IDENTIFICATION OF THE PHYSICAL CONTROLS ON THE DEPOSITION OF APTIAN AND ALBIAN DEEP WATER SANDS IN THE BREDASDORP BASIN, SOUTH AFRICA

TAMSYN VAN RENSBURG

OCTOBER 6, 2016

SUPERVISED BY DR BETH KAHLE (UCT) AND CO-SUPERVISED BY PETER DEKKER (PETROSA)

A Master's Degree Thesis in Geology through the University of Cape Town

Declaration

By submitting this thesis electronically, I declare that the entirety of the work contained therein is my own, original work, that I am the owner of the copyright thereof (unless to the extent explicitly otherwise stated) and that I have not previously in its entirety or in part submitted it for obtaining any qualification.

_____

Tamsyn van Rensburg

Date: 06 October 2016

Abstract

In the petroleum industry, the location of a new well is selected based on several factors, one of which is the presence of reservoir-quality sands. To determine the lateral extent of these sands away from well control, the depositional environment and character of the deposit must be adequately identified. This study aims to explain the physical controls on the deposition of the 13A (Aptian) and 14A (Albian) sequence sands within the deep water region of the Central Bredasdorp Basin through identifying the mass transport facies and processes and relating these to tectono-eustatic factors.

Since a primarily seismic-based approach was used to achieve the project objective, the results reflect findings based on 3D seismic data interpretations as well as seismic surface and volume attribute extraction supported by wireline well logs and well completion reports. This dataset contains information that enabled the identification of the structural and stratigraphic architecture of the 13A and 14A sequences as a whole, the location of the sediment provenances and possible triggers of the mass flows as well as the consequential sand distribution trends from the basin slopes to across the basin floor during the Aptian-Albian time. The onshore Tankwa Basin was studied as an analogue to the Bredasdorp Basin because it hosts world class outcrops of deep water lowstand fan deposits and therefore shows the finer-scale details of the associated depositional stratigraphy. The 13A and 14A sequence sands would have entered the Bredasdorp Basin in progradational pulses alternating with mud-rich successions associated with local sea level fluctuations that were on trend with the gradual global sea level rise from the Aptian to the Albian. These alternating successions are identified as lowstand, transgressive and highstand systems tracts in the seismic and wireline well log data used in this study.

The presented depositional model of the 13A sequence sands is a system of northwest to southeast sediment transport across the Central Bredasdorp Basin with indications of a final swing in orientation towards the east. The sands were mainly sourced from the paleo shelf edge on the northwest margin, although additional sediment input may have come from the west too. The faults that were active before and during the deposition of the Aptian-aged (13A) sands appear to have been the main control on sand distribution across the basin, guiding the sands from slope channels into basin floor fans and from shelf edge slumps into base of slope fans in a basinwide northwest-southeast trend.

The model of deposition of the 14A sequence sands is based on a channelised flow of sediment from the Central Bredasdorp Basin paleo shelf edge, down the slope and onto the basin floor primarily from the onshore source on the western margin. Supplementary sediment input may have originated from the Agulhas basement high on the southern margin of the basin in the form of less confined channels and mass wasting deposits. Inherited topography of the sea floor at the Albian time appears to have been the primary control on 14A sand distribution, causing bypass zones and giving rise to narrow, confined channel complexes despite some of the active faults possibly redirecting some of the sands from their initial trend.

Overall the pattern of deposition of the Aptian and Albian deep water sands in the Bredasdorp Basin appears to have been physically controlled by the regional paleo seabed topography and fault activity until the late Aptian.

Keywords: deep water, Bredasdorp Basin, controls on, mass transport deposits, sequence stratigraphy, lowstand, systems tract, progradation.

Acknowledgements

I would like to sincerely thank my project supervisor, Dr Beth Kahle (University of Cape Town), for her guidance and support through this study towards a Master's degree in Geology. Her enthusiastic contribution and reassurance of my ideas and findings gave me confidence in my project and fed my passion for this field of geoscience.

My appreciation is extended to Mr Peter Dekker, as my Masters project co-supervisor and my mentor at PetroSA. He offered practical advice and encouraged me to think "out-of-the-box" and to have more confidence in my own theories and interpretations.

PetroSA is acknowledged in this study as my full-time employer. Their technical and financial support in pursuing this degree is greatly appreciated.

As my mentor, Dr Alexis Carrillat (Schlumberger) empowered me with many of the skills and knowledge that I engaged in undertaking this project. His constant, encouraging support of me furthering my studies was highly valued.

Last, but certainly not least, I would like to convey immense gratitude and love to my family and friends that offered me encouragement and unwavering support on this journey.

Contents

List of Figures

List of Tables

Glossary

Definitions are sourced from the list of References.

Accommodation space: A sequence stratigraphic term for the amount of space available for sediment accumulation. Factors primarily influencing the amount of accommodation space are basin subsidence and sea level eustasy.

Aggradation: The accumulation of stratigraphic sequences by deposition in which beds stack vertically on one another during periods of a balance between sediment supply and accommodation space.

Amplitude: The deviation of the seismic wave from the zero crossing. The maximum positive amplitude is referred to as a peak and the maximum negative amplitude is referred to as a trough, resulting from a contrast in the seismic impedance.

Bypass: The transport of a sediment beyond a fixed area or geographical point. The bypassed sediment may include substrate material entrained during the passage of the flow which is deposited farther down in the system. Bypass usually occurs on a simple, steep slope which has a high level of confinement whereas a simple, toe of slope basin floor fan will be deposited where there is an abrupt change to a lower gradient and an associated lesser degree of confinement.

Conformable: Parallel strata that have undergone a similar geologic history and are deposited in succession without interruption.

Cycle orders: Sedimentary strata are deposited in rhythmic cycles and collectively form systems tracts, based on cyclic fluctuations of the sea level curve. Vail et. al. (1977) and Haq et. al. (1987) subdivide these depositional sequences into first to sixth order cycles based on duration in time.

First order cycles reflect sea level changes related to the movement of the global plates, occurring at a frequency of 250-300 myrs.

Second order cycles reflect sea level changes related to tectonic processes at a frequency of 9-10 myrs.

Third order cycles are 1-2 myrs in duration and represent the fundamental cycle on the proposed global eustatic cycle charts, typically consisting of the lowstand, transgressive and highstand systems tracts described above.

Fourth order cycles have a ~0.1 myrs frequency.

Fifth order cycles range from a 0.02 to 0.04 myrs frequency and have been interpreted as Milankovitch cycles since they appear to control high frequency variations in the global climate.

Formation Micro Imager (FMI): A high resolution electrical imaging device designed by Schlumberger to measure changes in micoresistivity in the rock formations intersected by a well. It is an advancement on dipmeter technology, used to identify sedimentary features and structural features (e.g. natural fractures) in sedimentary rocks in the form of a 2D image with a colour scale based on the angle of dip.

Progradation: The accumulation of sequences by deposition in which beds are deposited successively basinward due to the volume of sediment supply exceeding the available accommodation space. The position of the shoreline migrates into the basin during episodes of progradation in a process called regression.

Regression: The migration of the shoreline into a basin during progradation due to a fall in relative sea level. Deposition during a regression can juxtapose shallow water sediments onto deep water sediments.

Relay ramp: A feature that is formed during the growth of normal fault systems and recognised as an area of reoriented bedding between two normal faults that may overlap in map view and have the same dip direction.

Retrogradation: The accumulation of sequences by which beds are deposited successively landward because sediment supply is limited and cannot fill the available accommodation space. The position of the shoreline migrates backward onto the land in a process called transgression.

Shear: Deformation in which parallel internal surfaces slide past each other in a material substrate.

Shear stress: Co-planar with a material cross section from a force vector parallel to the cross section.

Shear strength: The strength of a material against structural failure where the material fails in shear.

Sinuous: A continuously differentiable curve. For example, a meandering channel.

Strata: Layers of sedimentary rock.

Transgression: The migration of shoreline out of a basin and onto land during retrogradation. A transgression can result in sediments characteristic of shallow water being overlain by deeper water sediments.

Tuning Effect: A phenomenon of constructive or destructive interference of seismic reflection waves from closely spaced events or reflections. At a spacing of less than one-quarter of the wavelength of the seismic wave, seismic reflections undergo constructive interference and produce a single event of high amplitude. At spacing greater than that, the event becomes resolvable as two separate events. The *tuning thickness* is the bed thickness at which two events become indistinguishable in time, and knowing this thickness is important to seismic interpreters who wish to study thinly-bedded reservoirs.

Turbidites: Here I define turbidites to be a fluidised, mixed sediment mass transport flow triggered by a catastrophic event causing a turbulent surge, beginning on the edge of the continental shelf or at the head of a canyon and progressing down the continental slope driven by the sedimentary load density under the influence of gravity. The resulting deposit is a sedimentary sequence of fining upwards sands with thinly interbedded mudstones on the basin floor, sometimes referred to as a partial Bouma sequence (illustrated below).

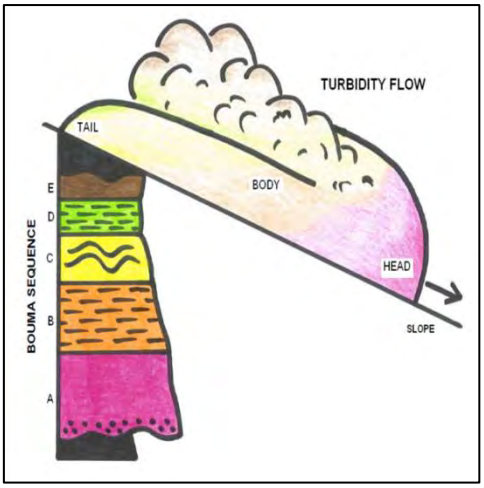

The relationship between the Bouma sequence units A to E and a turbidity flow. As a turbidity current progresses down a slope, the coarser grained sediments (i.e. sands), which are carried at the head of the turbidity flow, are deposited first due to their weight. Bouma sequence unit A is therefore deposited first – onto the scoured base of old muds on the basin floor. As the body and finally the tail of the turbidity flow move down the slope and lose energy, finer and ultimately the finest (suspended) sediments, i.e. silts and muds of Bouma sequence units B to E, are deposited sequentially on top of the sands. This forms an overall upward-fining sequence of massive sands (A), parallel laminated sands (B), cross laminated and rippled sands (C), followed by laminated silts (D) and finally pelagic and hemi-pelagic muds (E).

A complete Bouma sequence (Van Rensburg, 2012).

Unconformity: A surface between successive strata representing a missing interval in the geologic record of time, produced either by an interruption in deposition or by the erosion of depositionally continuous strata followed by renewed deposition.

Type 1 unconformity is characterised by stream rejuvenation and fluvial incision, sedimentary bypass of the shelf, and an abrupt basinward shift of facies and coastal onlap. This is interpreted to form when the rate of eustatic fall exceeds the rate of basin subsidence at the depositional shoreline break, producing a relative fall in sea level at that position.

Type 2 unconformity is characterised by subaerial exposure and a downward shift in coastal onlap landward of the depositional-shoreline break. It lacks subaerial erosion associated with stream rejuvenation and a basinward shift in facies; and is interpreted to form when the rate of eustatic fall is less than the rate of basin subsidence at the depositional-shoreline break.

Unconformities nomenclature: The alphanumeric nomenclature system of the unconformities bounding the South African stratigraphic sequences is one which has evolved over many years, originating from a hierarchal, operational type of naming system long before ages were assigned to the horizons and they are therefore frequency independent. Numerical symbols 1 to 22 were assigned in stratigraphic succession to prominent, unconformity-bound, seismically-distinct sequences or sequence sets. Less distinctive sequences were assigned alphabetical symbols A to E in stratigraphic succession within the numerically named sequences and sequence sets. Sequence-bounding unconformities are identified as either Type 1: t1 or Type 2: t2. Overall most sequences are designated by the symbol applied to their basal unconformity. The same principle applies to other types of stratigraphic surfaces, like a maximum flooding surface (MFS). For example, 13A sequence is bound by the basal Type 1 unconformity surface: 13At1. Additional alphabetical symbols are assigned to the 13A and 14A sequences in some studies to define the top of the sequence sand: ST and the base of the sequence sand: SB, for example 13AST and 13ASB. *See Appendix II and III*.

Well tops: The markers representing the unconformity surfaces intersected by a well with particular depth and time values.

CHAPTER 1

INTRODUCTION

1. Introduction

In the Bredasdorp Basin the Aptian-aged 13A and Albian-aged 14A sequence sands were deposited following the 13At1 (~124 Ma) and 14At1 (~108 Ma) unconformities, respectively, and are commonly recognised as hydrocarbon-bearing reservoirs off the south coast of South Africa. During this time, the basin was subjected to several episodes of subsidence separated by events of basin margin uplift and subaerial erosion in response to the separation of the South American and African plates (Brown *et. al*., 1995). The sands of the 13A and 14A sequences were transported from the continental shelf edge and basin margin basement highs downslope into the depocentre of the deep marine basin. Transport occurred under the influence of gravity in the form of slumps, debris flows and via slope channels which splayed as fans on the deeper basin floor in fining upward successions of alternating sand, silt and shale intervals, each spanning a period of approximately 2.5 million years (Brown *et. al.*, 1995). In this thesis, I will investigate the distribution of the mass transport deposits associated with the 13A and 14A sequences, since they have important implications in assessing the volume and distribution of the remaining hydrocarbon resource potential in the Bredasdorp Basin of South Africa.

The objective of this study is to perform a local assessment of the deep water, gravity mass flow sands of the Aptian 13A and Albian 14A sequences within the offshore Central Bredasdorp Basin and to determine the physical regional controls on their distribution (discussed in *Chapter 2)*.

In line with the objective, the Tankwa Basin in the SW corner of the greater Karoo Basin of South Africa was a good analogue because it hosts the world's best preserved Permian deep water turbidite fan complexes (discussed in detail later in this thesis) (Catuneanu *et. al*., 2002; Van der Werff and Johnson, 2003; Wickens and Bouma, 2000). Studying these onshore outcrops offers a better understanding of the spatio-temporal depositional evolution of prograding mass transport deposit successions (Wickens and Bouma, 2000). Combining this new knowledge with interpretations from a database of seismic surveys and wireline well logs creates the opportunity to construct a depositional model with a realistic perception of scale and one which may be used to establish an understanding of the physical controls on the deposition of the Aptian (13A) and Albian (14A) sequence sands across the Central Bredasdorp Basin.

The Bredasdorp Basin is one of five offshore sub-basins that developed within the larger Outeniqua Basin on the southern coast of South Africa in response to rift tectonics during the breakup of Gondwana from ~180 Ma (Broad *et. al*., 2006; Catuneanu *et. al*., 2002). The Bredasdorp Basin is bound by the Southern Outeniqua Basin beyond the 200 metre isobath to the south (Brown *et. al*., 1995), by the Agulhas Arch in the west and southwest and the Infanta Arch/Embayment in the northeast (Broad *et. al*., 2006) (**Figure 1**). Covering an area of approximately 18,000 km^2 (Wood, 1995), the Bredasdorp Basin acted as an ideal depocentre for weathered sediments sourced from subaerially exposed continental crust and the submarine shelf edge during the late Jurassictod Cretaceous periods (Davies, 1997; Tinker *et. al*., 2008). During this time, the sea level was rising globally but intermittent falls in the local sea level, influenced by pulses of basin margin uplift, caused

subaerial erosion of the basement structural highs and initiated sediment transport from the fluvial source into the offshore environment as mass flows from areas of unstable shelf edge quickly downslope onto the basin floor. Extrapolations from the δ-18 oxygen isotope records in the Southern Hemisphere found a sea surface temperature increase by approximately 3°C from the Aptian through the Albian, which resulted in an episode of intense global warming (Clarke and Jenkyns, 1999). The sea temperature change would have influenced water current circulation and organic matter deposition in the deep basin and this combined with atmospheric warming altered the geomorphology (e.g. fluvial and deltaic drainage patterns) of the onshore source locations thereby directly impacting the characteristics of the Aptian (13A) and Albian (14A) sequences in the Bredasdorp Basin.

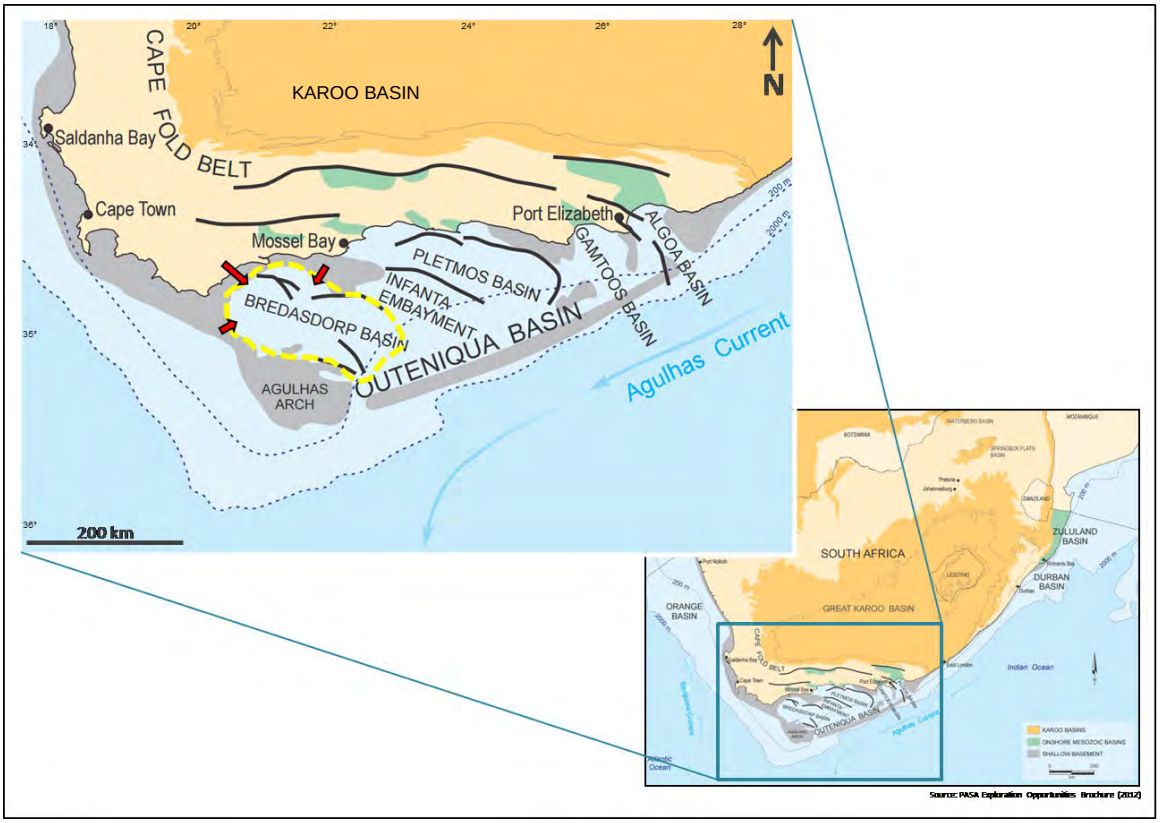

Figure 1 Regional location map of the Bredasdorp Basin within the greater Outeniqua Basin, bound by the Agulhas Arch and Infanta Arch/Embayment off the south coast of South Africa. Red arrows indicate the expected main sediment input directions. (Modified from PASA Exploration Opportunities Brochure (2012)).

The depocentre of the Bredasdorp Basin contains a concentration of fault-bound horst and graben structures as well as sedimentary deposits in the form of slumps, channels, fans and lobes. These features are key in addressing the study objective through building an understanding of the tectono-stratigraphic history of the 13A and 14A sequence sands in this basin (Burden and Davies, 1997). Brown *et. al*. (1995) describe the tectono-stratigraphic history episodes of thermal subsidence terminated periodically by basin margin uplift and associated erosion due to subaerial exposure and sea level falls. The deep water environment of the Bredasdorp Basin is classified as present day water depths greater than 200 metres in this study but at the initiation of the deposition of the 13A sequence the eustatic sea level was approximately 100 m lower than it is today and approximately

25 m lower than present during the initiation of the 14A sequence deposition (Brown *et. al*., 1995). The terrigenous sediments were sourced from the continental shelf at an average distance of ~145 km from the common 13A/14A depocentre and entered the basin in response to an externally initiated trigger of mass sediment flow.

The defined study area in the Central Bredasdorp Basin is 3,290 km² and was selected considering the above factors but also based on the quality and abundance of data coverage (**Figure 2**). Previously identified sand distributions of the 13A and 14A sequences and the proposed major faults intersecting the Bredasdorp Basin were taken into account too.

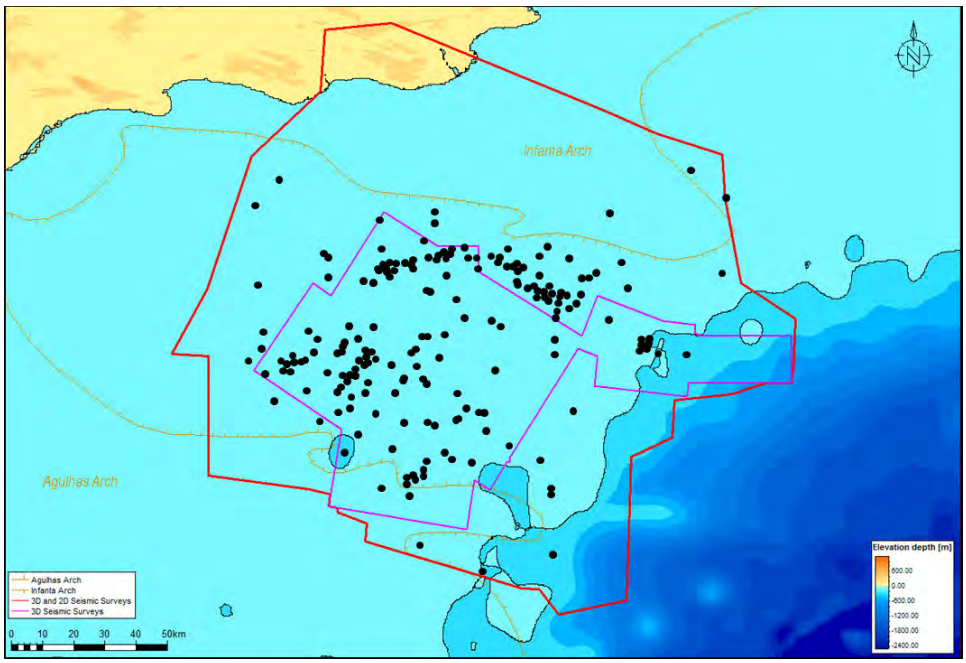

Figure 2 Seismic and well data coverage across the central to southern areas of the Bredasdorp Basin, with the full set of wells (black dots) and the coverage of the "3D and 2D" and "3D only" seismic survey sets (red and pink polygons, respectively).

CHAPTER 2

OBJECTIVES AND EXPECTED DELIVERABLES

2. Objectives and Expected Deliverables

The objective of this study is to determine the physical regional basin controls and local assessment in the sand distribution of the Aptian (13A) and Albian (14A) sequences within the offshore Central Bredasdorp Basin of South Africa and to identify the trigger mechanisms and sediment source locations of these mass transport flows. This may be achieved by considering the effect of environmental factors (e.g. sea level fluctuations, slope instability, localised faulting, thermal subsidence or tectonic-induced uplift, and variations in sediment influx) in addition to interpreting seismic facies, horizons and faults and the relevant wireline well data but also through applying knowledge gained from literature reviews and a case study of the onshore Tankwa Basin.

The methodology applied in this study (discussed later in this thesis in *Chapter 5*) expected to deliver the following results:

- Mapped top and base surfaces of the 13A sequence and the 14A sequence and seismic attribute extraction maps.
- Faults interpreted across the study area – pre- and post-Aptian in age.
- A broad identification of the deep water mass transport deposit types of sands present within the 13A and 14A sequences.
- A case study of the Tankwa Basin deep water turbidite fan complex as an analogue for the Aptian and Albian gravity mass flow deposits in the Central Bredasdorp Basin.
- Identification of the source of the sands in the 13A and 14A sequences.
- Identification of the physical controls on the deposition of the 13A and 14A sequence sands from the source to the depocentre.
- Depositional models for the 13A and 14A sequence sands across the Central Bredasdorp Basin.

CHAPTER 3

GEOLOGICAL SETTING

3. Geological Setting

3.1 Plate Tectonics and Basin Evolution

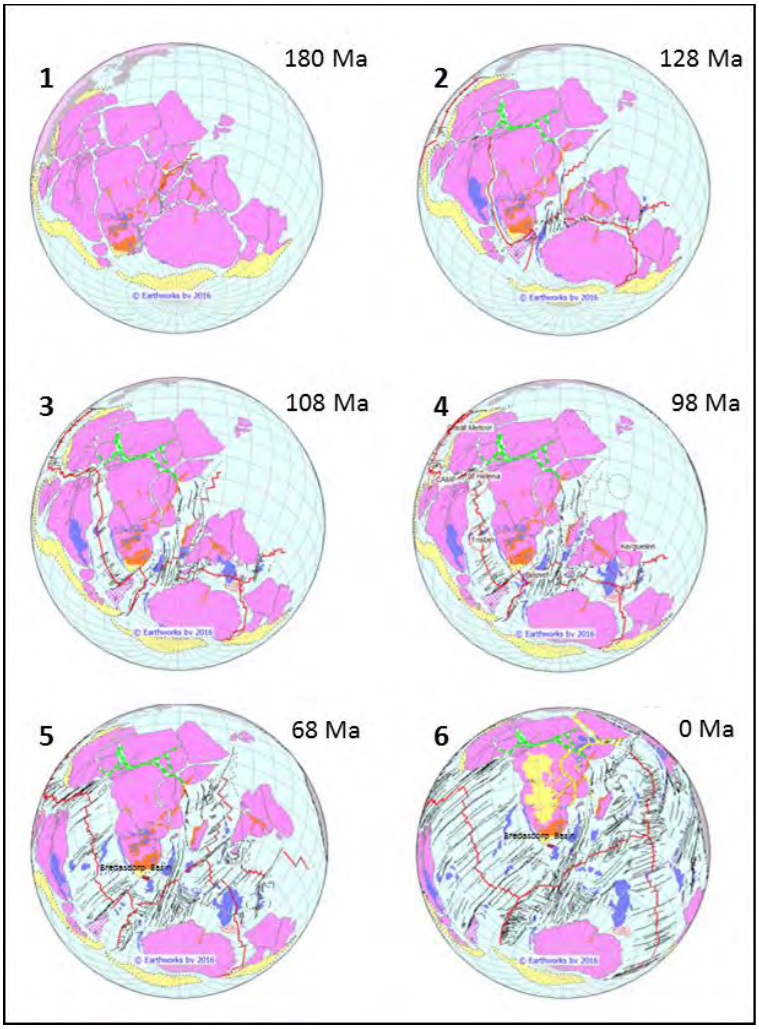

Figure 3 Schematic of the chronological-based stepwise breakup of the Gondwanan supercontinent from 180 Ma (1) to present day (6), illustrating the evolution of the offshore Outeniqua sub-basins and associated structural features (www.reeves.nl/gondwana).

The breakup of the Gondwanan supercontinent began in the mid-Jurassic (~180 Ma) (**Figure 3 (1 - 2)**) and around 80 million years later (late Jurassic) South America began drifting westwards from South Africa and the Falkland Islands (**Figure 3 (3)**), creating a fracture system influenced strongly by the ancient weak zones of the onshore Permian-aged Cape Fold Belt and due to the presence of the Tristan De Cunha plume and the Bouvet hot spot (Watkeys, 2006) (**Figure 3 (4)**). As largely dextral strike-slip movement occurred along fracture system lineament, an extensive NE-SW trending transform fault, named the "Agulhas Falkland Fracture Zone", developed along the southern edge of the African plate as the Falkland plateau began rotating away from it (Broad *et. al.*, 2006) (**Figure 3 (5)**). The strong trans-tensional stresses associated with the Agulhas Falkland Fracture Zone (AFFZ) triggered normal faulting (Du Toit, 1976; Fouché *et. al.*, 1992) along the older scars of compressional structures inherited from the Cape Fold Belt (Cartwright, 1989, Malon *et. al.*, 1990, Davies, 1997) (**Figure 3 (6)**). This developed a NW-SE trending series of en-echelon horsts and grabens along newly weakened zones of offshore continental crust on the south and east coasts of South Africa within the Mesozoic-aged (~271 Ma to ~67 Ma) Outeniqua Basin (Tinker *et. al.*, 2008), better known as the Bredasdorp, Pletmos, Gamtoos and Algoa sub-basins (**Figure 4**).

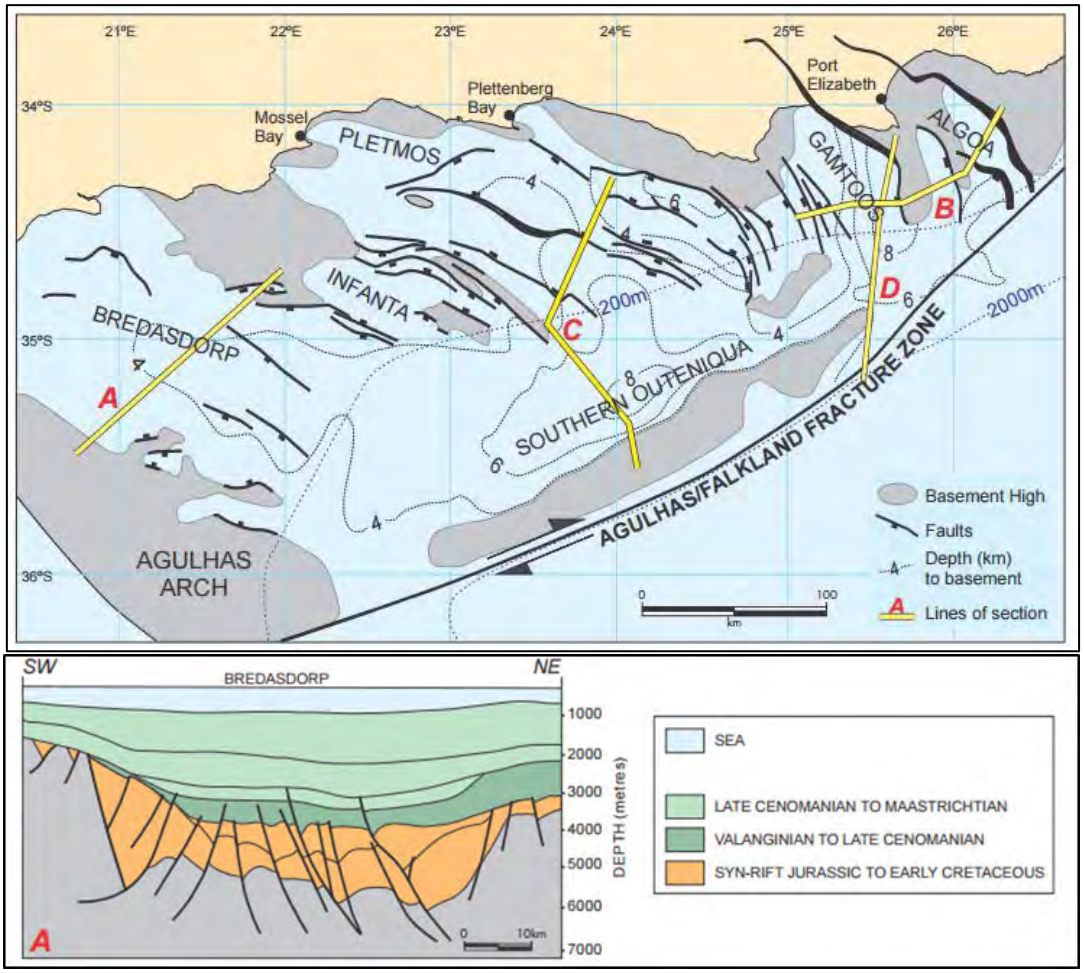

Figure 4 Major tectonic elements in the Outeniqua sub-basins and a schematic cross-section (A) to illustrate the horsts, grabens and major faults associated with sediments from the syn-rift (Jurassic) to recent within the Bredasdorp Basin. (PASA Exploration Opportunities Brochure (2012)).

Structural readjustments, rifts and collapse continued to occur in this region affecting the established Mesozoic-aged Bredasdorp Basin (McMillan *et. al.*, 1997) until the extensional tectonic activity ceased. The later separation and migration of the Falkland Islands from the African plate caused pulses of compressional tectonic activity in the sub-basins which prompted folding, uplift and intensive subaerial erosion (Brown *et. al.*, 1995). By this time, thermal subsidence was occurring in the Bredasdorp Basin (Davies, 1997; Jungslager, 1996; McMillian *et. al.*, 1997) in episodes of 9-12 million years in duration, each terminated by a brief uplift of the basin margins and the subsequent erosion to form a Type 1 unconformity due to further plate separation movements between Africa and South America (Brown *et. al.*, 1995). These periodic tectonic pulses interacted with eustatic fluctuations as well as the sediment supply, thereby all working to drive the transport and deposition of mass flow deposits, such as those in the 13A and 14A sequences (Brown *et. al.*, 1995).

3.2 Tectono-Stratigraphic History

The pulses of sedimentary filling of the Bredasdorp Basin have been associated with specific concurrent tectonic episodes in the basin (Jungslager, 1996) (**Figure 5**). This enabled the division of the Bredasdorp Basin sedimentary history into four major tectono-stratigraphic phases: pre-rift, syn-

rift, transition and drift. The pre-rift phase is associated with the basement rocks and the sequences deposited prior to the formation of the Valanginian-aged (~139 Ma) 1At1 unconformity and is therefore not discussed in detail in this study. Separated by the 1At1 unconformity and a brief episode of thermal basin subsidence (i.e. the transition phase), the syn-rift and drift phases represent not only unique sedimentary characteristics but also different tectonic episodes in the history of the Bredasdorp Basin (McMillan *et. al*., 1997). The drift phase is key in this study as it includes the Aptian-aged 13A sequence, between the 13At1 unconformity (~124 Ma) and the approximately 2.5 million years younger sequence top, and the Albian-aged 14A sequence bound by the 14At1 unconformity (~108 Ma) below and the sequence top corresponding to a surface of approximately 105.5 Ma in age. These ages are sourced from the latest international chronostratigraphic chart (ICS, 2016) (**Appendix II**) and were applied in principle to the second and third order unconformities reflected on the Cretaceous chronostratigraphic chart of the Bredasdorp Basin from Brown *et. al.* (1995) (**Appendix III**). These considerations are reflected together in the sequence chronostratigraphic chart of the Bredasdorp Basin below (**Figure 5**).

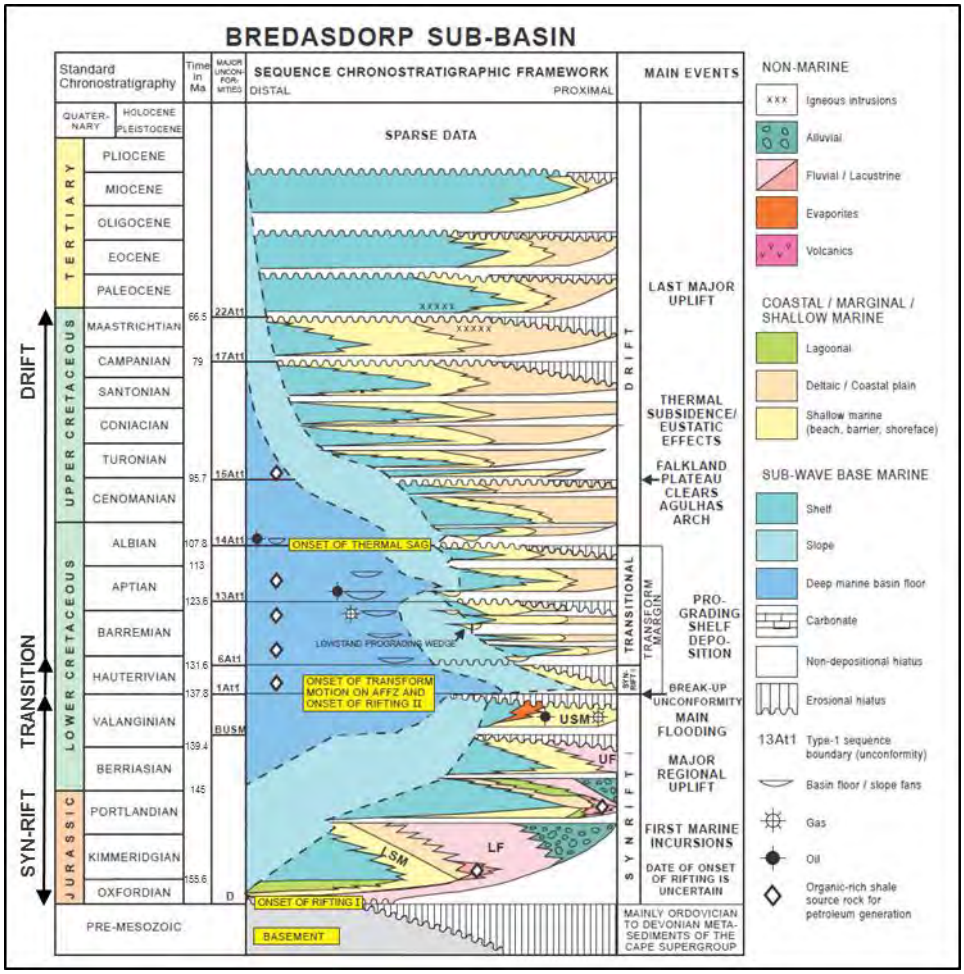

Figure 5 Sequence chronostratigraphic chart of the Bredasdorp Basin illustrating the syn-rift, transition and drift phases (Modified from Brown *et. al*., 1995).

3.2.1 Syn-rift Phase

The syn-rift phase marks an episode of extension, causing the continental crust to stretch and thin and in some parts to fail as faults. The syn-rift phase is represented by a succession of sequences bound by a basement unit of Ordovician to Devonian (~480 – 360 Ma) slates and quartzites of the

Cape Supergroup and capped by the Hauterivian-aged (~137 Ma) 1At1 unconformity. The deposition of the late Jurassic to early Cretaceous syn-rift sedimentary deposits between ~160 Ma and ~100 Ma varies in character from alluvial fanglomerates to braided and meandering fluvial channel sands overlain with shales (Burden, 1992; McMillan *et. al*., 1997; Davies, 1997) and resting unconformably on the faulted basement. Clastic continental sediments, such as orthoquartzites and slates of the Cape Supergroup and sandstones and shales of the Karoo Supergroup, originated from the erosion of the onshore Cape Fold Belt and became intercalated with shallow marine sediments sourced from the paleo basin shelf (McMillan *et. al*., 1997) during the early Cretaceous.

Rifting ceased in the early Valanginian (~139 Ma) and was followed by a marine regression, which led to the formation of the 1At1 unconformity at the same time of the initiation of movement along the AFFZ (Jungslager, 1996). The associated dextral strike-slip faulting activity caused regional uplift and erosion, thereby marking the end of the syn-rift phase and a drastic change in the depositional environment of the Bredasdorp Basin.

3.2.2 Transition Phase

The first sediments of the transition phase were deposited following the deposition of the maximum flooding surface shales of the 1At1 unconformity (~137 Ma). At this time, the Bredasdorp Basin experienced asthenospheric cooling and an associated episode of rapid thermal subsidence along the rift faults. This activity prompted the central parts of the basin to deepen and thereby leading to restricted water circulation and the formation of a poorly oxygenated environment. The initial sedimentary deposits into this depocentre were identified as deep marine muds, which became intercalated with occasional mass flow sands (McMillan *et. al*., 1997; Broad *et. al*., 2006) that were deposited in aggradational successions concentrated within the deepest depocentre as sequences 1A to 5A (Brown *et. al.*, 1995).

3.2.3 Drift Phase

As the rate of subsidence began to slow down, a transpressional event caused uplift in the Bredasdorp Basin thereby terminating the transition phase of deposition and prompting the formation of the 6At1 (~132 Ma) unconformity as the base of the drift phase of tectono-stratigraphic deposition. There is no precise marker, per se, that defines the commencement of the drift phase but the approximate timing has varied over the years (for example Brown *et. al*. (1995) (**Figure 5**) place the 14At1 unconformity as the start of the drift phase) but has been delineated as the 6At1 unconformity in this study, based on the latest interpretations conducted across the Bredasdorp Basin using the most recent, available sources of data.

During periods of low relative sea level, submarine canyons and channels developed in the Bredasdorp Basin from the shelf and basin margin highs. The submarine canyons incised into the paleo basin shelf and fed sands into the slope channels that acted as pathways for the mass flow sands from the shelf edge to the depocentre of the basin, thereby adding further loading and contributing to active crustal depression and subsidence. As a result, most of the sands were preserved as depositional sequences of fining upward basin floor fan complexes and lowstand wedges as the sands were transported downslope under the influence of gravity (Mutti, 1985). This occurred coincidently with intermittent regressive sea level phases during the late Hauterivian to Aptian and specifically between the 6At1 (~132 Ma) and 13At1 (~124 Ma) regional unconformities (Davies, 1997; Burden, 1992), which formed due to episodic events of local uplift and subsequent widespread subaerial erosion in the Bredasdorp Basin (Brown *et. al*., 1995). The most significant unconformities in this study are 13At1 (~124 Ma) and 15At1 (~96 Ma) as they represent the limits of

the broader interval of investigation which encompasses the important 14At1 (~108 Ma) unconformity too.

The 13At1 unconformity formed due to uplift and the associated intensive subaerial erosion due to the tectonic action of the Falkland plateau moving past the Agulhas platform (Brown *et. al*., 1995). A later fall in the local sea level enabled the basin to receive this eroded sand input from the shelf in the north-northwest and with the regression of the coastline the 13A sands were transported as far as into the basin depocentre and deposited as a lowstand package. A period of sand starvation followed as the local sea level rose and sediment supply periodically diminished, which prompted organic-rich shales to be deposited as a basinwide transgressive package associated with the 13A maximum flooding surface (Brown *et. al*., 1995; Broad *et. al*., 2006). After the deposition of a highstand package in the form of submarine progradational sequences during a higher sea level, a brief episode of basin margin uplift erosively formed the 14At1 unconformity (Broad *et. al*., 2006). Local sea level fluctuations then caused influxes of sand into the basin during episodes of renewed subsidence, albeit gradually slower subsidence over time, and a coincident sea level fall (Brown *et. al*., 1995) which ultimately led to the deposition of the 14A sands in a distributional pattern extending from the paleo shelf in the west into the depocentre of the Bredasdorp Basin further east. Subsequent cycles of basin sag and an accompanying local sea level rise in the Bredasdorp Basin yielded thick depositional successions of shales basinwide between the lowstand packages of the 14A and 14B sands, in the form of transgressive and highstand systems tracts successions. This took place until the basin experienced some remnant uplift and erosively formed the regional 15At1 unconformity (Brown *et. al*., 1995). Open shelf sedimentation prevailed with the complete separation of the South American and African plates (Broad *et. al*., 2006) and aggradational shelf deposits continued to overlay the 15At1 unconformity, only periodically interrupted by brief erosional episodes until the end of the Cretaceous (~67 Ma) (Roux, 1997).

CHAPTER 4

DATABASE

4. Database

4.1 Study Area

The study area covers 3,290 km² of the central part of the Bredasdorp Basin, located off the south coast of South Africa. The image below (**Figure 6**) captures the proximity of the study area to the present day shoreline but also the location of the study area from the continental shelf edge and onshore Cape Fold Belt source of sediment.

Figure 6 The study area (yellow polygon) of this project located on the present day continental shelf off the south coast of South Africa.

4.2 Seismic Data

The seismic data provided by the Petroleum Oil and Gas Corporation of South Africa (Pty) Ltd (PetroSA) offers dense coverage of the Central Bredasdorp Basin, consisting of 3D seismic cubes and 2D seismic lines. The 3D seismic surveys cover a total area of ~7,345 km² with vintages ranging from 1994 until 2012; and the 2D seismic line coverage equates to 45,000 km of original and reprocessed data. After a high level verification of the 3D and 2D seismic data, it was decided to restrict the seismic database to a set of two 3D surveys for this study, with the extent of the surveys fully covering the "Study area" polygon (**Figure 7**).

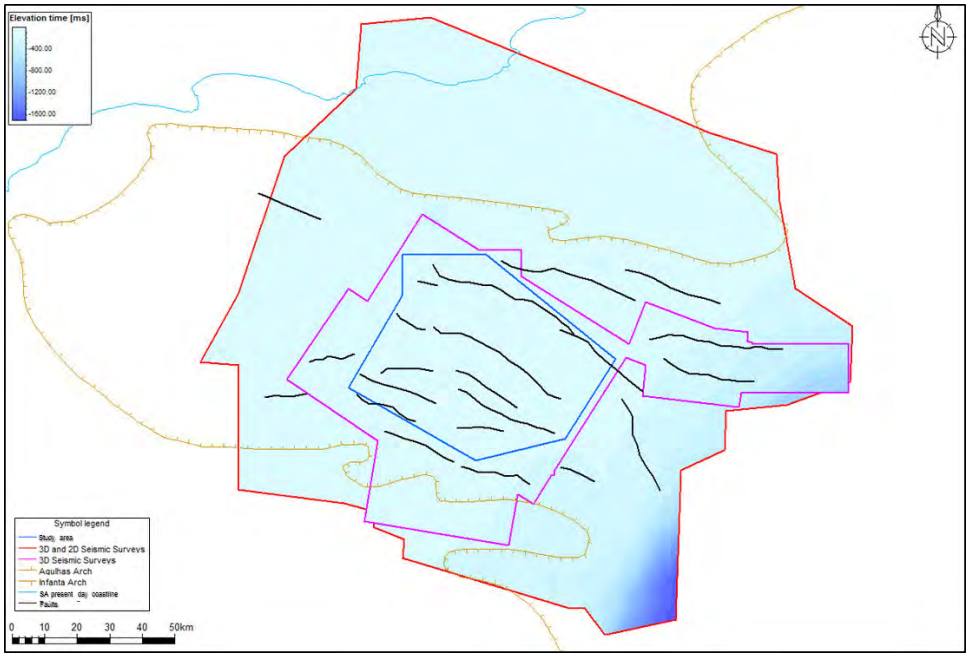

Figure 7 A comparison of the extent of various sets of seismic data coverage: "3D and 2D" – red polygon, "3D only" – purple polygon, Study area – blue polygon. Displayed on my interpretation of the present day seabed time surface with the key structural elements, such as the basin bounding highs and legacy fault interpretations, in the Bredasdorp Basin.

The most recent 3D seismic survey in the database of this project was performed over the Central Bredasdorp Basin and processed in 2012. This survey covers the full study area and was used as the primary seismic data for interpretation, complemented by the 1996 3D seismic survey where its boundary is close to the edge of the study area.

The high resolution 2012 3D seismic survey was acquired over the Central Bredasdorp Basin using an "over/under" technique. This geometry of acquisition (the streamers) was promoted as the DISCover (Deep Interpolated Streamer Coverage) technique by Western Geco. This broadband acquisition technique was developed to deliver 3D seismic data with an enhanced bandwidth (www.slb.com). The enhanced bandwidth is achieved by combining the low frequencies recovered from the deeper-towed streamers (and therefore not affected by swell and other environmental noise) with the higher frequencies recovered from the shallower-towed streamers after discarding the noise contaminated lower part of the upper stream spectra that has been affected by swell and other noise. The streamer technology used Western Geco's patented "Q-marine point-receiver marine seismic system" which records the seismic data at high spatial frequencies to allow better attenuation of environmental and streamer noise.

The survey layout plan consisted of roughly east-west trending sail lines orientated in the strike direction of the main structural features of the Bredasdorp Basin geology, although a dip orientation to the intervals of interest would have been better from an imaging perspective. 3D surveys in the southern offshore are typically oriented in a roughly east-west condition for operational and environmental considerations. This orientation is approximately perpendicular to the dominant and ubiquitous swell which originates in the deeper oceans toward the southwest and theoretically

movement along the streamers is therefore reduced. Currents in the survey area may reach up to 2 knots but they are generally unpredictable and dependent on weather. Onboard current meters closely monitor data recorded from compasses on the streamers and the Q-fins are steered to re-orient the streamers when necessary. The Agulhas current intersected the survey area to the far south and only affected the streamers during line changes. Further details about the 2012 3D seismic survey are described in **Appendix I**.

The initial sequences of the seismic data processing were performed onboard the vessel by Western Geco. The onboard processing focuses on noise attenuation in the shot domain (attenuation of noise present in all seismic traces that originated from a common shot), identification and replacing of 'bad' traces (not meeting certain amplitude criteria). It also typically applies tidal corrections to the recording times and then decimates the volume of field data by sub-stacking or summing of adjacent traces since the processes applied later in the sequence do not require such regular spatial sampling. Onboard processing is also used to perform quality assurance and evaluate whether newly acquired data meets the acceptance criteria.

The processing was continued by Western Geco onshore. Residual noise attenuation, attenuation of short and long period reverberations and imaging methods completed the processing sequence (unpublished presentation by PetroSA). PetroSA was provided with full and partial stack cubes (near angle stack: 0-18°, mid angle stack: 18-36°, far angle stack: 36-54°) and the stacking velocity cube in which velocities were picked every 500 metres. Further details of the 2012 3D seismic survey and its data processing techniques (e.g. migration algorithms, velocity models, gain and frequency adjustments) remain unpublished.

4.3 Well Data

From over 200 wells drilled across the Bredasdorp Basin, a subset of 22 wells within the central part of the basin was selected for this study (**Figure 8**). The information gathered from these wells includes wireline well logs, geological well completion reports and drilling reports for the purpose of this study. PetroSA provided these data in a digital format, although paper-based copies of the well completion and drilling reports were available too.

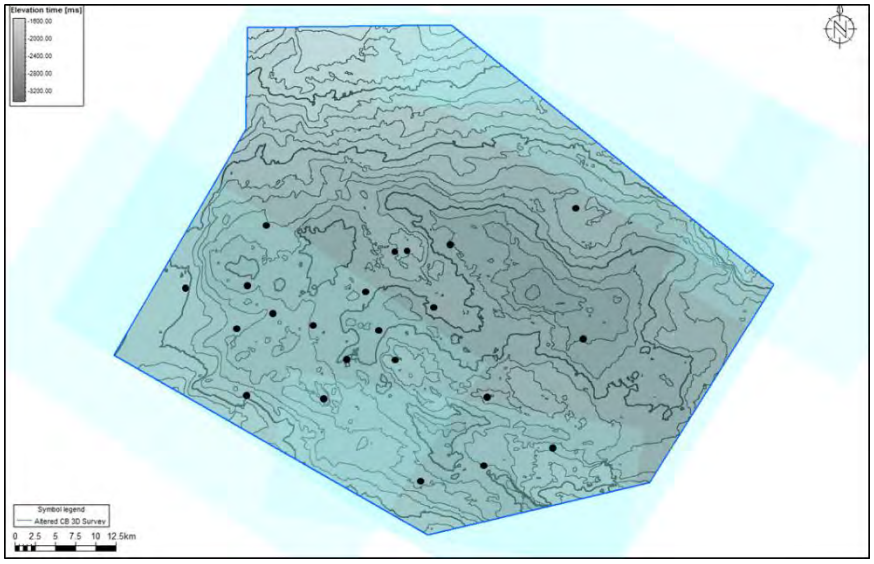

Figure 8 Location of the subset of wells for this study within the "study area" polygon. Blue shaded areas represent the 3D seismic survey coverage, displayed on the interpretation of the 1At1 time structure surface.

4.4 Checkshot Data

Time-depth curves and checkshot data are readily available for 21 of the 22 wells selected for this study. The time-depth curves are based on sonic log information, which is calibrated with seismic checkshot information. The checkshots in the Petrel project database were verified using the original checkshot data sheets as a comparison for each of the key wells.

4.5 Cultural Data

Maps illustrating features such as licence blocks, digitized polygons of seismic survey coverage, legacy faults, structural features and maps bearing the present day coastline and onshore mountain ranges are a few examples of the types of cultural data that were consulted in this study. These files were imported into the Petrel project database and geo-referenced. Some were used to create digitized features (e.g. Agulhas and Infanta arches) in the form of polygons which could be displayed in different types of windows in the project.

CHAPTER 5

METHODOLOGY

5. Methodology

5.1 Literature Review

Previous studies in the Bredasdorp Basin in the form of reports (public and unpublished), presentations and posters as well as theoretical models and interpretations were reviewed prior to and throughout this study. It should be noted that the majority of those studies used only 2D seismic data and hence there may be quality differences in the results and limitations would have been reached in achieving past study objectives.

There is the suggestion that the Bredasdorp Basin played host to prograding fan systems of mass flow and channelised sediments that were deposited in the deep submarine basin periodically throughout its history. These sedimentary packages are particularly dominant in the 9At1 to 13At1 interval (~128 - 124 Ma) and are generally recognised as sandstones interbedded with claystones/shales (as discussed in the *Chapter 3:* G*eological Setting*). For this study, the focus was narrowed down to the 13A and 14A sequences, broadly bound by the 13At1 and 15At1 unconformities.

5.2 Data Collection

A data listing was generated based on the study objectives set out during the proposal phase of this project. My active involvement in the South African petroleum industry assisted in giving me a fair idea of the extent of the available database and the range in data vintages. This knowledge assisted in planning the time allocation for data loading into the empty Petrel project.

5.3 Project Geo-Referencing

Creating a Petrel project requires the definition of the co-ordinate reference system (CRS) to globally geo-reference the different dataset types as they are imported into the project. A technical consultant from Schlumberger assisted me in creating a CRS to define the Petrel project as a "WGS 8434S ESRI 1128" system and to programme the immediate conversion of imported "Cape Clarke 1880" system data. This is necessary before populating the project because seismic and well data may be acquired and/or processed in different geographical reference systems, and bitmaps and other loaded maps and/or images need to be geo-referenced after being imported into the project, based on a single CRS.

An additional geo-referencing tool is the Map Service function in the Petrel. This tool activates a live satellite map view of the Earth, which was centred on South Africa for the purpose of this study. This function may be used to verify the position of imported, co-ordinate based data (e.g. literature-derived maps, wells, seismic surveys).

5.4 Data Import

Guided by the study objectives set out in the project proposal phase, the following types of data were collected and imported into the new, geo-referenced Petrel project:

- 3D and 2D seismic surveys
- Wells with wireline logs
- Checkshot data

- Cultural data (e.g. maps, images, polygons)

5.5 Data Analysis

A review of the dataset was undertaken at the beginning of the project to assess its validity and applicability to the scope of this study by considering factors such as basin coverage, depth, vintage, complexity and quality.

The 3D and 2D seismic surveys were compared in vertical and areal extent, the quality of the ties between them was checked and the phase correlations and time shifts were reviewed across the datasets.

The wells were assessed by considering their spatial distribution across the Central Bredasdorp Basin and which wells intersect the 13At1 and 14At1 levels and therefore the targeted 13A and 14A sequences in the study area was taken into account too. The availability, comprehensiveness and quality of the well log data were checked around the same time that the loaded checkshot files were reviewed against the original checkshot data sheets. The study area was delineated so that subsets of seismic and well data could be selected, bearing in mind the outcome of the data review/validation phase. Ultimately the database was refined to include only two 3D seismic surveys and 22 wells with their gamma ray, sonic, density and caliper wireline logs.

5.6 Synthetic Seismogram Generation

For the synthetic seismogram generation, the Integration Method was applied in the Well-Seismic Tie tool in Petrel. This method was chosen for this study because it is a time-based (TWT) template that incorporates the well-seismic tie steps of sonic calibration and synthetic generation into a single process (this is the integration) as opposed to two separate processes. Input data for the Integration Method consisted of a preloaded well with checkshot data, sonic and density logs, a seismic survey as a reference and a seismic wavelet (**Figure 9**). The ties across the 13At1 and 14At1 unconformities were of particular importance in this study because they were considered to be the basal surfaces of the 13A and 14A sequences, respectively. For some of the wells a theoretical seismic wavelet was used to generate the synthetic seismogram and in others a wavelet was extracted from the referenced seismic survey (i.e. the most recently acquired 3D survey in this study) and over a specified time window. An average wavelet frequency of 25 Hertz was applied in the synthetic seismogram generated in this study as this was the frequency of the reference seismic survey in this process. Where necessary, the resultant synthetic trace was bulk shifted in time or stretched and squeezed to better align it with the real seismic data traces at the well location, however manipulating the resultant trace was kept to a minimum and in some wells no bulk shift was applied. Overall the synthetic seismograms were bulk shifted over a range of 2 to 30 milliseconds. This was followed by the activation of the final synthetic seismogram as the calibrated time-depth relationship (TDR) curve in the well to ensure that the tie was applied.

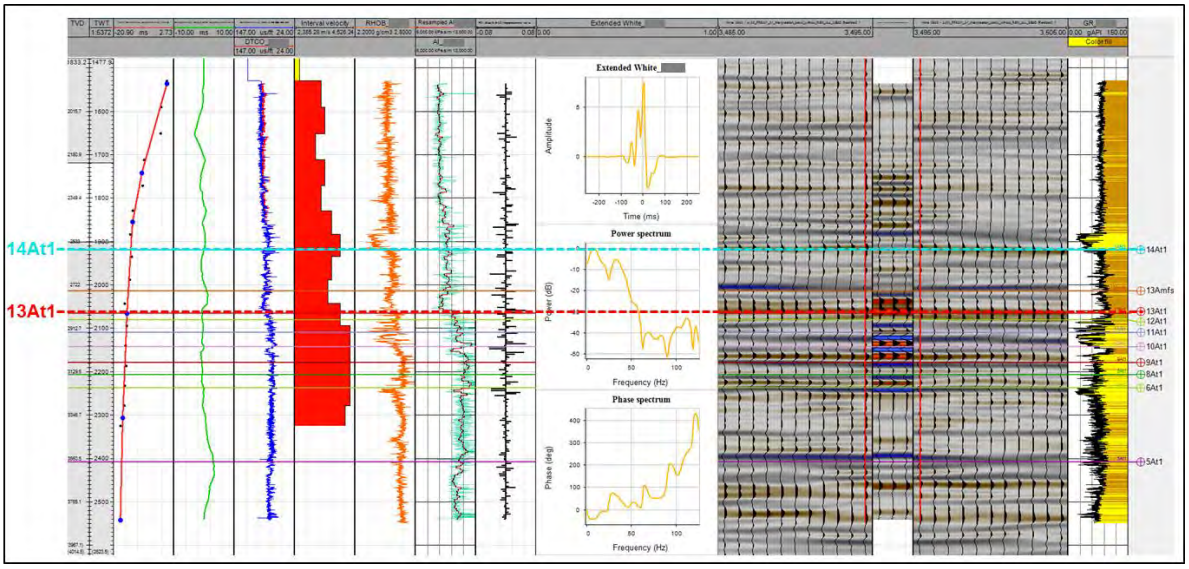

Figure 9 An example of the variables used and produced in the generation of a synthetic seismogram, listed from left to right: depth (TVD), time (TWT), checkshot points overlain with a drift curve, the residual curve, original sonic curve (red, DTCO) and calibrated sonic curve (blue), density curve (RHOB), AI curve (turquoise) overlain with Resampled AI curve (blocky red), reflection coefficient spikes, convolutional wavelet, original seismic traces displayed as two panels on either side of the resultant synthetic seismogram, gamma ray log.

5.7 Seismic Interpretation

Seismic interpretation is performed to analyse the seismic data by mapping reflection events using the markers of the horizons at the well locations (i.e. well tops) to create stratigraphic-based time correlations across the basin. As part of the seismic data review process, initially the seabed horizon was interpreted in the 3D and the 2D surveys but after scrutinizing the output surface, the extent of the study area and the time required to perform this task, a decision was made to limit the seismic data to a smaller subset of 3D surveys only.

Initially a standard 200 by 200 inline-crossline increment was applied in the manual interpretation of the regional unconformities and surfaces: Basement, 1At1, 12A sand top, 13At1, 14At1, 15At1 and the present day seabed. 3D autotracking was then applied to the manual interpretation to fill in gaps and to reguide the horizon in uncertain or mistied areas. As a form of quality control during the initial picking and during the 3D autotracking, composite seismic sections were made across the study area in random orientations to purposely intersect the brightest amplitudes of the broadly distributed 13A sands and the more confined 14A sands in approximately north-south and west-east orientations. It was recognised in this study that the 13A and 14A sands overlay the 13At1 and 14At1 unconformities, respectively, identified as a bright red reflector on the full- and far-stack seismic sections representing a seismic wavelet peak (positive standard polarity) and indicate an increase in acoustic impedance and hence the sand base (i.e. 13ASB and 14ASB). Above the sand base (peak), the sand tops (i.e. 13AST and 14AST) can be seen more clearly in the far-stack seismic sections as a bright blue seismic wavelet trough (negative standard polarity) due to the decrease in acoustic impedance caused by the porosity-driven decrease in bulk density and a density contrast between the softer shales above. The 13At1 peak appears as a doublet (i.e. double peak) in some areas of the seismic section but as a single

peak elsewhere and this is due to the effect of tuning thickness. For consistency, the 13At1 pick was made on the lower peak of this doublet (**Figure 10**).

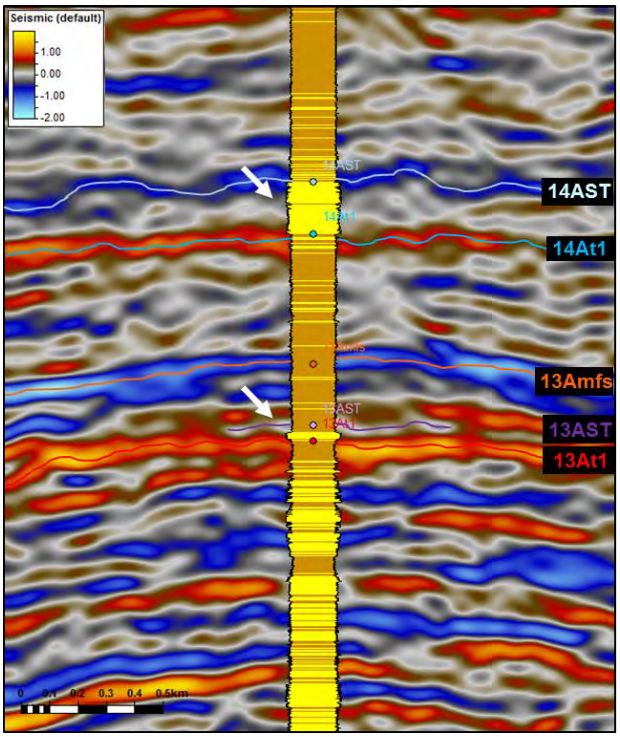

Figure 10 Seismic section (full stack) intersecting a well with its key well tops/markers displayed. The 13At1 doublet is present below the 13A sand for which the top is picked as the trough in between the two peaks of the 13At1 doublet.

5.8 Surface Mapping

Surface mapping is the process of creating a solid 2D grid based on point data, polygons, horizon interpretations, bitmaps and/or well tops through applying an algorithm-based method in Petrel. Gridding algorithms that may be applied include: Convergent Interpolation, Moving Average, Minimum Curvature, Kriging, Cos Expansion, Gaussian Simulation, Surface Resampling, Isochore and Artificial Algorithms. Convergent Interpolation gridding was selected as the algorithm for converting the seismic horizon interpretations into surfaces in this study as it yielded the best results after it tunes the surface to an unlimited amount of neighbouring data points (Petrel Help, v.2015). Seismic horizon interpretation is required as the main input in the surface mapping (gridding) function but it may be complemented with other inputs such as faults, contours, lines and polygons to influence the topography and spatial extent of the resultant surface. The geometry of the surface was specified by defining the grid position, layout (X & Y increments) and size; and a boundary was defined to restrict the lateral extent of gridding. To validate the resultant surface and to assess the accuracy of the interpretation picks, the residuals between the surface and the well markers were calculated. Based on the residuals, the generated surface was edited to more precisely fit the well markers but alternatively an adjustment of the surface as a whole may be applied by changing the average Z-value (single depth or time value) to ensure a good tie between the horizons and accurately picking the markers.

5.9 Seismic Attribute Extraction and Volume Rendering

Seismic attribute extraction and volume rendering are two functions in Petrel that may be used to emphasize or highlight particular features of a seismic-derived surface or a seismic cube to better identify sands and to better delineate structural trends in the sand distribution. The functions are algorithm-based and operate by extracting and highlighting specific attributes of the seismic data as a visual reflection of the properties of the rocks and fluids. Seismic attributes analysis was focused in a window extracted from 13At1 to 30 milliseconds above the 13At1 surface and likewise for 14At1 to try capture more information about the distribution of the 13A and 14A sequence sands.

In this study, the following surface attribute extraction algorithms were applied: Dip Angle, Dip Azimuth, Maximum Amplitude, Maximum Curvature, Minimum Amplitude and Root Mean Square (RMS). The descriptions of these attributes (below) are modified from the Petrel manual and based on the function that they provided in this study. The best results are illustrated in *Chapter 9: Results*.

Dip Angle is a geometric attribute which measures reflector shape and estimates reflector orientations, based on a computation applied to each trace to determine the best fit plane (3D) or line (2D) between its immediate neighbour traces on a specific seismic horizon. The resulting surface shows the magnitude of dip (or gradient) of the plane or line in degrees measured from the horizontal plane so Dip Angle can be used to create a pseudo paleo-geologic map on a horizon or time slice or to even highlight areas of sharp geological breaks (e.g. paleo-shelf edge, faults etc.).

Dip Azimuth is a geometric attribute which measures reflector shape and estimates reflector orientations, based on a computation applied to each trace to determine the best fit plane (3D) between its immediate neighbour traces on a specific seismic horizon. The resulting surface illustrates is the direction of maximum slope (or dip direction) clockwise from north, measured in degrees. Dip Azimuth can be applied to highlight the trending orientation of sharp geological breaks (e.g. paleo-shelf edge, faults etc.).

Maximum Amplitude is a seismic attribute that computes the maximum positive value of the absolute value amplitudes within a defined time or depth window. It measures lateral reflectivity changes in acoustic impedance contrast and can therefore be used to map the strongest positive Direct Hydrocarbon Indicators (DHIs), like a bright spot, within a specified zone. Since Maximum Amplitude recognises positive amplitude values, it can be applied to highlight the likely distribution of fluid-bearing or highly porous sands through the strong peak that is typically associated with the top of the sands, although this may be challenging in areas where the base of the reservoir sand coincides with a regional unconformity reflector.

Maximum Curvature is a partial derivative of the *Dip* surface attributes in the form of a measure of the change of dip of the reflectors as a function of azimuth. Maximum Curvature is calculated from the magnitude or direction of maximum curvature of a specified seismic horizon and it can be used for identifying structural features (e.g. paleo-shelf edge, sediment accumulations, basement highs, slope collapse etc.), based on areas of the surface with the greatest change in dip.

Minimum Amplitude is a seismic attribute that computes the maximum negative value of the absolute value amplitudes within a defined time or depth window. It measures lateral reflectivity changes in acoustic impedance contrast and can therefore be used to map the strongest negative DHIs, like a bright spot, within a specified zone. Since Minimum Amplitude recognises negative amplitude values, it can be applied to highlight the likely distribution of fluid-bearing or highly porous sands through the strong trough that is typically associated with the top of the sands.

RMS is a mathematical product of the square root of the sum of squared amplitudes divided by the number of samples within the specified time window. It can be used to measure the reflectivity associated with several factors: DHIs in a target zone, porosity or fluid content in a reservoir or geological-driven amplitude changes (e.g. sequence boundaries, unconformity surfaces and discontinuities).

The volume rendering algorithms that were experimentally applied to the seismic cube in this study to enhance the seismic attributes included: Edge Effect, Envelope, Graphic Equalizer, Instantaneous Frequency, Relative Acoustic Impedance, Standard Deviation, Sweetness and Variance. The descriptions of these attributes (below) are modified from the Petrel manual and based on the function that they provided in this study. The Sweetness and Variance attributes are illustrated in *Chapter 9: Results*.

Edge Effect is a statistical edge enhancement method that can be used to detect and enhance sharp or vague edges, such as faults. It identifies where the values on a line segment differ significantly from the surrounding values in all directions. The result is the best evidence of a line passing through a particular point and ultimately the better the evidence, the higher the output value. This function of the Edge Effect makes it a useful tool in the Ant-tracking process.

Envelope is an attribute which highlights subtle lithological changes and also detects bright spots. It is similar to reflection strength in that its total instantaneous energy is independent of phase.

Graphic Equalizer is an attribute which is used to enhance or reduce selected frequency components of the input signal by applying high, low or bandpass filters to the input seismic volume. It highlights consistent reflectors at different bandwidths and therefore guides interpretation in ambiguous areas (e.g. in areas with truncations, unconformities, onlapping etc.).

Instantaneous Frequency is an attribute which is independent of phase and amplitude, and it indicates reservoir rock properties and thickness or lateral lithology variations.

Relative Acoustic Impedance (RAI) is mathematically the sum of regularly sampled amplitude values, which is calculated by integrating the seismic trace and running it through a Butterworth filter to reduce the introduced low frequency noise. The RAI attribute highlights an apparent acoustic contrast and thereby indicates sequence boundaries, unconformities ad discontinuities. It may also show reservoir porosity or fluid content.

Standard Deviation is a measure of dispersion of the Variance values by means calculating the square root of the Variance cube. This attribute helps refine the resolution of the Variance cube.

Sweetness is a seismic volume attribute which is the product of combining *Envelope* and *Instantaneous Frequency* that is used to identify features where the overall energy signatures change in the seismic data (e.g. a progressing channel).

Variance represents an estimation of the local variation in the seismic signal and can be described as a measure of dissimilarity of adjacent traces, rather than the inferred similarity. It is used to produce a seismic based cube which offers enhanced the imaging of faults and produces sharper vertical lithology definition.

5.10 Well Markers Analysis

Well markers were initially placed on the gamma ray wireline logs of the key wells by using the depth values of the unconformity surfaces recorded in the well completion reports. The significance of picking accurate well markers in the role that they play in tying the well data to the seismic data (also known as well-seismic ties) but they are also essential in generating attributes like sand fraction pie charts and net-to-gross. In this study, the wells were assigned alternate names ("A" to "V") for the sake of well identification confidentiality. The analysis is discussed in further detail in *Chapter 9: Results*.

5.11 Calculating Sand Fraction Pie Charts

Sand fraction pie charts for the 13A and 14A zones in the key wells across the basin were calculated to reflect the proportion of sand that is present between the stratigraphic markers (i.e. well tops) bounding the 13A and 14A sequence sands. In this study, the well markers of the key seismic horizons (i.e. 1At1, 12At1, 13At1, 14At1, 15At1, Seabed) were checked and the markers representing the tops of the 13A and 14A sequences were created. Following this exercise, the facies-based lithology attribute was calculated using the simple equation below.

Sand facies = If (GR<=75, 0, 3)

The equation calculates the proportion of sand facies (percent or fraction) over a defined interval of the gamma ray (GR) log and uses the predefined litholog facies classification scheme of "0" for a sand and "3" for a shale. The equation states that if the GR log has a value of less than or equal to 75 API units that the data point must be classified as sand facies ("0") or else the data point must be classified as shale facies ("3"). The 75 API unit cutoff will not be applicable in every well due to the natural radioactivity ranges in the sediments across the basin so the initial resultant lithology attribute must be reviewed for each key well in a well correlation window to assess how accurately its sand/shale facies segments represent the gamma ray log signature and suggestions. The cutoff value may then be adjusted accordingly.

Finally, a new continuous attribute was created in the well marker set to populate the attribute with lithology data and values were assigned to the attribute "By Zone" using an average method of "Fraction" for the "Sand – 0" facies classification. Repeat as above to generate the shale facies for

this marker set by selecting the "Shale – 3" facies classification. The sand fraction pie charts were displayed in a map window with a background surface (e.g. an amplitude map) and compared to the well report records to assess validity of the interpreted sand content of the 13A and 14A zones.

5.12 Generating Isochron Maps

An isochron map illustrates the time difference between two surfaces, reflected as thickness, to show the time thickness variation over the key intervals (i.e. 13A and 14A). Gross thickness maps were generated for 13At1-14At1, 14At1-15At1, 13At1-13AST and 14At1-14AST in Petrel. Sand thickness maps were generated too by using two well markers as the limits to a particular zone of the gamma ray wireline log and the associated sand fraction pie charts. Overall, the 13A and 14A sequences were represented by sand thickness maps generated between the 13A sand top and 13At1/13A sand base surfaces and between the 14A sand top and 14At1/14A sand base surfaces.

5.13 Fault Interpretation

Faults are structural features along which relative displacement has occurred to create vertically and/or laterally-offset blocks. Uplifted blocks are subjected to erosion and therefore promote the release of sediments into the environments adjacent to them. Downthrown blocks produce structural lows in the environment and therefore act either as conduits for sediment flows or as sedimentary sinks, since the downfaulting creates accommodation space. In this regard, faults play a significant role in sediment generation, dispersal and trapping. It is this principle which supports their importance in this study in determining if and how they played a role in the 13A and 14A sequence sands distribution. The faults were interpreted as three sets of classification: (1) extending from the Basement through 14At1, (2) extending from the Basement to just above 1At1, and (3) mostly deep-seated and elongated perpendicular to the main faults (i.e. orthogonal). As an initial form of validation, the interpreted faults were compared to legacy (literature-based) fault polygons in the Central Bredasdorp Basin. A second form of validation involved overlaying the newly interpreted faults onto maps of the key seismic horizons to determine if there is a clear relationship between the contour-based structure of the horizon and the fault trends. It should be noted that despite the faults not intersecting the 13A and 14A sequences in some areas of the basin, they may still have played a role in influencing the hereditary structure of the basin (i.e. topography) and created associated structural weaknesses in the younger rock sequences.

5.14 Generating and Interpreting Composite Maps

Composite maps were generated to identify the possible distribution of the 13A and 14A sequence sands by visually analysing the combined interaction of multiple seismic and well-based interpretations. Basic surfaces (seismic horizons) or isochron maps were overlain with attributes and captured as an image in Petrel, which was then edited with cartoon interpretations. A particularly useful example is a sand thickness map overlain with an amplitude surface, sand fraction pie charts and faults polygons. Examples are illustrated later in this thesis.

5.15 3D Horizon Probe

The 3D horizon probe tool in Petrel offers a similar interpretative process to the analysis based on seismic volume extraction, although it takes it a step further by producing a single cube of two or three seismic volume attributes over a predefined interval between two surfaces or based on one surface with the seismic cube clipped at a specified Z-value (time) above or below it. The tool essentially allows you to slice the seismic cube at any level to view the attribute and the features that it highlights at that specific point in time.

5.16 Depositional Models Proposal and Preferred Model Selection

One of the ultimate outcomes of this study is the proposal of depositional models for the 13A sequence sands and the 14A sequence sands. Recognising particular features in the seismic attributes extracted in and around the 13A and 14A intervals contributes to the findings gained from the analysis of the time structure surfaces, seismic attribute maps, sand fraction pie charts, isochron maps, fault interpretations, 3D horizon probe tool and previous interpretations. These results were combined figuratively to generate possible models of deposition of the 13A sequence sands and 14A sequence sands individually across the Central Bredasdorp Basin. Two models were proposed for each sequence but ultimately a preferred model was selected for each sand sequence.

CHAPTER 6

DEEEP WATER MASS TRANSPORT DEPOSITS

6. Deep Water Mass Transport Deposits

6.1 Introduction

According to Boggs (2006), mass transport deposits are described as a sedimentary succession that became remobilised after initially being stratigraphically (chronologically) deposited, but also prior to being lithified, and was transported downslope by gravitational-driven processes as non-rheological units. Based on this definition and as illustrated in the table in **Figure 11** below, mass transport deposits (MTDs) are controlled by fluid turbulence and gravitationally driven by either elastic mechanical behaviour to form falls, glides, slides and slumps; plastic mechanical behaviour to form mass sediment gravity flows (e.g. debris flow); or by viscous mechanical behaviour to form fluidal sediment gravity flows (e.g. turbidity flow).

Mass transport processes				Mechanical behaviour	Transport mechanism and sediment support
Rock fall				Elastic	Free fall and subordinate rolling of individual blocks or clasts along steep slopes
Slide		Glide			Shear failure among discrete planes with little internal deformation or rotation
		Slump			Shear failure accompanied by rotation along discrete shear surfaces with little internal deformation
Sediment gravity flow	Mass flow	Debris flow		Plastic limit	Shear distributed throughout sediment mass; strength principally from cohesion due to clay content; additional matrix support possibly from buoyancy
		Mud flow		Plastic	
		Grain flows	Inertial Viscous	Liquid limit	Cohesionless sediment supported by dispersive pressure; flow in inertial (high-concentration) or viscous (low-concentration) regime; steep slopes usually required
	Fluidal flow	Liquefied flow		Viscous fluid	Cohesionless sediment supported by upward displacement of fluid (dilatance) as loosely packed structure collapses, settling into a more tightly packed framework; slopes in excess of 3° required
		Fluidized flow			Cohesionless sediment supported by the forced upward motion of escaping pore fluid; thin (< 10 cm) and short-lived
		Turbidity current			Supported by fluid turbulence

Figure 11 Table of classification of mass transport deposits (Redrawn from Boggs, 2006).

Practically, MTDs form when shear strength is exceeded by shear stress. For example, when sediment is rapidly deposited an overpressure may develop and this will result in a decrease in sediment strength (Sawyer, 2006).

MTDs typically form in a deep water margin setting where they splay from an unstable basin shelf edge or slope onto the basin floor (**Figure 12**). The presence of elements that may trigger this downslope, gravity driven movement are most commonly associated with a fall in sea level which initiates a large-scale collapse of the basin margin and this activity overcomes the material strength to induce slope failure and cause a mass sediment movement.

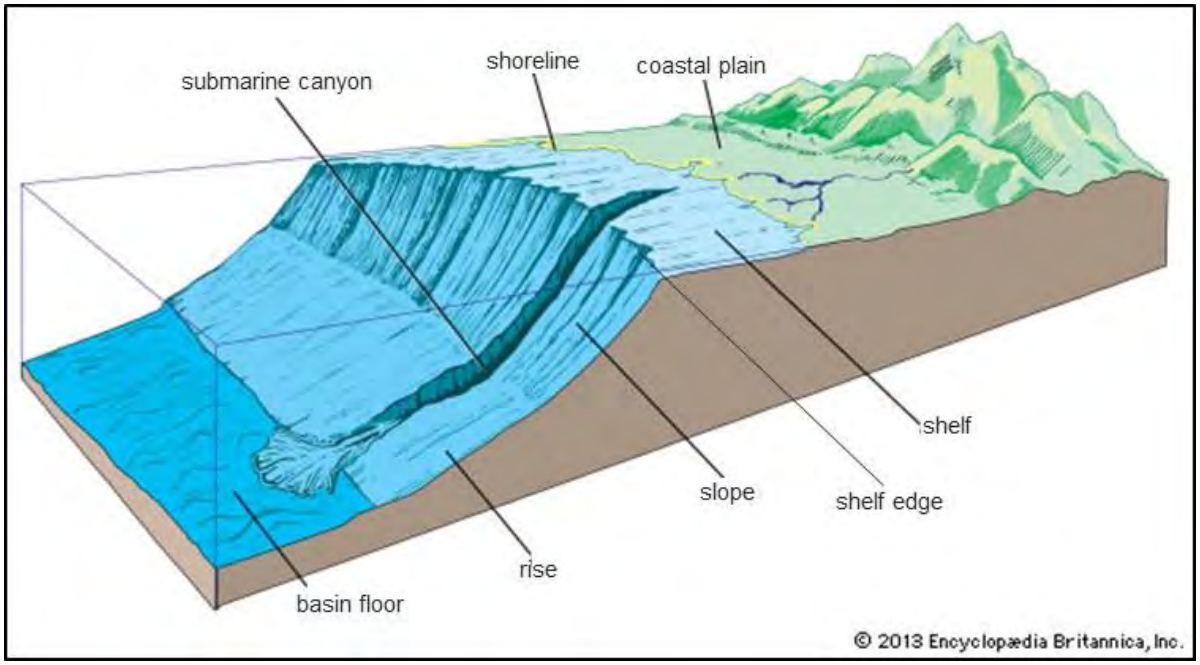

Figure 12 An artistic impression of the range in basin settings covered by a flowing mass transport deposit (Modified from Encyclopedia Britannica Inc. (2013)).

In this study, the "rock falls" type of MTD listed in **Figure 11** was irrelevant because only mass wasting in the form of slumps, debris flows and turbidity flows have been identified in the Bredasdorp Basin to date (**Figure 13; Appendix IV**). *Slumps* are described as shear failure of a sedimentary mass accompanied by rotation along a shear plane, resulting in internal deformation of the mass. *Mass sediment gravity flows*, on the other hand, are commonly initiated through a high sediment influx into a basin by severe fluvial floods and large-volume turbidity currents (Meiburg and Kneller, 2010). They may also be triggered by slope instability, sediment dilution, storm wave activity or sea surface winds initiating downwelling currents (Martin-Algarra *et. al*., 1992).

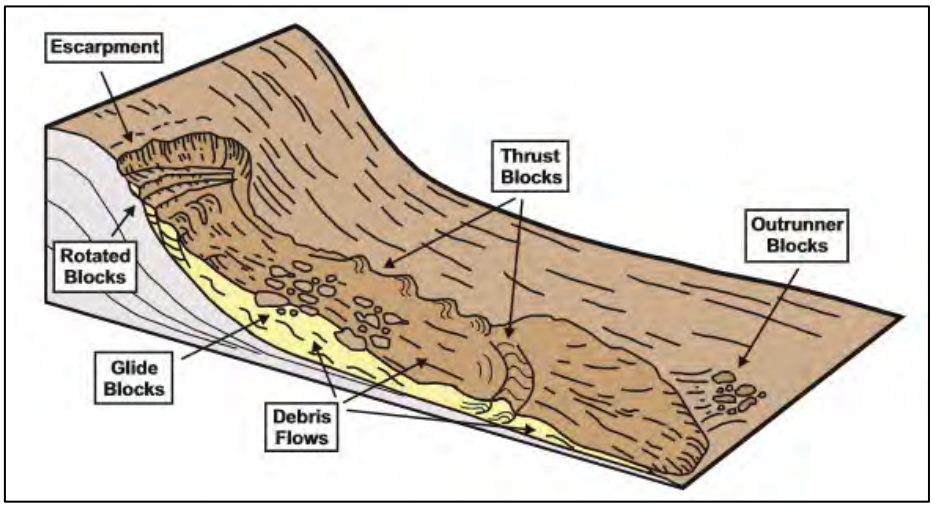

Figure 13 A schematic illustrating the different facies present in mass transport deposits system, including slide blocks (rotated, glide, thrust) and areas of chaotic sediments interpreted as debris flows. Individual glide blocks are present within a more deformed matrix. (Modified from Prior *et. al*., 1984).

6.2 Identifying Mass Transport Deposits

High resolution 3D seismic data can be used to recognise buried sedimentary deposits in terms of their distribution, geometry, scale and depositional setting and it may be complemented with other geological data like wireline logs, Formation Micro Imager (FMI) log images and well cores (Janocko *et. al*., 2012). Seismic attributes extraction is often applied to highlight structural features in the seabed that are associated with deep water MTD environments such as terraces, sand fairways, canyons and sinuous channels, over distances of greater than 50 km (Sawyer, 2006; Weimer and Slatt, 2007). Isopach maps can also be generated to identify gross and/or sand thickness distribution in the two-way time or depth domain to gain further understanding from the seismic and well data.

MTDs are typically amalgamated (Posamentier and Martinsen, 2006) so surfaces between the successive deposits may be difficult to recognise but generally the seismic facies vary from parallel beds, to rotated blocks thrust by low angle faults, to chaotic and hummocky reflections with poor to fair continuity and variable amplitude values (Weimer and Slatt, 2007; Janocko *et. al*., 2012).

6.3 Physical Distribution of Mass Transport Deposits

The distribution and character of a sand facies throughout a submarine basin and particularly in a package of MTDs is dependent on two types of controls: extrinsic and intrinsic (Sprague *et. al*., 2005). *Extrinsic controls* include elements that originate outside of the basin like climate, provenance type, characteristics of the drainage basin, sediment type and volume, sediment delivery mechanisms and flow types. *Intrinsic controls* are elements that are present within the basin such as shelf width and gradient, structurally controlled sediment traps, slope tectonics, sea floor gradient and confinement as a control on flow distance and the location of deposition, and structural and/or depositional inherited topography, which controls local sea floor gradient changes. Internal forcing through the interplay of valley incision depth, base level change, the turbidite system equilibrium profile and the slope aggradation rate may affect accommodation space and therefore act as an intrinsic control too.

MTD sands mostly occur as channel-fill and lobe deposits (**Appendix V**) and the conduit in which they form may be leveed, confined or distributary in nature depending on the topography of the seafloor and the presence of other structural influences (Sprague *et. al*., 2005) (**Figure 14**). A succession of channel-fill deposits and the associated channel bar deposits within a single conduit are collectively referred to as a channel belt and several stacked channel belts may be identified as a channel belt complex (www.seddepseq.co.uk). The confinement of the MTD sands may be structurally-induced by sea floor movements or influenced by older deposits to form ponded or intraslope basins that are typical of a distributary system that is located high on the regional slope (Sprague *et. al*., 2005) (**Figure 14**). Alternatively, further down the regional slope sedimentological confinement may be provided by conduits, like channels, or between adjacent shale-controlled sea floor highs (Sprague *et. al*., 2005). In summary, confinement and gradient are the controls of sediment dispersal in the deep water slope and basin floor settings (Sprague *et. al*., 2005).

In the case of the Bredasdorp Basin, the submarine valley-fill complexes are sourced from mass flows that originated on the slope and became sand-rich, meandering channel belts overlain by a multi-storey level of sand-rich, isolated leveed aggradational channel belts with a decreasing sinuosity and an overall upward decreasing sand content, fining upwards into a mud-rich succession on the basin floor (Janocko *et. al*., 2013).

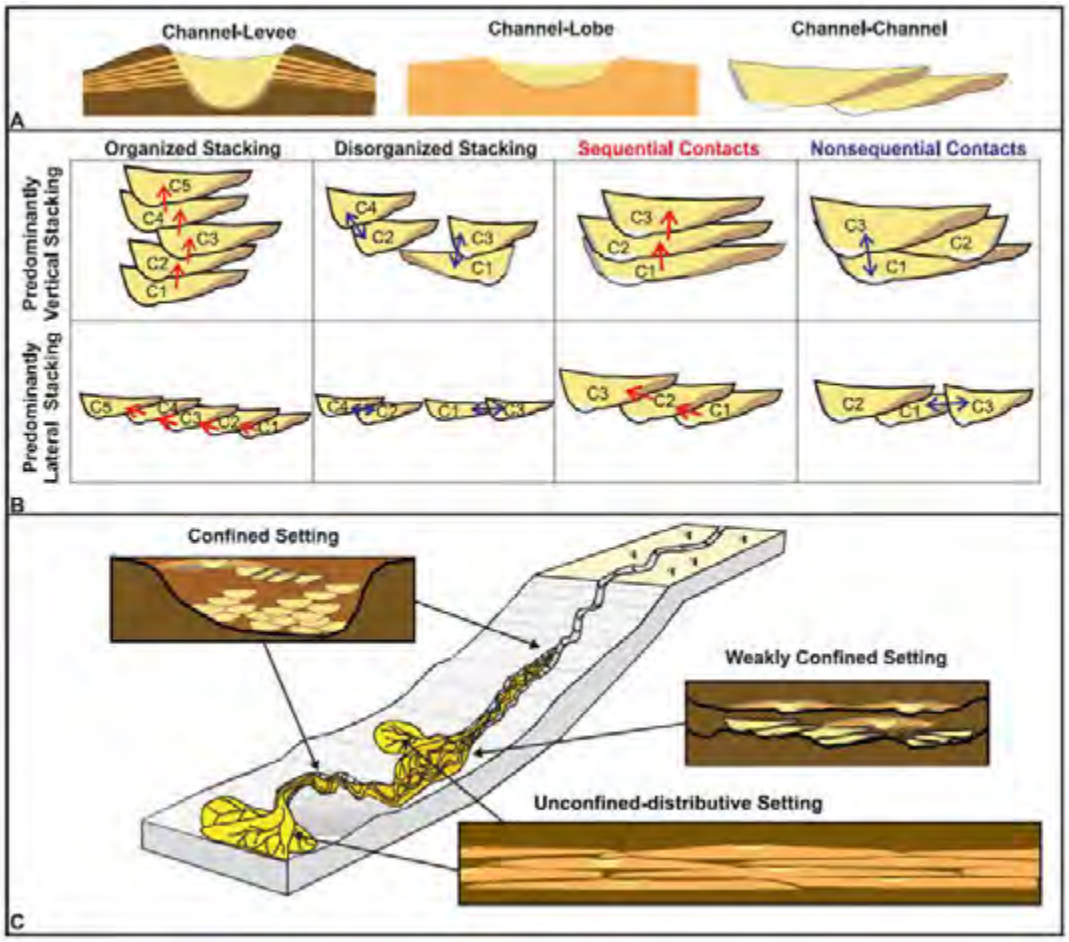

Figure 14 A schematic illustrating the different forms of channel stacking, the associated contacts and settings of channel confinement (www.sepmstrata.org).

Levees are the most extensive and largest sand-prone architectural element of the sinuous channel belts and can be more readily identified by their higher seismic amplitude reflections than the associated channel-fill deposits. An example of the architecture and lithology of a channel-fill complex is a basal portion of slumped, older channel-fill strata and a channel axis populated with deposits of medium-grained sandstone. The off-axis region of the channel conduit hosts deposits of fine-grained, parallel-laminated sandstones interbedded with medium-grained sandstones; and the channel margins contain very fine-grained, thinly-bedded, current-rippled sandstones interbedded with shales (Sprague *et. al*., 2005).

This study aims to broadly recognise the MTD types of the 13A and 14A sequences and to best delineate their sand distribution across the Central Bredasdorp Basin, using a combination of seismic

interpretation and facies identification supported by well data and literature with the concept of sequence stratigraphy in application too.

CHAPTER 7

SEQUENCE STRATIGRAPHY

7. Sequence Stratigraphy

The concept of sequence stratigraphy, as outlined by a number of authors, including Vail (1975), Vail *et. al*. (1977), Mitchum (1977), Posamentier *et. al*. (1988), Van Wagoner *et. al*. (1990), Brown *et. al*. (1995), Mitchum *et. al*. (2002), Weimer and Slatt (2007), and Miller *et. al*. (2011), was a key principle applied in performing the data interpretations and analysis in this study. Sequence stratigraphy is explained in detail in **Appendix VI**.

With a particular focus on the 13A and 14A sequences, their bounding unconformities were used to pinpoint the relationship between their identified age, the associated eustatic curves and the corresponding relative change in coastal onlap (Brown *et. al*., 1995). The results illustrated in **Figure 15** show that despite the global rise in sea level and hence landward direction of coastal onlap from the Aptian through the Albian, the 13A and 14A sequences were deposited during a local regression of the shoreline in the Bredasdorp Basin, over a period of ~2.5 million years each. This activity usually results from a fall in the local sea level, possibly combined with the thermal subsidence of the Bredasdorp Basin. Additionally, an increase in the sediment supply into the basin may have further influenced the regression to the point at which the shoreline was unable to erode and hence migrated basinward, forming progradational sedimentary packages (Miller *et. al*., 2011).

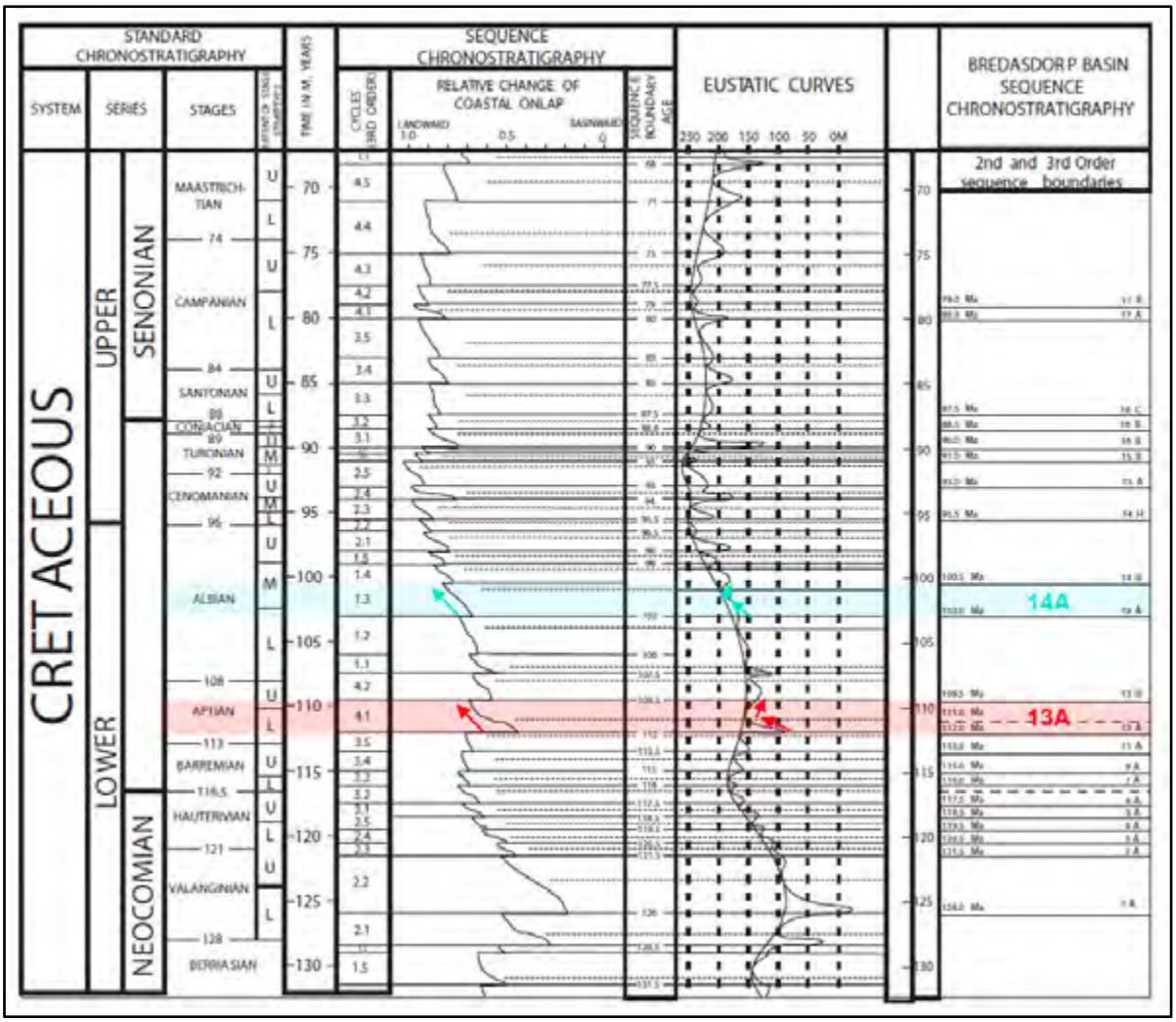

Figure 15 Second and third order global coastal onlap and eustatic curves for the Cretaceous (Haq et. al., 1987). Second order cycles are numbered 2 to 4. Third order cycles are numbered e.g. 2.1-2.5. Third order eustatic curve is characterised by abrupt rises and falls in sea level. Second order eustatic curve is smoother. This example illustrates the interpreted second and third order cycles of the Bredasdorp Basin, offshore South Africa (After Brown *et. al*., 1995).

Since sedimentary strata are deposited in rhythmic sequences relating to cyclic fluctuations of the sea level curve, internally a single sequence should consist of the three depositional systems tracts: lowstand systems tract (LST), transgressive systems tract (TST) and highstand systems tract (HST) (Brown *et. al*., 1995) (**Appendix VI**). Vail *et. al.* (1977) and Haq *et. al.* (1987) subdivide these depositional sequences into first to sixth order cycles based on their relative duration in time (See **Appendix VI** for a tabulated summary of sea level order cycles). Stacking of several fourth order sequences in a single third order sequence was first recognised by Mitchum and Van Wagoner (1990, 1991) as a predictable pattern of composite sequences distribution. Jeanette *et. al*. (2000) recognised a similar trend in the deep water systems of the central North Sea, which is a sag (post-failed rift) basin setting. Four third order sequences of sand-rich depositional systems, composed of higher frequency facies with distinct lithologies and architectures. Large-scale compensational stacking is demonstrated by a heterolithic basal unit of mud-rich debrites and sandstones deposited as broad, channelised bodies and overlain by more sand-rich sinuous to linear channel bodies. This vertical

change in sand content has been attributed to changes in the composition and volume of sediment gravity flows delivered to the shelf edge; and the variation in progradational dip is due to accommodation changes (Weimer and Slatt, 2007).

The findings made by Jeanette *et. al*. (2000) are very similar to the observations described previously by Brown *et. al*. (1995) in a study of the cycles of the deposition in the early Cretaceous sequences of two divergent basins in offshore South Africa: Pletmos and Bredasdorp. Second, third, and fourth order cycles were recognised in both of the basins and three third order sequences were recognised in the Bredasdorp Basin, in particular, in the late Barremian-late Aptian interval (e.g. 13A and 14A) (**Figure 16**). Only six fourth order depositional sequences were recognised in the Bredasdorp Basin and although these are not resolvable on seismic they have been found in alternating successions of prograding (LST/TST) and aggrading (HST) packages, developed during the corresponding fall and rise of the third order eustatic curve (Brown *et. al*., 1995) (**Appendix VI**). In the Bredasdorp Basin, lower rates of subsidence allowed only minor development of the higher frequency sequences and the lowstand sequences that have been drilled in the basin intersected more sand (Brown *et. al*., 1995). Brown *et. al*. (1995) recognised second order cycles on an average frequency of 5.5 to 10 million years in length and attributed these to a combination of tectonic and eustatic factors but discovered through well data that large volumes of (reservoir) sands had entered the Bredasorp Basin during the overlap of second and third order sequence boundaries, for example in 13A.

7.1 Applying Sequence Stratigraphy to this study

The hierarchy of the sedimentary architectural elements of a deep water depositional system is based on the physical stratigraphy of the strata with a thickness independent of time (Sprague *et. al*., 2002). There is a progressive increase in thickness with the progression from a bed, or single gravity flow, to a basin floor succession with the gross depositional relationship being strongly influenced by the seafloor topography, the geomorphology of the basin and the source location (www.sepmstrata.org). In the case of the Bredasdorp Basin, the generalised sequence stratigraphy architectural model of Posamentier *et. al*. (1988) and Galloway (1989) seems to be the most appropriate because it describes a divergent continental margin basin setting. As suggested by the Jeanette *et. al*. (2000) and Brown *et. al*. (1995) studies, however, there is a diversity in sequence stratigraphy models even within one type of tectonic setting.

Since most deep water systems are deposited in the lowstand systems tract (Weimer and Slatt, 2007), sequence stratigraphy was applied in this study as a principle to identify seismic facies in the third order Aptian (13A) and Albian (14A) sequences of the Central Bredasdorp Basin. Bound by a basal subaerial erosional unconformity, namely 13At1 for 13A and 14At1 for 14A, each sequence of retrograding deposits was overlain by a maximum regression (flooding) surface (**Appendix VI**). Considering the resolution of the seismic data in this study as well as its tuning thickness, only the tops and bases of the 13A and 14A sequence sands could be picked for the stratigraphic sequences identification, as illustrated on the seismic cross-section through the Bredasdorp Basin in **Figure 16**. The application of seismic surface attribute extraction and volume rendering, however, enabled the

distribution of these sands to be inferred across the Central Bredasdorp Basin and wireline well log studies over the key sequence intervals of this project to interpret properties like sand fraction and sand thickness distribution, using the gamma ray log motifs as guides in the possible depositional environments of the Aptian-Albian.

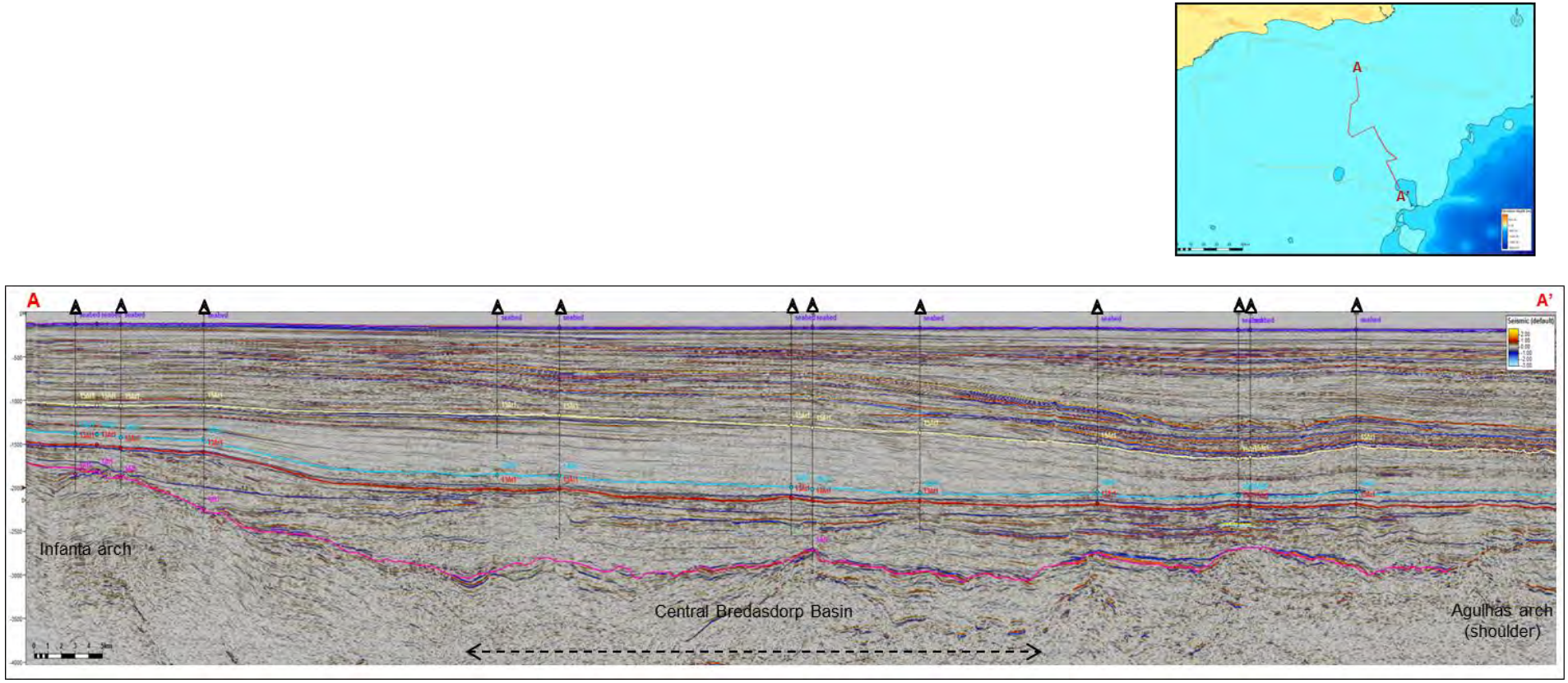

Figure 16 Composite seismic line extending from approximately north to south extending from the Infanta Arch through the Central Bredasdorp Basin to the Agulhas Arch (shoulder). Interpreted seismic stratigraphic sequence boundaries are shown in coloured lines. Wells intersected are marked with symbols. Notice the positive relief structure in the centre of the Central Bredasdorp Basin.

CHAPTER 8

CASE STUDY: THE TANKWA BASIN AS AN ONSHORE ANALOGUE

8. Case Study: The Tankwa Basin as an onshore analogue

8.1 Introduction

The onshore Tankwa Basin serves as an ideal analogue to the mass transport sands of the Aptian (13A) and Albian (14A) sequences of the offshore Bredasdorp Basin because it hosts the world's best preserved outcrops of Permian-aged deep water lowstand basin floor and slope turbidite fan complexes (Catuneanu *et. al.*, 2002; Van der Werff and Johnson, 2002; Wickens and Bouma, 2000). Studying these onshore outcrops in the field offers a better understanding of the spatio-temporal evolution as well as the mechanisms of channel distribution and fan-lobe deposition across the Tankwa Basin (Wickens and Bouma, 2000). Ultimately, this creates insight into the physical controls on the sand distribution in a deep water environment and this understanding will assist in determining the possible factors that affected the sand deposition in the 13A and 14A sequences in the Central Bredasdorp Basin. Combining the knowledge gained from field studies with the interpretations made in the desktop (software based) study contributed to constructing a theoretical depositional model (Sonibare *et. al.*, 2011) with a realistic scale, with the aim to apply it to generate a better understanding of the sand distribution in the Bredasdorp Basin (Sullivan *et. al.*, 2004) and to largely identify the 13A/14A mass transport deposit types.

8.2 Background

The Tankwa Basin is located in the southwestern corner of the greater Karoo Basin (Hodgson, 2009) (**Figure 17**). This area offers exposed outcrops of five Skoorsteenberg Formation deep water fans: Fans 1, 2, 3, 4 and 5, and serves as multi-scale record of a depositional episode in the history of this foreland basin.

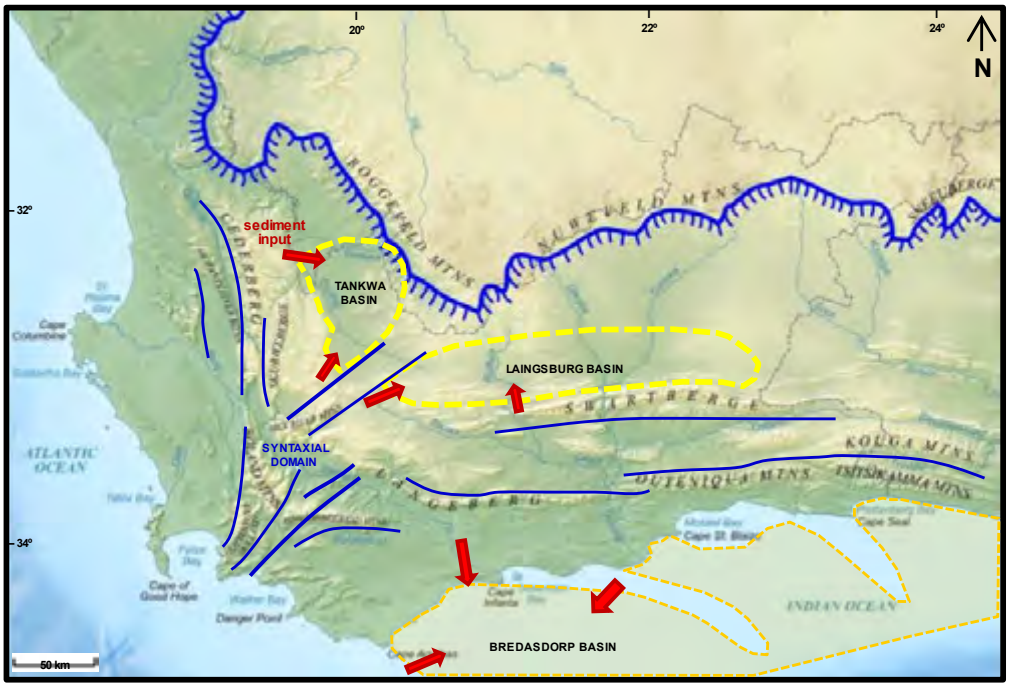

Figure 17 Structural surroundings of the onshore Tankwa Basin (relative to the offshore Bredasdorp Basin) with the directions of sediment input into the basins indicated with red arrows (Modified from *www.en.wikipedia.org/Cape_Fold_Belt*).

8.2.1 Tankwa Fan Complex

The core of the Karoo Supergroup is the Skoorsteenberg Formation within the Ecca Group (Van der Werff and Johnson, 2003) (**Appendix VII**). It is a succession of arenaceous, mud-rich turbidite fan systems that were deposited from an elevated basin margin source into the gradually-shallowing Tankwa Basin (Hodgson, 2009) over a period of ~20 million years (Heezen and Ewing, 1952; Meiburg and Kneller, 2009). 20 to 60 m thick sandstone beds alternate with siltstone and shale units within each fan system of this formation (Van der Werff and Johnson, 2003) and coincide with local sea level fluctuations as a result of tectonic activity or isostatic factors at play at the time of deposition (Catuneanu *et. al*., 2007; Smith, 1990). The fans appear as cyclic alternations of massive sandstone beds spanning for tens of metres as almost symmetrical channel-fills, pinching out laterally into overbank deposits of finer and thinner bedded siltstones and shales (Fildani *et. al*., 2007). The provenance of these turbidite fan sands is primarily the basement batholiths exposed in the south/southwest region of the basin (Fildani *et. al*., 2007) (**Figure 17**). The depositional setting, trend, thickness and lithological characteristics of each Tankwa fan are summarised in **Table 1**.

Fans 1 to 5 were deposited into the deep water environment of the Tankwa Basin but it is believed that a subsequent tectonic uplift event caused a decrease in the water depth and Fan 6 was therefore deposited into a shallower marine environment (Wach *et. al*., 2000). A second cycle of submarine fan systems was deposited in the late Permian in a prodelta environment as the local sea level was falling. These yielded a succession of less massive sandstones and proportionally finer deposits (Sonibare *et. al*., 2011) overlain by slope edge to deltaic shelfal deposits. Intermittent sea level fluctuations followed, until the foredeep was uplifted and drained to give rise to the present subaerial Karoo Basin. Unfortunately, due to the subaerial exposure of these deposits most of the fans have been subjected to erosion which has left only portions of the fan complex preserved, as illustrated in the aerial schematic view of Fans 1 to 5 in **Appendix VIII**.

	DEPOSITIONAL SETTING	DIRECTIONAL TREND	TOTAL THICKNESS	LITHOLOGICAL CHARACTERISTICS
FAN 1	**Upper-mid slope**	**Towards NE**	**20 metres**	**Basal sands are sharp contact sheet sands, followed by a lower unit of lens-shaped, channel-fill sands and then an upper unit of thin, sheet-like sands. An abrupt top (i.e. sand termination) of the fan suggests later lobe switching and abandonment.**
FAN 2	**Upper-mid slope**	**Towards NNE**	**45 metres**	**Three large, channel-fill sand units representing "mini fans" separated by 1-4-metre-thick shales.**
FAN 3	**Lower slope-base of slope**	**Towards NE then N**	**50 metres**	**Represents a complete turbidite system – thinning upwards amalgamated, stacked channel-fill sands interrupted by thin siltstone/claystone layers, erosional sedimentary features are visible at the base of the uppermost sand beds and in the distal fan the sands are more representative of overbank deposits.**
FAN 4	**Base of slope-basin floor**	**Towards ENE**	**60 metres**	**Six depositional packages but generally a lower unit of sheet-like, tabular sands separated from an upper unit of amalgamated channel sands by subtle erosional features and interrupted by mud-rich layers.**
FAN 5	**Base of slope-basin floor**	**Towards N**	**45 metres**	**Massive, amalgamated channel sands in the lower unit overlain by thinly bedded sands in the upper unit, interbedded with thin shales.**

Table 1 Summary of the depositional setting, directional trend of deposition, total thickness and lithological characteristics of Fans 1 to 5 in the Tankwa Basin (Based on field observations by Van Rensburg (2012)).

8.3 Findings

8.3.1 Structural Observations

The timing of the deposition of the Skoorsteenberg Formation fans is said to be due to the effect of active tectonics in the Tankwa Basin, including the isostatic uplift of the forebulge and the growth of anticlinoria in the southwestern corner of the basin (Wickens, 1994) (**Figure 17**). Structurally, bed-scale vertical jointing, faults and folds may be observed in the fan outcrops in the field, which indicate that there were extensional and compressional forces acting in the Tankwa Basin, possibly related to the activity of the Cape Fold Belt (CFB) (Wickens and Bouma, 2000).

The five fans in the Tankwa Basin bare similar depositional and cyclic characteristics which suggests that multiple, regular gravity-driven mass transport movements must have occurred (Van der Werff and Johnson, 2003). This observation narrows down the possible triggers of mass sediment transport to either slumping off the CFB, due to episodic uplift, or the failing of a canyon as it carried sediment from the marginal highs across the shelf of the basin and onto the deepening basin floor during forebulge flexure (Wickens and Bouma, 2000). The tectonic activity most likely initiated instability and caused gravity-driven sediment flows, like turbidity currents, under catastrophic and unpredictable conditions (Meiburg and Kneller, 2009), consequentially forming fans on the slope and basin floor. Fans 1 to 5 were deposited approximately 100 km from their source and horizontally into the wide, shallow Tankwa Basin. The minor 1 to 3 degrees tilt of the basin in the east (Bouma, 2004) allowed the tectonic activity on the basin margins to trigger the turbidity flows without affecting the distal depositional architecture.

8.3.2 Sedimentological Observations

There is a clear progression from deep water sediments to shelfal, deltaic and ultimately fluvial sediments (**Figure 19**) in a north/northwest direction through the Tankwa Basin from the main source in the southwest (Van der Werff and Johnson, 2003). This progressional order of the deposits represents the continuous reduction in water depth within the Tankwa Basin as tectonic uplift of the margins and downwarping of the central basin occurred in response to active compressional forces within the CFB causing extensional activity in the Bredasdorp Basin at that time (Hodgson, 2009; Smith, 1990; Wickens and Bouma, 2000).

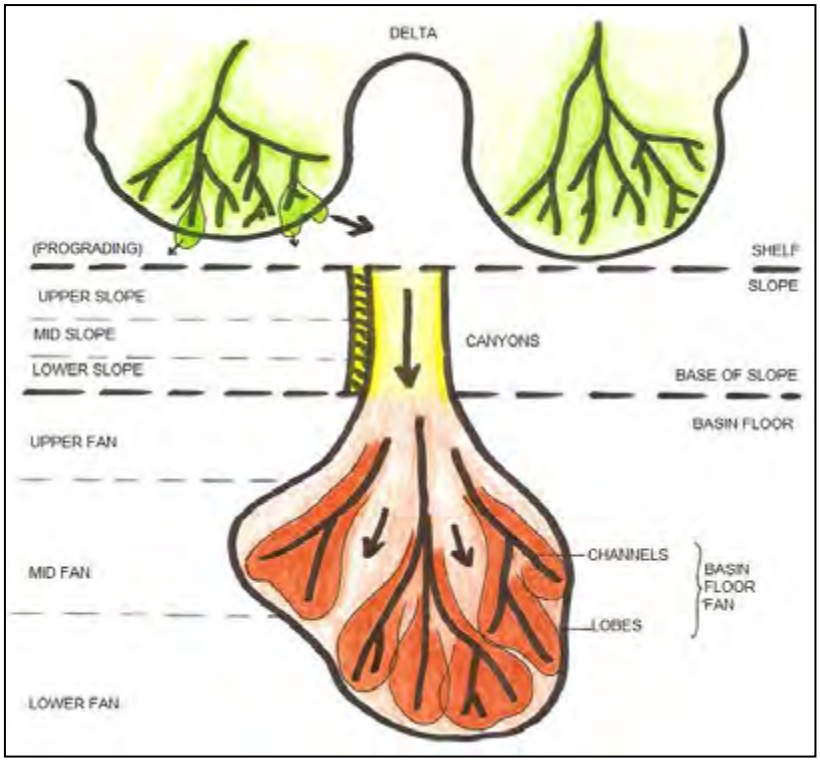

Figure 18 A prograding delta usually deposits sediments at the shelf edge which are then transported down the slope to the base where they splay out as a basin floor fan via several channel-and-lobe distributary systems (Van Rensburg, 2012).

8.3.3 Depositional Characteristics

The Tankwa fans were sourced primarily from the west/southwest, as suggested by horizontally-deposited, massive channel-fill sandstone beds that thin and pinch out towards the east/northeast (Meiburg and Kneller, 2009) (**Figure 19**). The pinching out suggests that the channel-fill deposits could merge into the adjacent overbank siltstones and shales or that there was simultaneous but minor sedimentary input from the east, thereby leading to the skewness in the channel-fill architecture and hence thicker sand deposition in the eastern side of the channel alongside the Karoo foreland system forebulge.

Figure 19 Fan 4 from a distance (**Top**) and zoomed-in views of the massive sandstones of the fan system (**Left**) (14cm pen for scale, circled in yellow) and the interfan succession of silty and shaley deposits (**Right**) (Field observations by Van Rensburg (2012)).

The local sea level fell consistently during the deposition of the fans and the sediments within the Tankwa Basin continued to prograde from the primary source as the deep water basin floor transformed into a slope–prodelta environmental setting. This sequence of changes may be seen recorded in the stratigraphy of the preserved outcrops and in road cuttings (on the north/northeast margin of the Tankwa Basin) in which the deltaic deposits advance vertically from channel-fill sandstones and overbank siltstones and shales to thinner, parallel beds of alternating sandstone, siltstone and shale. Prodelta deposits are generally chaotic in nature, attributed to the high energy environment and sometimes rapid influxes of water and sediment thereby leading to reworking, overlapping channel-fill deposits, deformed beds, sand lenses and a mixed sediment composition. The youngest sands in the Tankwa Basin were deposited in a fluvial setting and therefore represent the progradationally adjacent environment of deposition (Fildani *et. al.*, 2007). In the field trip to the Tankwa Basin, the fluvials were only observed at a distance on the north/northeast margin as this formation was not significant to the objectives of the study.

8.4 Discussion

The forebulge of the Tankwa Basin is dominated by deltaic and fluvial sediments, whilst the foredeep on the proximal rim of the Tankwa Basin is filled with deep water sediments that were deposited by mass gravity flows in the form of turbidity currents, submarine basin floor fans and lobes. Each fan in the Tankwa Basin is divided into distinct depositional packages, with sandstone beds varying in

thickness from 1 mm to >1 m, due to fluctuating flow velocities. The three primary controls on fan development are the sediment type and supply, tectonic setting and activity, and sea level fluctuations (Bouma, 2000 and 2004).

Generally, the Tankwa fan complex represents an pre-existing deep water environment from the upper slope to the basin floor setting overlain with channel, fan and lobe sands.

- Channel-fill deposits are dominantly sand. Within the channel axis they tend to be massive and amalgamated but in the channel margins they are more bedded and may even contain very thin silty interbeds (Van der Werff and Johnson, 2003). They may be vertically and/or laterally stacked, particularly in the slope to base of slope environment (Bouma, 2004).
- Overbank deposits are characterised by alternating thin and very thickly-bedded sheet, lobe and channel-fill deposits. In the Tankwa Basin, turbidite sands separated by silts and shales aggrade in the channels and laterally connect via sheet-like lobe deposits.
- The lobes are typically bare of channel architecture but may contain sedimentary features in an unconfined depositional setting (Dudley *et. al*., 2000).
- The mid fan comprises of aggradational and progradational channel lobe deposits as thickly-bedded core flanked by medium to thick bedded sandstone.
- The distal fan deposits are associated with the transition from mid fan channels and lobes to sheet deposits.
- The terminus of the fan comprises of channel-fills up to a few metres thick and displaying basal scour marks to pinching out channel-fills (Van der Werff and Johnson, 2003).

8.5 Relevance to the Bredasdorp Basin

The sedimentary deposits within the Skoorsteenberg Formation of the Tankwa Basin and those of the 13A-14A sequences of the Bredasdorp Basin are derived from continental sources located within the range of 100 to 160 km from the basin depocentre. The fan complex in the Tankwa Basin was deposited over a period of ~20 million years and the relative sea level fall during that time generated progradational sedimentary sequences. The deep water mass flow deposits of the 13A and 14A sequences in the Bredasdorp Basin were deposited during a local sea level fall too, resulting in progradational sedimentary sequences deposited broadly over ~16 million years between 13At1 and 14At1 but more precisely over ~5 million years in total for the 13A and 14A sequences.

The Tankwa Basin began receiving sedimentary input from ~280 Ma (Smith, 1990) from the west and southwest as sediments eroded from the western limb of the Cape Fold Belt mountain range and the adjacent anticlinoria during episodic uplifts. At this time, the Tankwa Basin was part of a flooded foredeep, also referred to as the Karoo Sea, located inland of the CFB. The Bredasdorp Basin received sedimentary input from ~160 Ma from the weathered onshore formations of the southern limb of the CFB via rivers but it also received direct sedimentary input from the basement highs on the basin margins in the north and south (Fildani *et. al*., 2007).

The direction of sediment input and hence the source locations in the Tankwa Basin was determined using field observations to recognise particular features such as pinch out, amalgamation, bed thickness variations, grain size and sorting, lithological variations, etc. and through combining these

with the use of borehole wireline log data, such as FMI measurements and ispoach maps. Technically, the same principle could be applied in the study of the Bredasdorp Basin although the scale of observation would be quite different (discussed in the poster in **Appendix IX**) and the non-exposure of the sequences is a challenge. Outcrop studies provide information in the vertical and lateral domains, based on observations that cover millimetres to kilometres in scale and can therefore be used to characterise detailed bed-scale architectures and internal heterogeneities. Seismic data provides information on the scale of hundreds of metres to kilometres in the horizontal domain, thereby yielding information about the structure of the basin as a whole although the interaction between individual sand bodies may also modify the seismic signatures and make individual channels unresolvable. Well data, such as wireline logs and cores, offers information ranging in scale from millimetres to metres in the vertical domain but is limited horizontally to the control points. The role of scale was demonstrated in this study by comparing the results of the outcrop studies performed in the onshore Tankwa Basin to the results obtained from studies based on a combination of seismic and well data in the offshore Bredasdorp Basin. This contributed to a better understanding of the past depositional environments in the Bredasdorp Basin, such as the multifaceted complex of deep water mass transport deposits, and played an important part in proposing accurate depositional models (Sullivan *et. al*., 2004) (**Appendix IX**).

8.6 Conclusion

From a broad perspective, the primary objective of the case study was achieved since the field observations of the onshore Tankwa Basin turbidite fan complex contributed to the understanding of the cycles of deposition into the deep water environment of a submarine basin through viewing the sedimentary deposits in outcrop after studying them in literature. The field study also gave the true perspective of scale and provided some insight into the proposed models of deposition of the Tankwa fans in terms of their modes of sediment transport, controls on deposition across the basin, the direction of source input and propogation, and the influence of extrinsic factors (Bouma, 2000). The time available to perform the field study and its post-study analysis was limited but a good source of references was available.

The exposure of the fans in outcrop form in the Tankwa Basin means that the physical elements that most likely contributed to their paths of transport and deposition are absent and this makes it difficult to explain the precise controls on the sand distribution and the timing thereof. In the Central Bredasdorp Basin, the physical controls on the paths of sand transport and deposition are preserved in the subsurface but the scale at which we can study and interpret these is limited to the resolution of the seismic data and limited spatially to the data control points (i.e. wells and seismic surveys). It therefore proved most beneficial to apply the knowledge gained about the stratigraphic and lithological character of turbidites of the Tankwa fan complex as well as the spatial distribution characteristics to complement the study of the 13A and 14A gravity mass flow sands in the Central Bredasdorp Basin.

CHAPTER 9

RESULTS

9. Results

9.1 Well Correlation and Wireline Log Interpretation

As mentioned under *Chapter 5: Methodology*, alternate well names were used for the sake of confidentiality of the 22 wells ("A" to "V") and the well completion report interpretations of the 13A and 14A sequence sands is captured in **Table 2**.

Before interpreting the gamma ray log values as a lithology indicator to identify the MTD sand types and using the gamma ray (GR) log motif to infer the depositional environment, I used the well completion report as a guide in picking the well tops (markers) and added additional markers to represent the tops of the 13A and 14A lowstand sequence sands. The tops guided the focus to the key intervals (i.e. 13A and 14A) on the GR log curve and determining the depositional character of the sequences as either fining upwards or coarsening upwards, based on a comparison to the literature-derived sketches of the GR log motifs and through consulting the summarised interpretation captured in **Table 2**. This analysis guided me in visualizing a basin-scale depositional environment particular to that of the Bredasdorp Basin during the Aptian-Albian time, which just needed a supportive seismic data-based perspective and possibly additional information, as demonstrated later in this thesis.

WELL	13A SAND PRESENCE	14A SAND PRESENCE
A	Stacked, deep marine fan lobe with channel/levee units	Stacked, mass flow overlain by upward-fining channelised mass flow abandonment unit
B	Stacked, deep marine basin floor fan lobe sequence (channelised, levee grain flows, sandy turbidites)	Stacked, mass flow sandstones
C	Interbedded turbiditic sands	Mass flow turbidite sand
D	Arenaceous sands	Slope sand stringers
E	Minor sand interbeds	NO SAND
F	Thin, turbiditic mass flow sands	Basin floor mass flow sands
G	Massive, deep marine mass flow sands	Submarine turbidite fan sands
H	Interchannel sand stringers	NO SAND
I	Thin sand interbeds	Base of slope fan complex with stacked, mass flow sands
J	NO SAND	Prograding, mass flow sand stringers
K	Interbeds of turbiditic channel and fan lobes	Poorly developed mass flow sands
L	Gravity flow sands	Channel sands
M	Interbeds	Massive, amalgamated mass flow sands
N	Occasional interbedded turbiditic sands	NO SAND
O	NO SAND	Base of slope mass flow sands
P	Thin gravity flow sands	Massive, amalgamated deep marine mass flow sands
Q	Turbiditic sands	Mass flow sand stringers
R	Interbeds	Minor sand interbeds
S	Minor deep marine mass flow sands	High energy mass flow sands
T	Stacked, deep marine fan lobe/channel sand units	NO SAND
U	Mass flow sands	High energy mass flow sands
V	Stacked, deep marine mass flow fan lobe sands	Interbedded, deep marine, mass flow turbiditic-type sands

Table 2 A summary of the well completion report descriptions of the 13A and 14A sequences in terms of sand content and depositional character for the subset of wells selected in this study.

9.2 Seismic Horizons Mapping

As part of the seismic data review process, the seabed reflector was interpreted using the 3D seismic surveys and then extended onto the 2D seismic lines to cover the parts of the Bredasdorp Basin beyond the 3D data coverage, as it is the easiest horizon to pick (**Figures 20** and **21**). A conclusion was reached that the challenges of interpreting on 2D seismic lines for vintages ranging from 1975 to 2011 was not contributing a significant amount to the study and hence the decision was taken to limit the seismic interpretation to the 3D dataset. Horizon interpretation efforts were then focused on using a selected set of 3D seismic surveys, ranging in vintage from 1994 to 2012, with a particular focus on the central part of the Bredasdorp Basin. This is illustrated under section *9.2.7 Seabed*.

Regionally, the unconformities are described as a "hard event" distinguished by a sharp increase in acoustic impedance between the typically porous reservoir sand above and the more compacted (denser) shale below and are therefore interpretatively picked through the apex of a basin-wide, strong peak wavelet (as described in the *Chapter 5: Methodology*). The unconformities and surfaces interpreted in this study include: Basement, 1At1, 12A sand top, 13At1, 14At1, 15At1 and present day seabed. The seabed and Basement serve as the uppermost and lowermost vertical limits whilst the other regional unconformities are guides to the sequences of interest in this study, namely 13A and 14A, as they mimic the deformation and uplifting of the Cape Supergroup rocks due to activity associated with the Agulhas Falkland Fracture Zone.

9.2.1 Basement

The Basement is also referred to as the pre-rift unconformity which represents a basinwide erosional event after the deformation and uplift of the Cape Supergroup in response to activity associated with the Agulhas Falkland Fracture Zone (discussed in the *Chapter 3: Geological Setting*). From a regional perspective, it is quite challenging to interpret the Basement reflector in seismic sections as it is not a continuous unconformity and shows a frequent change in polarity due to the contrasting densities with the chaotic composition of the underlying interfolded quartzites and slates, particularly where there are variations in the erosion depth. It is also not intersected by any wells within the study area, which creates some uncertainty. Interpreted on a peak, the Basement horizon undulates greatly across the basin as it aligns with the upper surface of the intensely folded and faulted Table Mountain Group below. The motive for interpreting this unconformity in this study is that it serves as an important guide in the interpretation of the main faults within the Central Bredasdorp Basin and it may play a role in influencing the inherited structure of the younger 13A and 14A successions. The interpreted Basement surface can be seen in **Figure 22**. The colour gradient, which ranges from 2200 to 5400 ms TWT (red to pink, respectively) and the time structure contours indicate that generally the Basement has a NW-SE elongated trend with the highest topography of the basin represented by the paleo shelf and Infanta Arch in the north and the Agulhas Arch with a more gradual slope on the southern margin. The deepest part of the surface appears to be isolated as two embayment-like depressions with steep slopes against the higher northern margin and perhaps indicate the mode of sedimentary transport into the basin, resulting from faulting or sea level fluctuations. There is also a slight structural high in the centre of the basin, which is the "Bredasdorp Central Horst", associated with the tectonic activity around the initiation of the breakup of Gondwana.

9.2.2 1At1

1At1 is a regional unconformity which represents a highly erosional event in the Bredasdorp Basin and it can be quite easily identified in seismic sections as a bright peak and an erratic reflector cutting into the layers of rock just above the pre-rift unconformity (i.e. Basement reflector). On a finer scale, there is a frequent change in polarity of the 1At1 reflector due to the change in densities of the unconformity surface and the rock layer below, particularly where there are contrasting degrees of erosion as it is in the case of the Basement reflector. The relevance of interpreting 1At1 in this study is that it serves as an important guide in the interpretation of the main faults. 1At1 is illustrated in **Figure 23**. The colour scale, ranging from 1400 ms TWT (red) to 3400 ms TWT (pink), and the time structure contours indicate a topography of the 1At1 level which is one of high basin margins gradually sloping into the deeper depocentre concentrated in the central part of the basin. The paleo shelf at this time seems to have been quite prominent in the north with the Agulhas Arch in the south being structurally more subdued at this time. The slightly shallower area in the southeast corner of the basin corresponds to part of the structural high identified on the Basement time surface so the relief may be attributed to the underlying structure. The 1At1 surface does not have clear embayment-like depressions against the northern basin margin like the Basement surface but rather a single, more elongated depression trending parallel to the margin. A second depression also appears to be present between the southern margin boundary (i.e. Agulhas Arch) and the small intrabasinal structural high in the southeast thereby suggesting that sediment transport deflection towards the south may have been possible due to the available accommodation space at the time.

9.2.3 12A Sand Top

The 12At1 unconformity is difficult to interpret in the seismic data due to the fact that it is not a regionally continuous reflector and more dominant unconformities occur above (13At1) and below (10At1), leading to the tuning effect. The 12A sand top (trough) was therefore interpreted on the far stack seismic data because it displays the 12A sequence more clearly than the full stack seismic data and as a brighter, broader reflector. The 12A sand top interpretation does not cover the full extent of the study area polygon hence there are structureless, extrapolated contours in the shallower southwest-west-northwest margins of the basin. The colour gradient, which ranges from 1620 ms TWT (red) to 2460 ms TWT (pink), and the time structure contours of the 12A sand top surface (**Figure 24**) demonstrate that the paleo shelf was most likely in the northern to northwestern part of the Bredasdorp Basin at around 121 Ma (early Aptian) and that the Agulhas Arch on the basin margin in the south/southwest was still a structurally subtle feature. The very steep paleo slope most likely fed sediments from the shelf into the large, circular depression in the east of the study area. This observation suggests a very significant change in the topography of the Bredasdorp Basin from the syn-rift to the drift. The relevance of interpreting the 12A sand top in this study is that it serves as a secondary guide in the possible distribution of the 13A sands deposited shortly after it and since there was a minimal time gap between the deposition of these two sequences and it is presumed that the same intrinsic elements were still in place in the Bredasdorp Basin over that period of < 2 million years (Brown *et. al.*, 1995).

9.2.4 13At1

The 13At1 surface (**Figure 25**) is a key seismic horizon as it represents the topographic structure of the basin floor just before the deposition of the 13A sequence and hence it had a strong impact on the distribution of the sands deposited from ~124 Ma, during the Aptian. It represents an erosional event caused by uplift in the basin and a simultaneous sea level fall so it is quite readily identified in the seismic data as a strong peak reflector across the basin. The 1350 to 2500 ms TWT range in the colour gradient together with the time structure contours suggest that, like during the 12A time, the paleo shelf was in the northern part of the Bredasdorp Basin. There is a change in the prominence of the south/southwestern margin since 12At1, however, in which the Agulhas Arch suddenly stands out as a high relief feature of the basin with a slope that is much steeper than that of the northern margin high (i.e. Infanta Arch). This observation does not appear to have an effect on the overall trend of topography at the Aptian time because the basin maintains a trend of deepening from west to east, although there is some additional deepening towards the southeast as a possible extension of the depocentre.

9.2.5 14At1

The 14At1 seismic horizon (**Figure 26**) plays the same role in influencing the distribution of the younger 14A sequence sands during the Albian as that of the 13At1 for the 13A sequence sands. 14At1 represents a highly erosional event due to an episode of uplift, following basin subsidence, and the accompanying fall in sea level. The reflector is not a strong peak in the seismic data but it can be picked across the basin by locating it using the overlying strong trough (i.e. 14A sand top reflector). The colour gradient ranges from 1250 to 1350 ms TWT and the time structure contours of the 14At1 unconformity surface show a trend similar to that of the 13At1 unconformity surface as a deepening of the basin floor at the Albian time towards the east into a large, circular depression. There is a very slight indication of an extension of the main basin depocentre towards the southeastern part of the Central Bredasdorp Basin too but this may be an effect of extrapolation since it falls on the edge of the interpreted study area. The 14At1 surface suggests that at around 108 Ma (Albian) the basin bounding highs were the paleo shelf in the north/northwest part of the Bredasdorp Basin and the Agulhas Arch in the south/southwest, yielding the same general depositional trend as seen on the other seismic horizon maps as a west to east direction of transport.

9.2.6 15At1

The 15At1 surface (**Figure 27**) was not as erosional as the 13At1 and 14At1 unconformities since it formed during a time of sustained basin subsidence with an overall higher global sea level from around ~96 Ma. In seismic sections, the 15At1 peak reflector stands out from the thick shale-rich successions deposited below and above it due to the contrast in density and hence velocity of the beds. The 950 to 2000 ms TWT range in the colour gradient and the time structure contours of the 15At1 surface suggest that the paleo shelf was still prominent in the north/northwestern part of the Bredasdorp Basin in the late Cenomanian but the Agulhas Arch on the basin margin in the south/southwest is not reflected in the map. The map shows a trend similar to the one seen on the 13At1 and 14At1 surfaces in which the basin deepens from west to east with the depocentre located in the eastern side of the basin centre although the contours depict a very different topographic

structure to 13At1 and 14At1. The illustrated basin floor structure at the time of 15A deposition was one in which there is a broad, gentle slope from the paleo shelf in the north/northwest and steepening slightly into the depocentre in the east. There is also the suggestion that the source may have been located in the west where the contours are slightly more concave.

9.2.7 Seabed

The maps of the seabed surface reflect the seismic interpretation results of using a combined set of "3D and 2D" seismic surveys in comparison to a set of "3D only" seismic surveys (**Figures 20** and **21**). The maps have been displayed with the same contour interval (100 m) and the same colour scale range (0-1800 ms TWT) but on the "3D and 2D" map there is a clear indication that the seabed is shallowest in the northwest and deepens in a southeast direction. On the "3D only" map the trend appears to reflect the seabed deepening to the east/southeast because of the extent of data coverage, i.e. there is no 3D data south of the easternmost extent of the surface. The extent of the 3D data coverage is not a problem since the focus of the study is on the Central Bredasdorp Basin, which is covered fully by the selected subset of "3D only" seismic surveys. Overall, both time structure maps of the seabed show a mostly flat topography over the study area with a subtle change in gradient towards the southeastern corner of the basin, representing the most recent position of the shelf edge as indicated by the dataset.

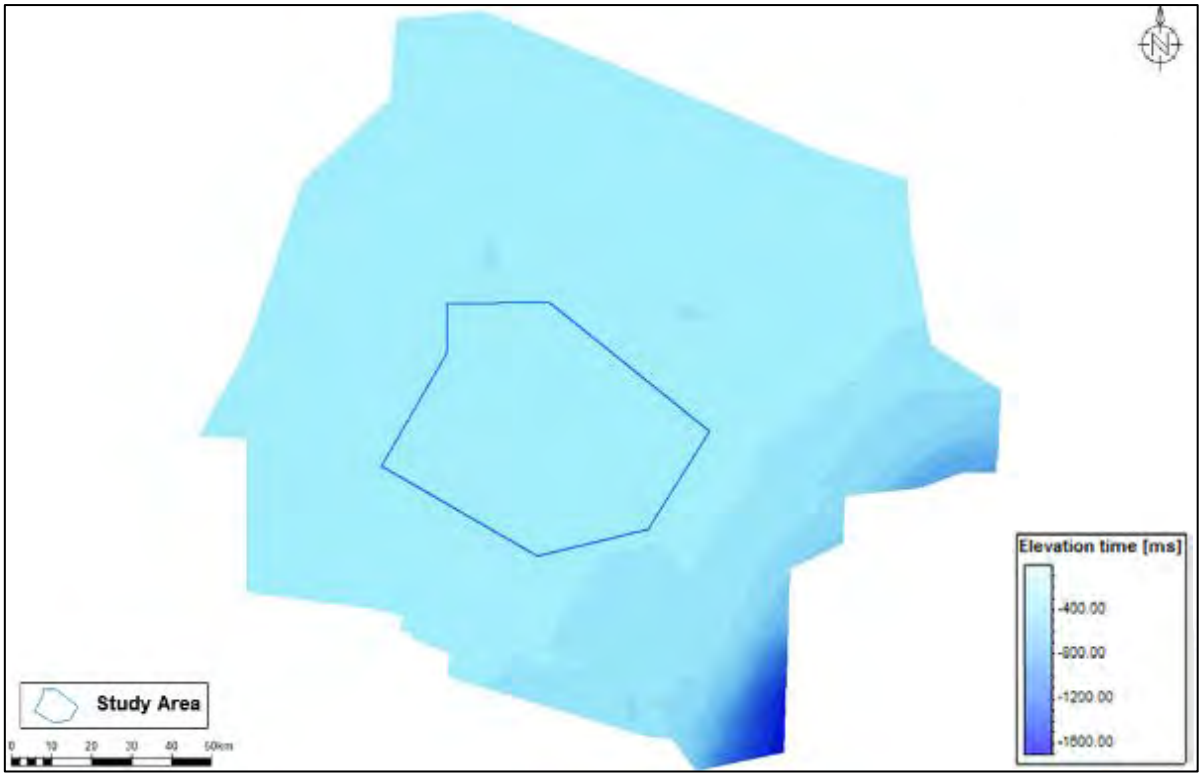

Figure 20 Seabed interpretation surfaces (TWT) using the combined set of 3D and 2D seismic surveys.

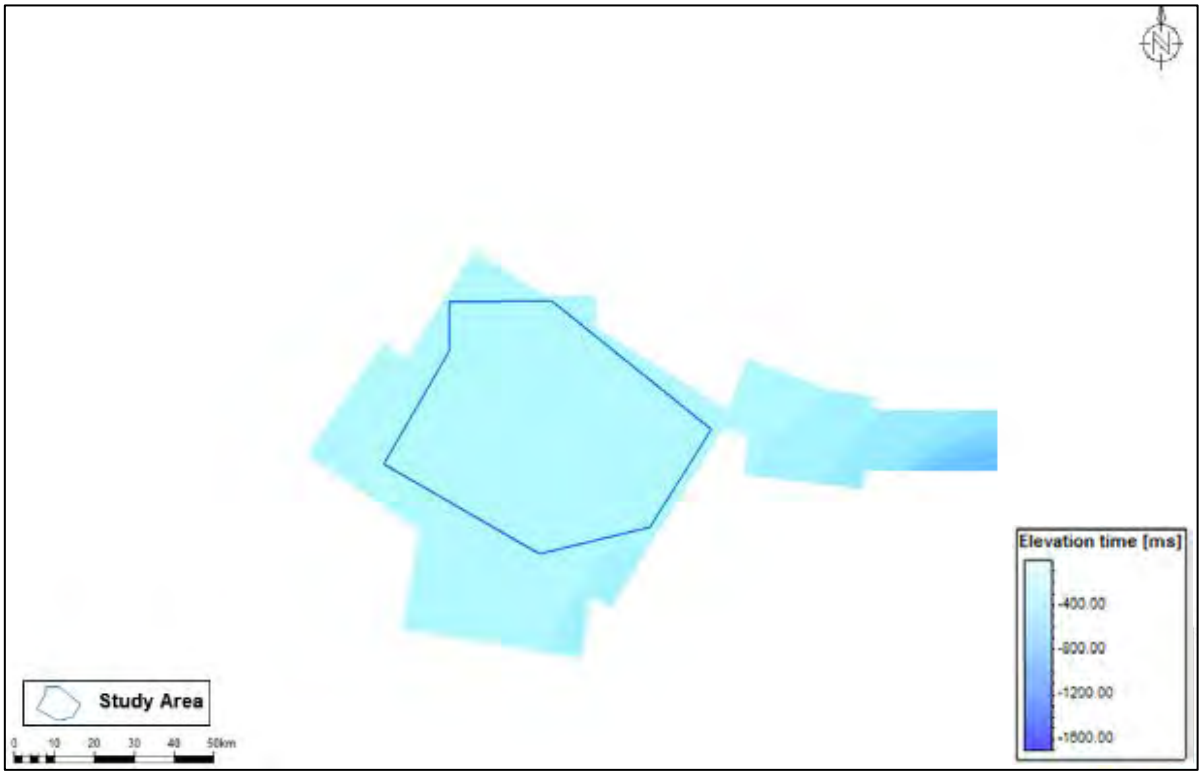

Figure 21 Seabed interpretation surfaces (TWT) using the set of 3D seismic surveys only.

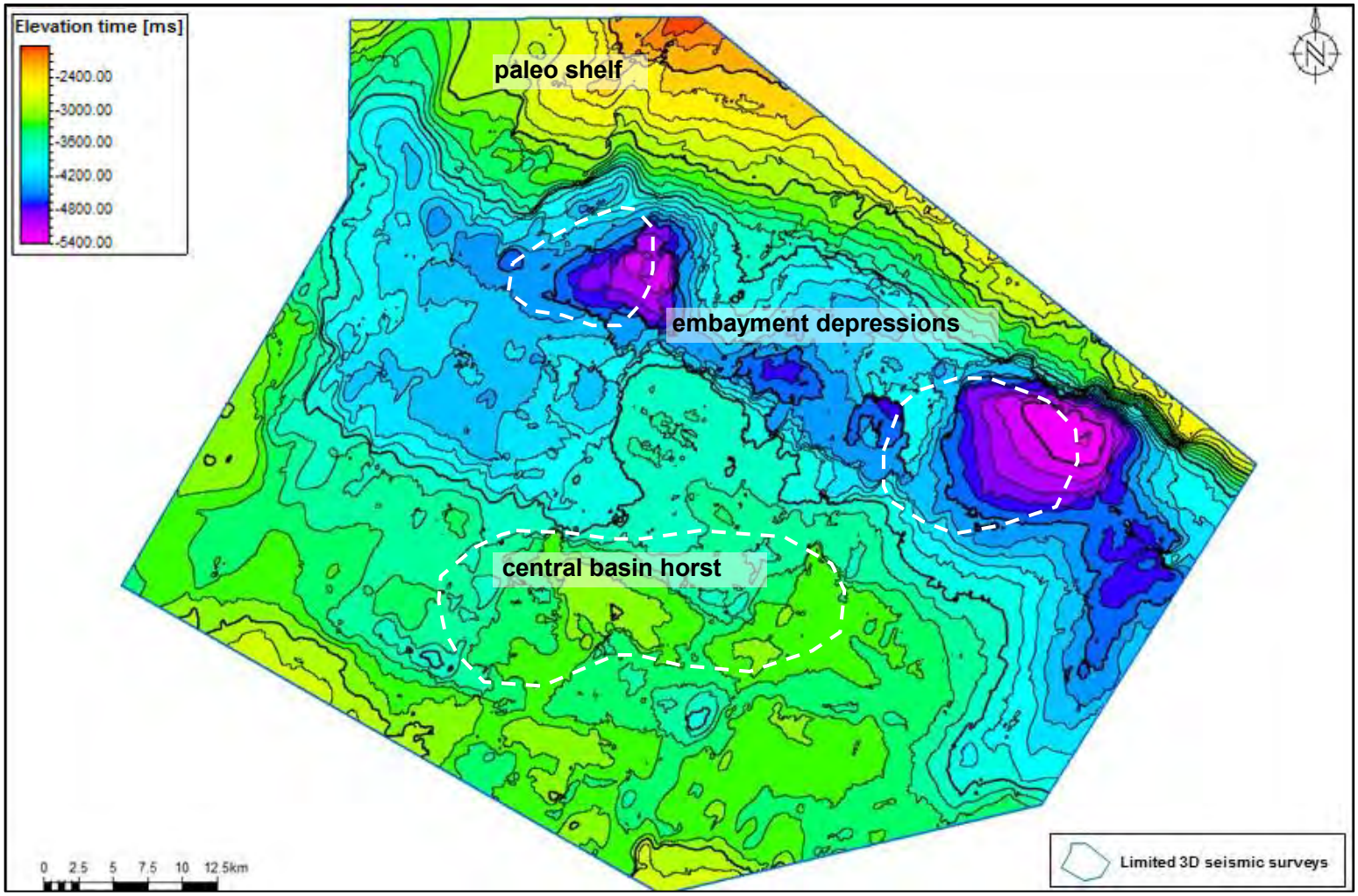

Figure 22 Time structure map of the Basement horizon over the study area in the Central Bredasdorp Basin.

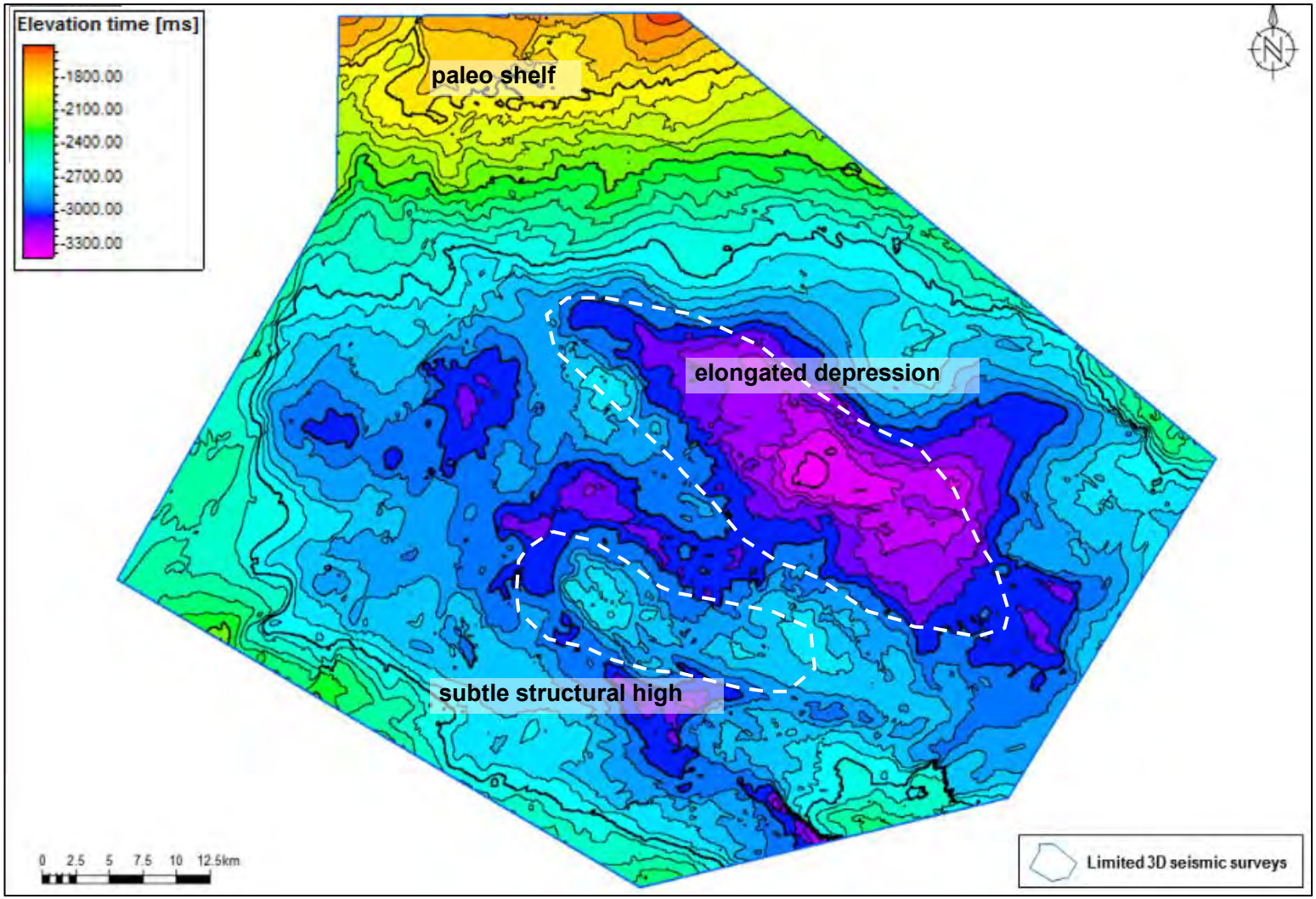

Figure 23 Time structure map of the 1At1 horizon over the study area in the Central Bredasdorp Basin.

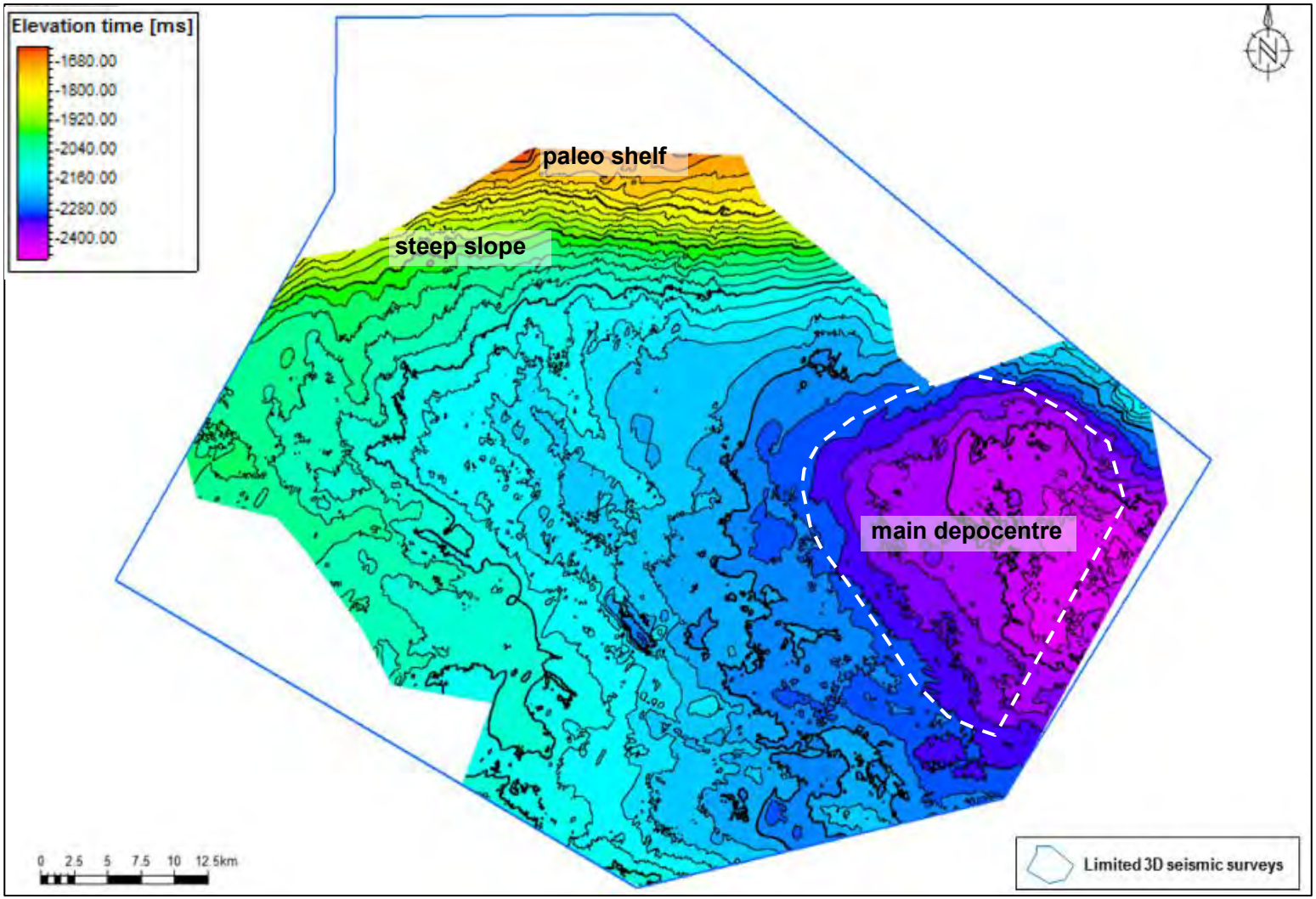

Figure 24 Time structure map of the 12A sand top horizon over the study area in the Central Bredasdorp Basin.

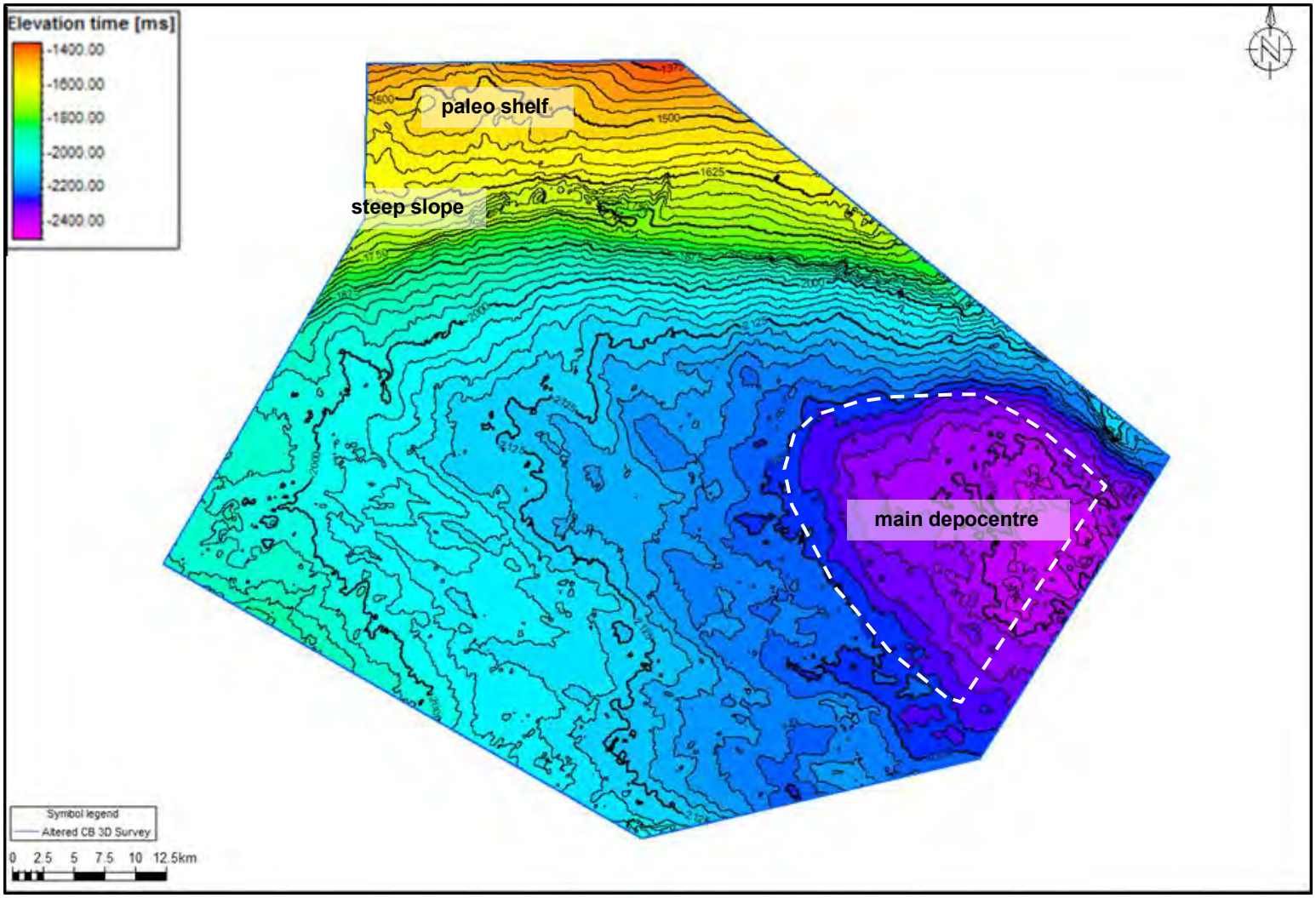

Figure 25 Time structure map of the 13At1 horizon over the study area in the Central Bredasdorp Basin.

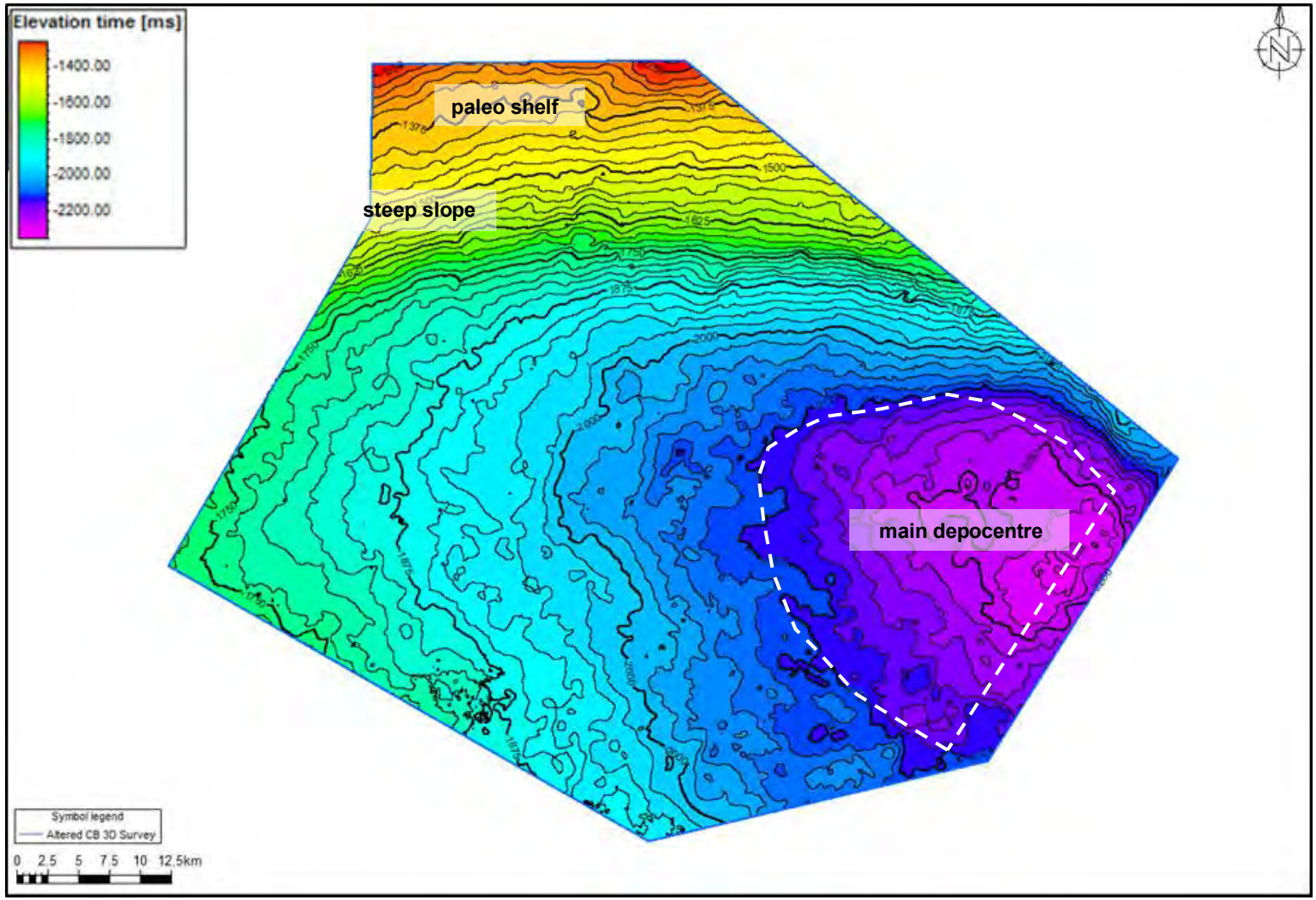

Figure 26 Time structure map of the 14At1 horizon over the study area in the Central Bredasdorp Basin.

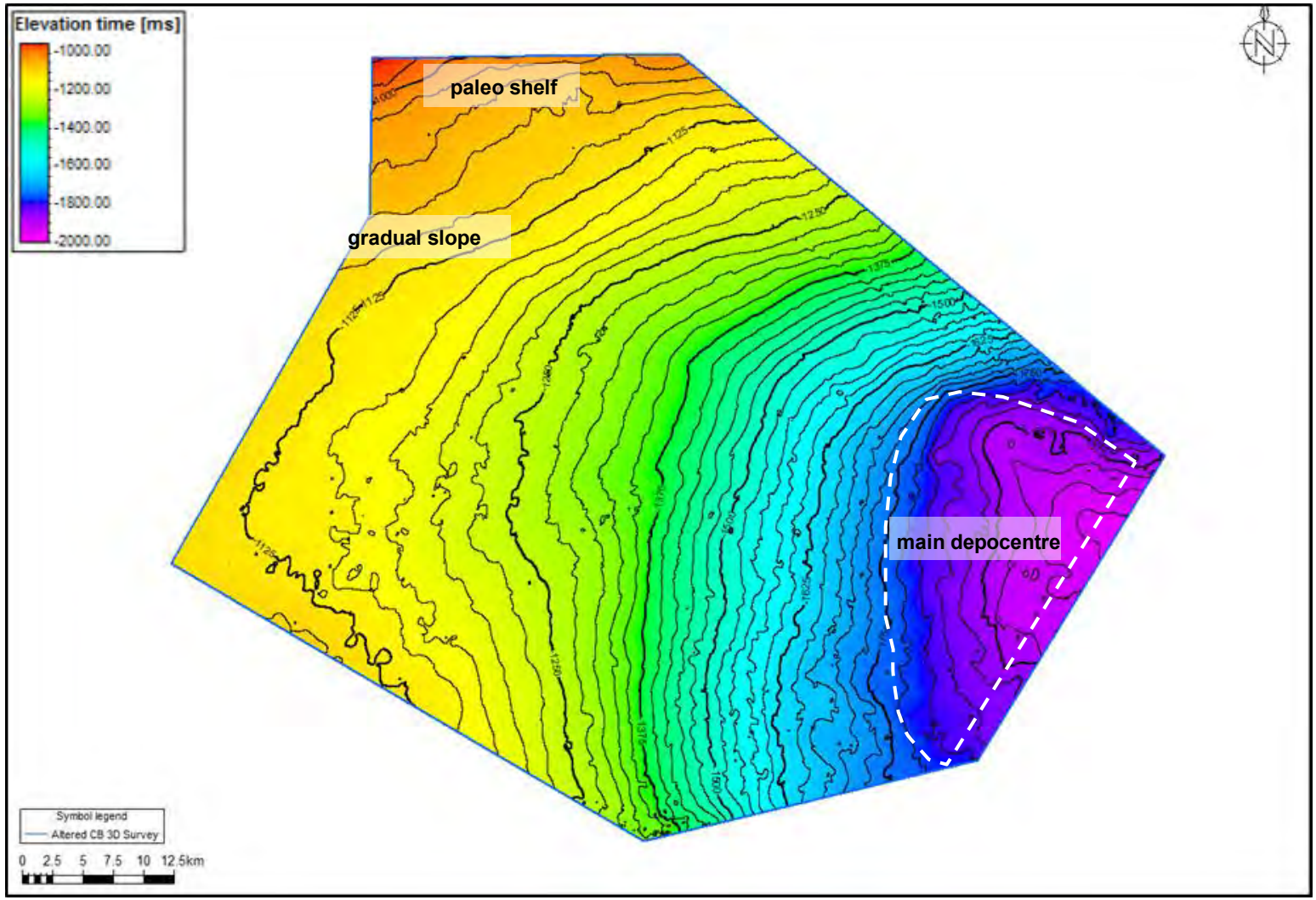

Figure 27 Time structure map of the 15At1 horizon over the study area in the Central Bredasdorp Basin.

9.3 Isochron Maps

To represent the time thickness variation of the 13A and 14A sequences, two types of isochron maps were generated in this study. The gross time thickness maps were generated using seismic surfaces as an input and ultimately reflect the combined thickness of shales and sands between: 13At1-14At1, 14At1-15At1, 13At1-13A sand top (13AST) and 14At1-14A sand top (14AST). The sand thickness maps were generated using the litholog facies attributes derived from well log data as an input for the 13At1-to-13AST interval to represent the 13A sequence and for the 14At1-to-14AST interval to represent the 14A sequence.

The 13At1-14At1 gross time thickness map (**Figure 28**) indicates that the thickest package of deposits in this interval is in the west/southwest. This finding fits the interpretation and assumption that one of the main sedimentary sources was located onshore in the west from which rivers deposited massive amounts of sediment just as they flowed into the offshore Bredasdorp Basin. The Agulhas Arch in the southwest most likely acted as a minor additional source of sedimentary input. The thinner areas of the 13At1-14At1 package appear dominant along the paleo shelf on the northern margin of the mapped area, as recognised on the 13At1 and 14At1 time surfaces in the eastern part of the basin due to the sediment supply diminishing with the increasing distance from the source during the Aptian-Albian times. There are also two thinner accumulations in the northern part of the central basin which may be inherited structural highs, formed as a lag effect of prior sediment accumulation into these areas which coincide with the embayment-like depressions that were present in the Basement topography. The thickness trend of the sediment in the 13At1-14At1 interval seems to have bypassed the above-mentioned accumulations, possibly within slight depressions, in a forked west-east directional trend.

The 14At1-15At1 gross time thickness map (**Figure 29**) illustrates that the thickest part of this interval is in the southwest part of the Central Bredasdorp Basin, despite the 14At1 and 15At1 time surfaces suggesting a depocentre located more in the eastern part during the Albian-Cenomanian time (refer to *Results* chapter, *Section 9.2*, p. 50). The thinning of the package around the semicircular-shaped depocentre shows a trend of pinching out and onlapping of the package against the northern basin margin, or paleo shelf–slope edge, but also towards the northeast against the Infanta Arch. An indication of thinning of the package in the east of the basin may be due to data interpretation constraints or, more practically, a representation of how the sediment supply diminished with increasing distance from the onshore sediment source in the west**.** The "flatter" nature of this map, as interpreted from the contours, in comparison to the 14At1-15At1 gross time thickness map is probably due to the difference in the thickness of the interval between the unconformities.

To better represent the distribution of the sands in the 13A and 14A sequences, gross time thickness maps were generated over a more restricted interval of the 13At1 to 13AST and the 14At1 to 14AST, respectively.

The 13At1-13AST gross time thickness map (**Figure 30**) indicates a proposed pattern of sand distribution in which failure on the shelf edge–slope initiates a mass sediment flow down the slope, splaying at the base and onto the basin floor as fans and lobe-like geometries with a NW-SE

orientation. Broad, thick sand "corridors" on the isochron map trend NW-SE and north-south, appearing to be sourced from the northwest and north/northeast, respectively, whilst thinner areas of sand like the circular accumulation in the central part of the map may be the result of underlying structures, like ridges or faults, which cause the sands to bypass. As a working interpretation, these clusters of thicker and thinner sequence accumulations have an alternating offset pattern located adjacent to each other across the basin. This prompted the sketching of boundaries between the clusters, which became referred to as thickness-based "transfer zones". The 13A gross isochron map overlain with the sand fraction pie charts appears to indicate a thicker, sand-dominated area in the western part of the basin, suggesting that there may have been sedimentary input from that direction and generally the pie charts bearing a larger fraction of sand are coincident with the areas of moderate to high thickness on the 13AST1-13At1 gross time thickness map.

At first glance, the 14At1-14AST isochron map (**Figure 31**) does not show a distinct trend of sand distribution across the Central Bredasdorp Basin. The relationship between the sand fraction pie chart results and the 14A isochron map appears to be weak too. However, through applying the same overview of the variation in the thickness of the 14A sequence across the basin the presence of a transfer zone trend becomes apparent, like the one recognised on the 13A sequence gross isochron map. The trend showing of a thicker sand accumulation against the W/NW parts of the basin and an isolated, very thin to sand-less accumulation in the central part of the basin between the northern and southern west-east trending sand dispersions. Comparatively, the thickness-based transfer zone boundaries identified on the gross isochron maps of the 13A and 14A sequences mirror one another in terms of approximate length, spacing and orientation which suggests that there must be a common feature at play. The area of positive structural relief and the associated 14A sequence thinning in approximately the central part of the basin is a feature that is coincident with the position of the structural high identified on the Basement and 1At1 time structure maps and present on the 13A isochron map too.

The findings described above prompted the generation of sand thickness maps using zones delineated by the well tops as the main input but to include the seismic interpretations as a trend surface to determine if a stronger pattern of sequence thickness versus transfer zone control would emerge from the wells instead. The 13A and 14A sand thickness maps do not, however, show a clearly interpretable trend due to the sparseness of the data points (i.e. wells) (**Figures 32** and **33**). Overall there is a common trend of an increasing sand thickness from west to east for the 13A sequence and the 14A sequence and this agrees with the previous findings that strongly suggest the presence of the main sedimentary depocentre located in the eastern part of the Central Bredasdorp Basin at the Aptian-Albian time.

In summary, **Figure 34** is a seismic cross-section from west to east across the Central Bredasdorp Basin, illustrating the thinning of the 13A and 14A sequences towards the east as identified on the gross isochron maps of 13At1-14At1 and 14At1-15At1.

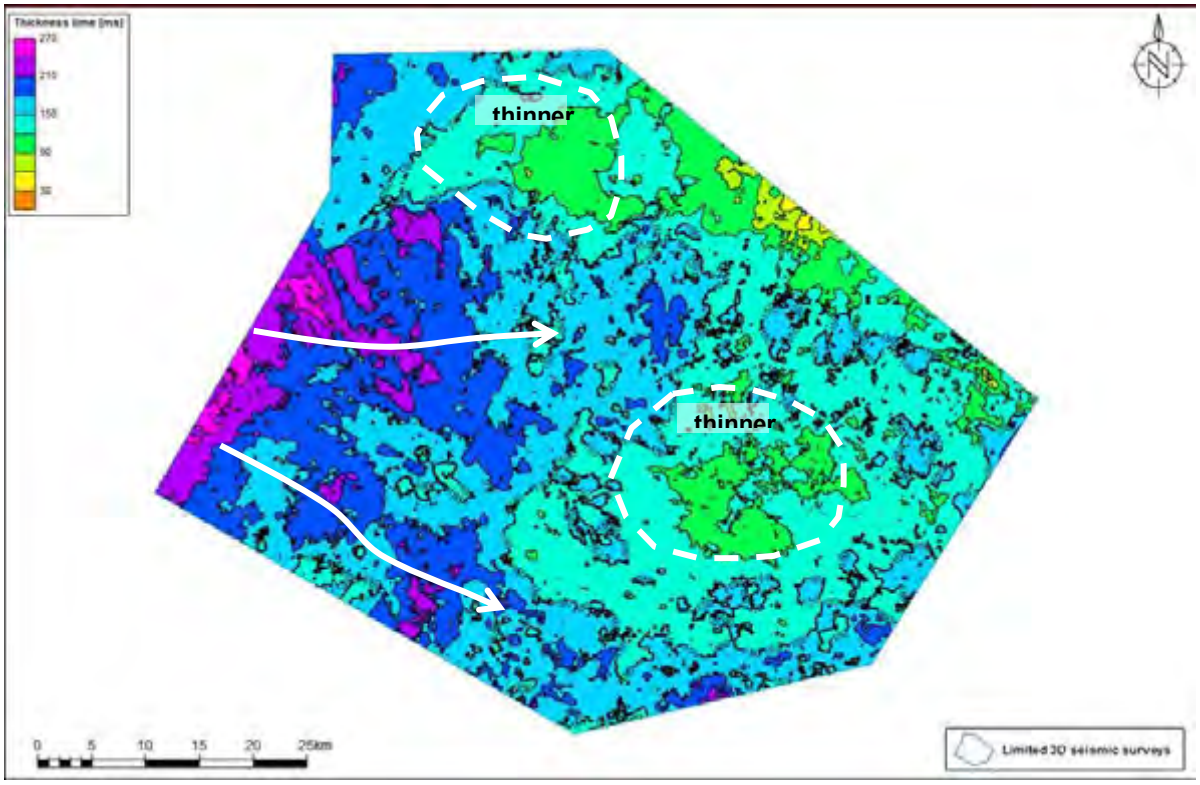

Figure 28 Gross isochron map of 13At1 to 14At1. Annotated with likely sediment transport directions (white arrows) coinciding with the thicker accumulations and the thinner accumulations circled in white.

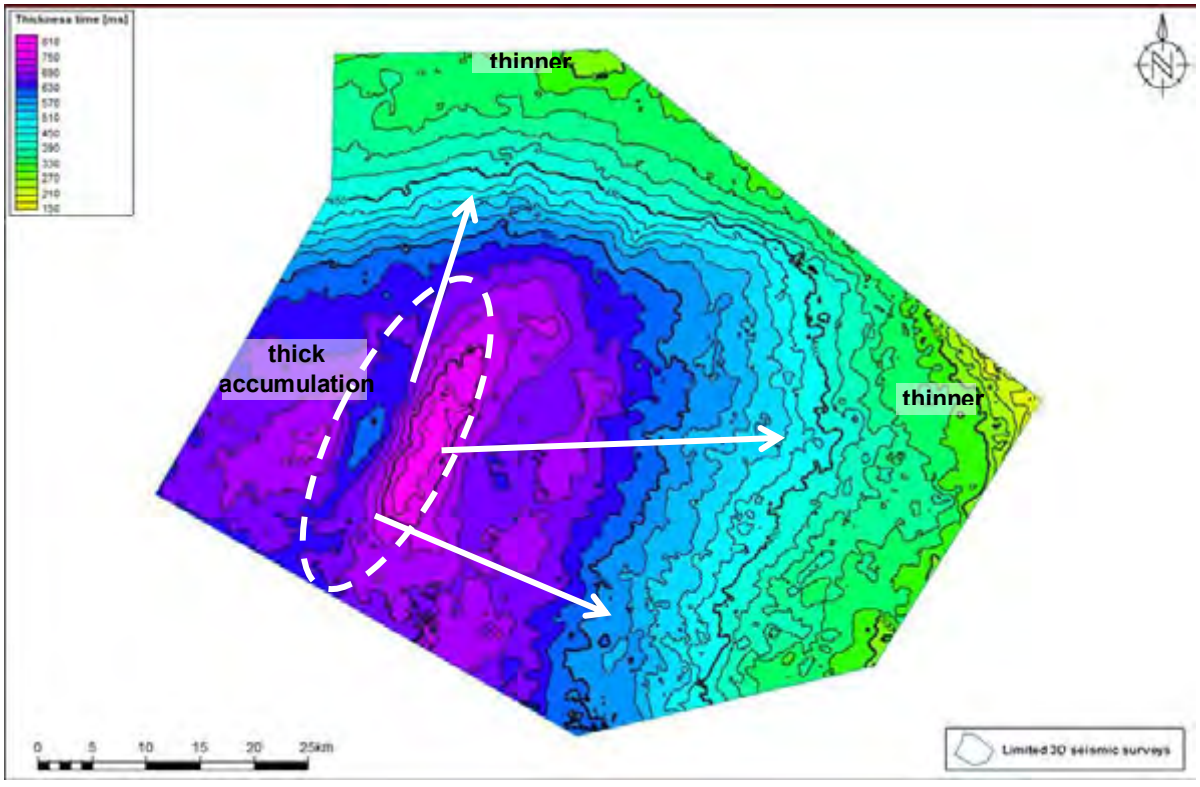

Figure 29 Gross isochron map of 14At1 to 15At1. Annotated with multiple possible sediment transport directions (white arrows) from the thick central accumulation towards the thinner accumulations on the basin margins.**.**

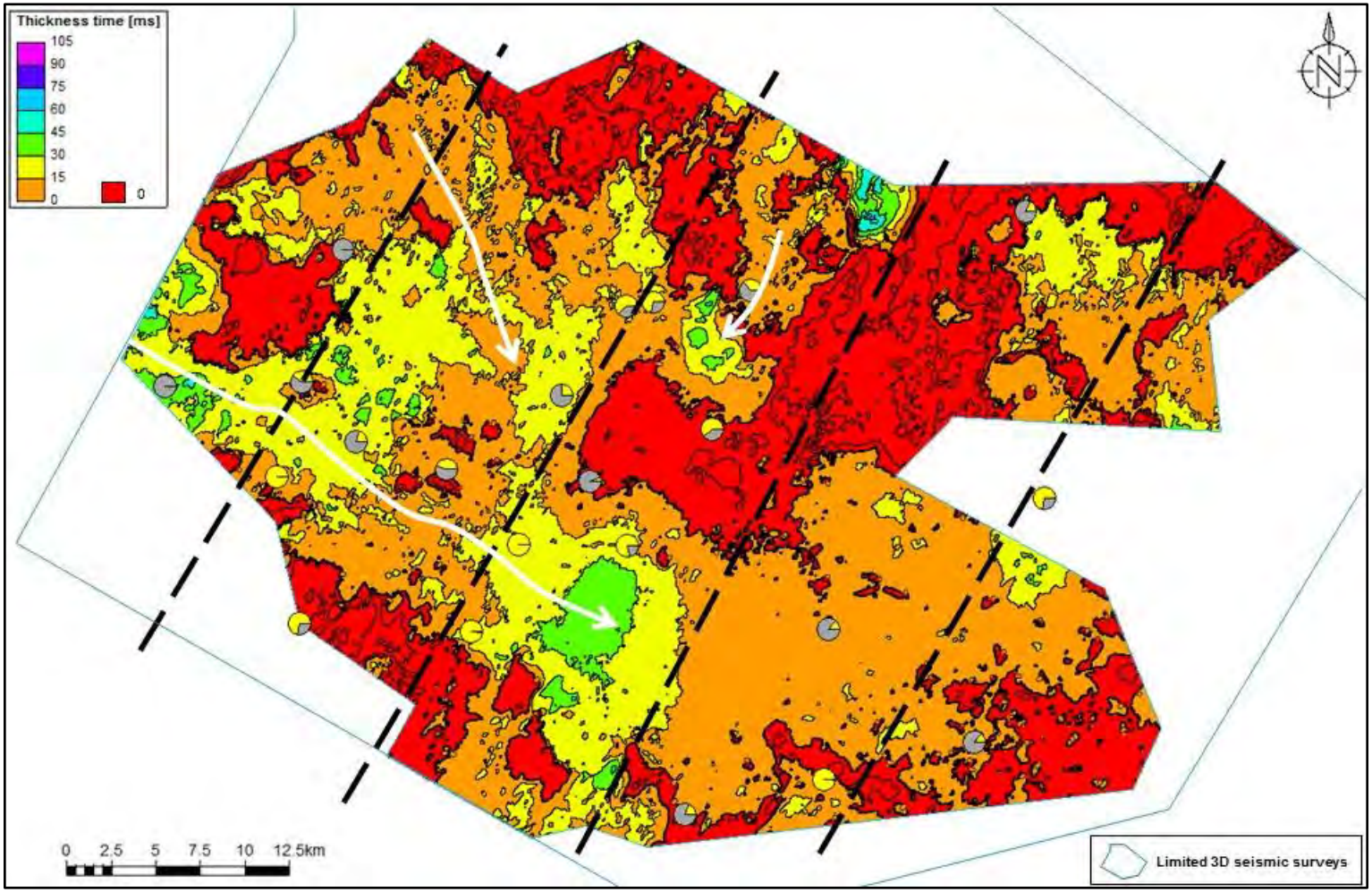

Figure 30 Gross isochron map of 13At1 to 13A Sand Top with sediment transport directions (white arrows) coinciding with thicker sand dispersions and transfer zones (bound by black dashed lines) delineating segments of alternating sand thickness.

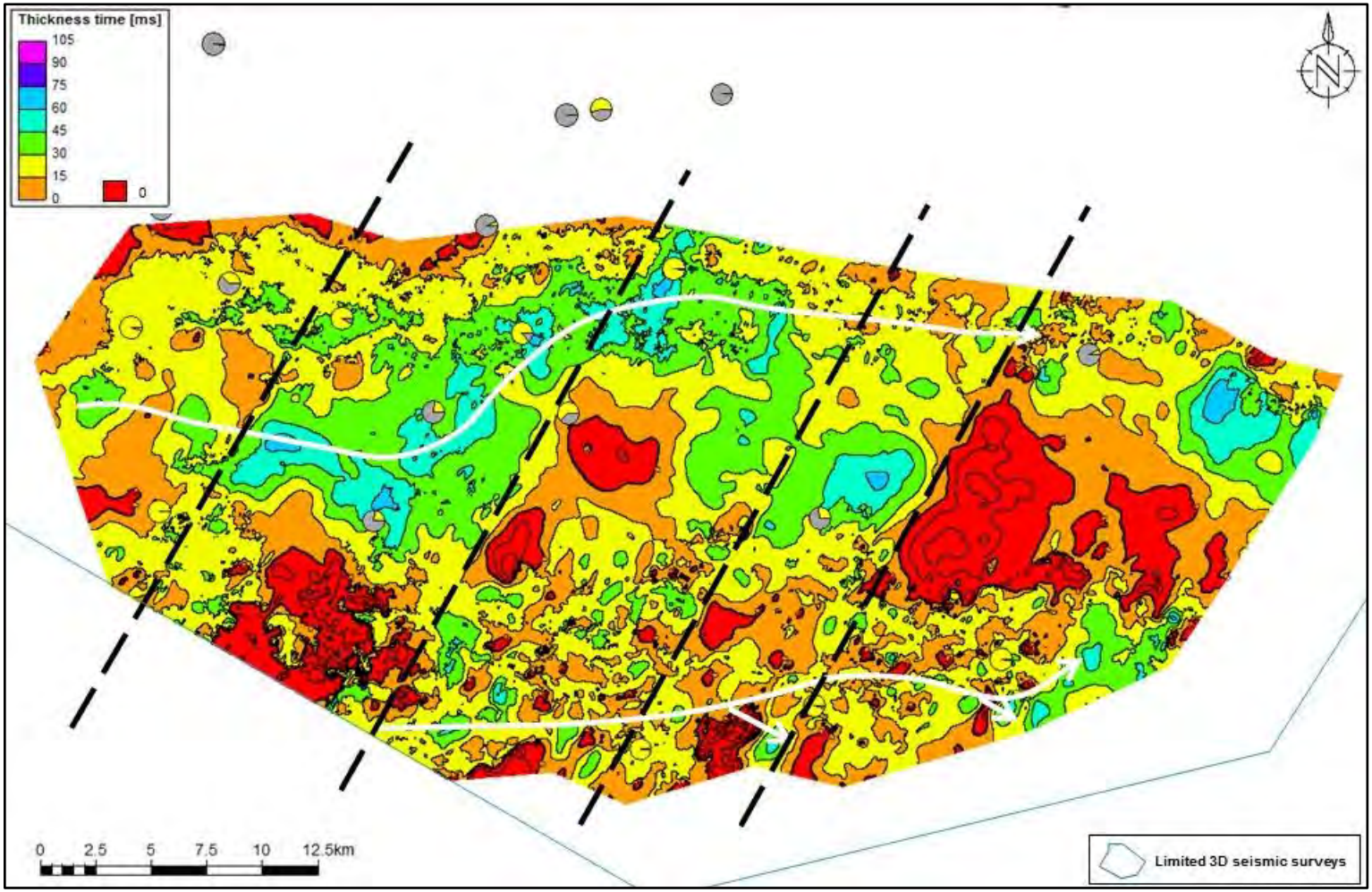

Figure 31 Gross isochron map of 14At1 to 14A Sand Top with sediment transport directions (white arrows) coinciding with thicker sand dispersions and transfer zones (bound by black dashed lines) delineating segments of alternating sand thickness.

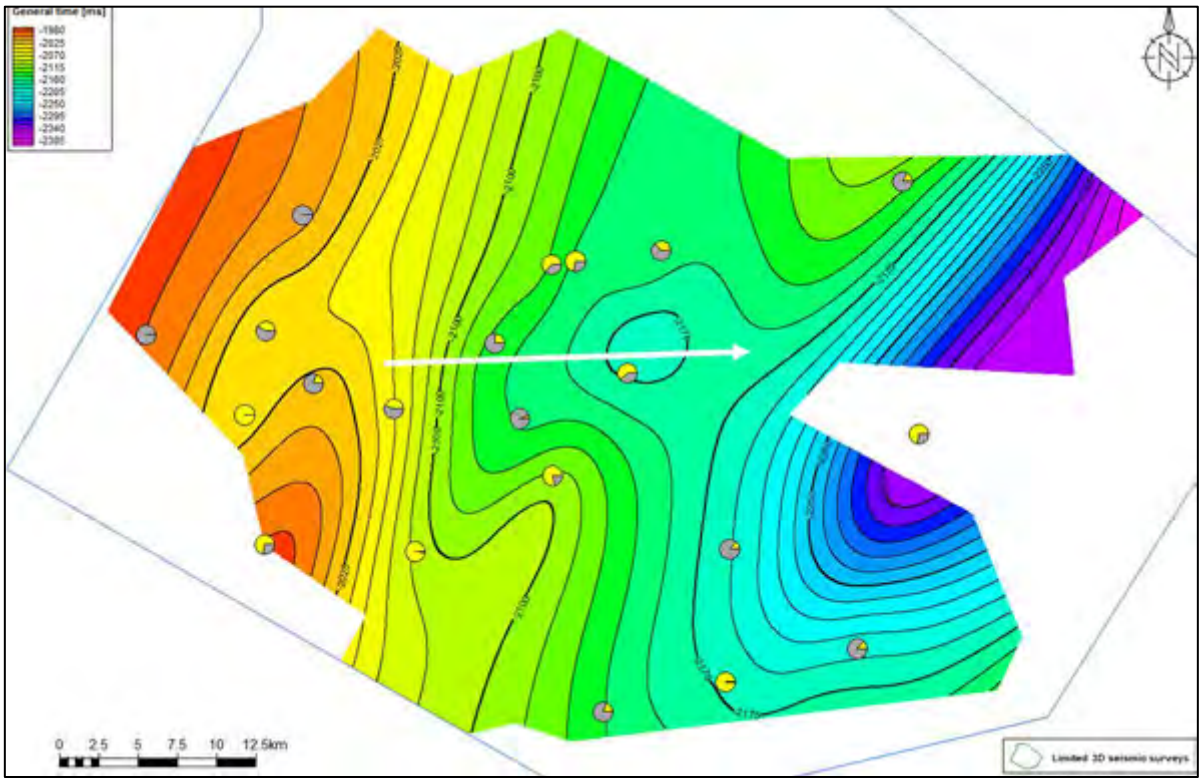

Figure 32 Sand isochron map of 13At1 to 13A Sand Top with sand fraction pie charts for the 13A zone.

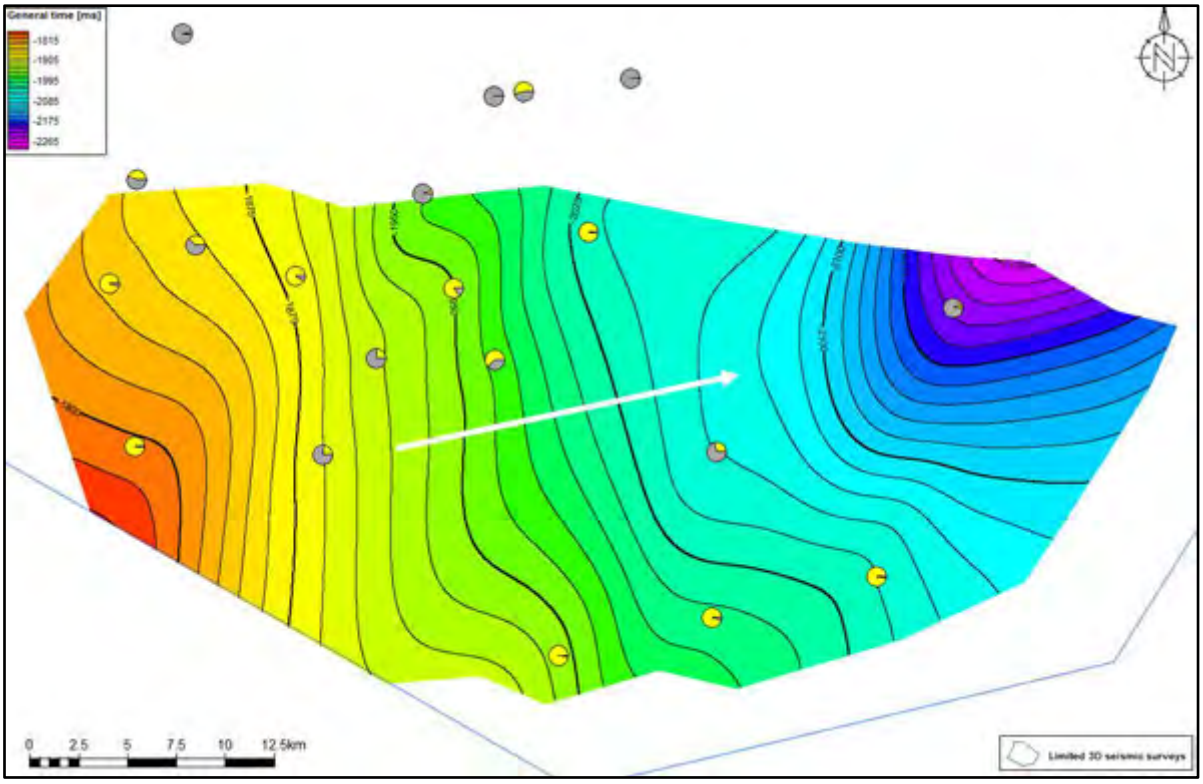

Figure 33 Sand isochron map of 14At1 to 14A Sand Top with sand fraction pie charts for the 14A zone.

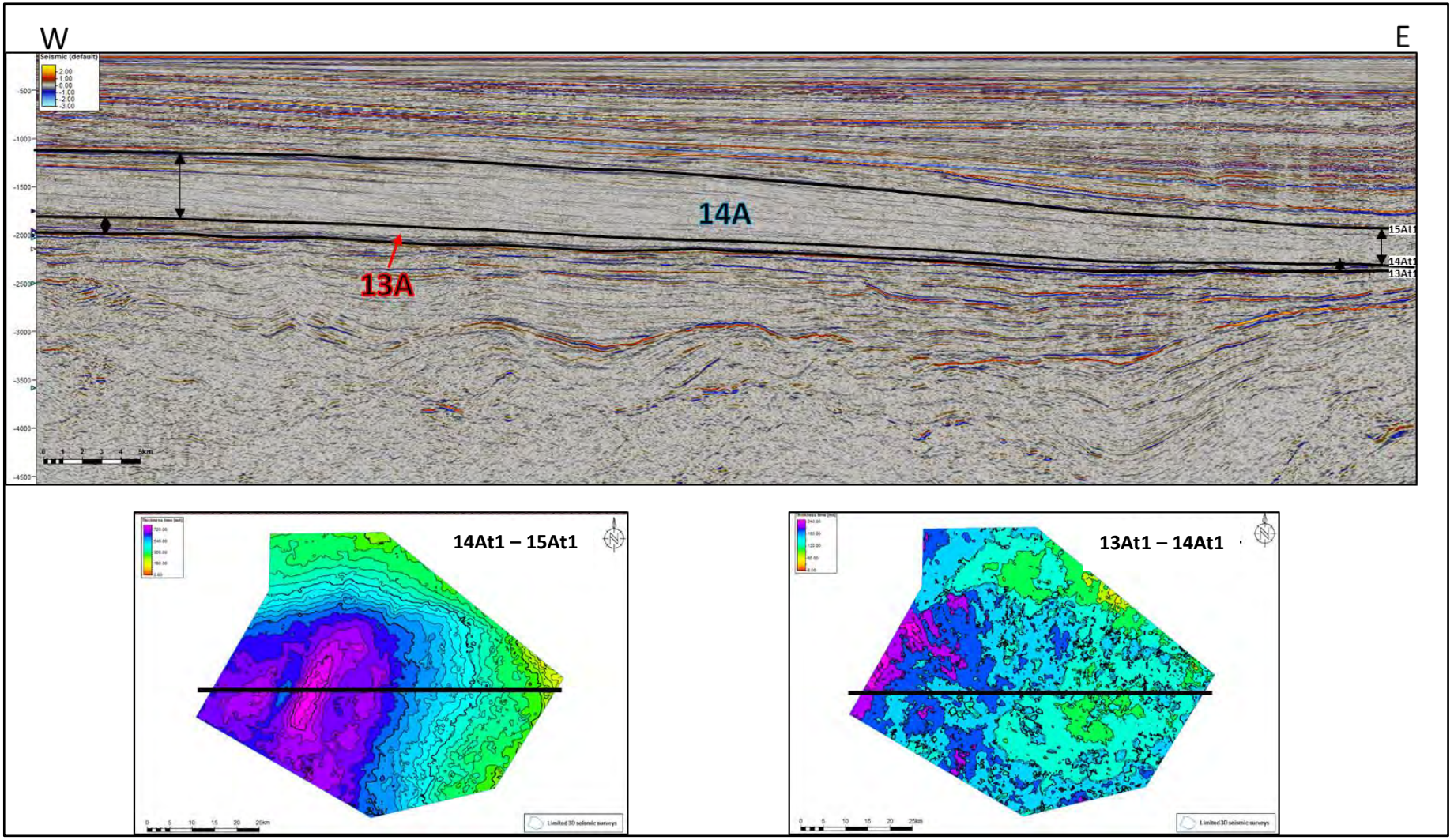

Figure 34 Seismic cross-section from west to east across the Central Bredasdorp Basin, illustrating the thinning of the 14A and 13A sequences towards the east as seen in the gross isochron maps below (14At1-15At1 and 13At1-14At1).

9.4 Seismic Attributes Interpretation

The first step in determining the likely sand distribution of a seismic sequence, such as 13A and 14A, is to extract the amplitude attribute for the basal surfaces of the sands. In this study, the amplitude attribute was extracted for the 13At1 and the 14At1 interpretation surfaces. The range in positive and negative amplitude values give an overview of the depositional trend associated with the 13A and 14A sequences, with the assumption that the more positive amplitude values are associated with the sands. In **Figures 35** and **36** the likely distribution of the 13A and 14A sequence sands is illustrated, respectively.

The principles of seismic attribute extraction and volume rendering are described in detail in *Chapter 5: Methodology* and the results of the selected few attributes (*viz.* Minimum Amplitude, RMS, Dip Angle, Dip Azimuth, Maximum Curvature and Variance) are captured in **Figures 37** to **45**.

The amplitude map of the 13At1 interpretation surface suggests a broad distribution of the 13A sands in a pattern from NW to SE and then east and it emphasizes the location of the basin depocentre at the Aptian time as a cluster of strongly positive amplitude values in the southeast/east part of the study area. This feature is captured by the 13A gross thickness map too (See **Figure 30**). Since the 13A sand top is associated with a trough reflector and the 13A sand base is associated with a peak reflector, Minimum Amplitude (**Figure 37**) and Maximum Amplitude attributes were extracted to try highlight the brightest (strongest) amplitudes associated with the 13A sands but the results were not as informative as the RMS attribute which proved best at illustrating the sand distribution pattern across the basin (**Figure 38**) as it is generally renowned for highlighting features like thin turbidite and delta front sands as well as the exact slope break location (Zhao *et. al*., 2015). This is demonstrated with annotations in **Figure 39** and a comparison of the relative sand thickness may be seen in the gross isochron map of 13A in **Figure 30**.

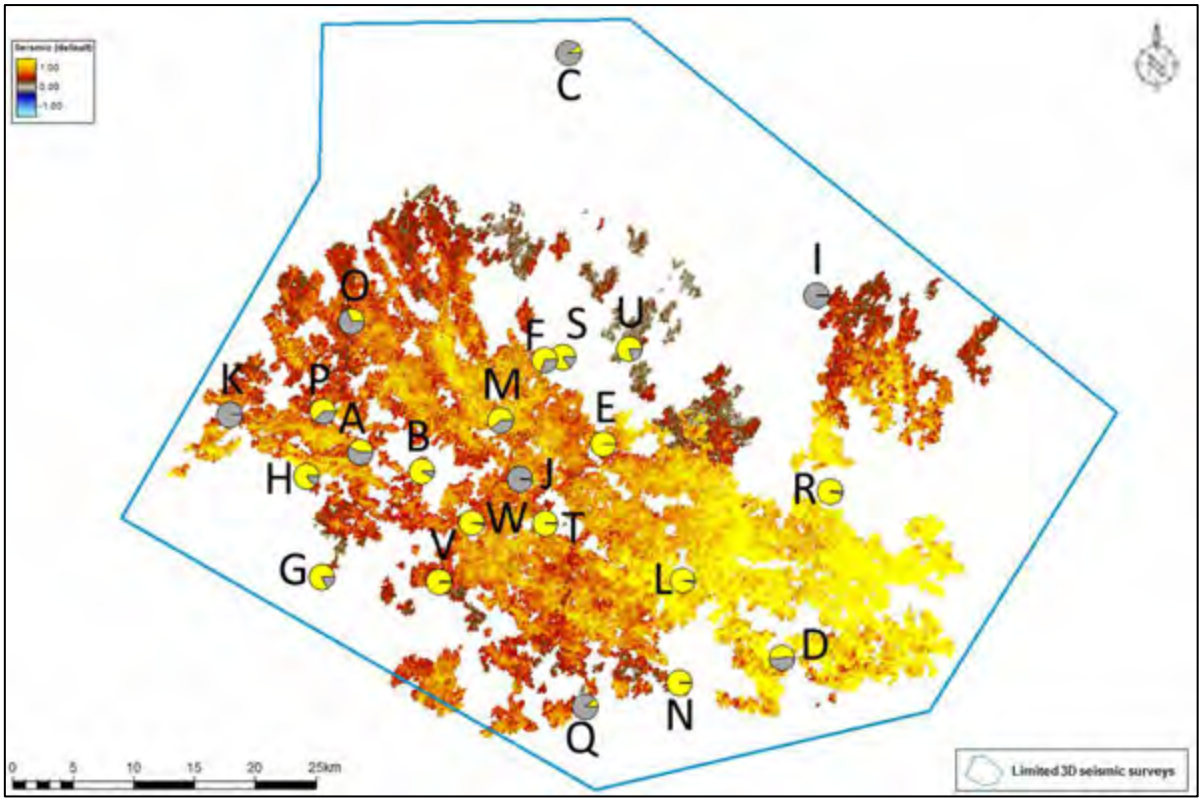

Figure 35 Seismic amplitude attribute displayed on the 13A sand base interpretation map.

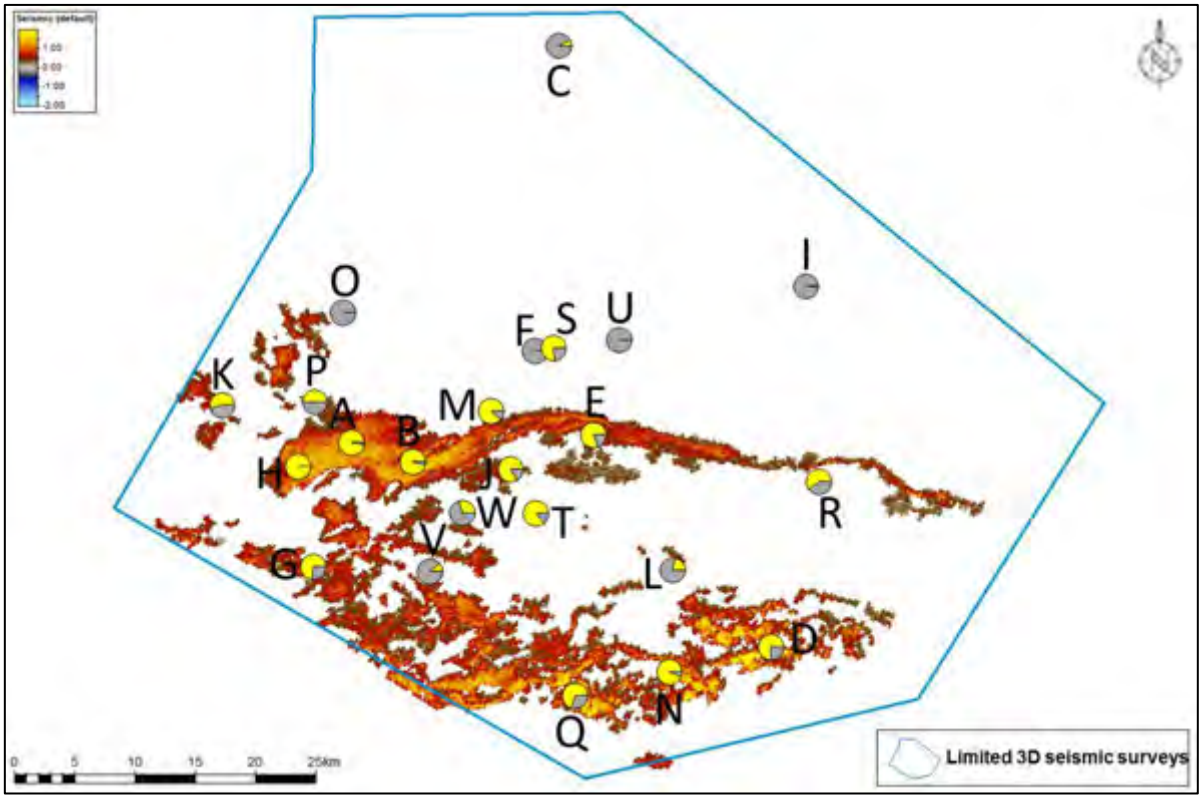

Figure 36 Seismic amplitude attribute displayed on the 14A sand base interpretation map.

The 13A sand distribution trend is very similar to that captured by the 13A sand base interpretation amplitude map (**Figure 35**). To illustrate the possible interaction of faulting and the distribution of the 13A sands, the dip angle and dip azimuth attributes were extracted on the 13At1 surface (**Figures 40** and **41**). The dip angle also showed the paleo shelf edge in the north quite clearly, as did the Maximum Curvature attribute map (**Figure 42**). The Aptian sand distribution trends across the Central Bredasdorp Basin were supported by the patterns on the Variance map of the 13At1 surface which also seemed to highlight channels on the north shelf flowing across to the shelf edge where apparent slump features give rise to slope channels and downdip splays as fans and lobes on the basin floor (**Figure 43**).
Overall, the features of channelised sands on the slopes and basin floor fans and lobes expected in this study are very clear on the amplitude map, derived from the seismic interpretation surface but they were further enhanced by applying seismic attribute extractions to generate RMS, Maximum Amplitude and Variance maps.

The amplitude map of 14At1 (**Figure 36**) suggests that sand deposition took place as two sub-parallel and separate west-east trending sand fairways of channel complexes. The northern sand fairway of the 14A sequence sands is narrower and more isolated with a gentle meandering pattern than the southern sand fairway of the 14A sequence sands, which is less isolated in a pattern of smaller, interwoven meandering branches off the main channel over a wider area in the form of channel splays and fans. Overlaying the sand transport interpretation from the amplitude map onto the 14At1-14AST isochron map highlights the west to east distributional trend of the 14A sequence with areas of greater thickness coinciding with the brighter, more positive amplitude values and therefore assumed sand concentrations. The only difference between the suggested sand distributional trends of the amplitude map and those of the isochron map is in the region of the northern fairway for which there is the variation in the source location in the west variation in the source location as suggested in the west by the amplitude map but southwest by the isochron map. To determine the possibility of faulting playing a role in guiding these fairways, the dip angle and dip azimuth attributes were extracted. Mapping of the 14A sand using seismic attributes was a bit trickier than that of the 13A sand as algorithms like Minimum Amplitude and Maximum Amplitude did not yield favourable results. The strong amplitude response of the 14A sand was best captured by the RMS attribute, which produced a clearer trend and one supporting that illustrated by the 14A sand base interpretation amplitude map. The RMS map (**Figure 44**) places an emphasis on the proximal part of the 14A deposits in the west of the basin at the Albian time by a concentration of strongly positive amplitude values, which is a feature captured by the 14A gross thickness map too. The Variance map of the 14At1 surface (**Figure 45**), however, shows a fair overview of the sand distribution trends across the Central Bredasdorp Basin and it seems to highlight the proximal 14A sand deposits best but overall demonstrating a prominent west-east pattern of distribution. The variance values also suggest the presence of a small, elongated positive structure between the two fairways, which is the structural high identified on the 14At1 time structure map and on the 14A gross thickness map.

Overall, the channelised distribution of the 14A sands is best resolved in seismic reflection data by using the RMS, Maximum Amplitude and Variance attributes in addition to the basic extraction of seismic amplitude values from the 14At1 interpretation surface.

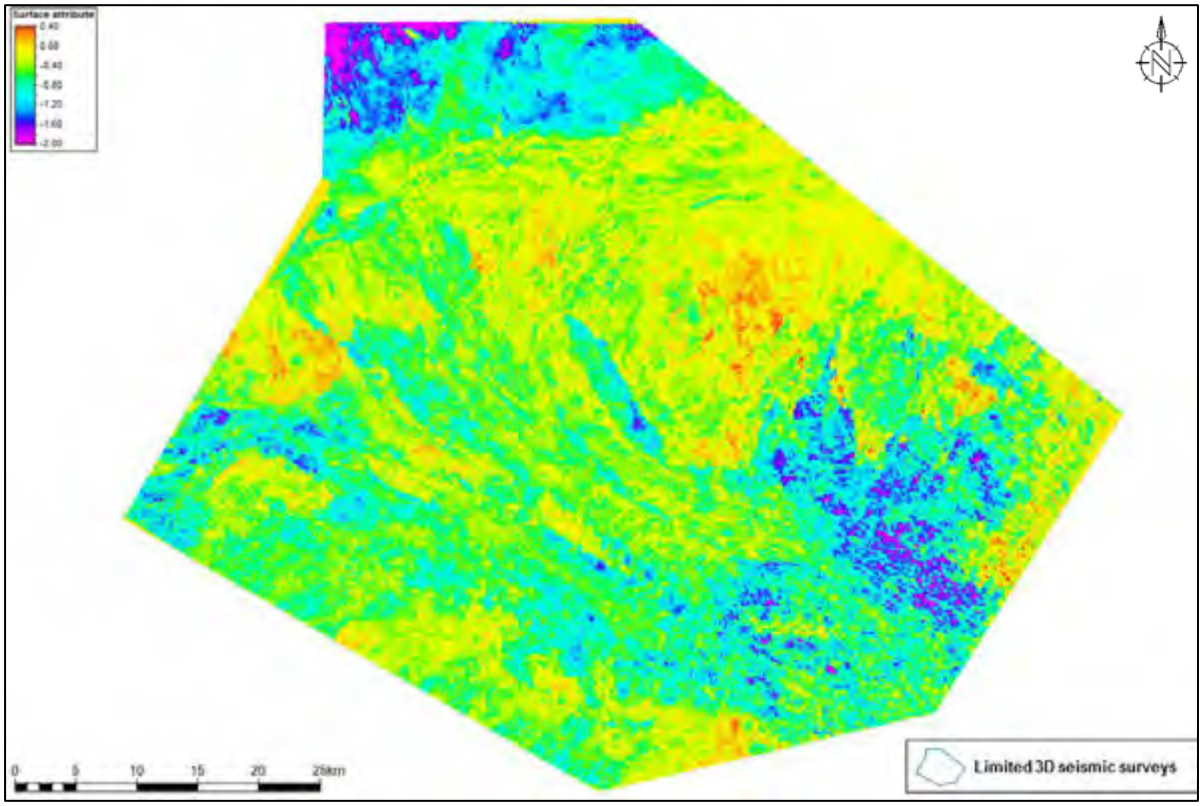

Figure 37 Seismic attribute extraction map of Minimum Amplitude of 13At1.

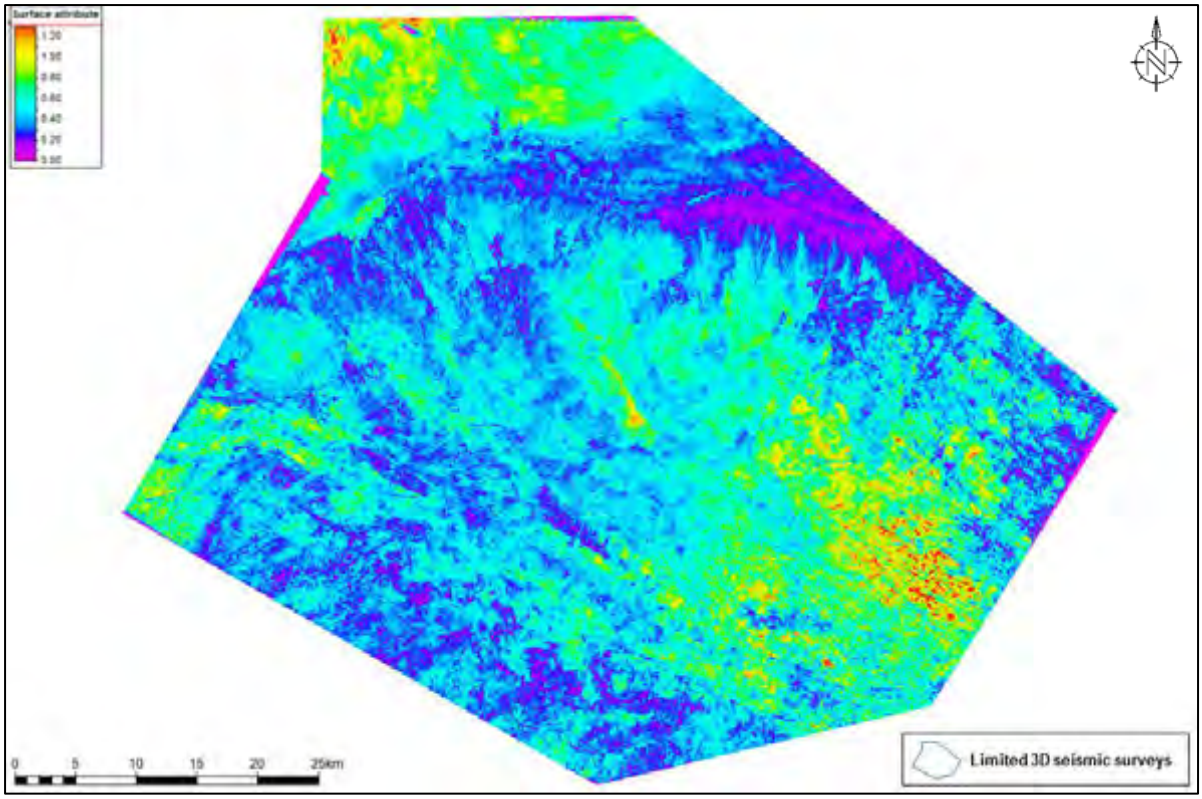

Figure 38 Seismic attribute extraction map of RMS of 13At1.

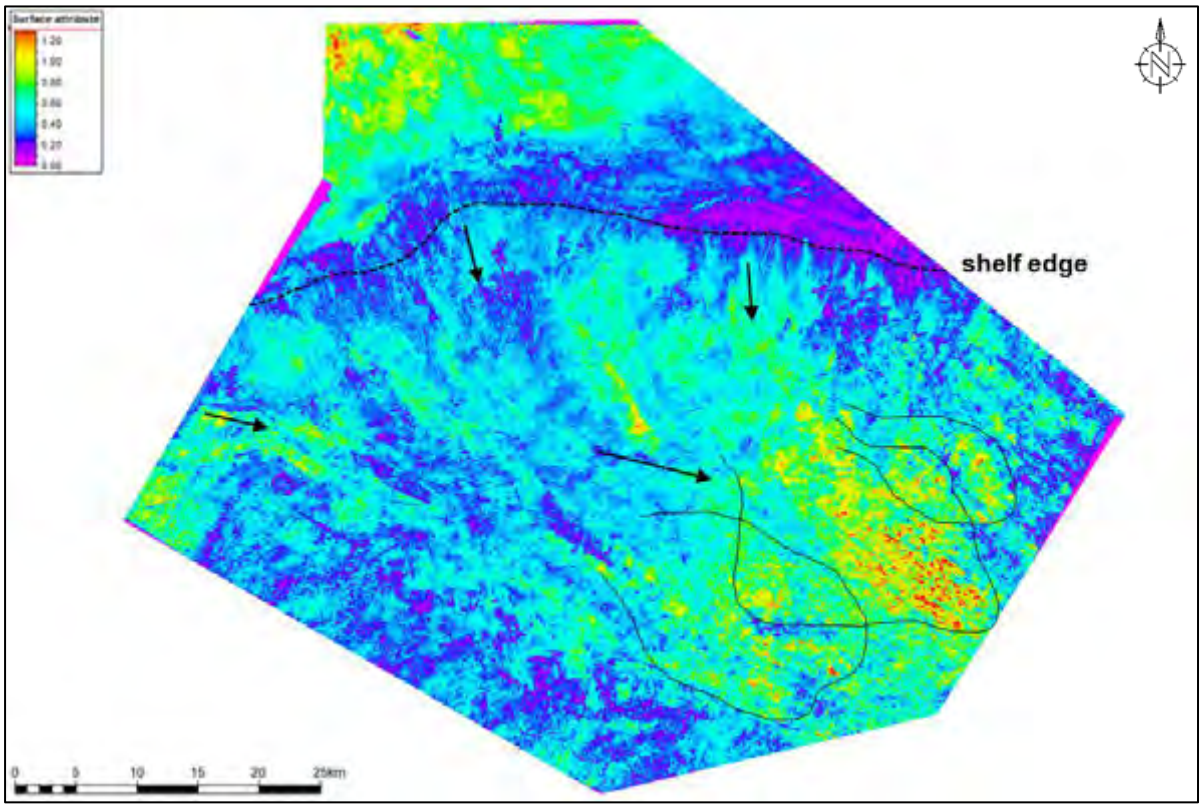

Figure 39 Seismic attribute extraction map of RMS of 13At1 overlain with line drawings to give an indication of the interpreted distribution of the 13A sequence sands across the Central Bredasdorp Basin.

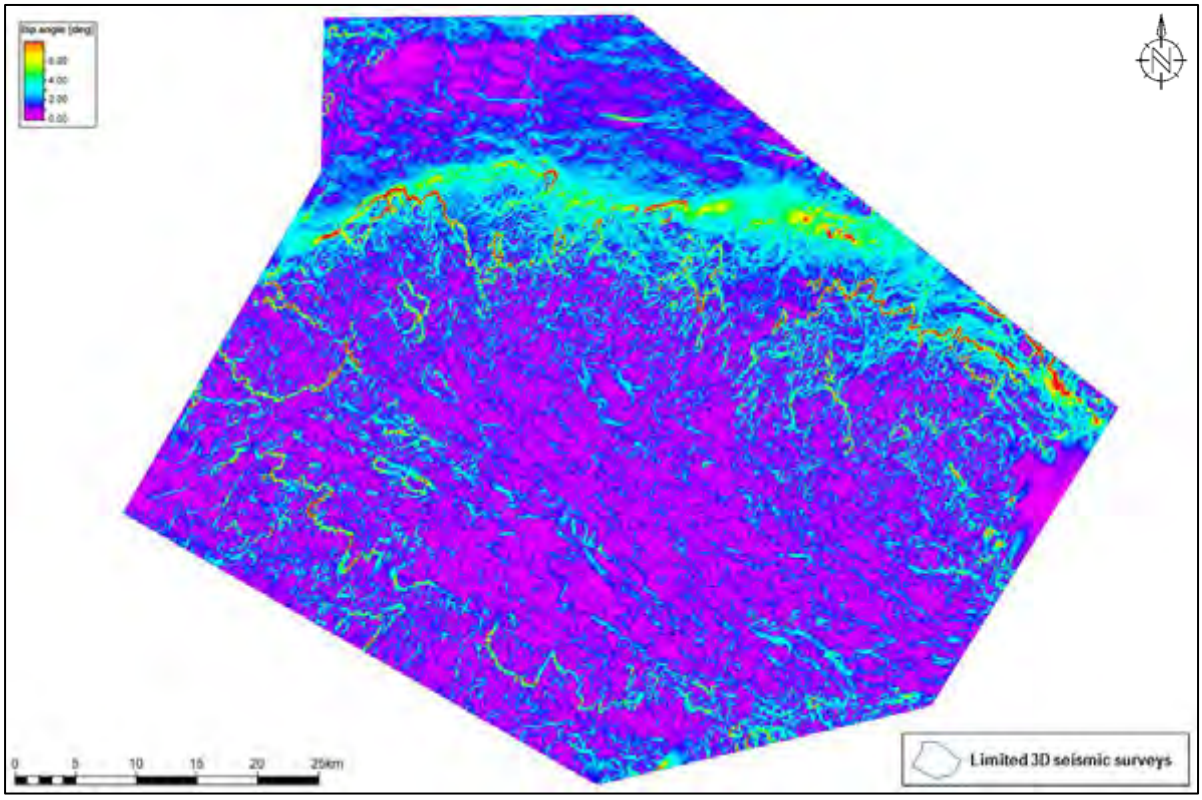

Figure 40 Seismic attribute extraction map of Dip Angle of 13At1.

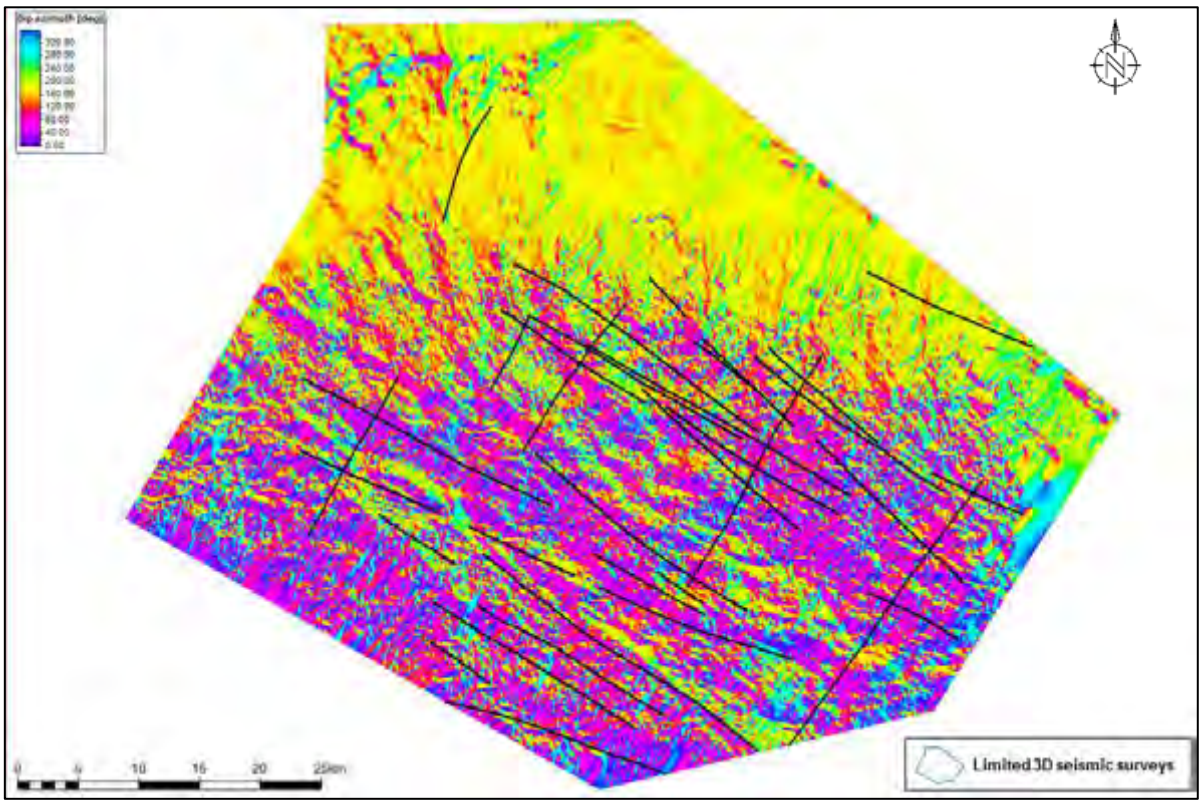

Figure 41 Seismic attribute extraction map of Dip Azimuth of 13At1 overlain with the faults that intersect the 13At1 level.

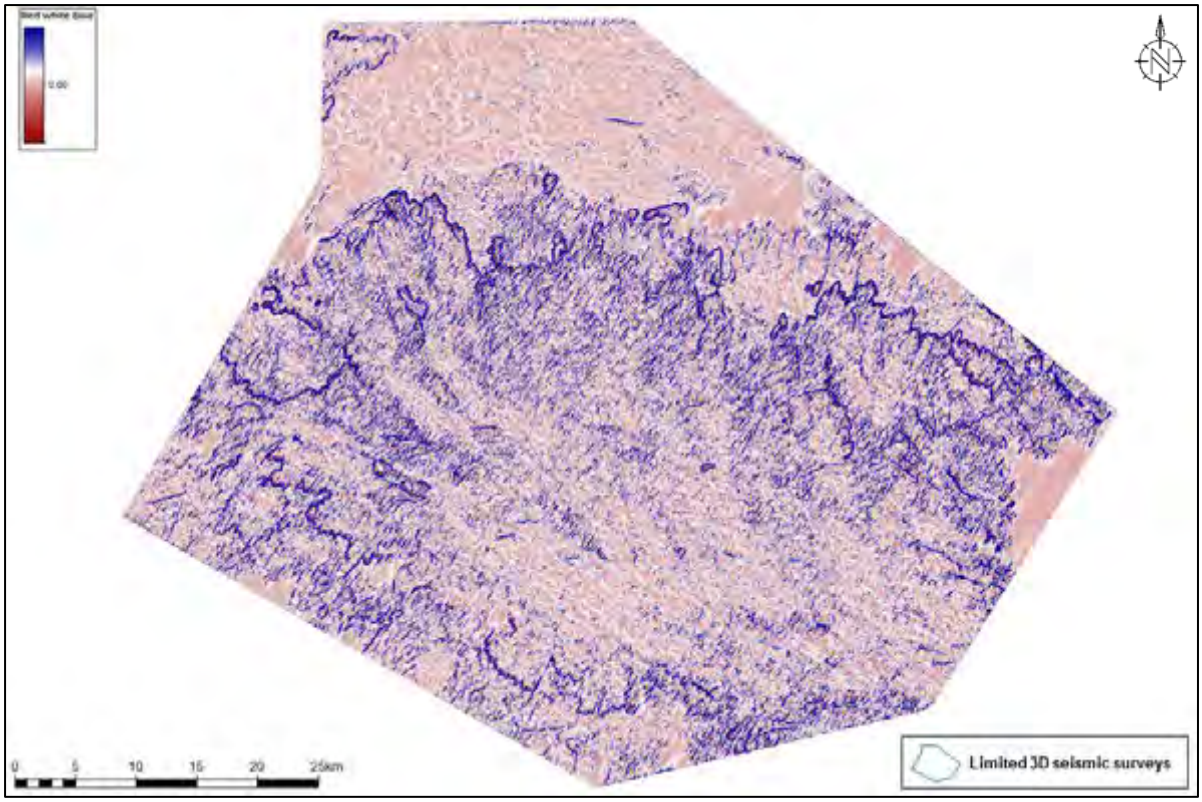

Figure 42 Seismic attribute extraction map of Maximum Curvature of 13At1.

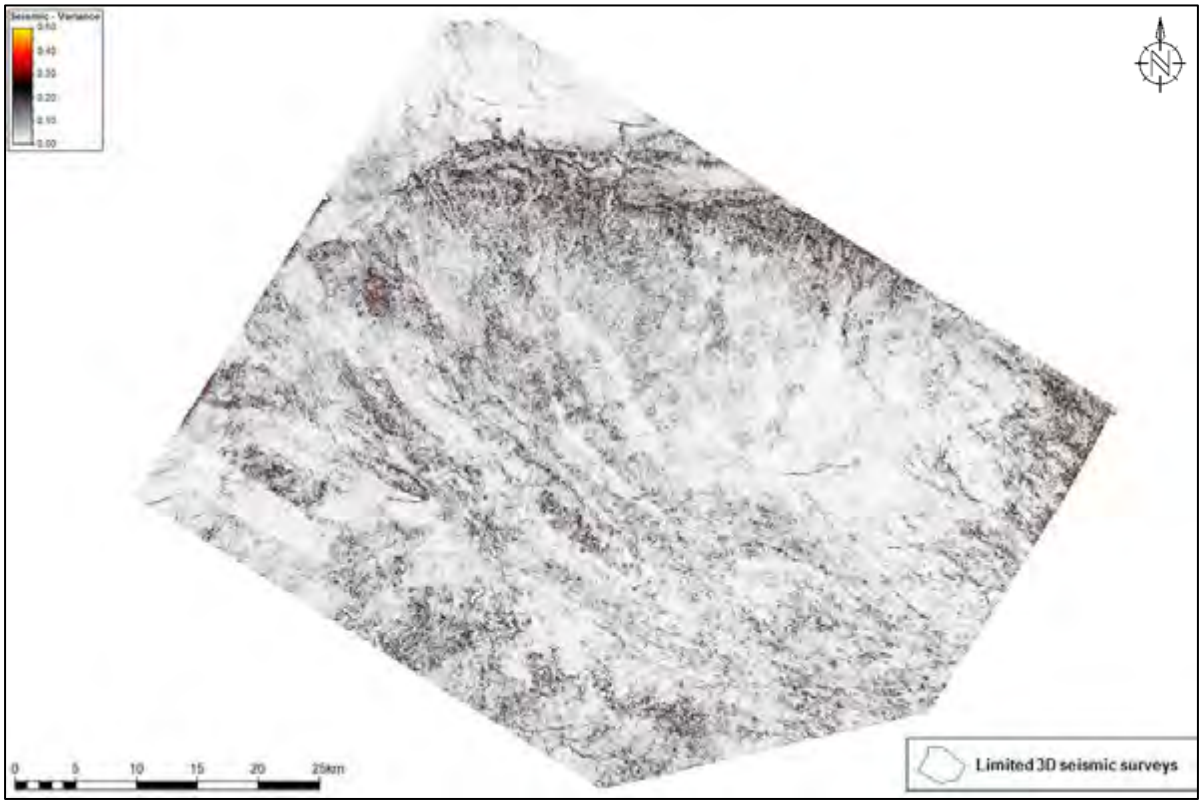

Figure 43 Seismic attribute extraction map of Variance of 13At1.

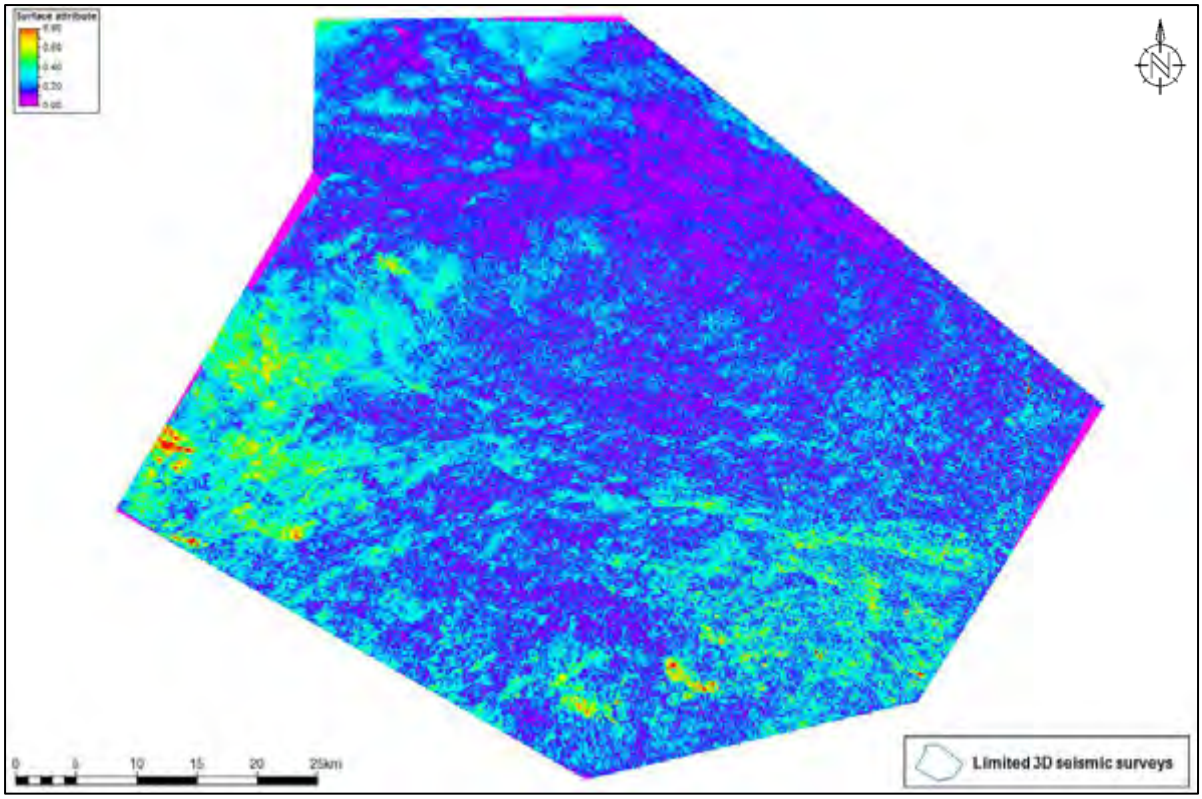

Figure 44 Seismic attribute extraction map of RMS of 14At1.

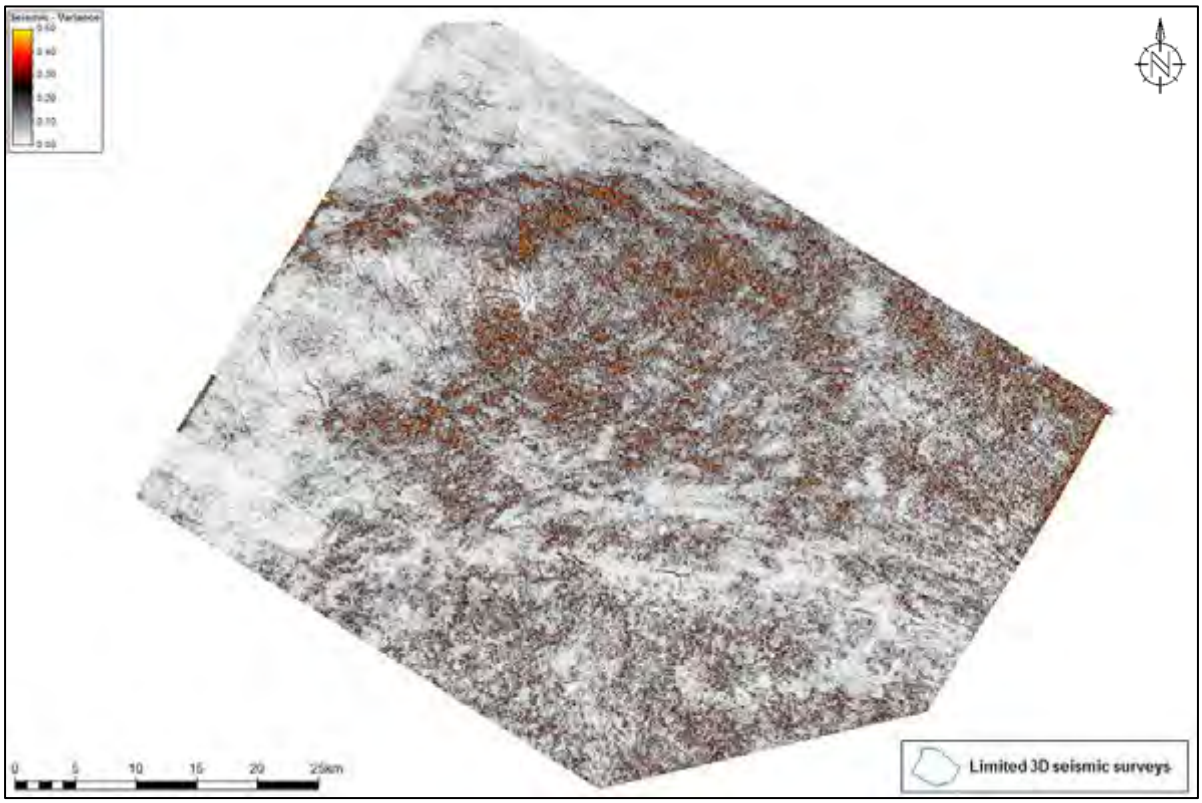

Figure 45 Seismic attribute extraction map of Variance of 14At1.

9.5 Fault Interpretation

To add a structural element to the proposed sand distribution patterns across the Central Bredasdorp Basin faults extending from the Basement upwards were mapped and yielded a major NW-SE trend. A selected few subordinate faults interpreted in the central part of the map were identified as orthogonal to the main faults (with a NE-SW orientation), which may be a reflection of the tectonic stresses acting on the basin from the late Jurassic to early Cretaceous times. Not all of these faults were active for the duration of deposition from the pre-rift to the post Albian 14At1 unconformity but they may have experienced episodic reactivation as the basin was subjected to readjustment, tilting, uplift and thermal subsidence.

Overlaying the faults on the Basement time structure surface (**Figure 47**) demonstrates a reasonable fit with the topography of the basin floor at that time, as suggested by the time-based contours showing alternating mini basins and embayments along the northern margin of the basin. The 1At1 time structure surface shows the same result (**Figure 48**) with a particularly dominant, elongated depression parallel to the northern basin marginal high. There is also a series of fault-bound "transfer zones" that lie parallel to the orthogonal faults that intersect the Basement and 1At1 maps, based on the concept illustrated in **Figure 46**. The fact that these fault-bound transfer zones coincidentally mirror the sequence thickness-based transfer zones (as discussed in *section 9.3: Isochron Maps*), probes further investigation into the deeper-seated physical controls on the distribution of the 13A and 14A sequence sands and the likelihood of sand distribution also being influenced by the relay ramp structural mechanism in the faulted Central Bredasdorp Basin.

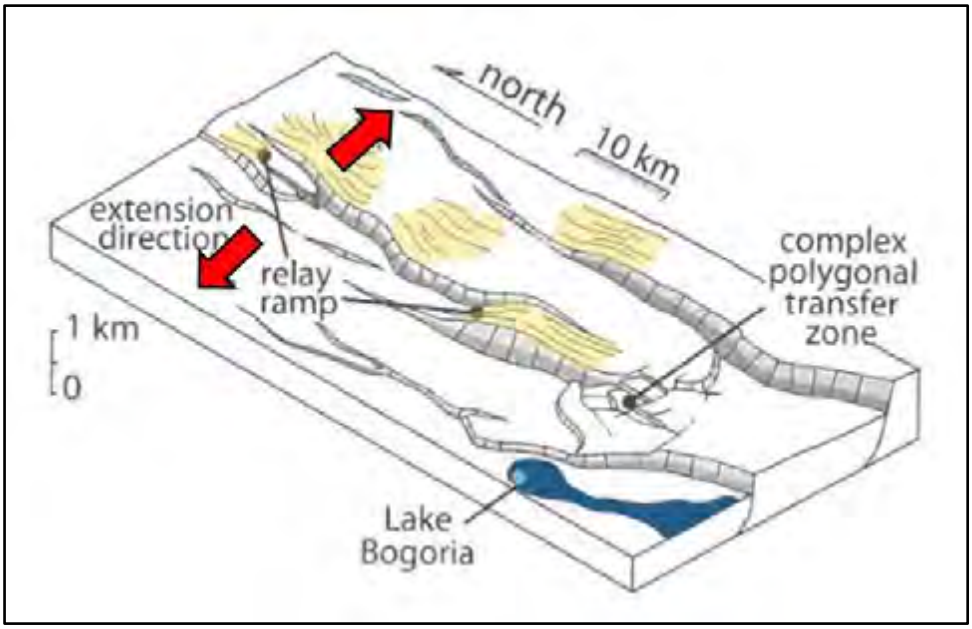

Figure 46 Schematic of fault-controlled transfer zones in an extensional environment, based on the East African Rift system (Modified from Burbank and Anderson (2012)).

Overlaying the faults on the 13At1 and 14At1 time structure surfaces (**Figures 49** and **50**) does not indicate a relationship as clearly as that displayed between the Basement and 1At1 maps and their

respective faults. A link can, however, be made between the deepening direction trend of the surfaces and the orientation of the main faults with the depocentre of the Aptian (13At1) and Albian (14At1) surfaces in the south/southeast part of the Central Bredasdorp Basin deepening from the north/northwest. The contours on the maps do not show any suggestion of the orthogonal fault-bound transfer zones so the tectonic activity that initiated them must have terminated before the Aptian time. This is also suggested in **Figure 51** in which the seismic section across the basin illustrates the cross-sectional view of the variation of thickness of the 13A and 14A sequences, whilst the positions and vertical extent of the faults demonstrates to what degree they may have had an influence on the sand distribution with the faults regularly intersecting the 13At1 horizon but not often reaching the 14At1 horizon, even where the positive relief (i.e. horst) structures have formed.

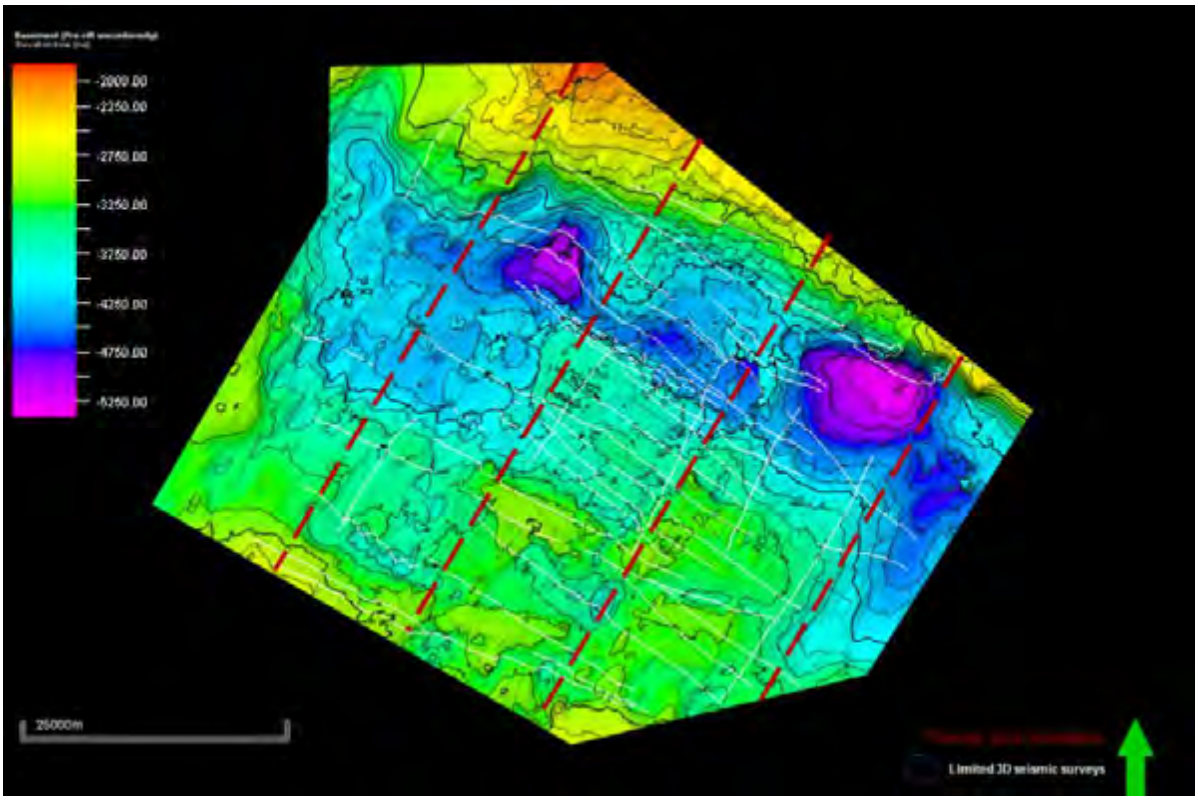

Figure 47 Time structure map showing the faults that intersect the Basement level. Dashed red lines represent the transfer zone boundaries identified based on the time structure contours of this Basement surface and coinciding with the transfer zones identified on the 13A and 14A gross isochron maps.

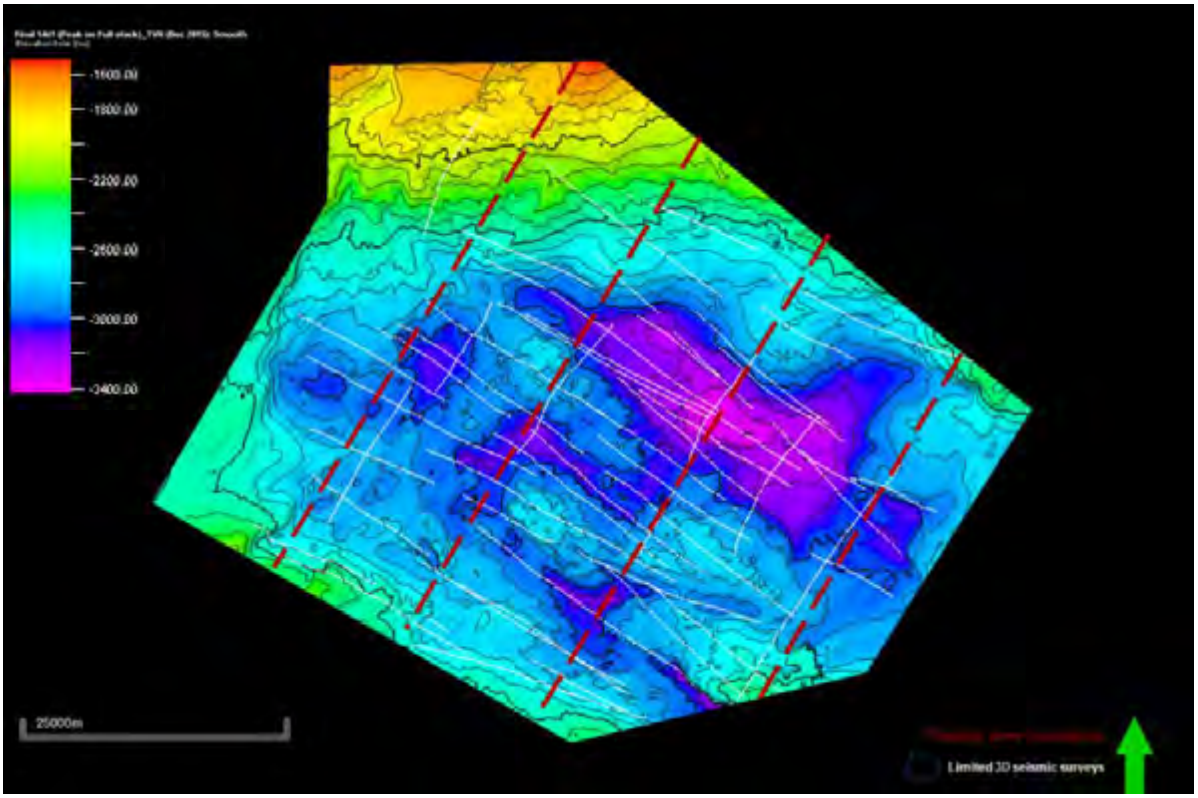

Figure 48 Time structure map showing the faults that intersect the 1At1 level. Dashed red lines represent the transfer zone boundaries identified based on time structure contours of this 1At1 surface, and coinciding with the transfer zones on the 13A and 14A gross isochron maps.

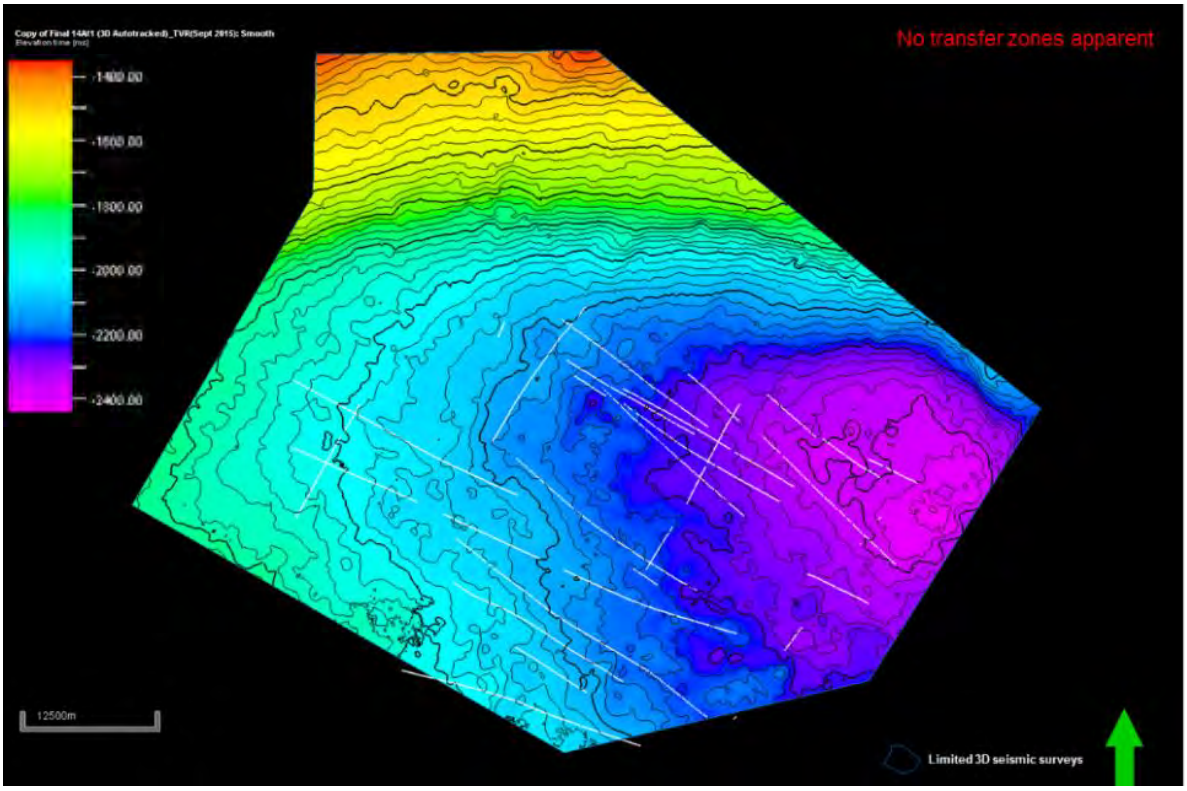

Figure 49 Time structure map showing the faults that intersect the 13At1 level. No transfer zones are evident from the time structure contours on the 13At1 surface.

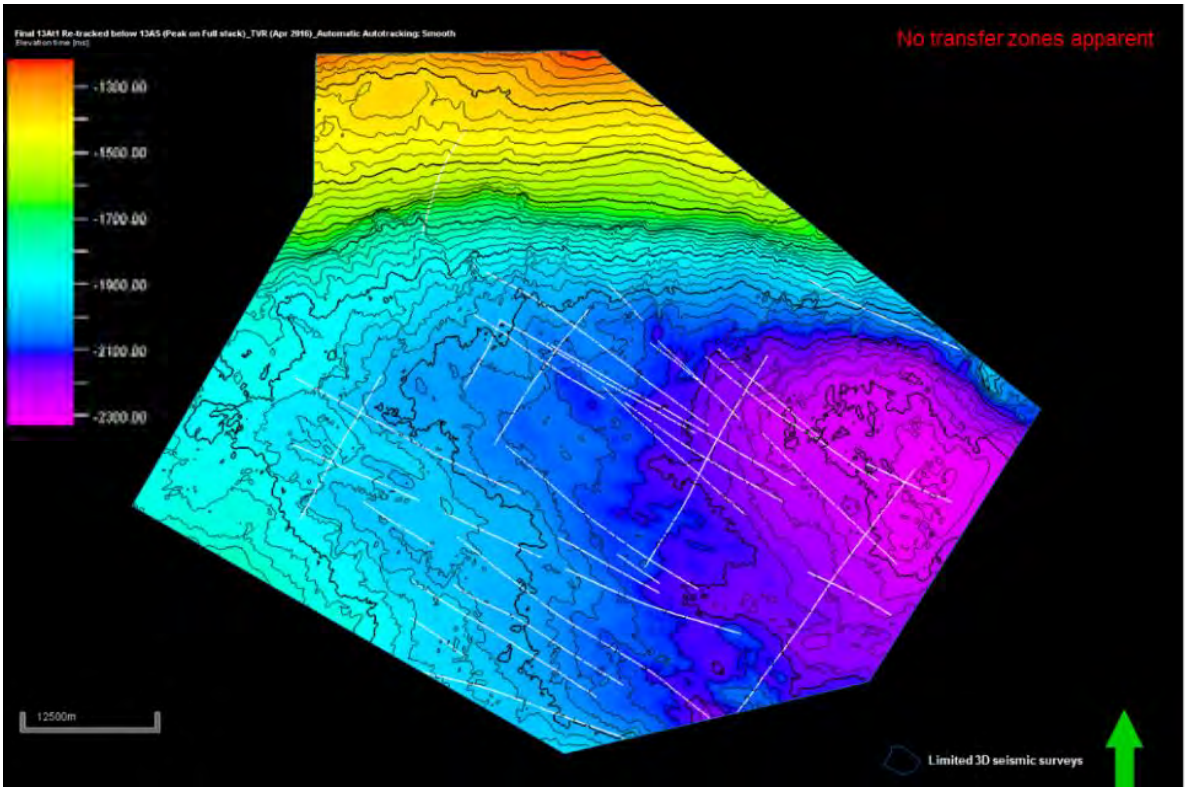

Figure 50 Time structure map showing the faults that intersect the 14At1 level. No transfer zones are evident from the time structure contours on the 14At1 surface.

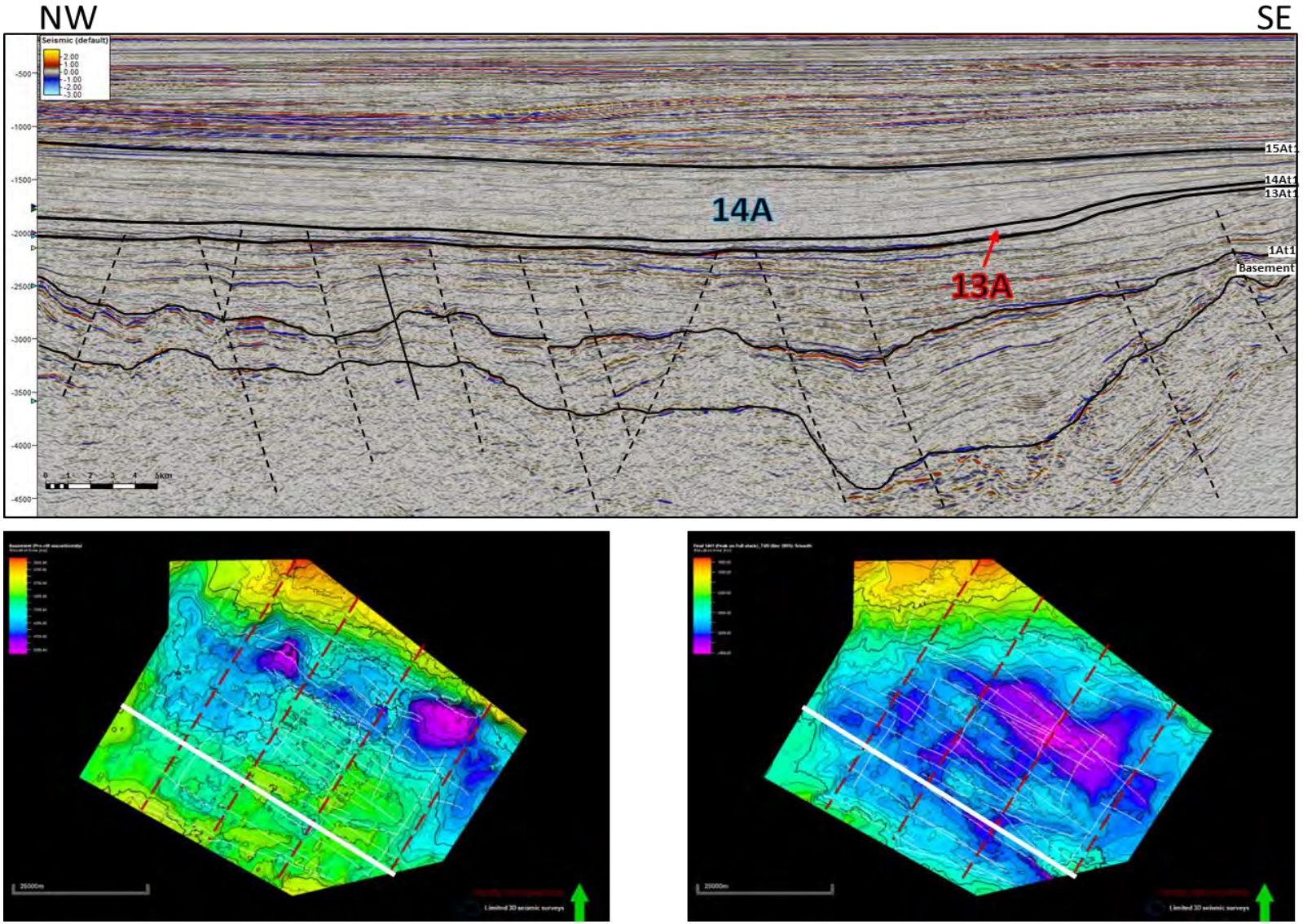
NW
SE
Seismic (default)
2.00
1.00
0.00
-1.00
-2.00
-3.00
-500
-1000
-1500
-2000
-2500
-3000
-3500
-4000
-4500
0 1 2 3 4 5km
15At1
14At1
13At1
14A
13A
1At1
Basement

Figure 51 Seismic cross-section from west to east across the Central Bredasdorp Basin, illustrating the thickness of the 14A and 13A sequences in relation to the position of the transfer zones and the underlying structure of 1At1 and the Basement surfaces below.

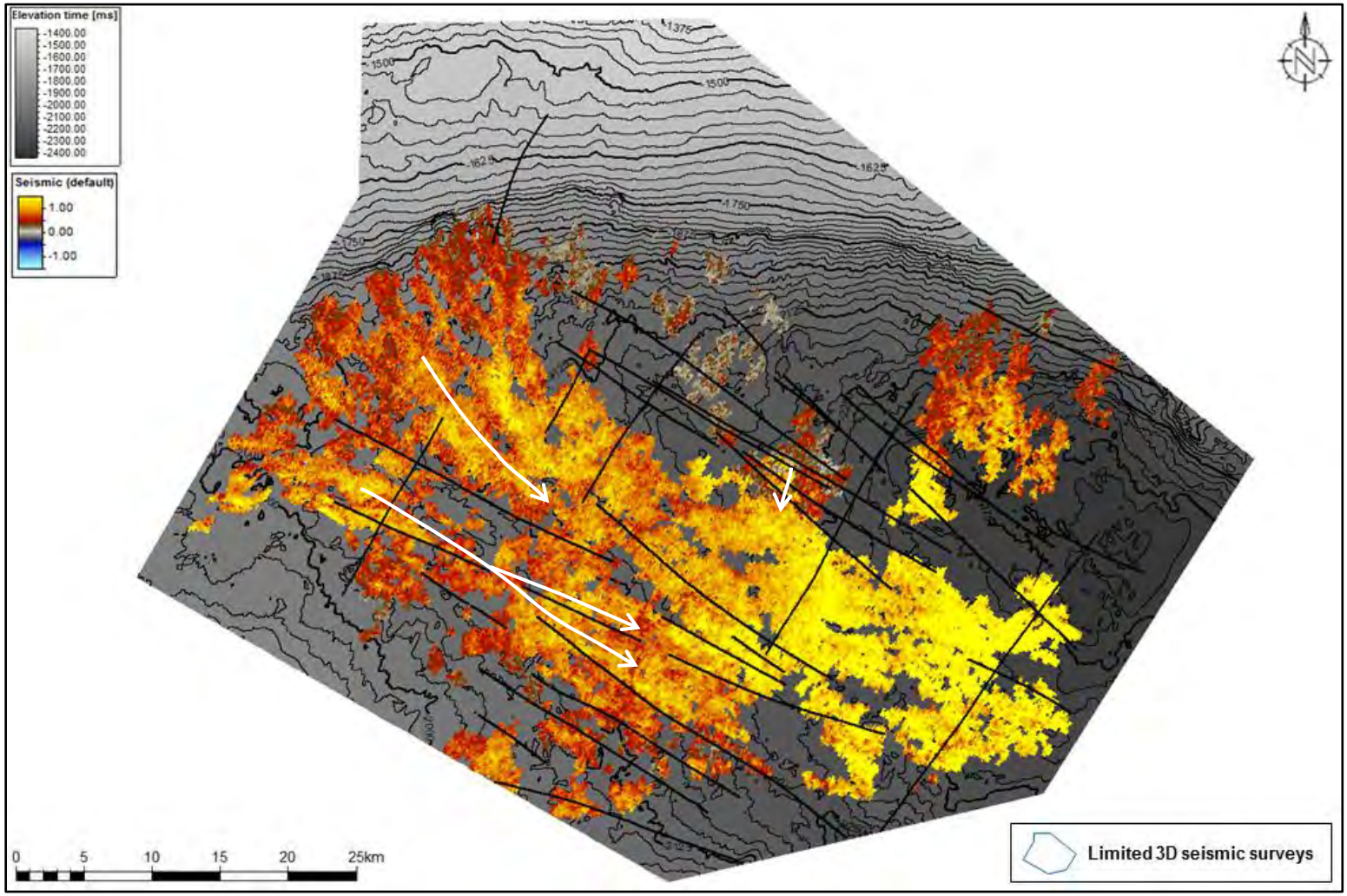

Figure 52 Time structure map overlain with sand base amplitude map and the intersecting faults for 13At1. Annotated with the main sand transport direction (white arrows).

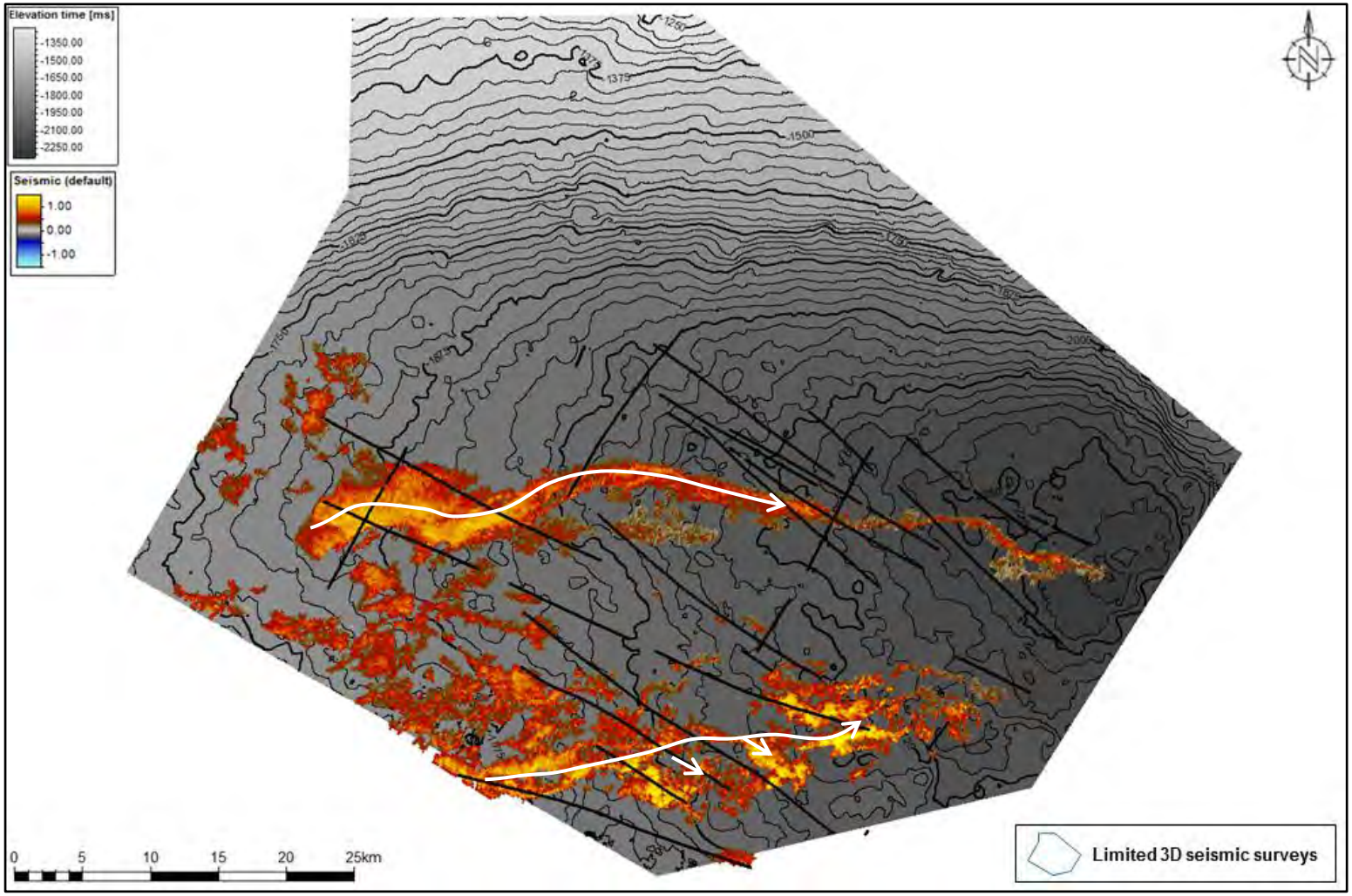

Figure 53 Time structure map overlain with sand base amplitude map and the intersecting faults for 14At1. Annotated with the main sand transport direction (white arrows).

Looking more specifically at the interaction of the structural contours of the 13At1 time surface with the intersecting faults and 13A sand base amplitude map (**Figure 52**), there is again a clear indication that the main faults played a role in physically controlling the pattern of 13A sand deposition, possibly acting as conduits from the source to the main basin depocentre because they appear to run parallel to some of the more obvious channel and fan-lobes. The orthogonal faults do not appear to have as much of an influence but they are present at the termination of some of the fan-lobes across the eastern part of the central basin.

Looking at the interaction of the faults with the 14At1 time structure surface and 14A sand base amplitude map (**Figure 53**) there is a subtle relationship between the bright positive amplitudes representing the 14A sands and the pattern of the time structure contours and is no clear form of depositional guidance by the main or orthogonal faults. A slight divergence of the general west-to-east- trend of the sands may suggest some underlying structural influence or perhaps that the faults are playing a role other than that of confining the mass sand flows.

Considering the above findings but using literature and previous studies for support, **Figures 54** and **55** show several images of the 13A and 14A sequence sands and the faults present around those intervals. The 3D views of the amplitude map-based representation of the sands' depositional extent give a good exaggerated impression of the interplay with fault presence. The orientation of the faults at the 13A level as seen in the 3D views and in the seismic cross-section (**Figure 54 (a)**) appear to guide the sands from the source and off the paleo shelf/shelf edge in the north/northwest towards the south before taking a gentle swing towards the eastern part of the basin. The 13A gross thickness map also illustrates a coincidental presence of many faults in the north/northeast corner of the basin and the limited presence-to-absence of the 13A sequence, suggesting again that the faults may play a significant role in guiding sand distribution. This model of fault controlled sand deposition is reflected in the sketched block diagram from Patton (2015) (www.earthjay.com) in **Figure 54 (a)** in which submarine fans are fed with sedimentary input from fault-controlled slope basins and splay from the steep slope of the faulted accretionary prism (~basin margin high) onto the base of slope-basin floor environment where sediments are suspended and transported in lobes and fan channels into a (possibly fault-guided) submarine channel. In the seismic cross-section (**Figure 54 (b)**), taken perpendicular to the main transport direction of the 13A sand deposits, the sands appear as well-confined into channels by the faults and are even accumulated above older horst-like structures which suggests that there was post-depositional uplift.

For the 14A sands the 3D views, seismic cross-section and maps of the 14A sequence does not give a strong indication of the faults playing a role in influencing the pattern of sand deposition. The images do, however, confirm prior suggestions that the faults were playing a role other than confining the mass sand flows by rather creating a terraces-like topography at the 14A level over which the 14A channel sands "jumped" and became diverted as a zigzag or meandering-like pattern across the basin floor from west to east. This model of fault control of sand deposition is reflected in the sketched block diagram in **Figure 55 (a)** (www.geologycafe.com) which depicts how offset faults can cause a diversion of fluvial drainage which can be applied to the Bredasdorp Basin in a submarine

environment in which offset faults laterally and perhaps slightly vertical deflected the channelised mass flow sands of the 14A sequence between the base of slope and the main basin depocentre environments. This is particularly clear in the seismic cross-section (**Figure 55 (b)**) taken perpendicular to the northern fairway axis.

Generally, the faults of the literature-based set and the interpreted set of this study follow the same NW-SE trend identified so far in this study (**Figure 56**). The literature-based faults are more extensive across the Bredasdorp Basin and appear to extend alongside the margins of the basin on a regional scale in comparison to the faults interpreted in this study which are concentrated in the Central Bredasdorp Basin. The literature-based faults do not appear to offer much additional control to the distribution of the 13A and 14A sands in this study but they served as a subtle guide and good comparative structural interpretation in general the regional character of the faults.

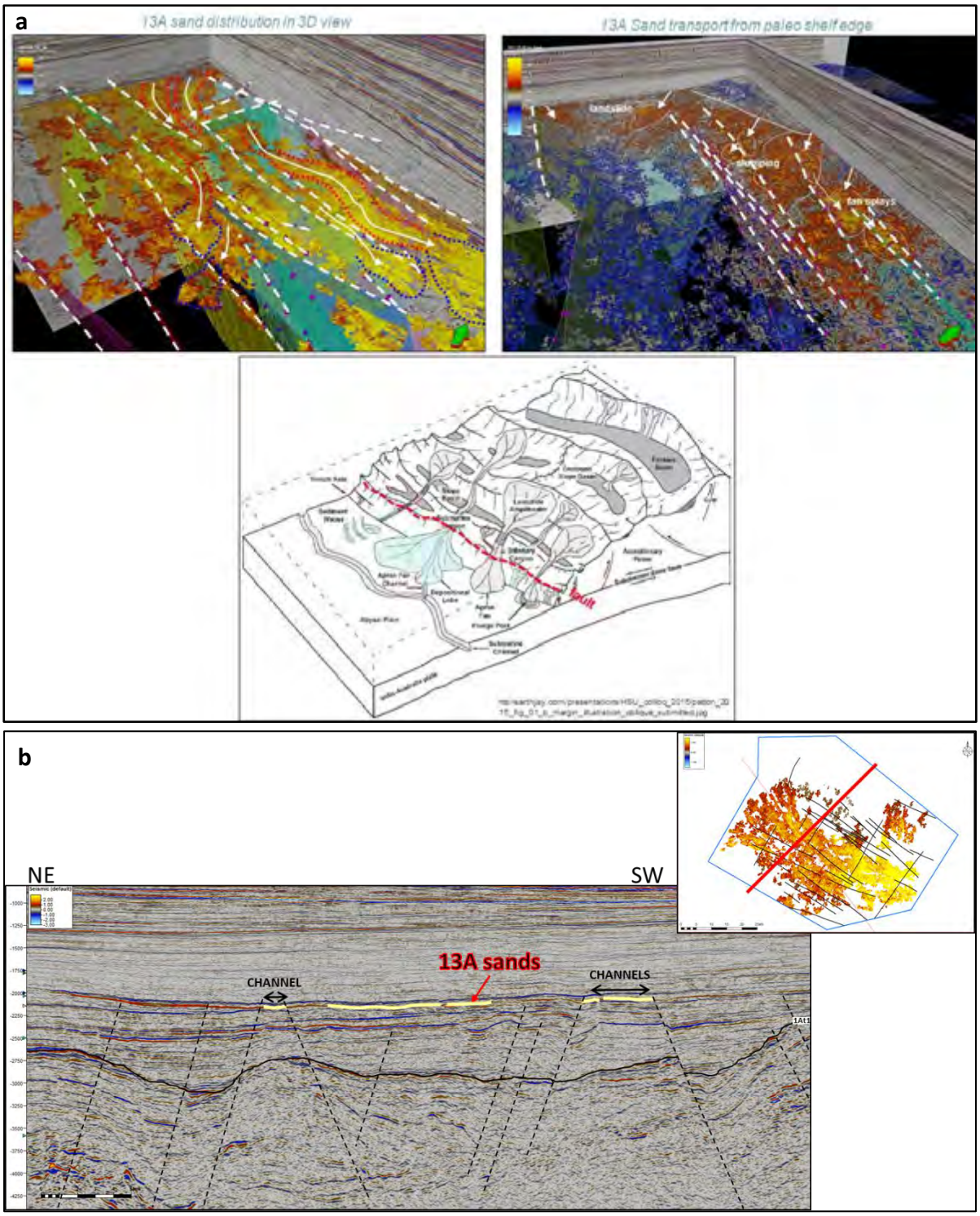

Figure 54 (a) 3D views of faults intersecting the 13A sands with a literature-based sketch model for support (www.earthjay.com) with accompanying schematics illustrating the influence of the faults on the sand flow direction and restricted distributional extent as shown in **(b)** the seismic section where sands are channelised by the faults.

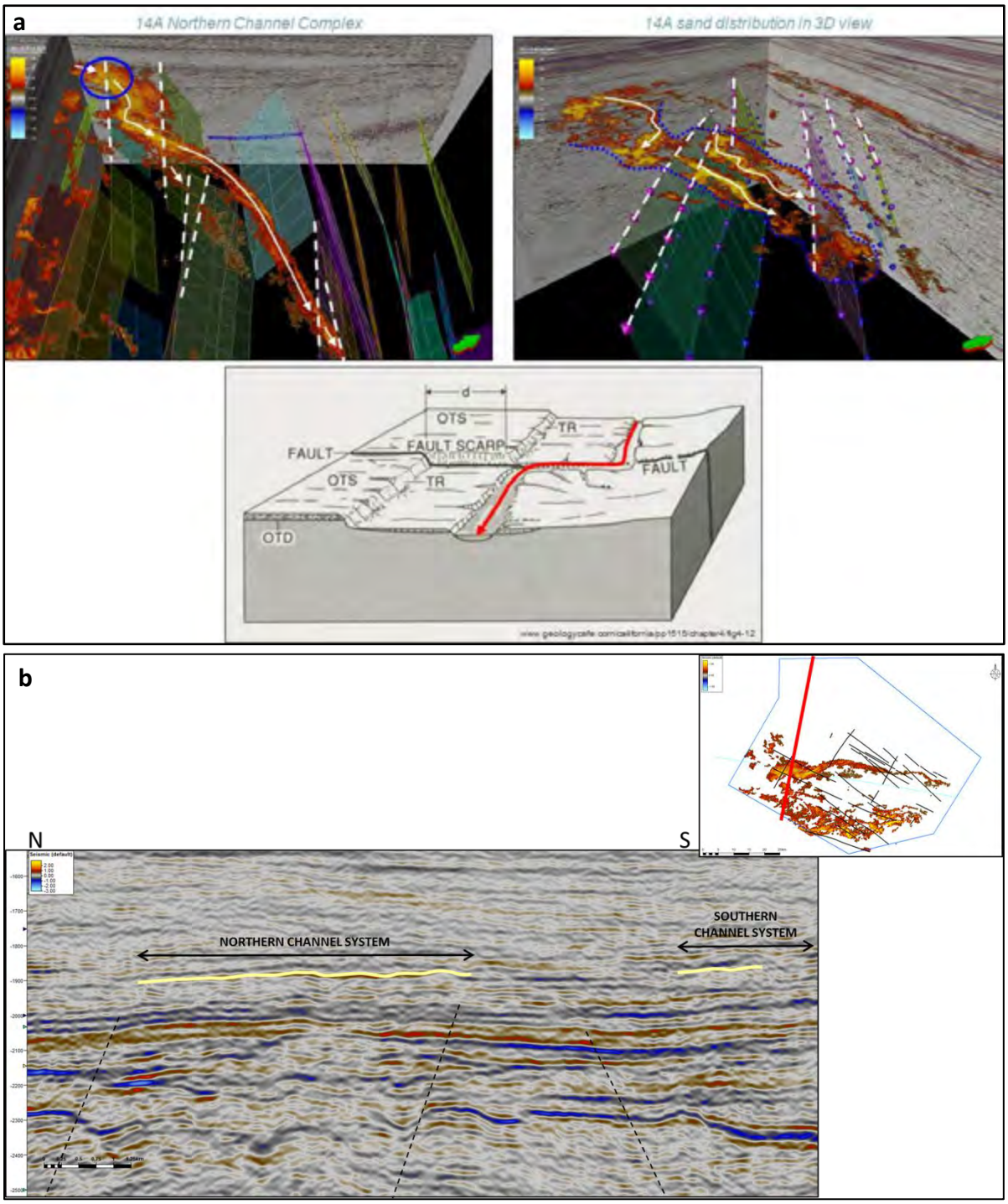

Figure 55 3D views of faults intersecting the 14A sands (**Top**) with accompanying schematics illustrating the guiding effect of the faults on the sand flow direction and distribution as shown in the seismic section in which the faults do not appear to intersect not restrict the 14A sand deposition (**Bottom**).

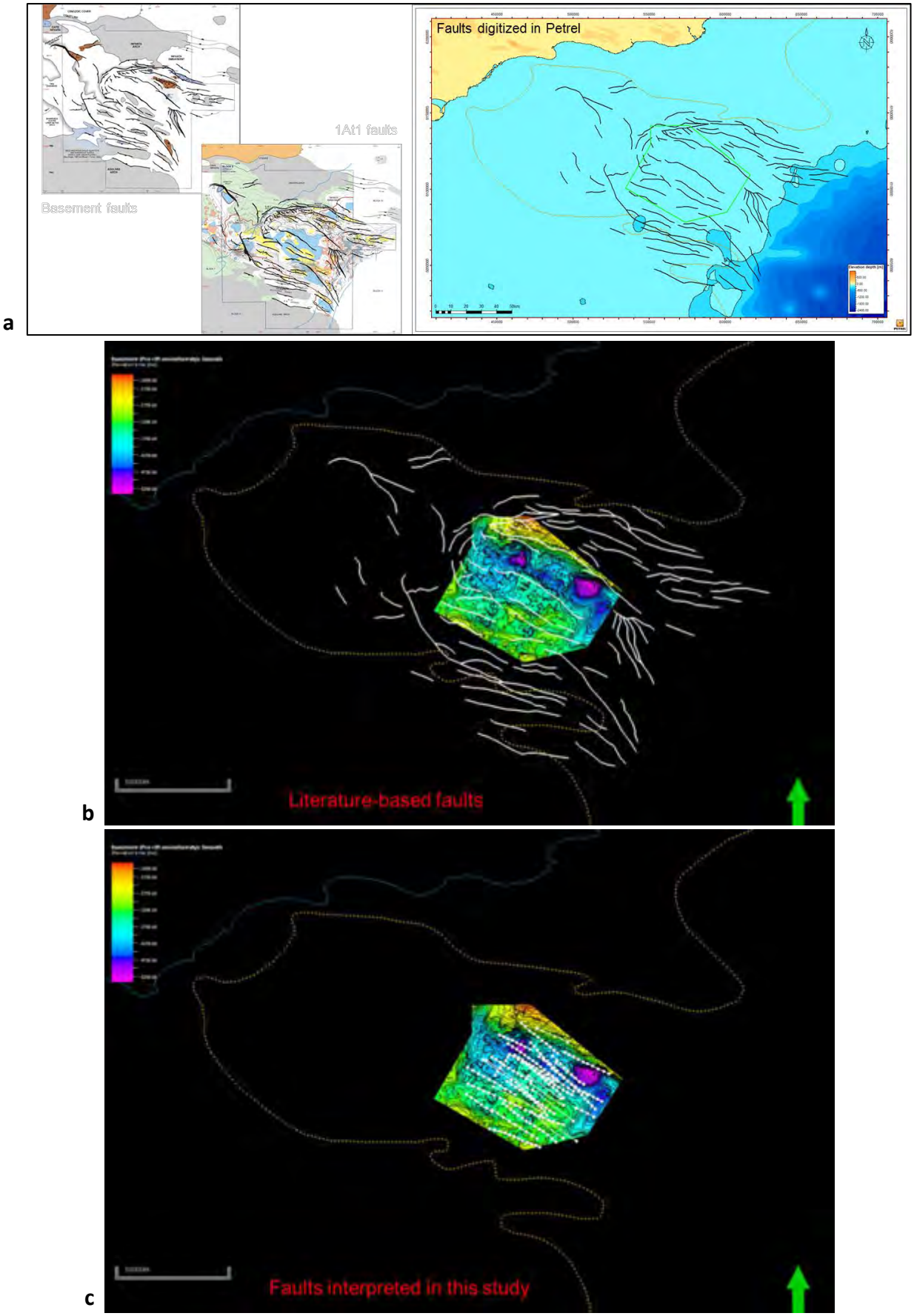

Figure 56 Images illustrating **(a, b)** the legacy faults derived from literature compared to **(c)** the faults interpreted in this study and their orientation and presence across the Central Bredasdorp Basin.

9.6 Composite Interpretation Sections

Composite interpretation sections were created to draw together the findings made from the seismic and well data sets. The seismic cross-sections were selected across the 3D seismic cubes such that they intersected some of the key wells that fell within the mapped strong positive amplitudes (i.e. sands) extent of the slope to basin floor deposits of the 13A sequence and on or close to the northern and southern fairways of the 14A sequence. This resulted in N-SE and W-E seismic sections through the 13A sequence sands (**Figures 57** and **58**) and W-E and NW-E seismic sections through the 14A sequence sands (**Figures 59** and **60**). The wells intersected by each of these seismic lines were displayed side-by-side in a correlation window in the same order that they are positioned on the map and along the extent of the seismic section so that their gamma log motifs could be interpreted to identify the type of mass transport sand deposit and the likely depositional environment intersected by each well (as described in *section 9.5: Fault Interpretation*). A comparison was made with the interpreted sand deposit types and environments recorded in the well completion reports (as summarised in **Table 2**) but it was decided to use the interpretations made in this study instead, as they took into account a number of additional factors as influenced by the development in skills and knowledge gained since those times. To emphasize the variation in sand thickness across the basin, "flattening" was applied in the well correlation windows to align the wells based on a specified well marker, for example 13At1 for the 13A sequence and 14At1 for the 14A sequence. To ultimately take into account the element of fault control on sand deposition and basin structure, the seismic horizons and interpreted faults are displayed on the seismic cross-sections in which the older pre-rift to syn-rift phases of structural geology appear the most dominant in terms of structural relief variability.

Based on **Figures 57** and **58**, the 13A amplitude map offers a high level trend of the 13A sand distribution cross the Central Bredasdorp Basin, which is sufficient detail for the scope of this study. Interpreting the 13A Sand Base using 3D autotracking of the brightest peak segments of the 13At1 trough-peak pairs produced the amplitude map mentioned above; and the 12A sand top surface was interpreted using the same principle to offer some guidance in verifying the distribution of the 13A sands. This was considered feasible since there is a short time lag of ~2 million years between the deposition of the 12A and 13A sequence sands. Using the sand fraction pie charts for the 13A zone, there is a suggested dominance of sand with an average of ~60-75% in the wells that intersect the curved north-south to NW-SE trend of the 13A sand base interpretation amplitude map across the Central Bredasdorp Basin. Wells bearing close to or equal to 100% shale are located off the amplitude map towards the west and south. Generally, there are more wells and greater sand fraction portions in the western half of the Central Bredasdorp Basin, coinciding with a brighter yellow, strongly positive amplitude cluster, hinting at a western-sourced flow of sand in a trend towards the basin depocentre in the east at some point during the deposition of the 13A sequence. Notice how the seismic cross-section reflects this structure too with sedimentary input from the north and small irregularities in the 13A package being a partial reflection of the underlying structural features. The above observation also agrees with the theory of the 14A sand source location (**Figure 36**); and these findings support the interpretation of the amplitude map as a viable sand distribution indicator. Cross-checking the above statements with the interpretative records in the key wells reports verifies

the interpretation of the amplitude map and validates the calculation of the 13A sand fraction pie charts. The relationship between the location of the sand-dominant fraction pie charts and the more negative values on the amplitude map is fair and the 100% shale fraction pie charts and the lack of positive amplitude values is moderate. The reports also give more specific information about the sands intersected in the 13A sequence, such as their abundance, the facies type and the depositional environment.

Based on **Figures 59** and **60**, the brightest and most positive values on the 14A amplitude map fall within the proximal and central part of the northern fairway and are intersected by wells with sand fraction pie charts that have close to 100% sand in the 14A sequence. In the mid region of the northern fairway, the bright yellow (positive) amplitudes appear to dim out and the pie charts located at wells drilled on the outer edges of the fairway indicate a fair to good fraction of 14A sand presence of ~75%. The pie charts updip of the northern fairway gradually decrease in sand fraction presence northwards and as the amplitude map fades and becomes more negative up to 100% shale. Fewer wells intersect the southern fairway of the 14A amplitude map but they show a similar relationship with the amplitude map as those in the northern fairway. Notice how the seismic cross-section reflects the sedimentary input from the west as the 14A package thins slightly eastwards. Slight variations in the 14At1 horizon partially reflect the form of the underlying older sequences and structural features. Cross-checking the above statements with the interpretative records in the key wells reports verifies the trends of the amplitude map and validates the calculated outcomes of the sand fraction pie charts. The reports also give more specific information about the sands intersected in the 14A sequence, such as their abundance and the facies type and therefore the depositional environment too.

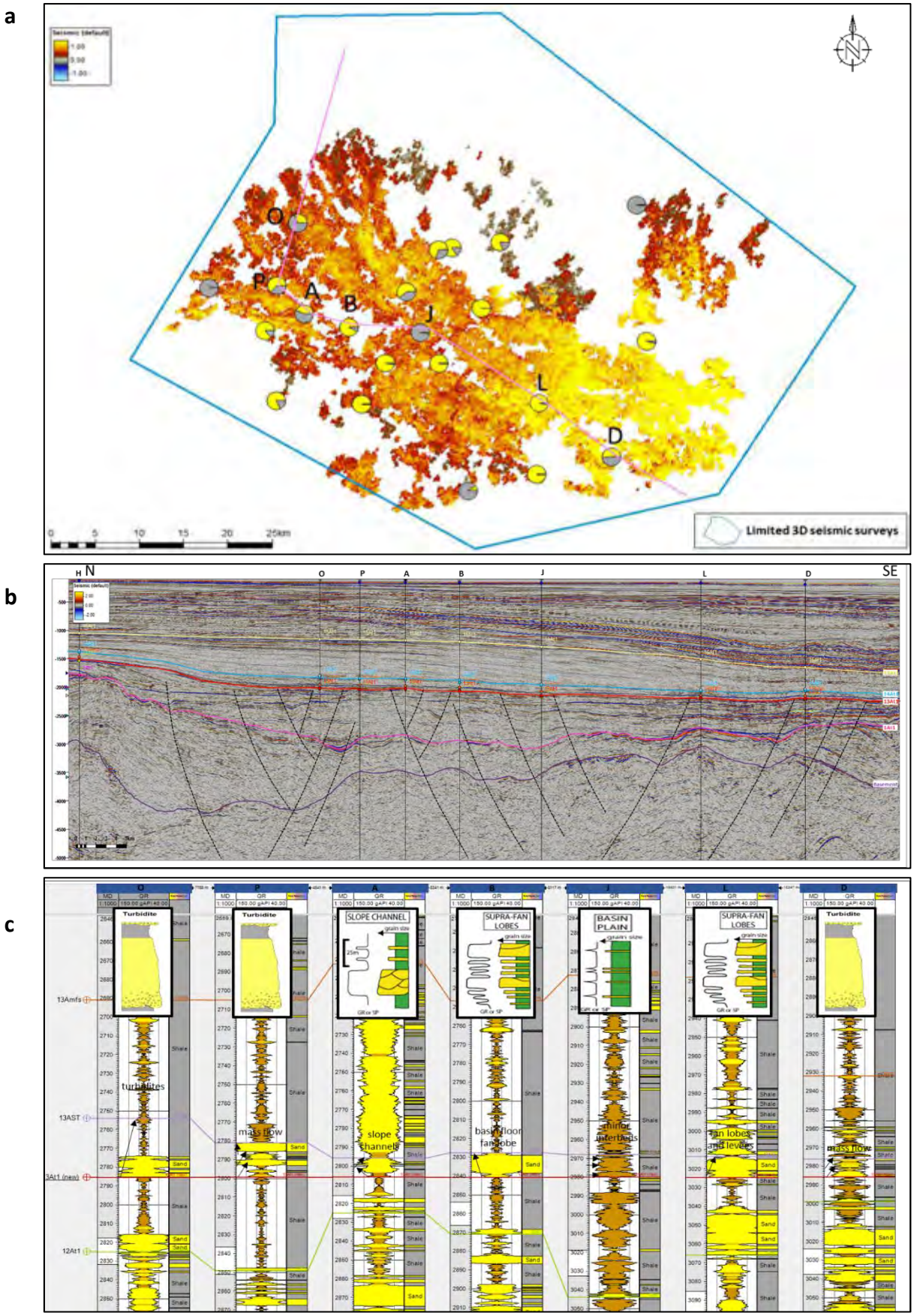

Figure 57 Key elements in the 13A sand fairway analysis. **(a)** Amplitude extraction map of the 13A sand base overlain with 13A sand fraction pie charts; **(b)** Composite seismic section through a selected few key wells with key seismic horizon interpretations and faults; **(c)** Well correlation panel with gamma ray log motif interpretations.

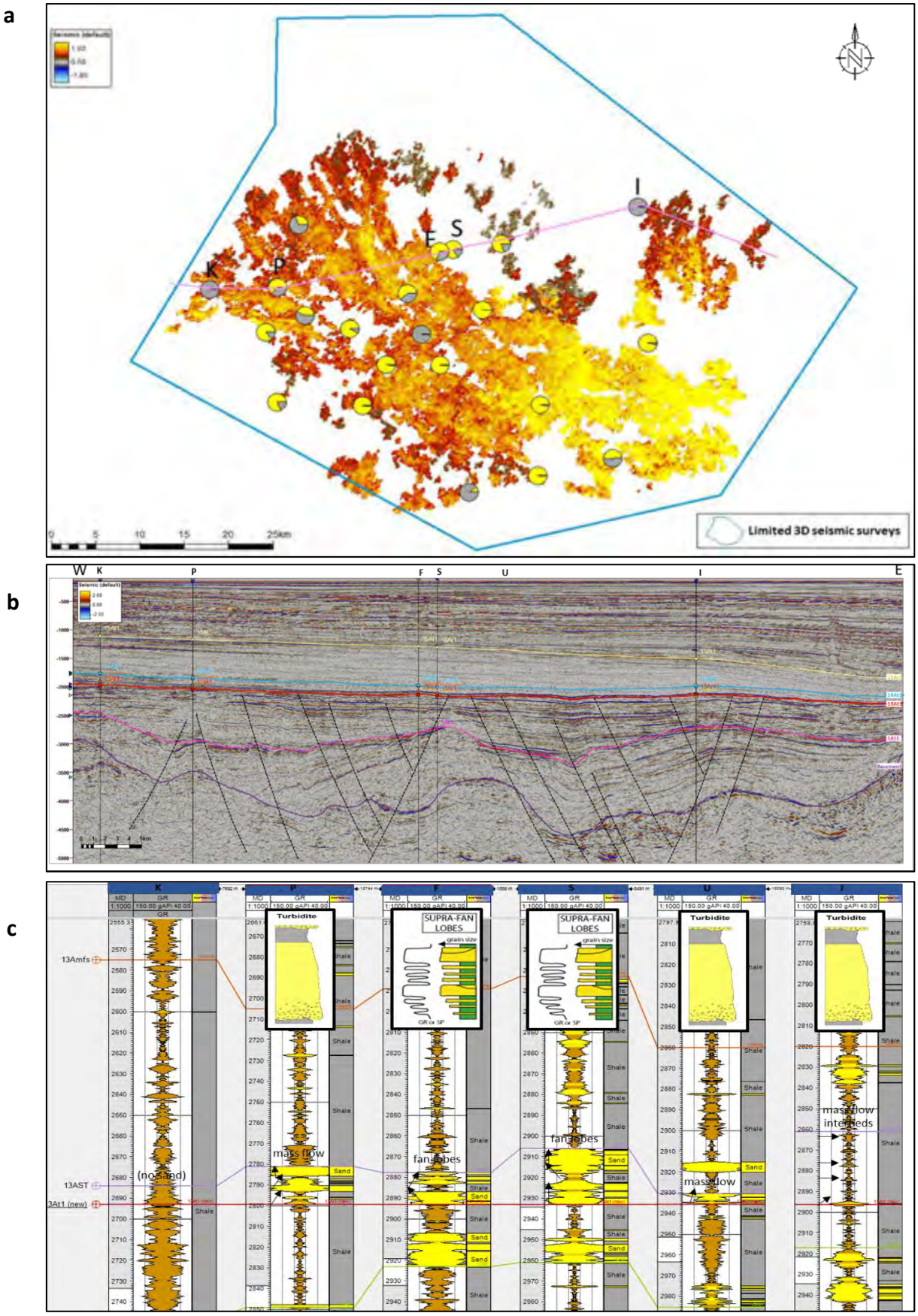

Figure 58 Key elements in the 13A sand fairway analysis. **(a)** Amplitude extraction map of the 13A sand base overlain with 13A sand fraction pie charts; **(b)** Composite seismic section through a selected few key wells with key seismic horizon interpretations and faults; **(c)** Well correlation panel with gamma ray log motif interpretations.

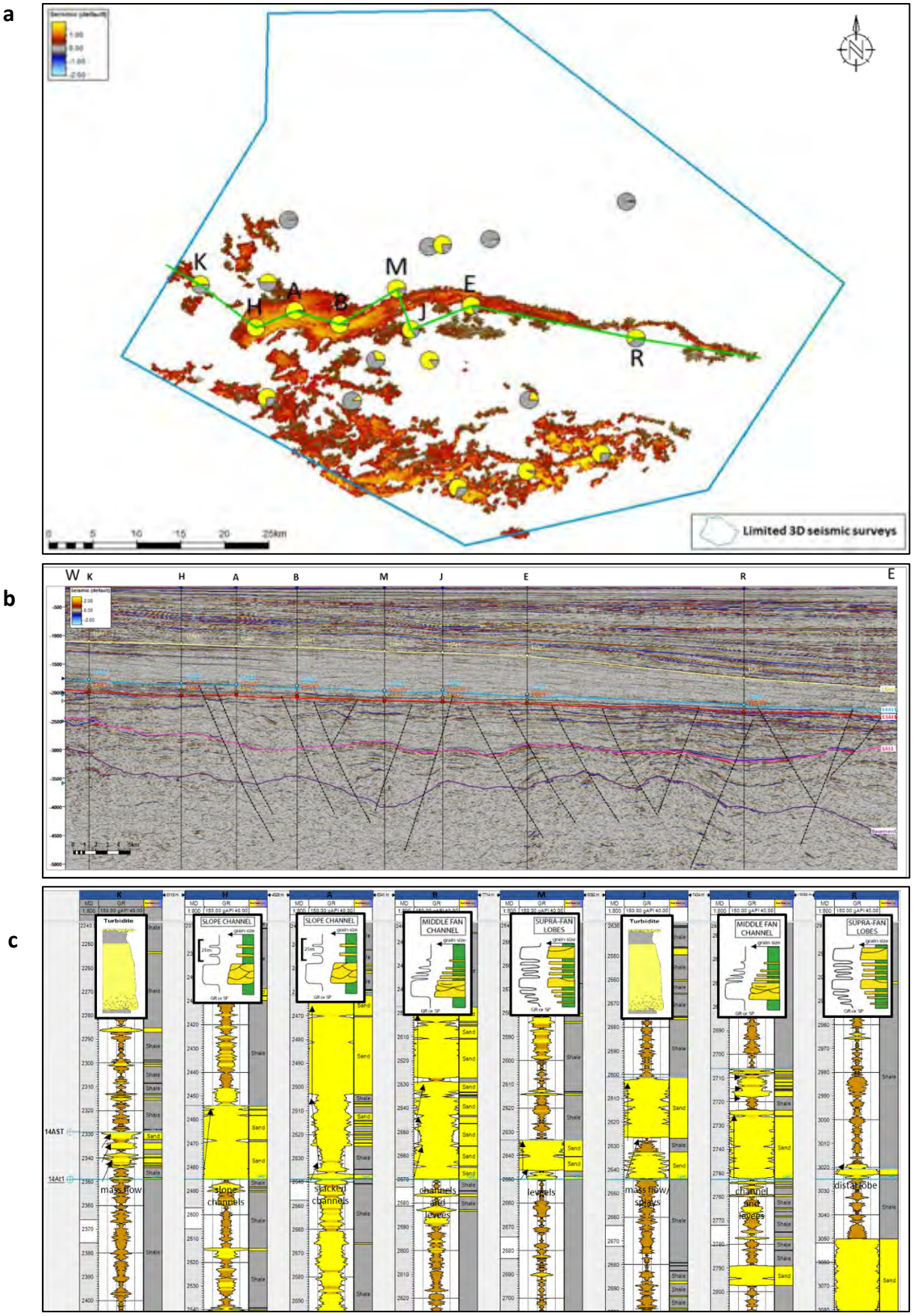

Figure 59 Key elements in the 14A northern sand fairway analysis**. (a)** Amplitude extraction map of the 14A sand base overlain with 14A sand fraction pie charts; **(b)** Composite seismic section through a selected few key wells with key seismic horizon interpretations and faults; **(c)** Well correlation panel with gamma ray log motif interpretations.

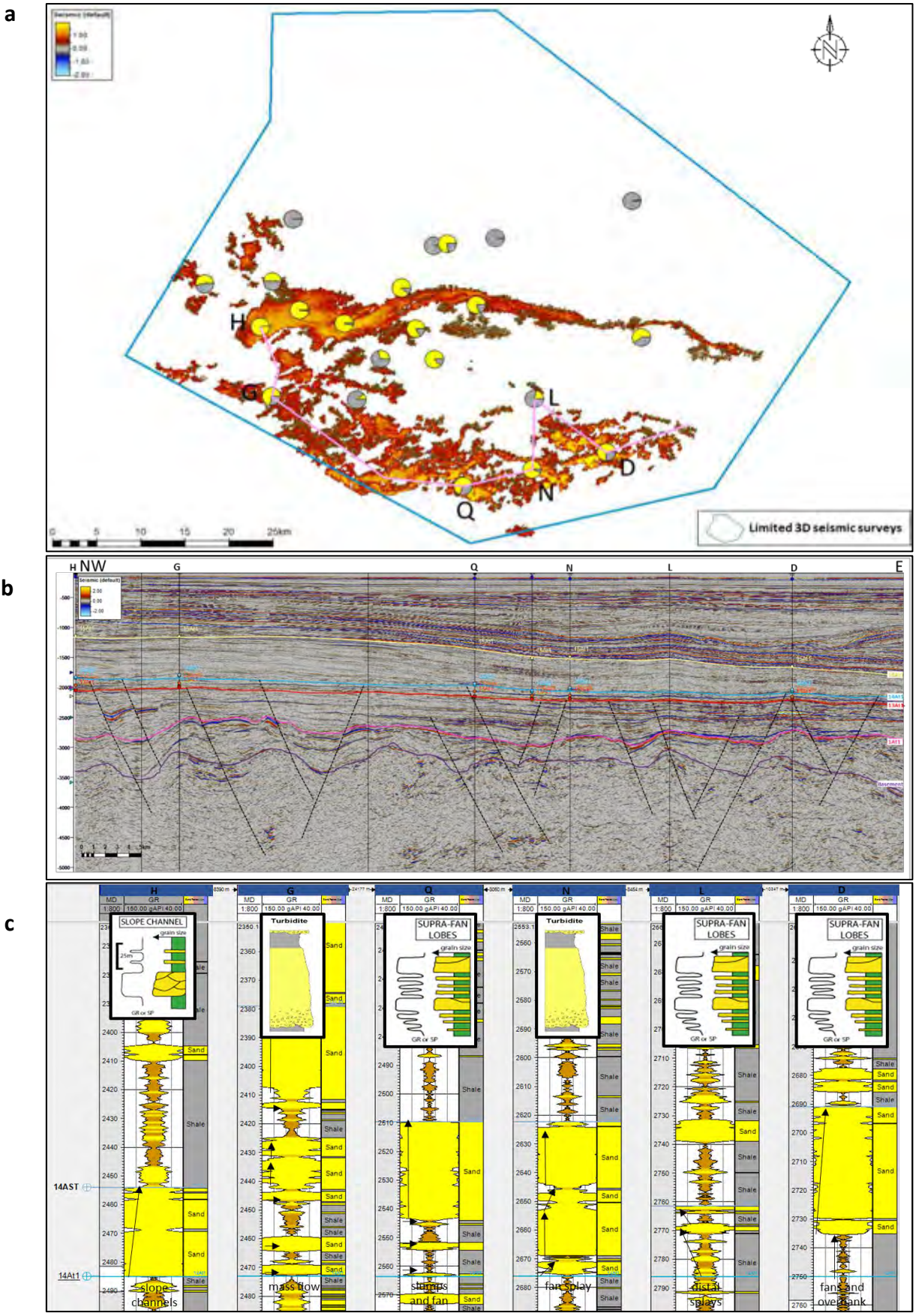

Figure 60 Key elements in the 14A southern sand fairway analysis. **(a)** Amplitude extraction map of the 14A sand base overlain with 14A sand fraction pie charts; **(b)** Composite seismic section through a selected few key wells with key seismic horizon interpretations and faults; **(c)** Well correlation panel with gamma ray log motif interpretations.

9.7 Deep Water Depositional Model

A general Aptian-Albian deep water depositional model representing the 13A and 14A sequences mass transport deposits distribution across the Central Bredasdorp Basin was generated. This exercise was performed by combining the interpretations of the horizon time structure maps, fault interpretations, seismic attribute extractions, gross isochron maps, sand fraction pie charts and gamma ray log motif interpretations to generate a 3D sketch model of the Central Bredasdorp Basin type of environment and the variety of settings within it (**Figure 61**). The schematic illustrates the range in depositional environments and associated geomorphological features that were present across the Bredasdorp Basin spanning the Aptian-Albian time, extending from the onshore fluvial source which fed sands via submarine canyons across the shallow shelf, where they accumulated on the shelf edge and ultimately flowed down slope in the form of slumps or via slope channels as the shelf edge became too unstable and collapsed. The slumped masses of sediment splayed at the base of the slope and became interbedded with sediments splayed from the slope channel terminus as base of slope fans (e.g. the 13A sequence sands) or with sediments that were suspended with enough energy to be carried in meandering channels from the slope onto the basin floor (e.g. the 14A sequence sands). Typically levees formed alongside the basin floor channels and at the channel terminus the sediments splay erratically as submarine fans and lobes (e.g. the 13A sequence sands) but pulses in energy may have driven the sediments to burst the banks of the channels as overbank splays. This gradual transition in depositional character from the onshore fluvial source to the distal submarine basin floor fans has been captured in the (gamma ray) log motifs too, which are positioned such that they reflect the different depositional settings and give an indication of the clear variation in the stratigraphic column of sand deposition across the Bredasdorp Basin. The element of fault control of sand deposition is represented in this sketch model too, where faults are illustrated as partially penetrating the seabed and subtly acting as guides in the extent of the sediment distribution, particularly the submarine basin floor fans and the older stacked channel lobes.

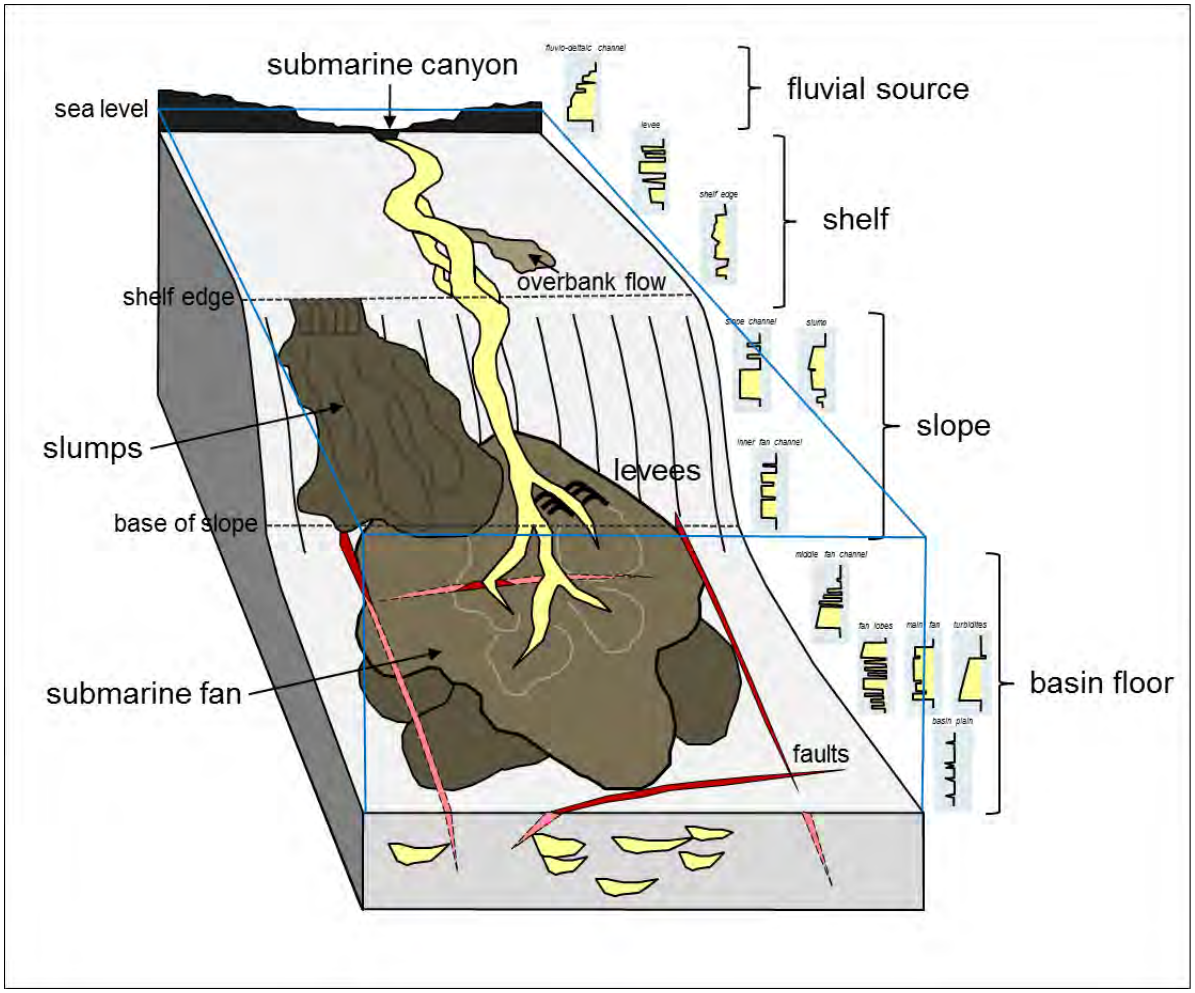

Figure 61 Summary schematic illustrating the general depositional process taking place in the Central Bredasdorp Basin during the Aptian and Albian times, represent the mass transport deposition of the 13A and 14A sequences.

Using the knowledge gained from the sketch model and the previous interpretation-based figures, **Figures 62** and **63** show the results obtained from applying the 3D horizon probe tool in Petrel in this study as a quick-look into the outcome of combining the seismic attribute properties extracted using the Variance and Sweetness algorithms. The aim of this exercise was to delineate the possible distributional trends of the 13A and 14A sequence sands using only the seismic reflection properties displayed on several random time slices through these sequences as well as at the 13At1 and 14At1 basal unconformities levels. The resulting observations and interpretations reflect those made from the seismic amplitude maps of the 13A and 14A sequences in *Chapter 9: Results*.

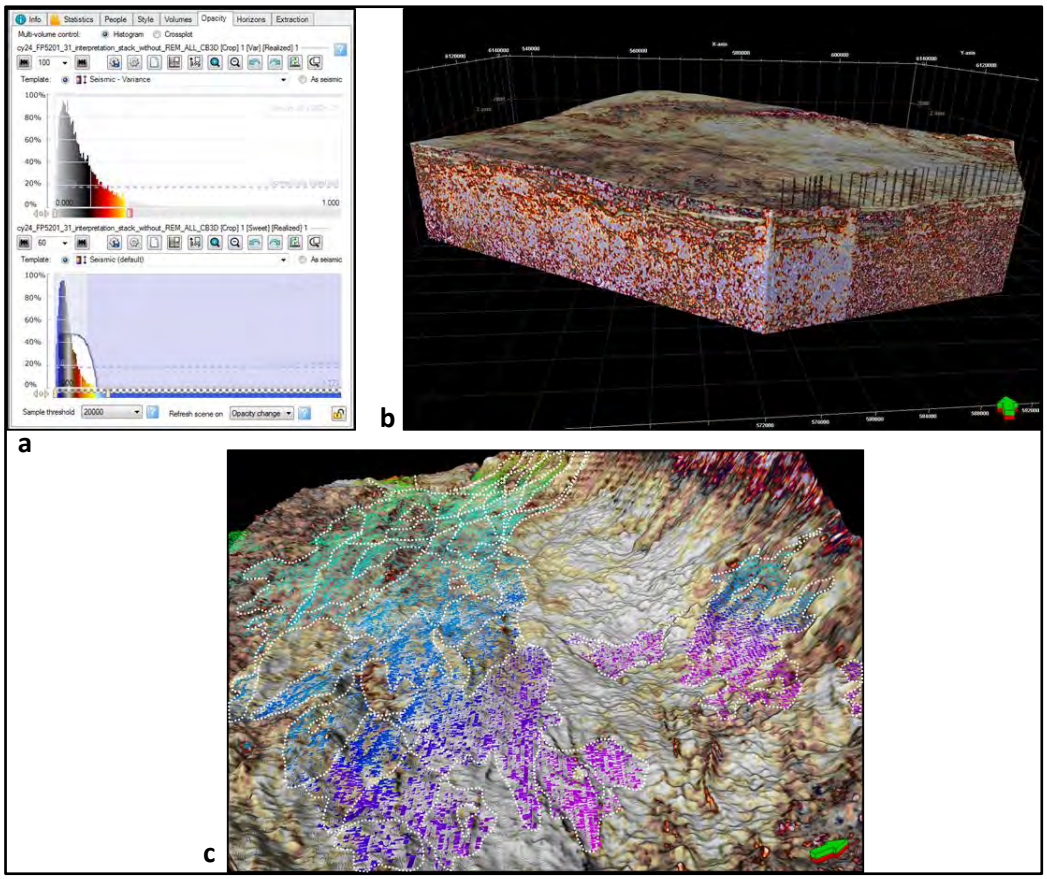

Figure 62 Horizon probe tool components are illustrated in **(a)** which captures the opacity window of the input Variance and Sweetness seismic attribute cubes. Note that the clipped colour palette for Sweetness, which is applied in **(c)** and overlain with the 13A sand interpretation surface [green-blue-purple]. The 3D view in **(b)** shows the 13At1 surface with rendering below in which some structural features are enhanced in the side walls of the cube. The 3D view of the 13At1 surface **(c)** illustrates how sand extent can be imaged using a combined cube of Variance and Sweetness.

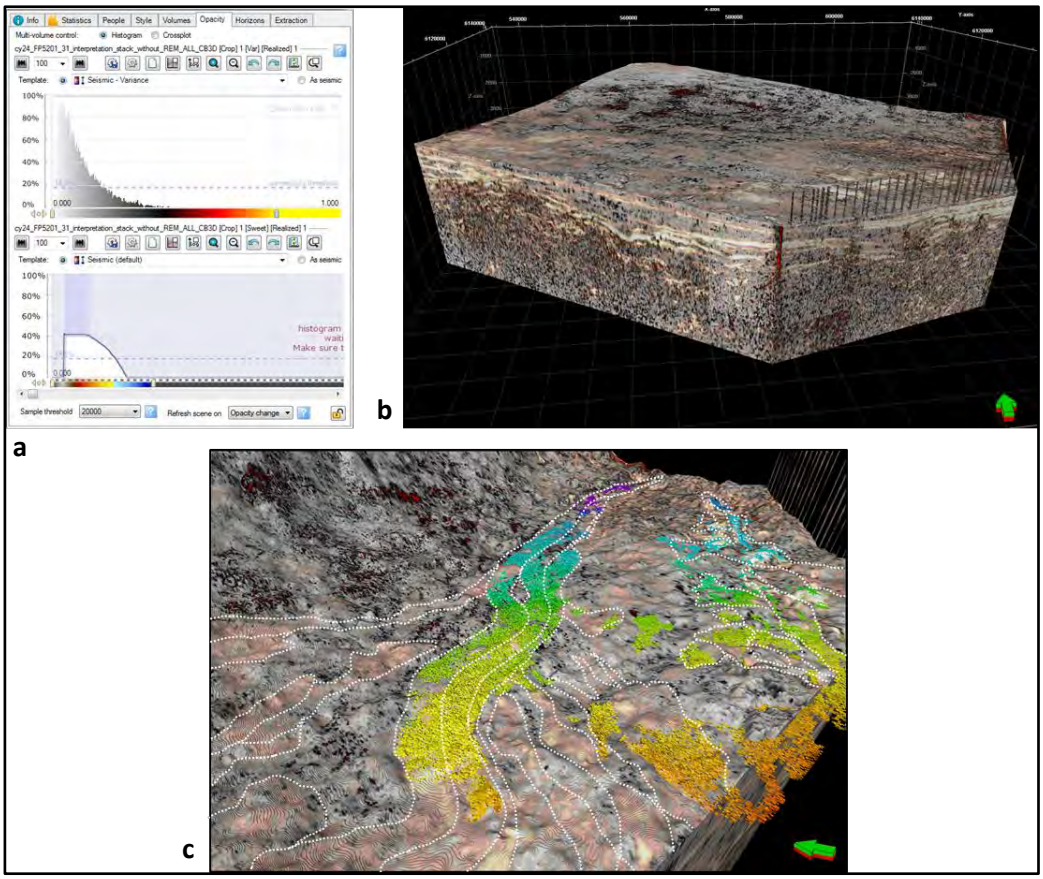

Figure 63 Horizon probe tool components are illustrated in **(a)** which captures the opacity window of the input Variance and Sweetness seismic attribute cubes. Note that the clipped colour palette for Sweetness, which is applied in **(c)** and overlain with the 14A sand interpretation surface [orange-green-purple]. The 3D view in **(b)** shows the 14At1 surface with rendering below in which some structural features are enhanced in the side walls of the cube. The 3D view of the 14At1 surface **(c)** illustrates how sand extent can be imaged using a combined cube of Variance and Sweetness.

Following the general Aptian-Albian model and the quick-look 3D horizon probe analysis, a more detailed study of the 13A and 14A sequences was carried out and led to the generation of two proposed models of sand deposition for each sequence. The schematics below (**Figures 64** and **65**) are working descriptions of the proposed depositional models described for the Aptian 13A sequence and the Albian 14A sequence, created using a combination of hard data and interpretative sketching.

9.7.1 13A Sequence Proposed Depositional Models

The Aptian-aged 13A sequence was deposited as a progradational package of continental-derived sediments during a time of a local sea level fall. The 13A sequence sands, specifically, are strongly associated with a lowstand systems tract and overall the sand distribution appears to have been guided by the NW-SE trending main faults as conduits into deeper basin where the sands eventually splayed as fans. The alternate models of the deposition of the 13A sequence sands into the Central Bredasdorp Basin are described below. See **Figure 64**.

9.7.1.1 *13A Model 1: Switching source input*

The regressive position of the coastline enabled the onshore deltaic channels to provide sedimentary input from the west and northwest directions and the falling local sea level prompted sediments to erode off the subaerially exposed basement high basin margins in the north (i.e. Infanta Arch) and in the south (i.e. Agulhas Arch). The sediments flowed primarily from the northeastern and south/southeastern corners of the Central Bredasdorp Basin into the main depocentre, driven by onshore sediment inflowing fluctuations and the effect of gravity on the stability of the sediments accumulating on the shelf edge. The steep gradient of the northern and southern basin margins provoked sediments to enter the submarine environment via the combination of mass wasting (e.g. slumps) and channels flowing down the slope and onto the basin floor. Incision of the slope with channels carried the sediments downwards to the lower slope and base of slope settings where they ultimately splayed as fans but this depositional style alternated periodically with slope slumping due to shelf edge failure due to a lack of accommodation space on the shelf coupled with the increasing weight of sediment building up on the shelf edge. Faults that were active at the time directed the sediment flow via conduits (channels) across the basin and where fault control became redundant the sedimentary load was deposited as fans and lobes. There is a subtle trend of a northern cluster of channels and fans, sourced primarily from the northwest, and a southern cluster of channels and fans, sourced apparently from the west, possibly caused by the influence of the small structural high in the central part of the basin.

9.7.1.2 *13A Model 2: Simultaneous input from multiple sources with faults driving channel avulsion*

The falling local sea level encouraged sediments to erode off the subaerially exposed basement high basin margins in the north (i.e. Infanta Arch) and in the south (i.e. Agulhas Arch), flowing into the main depocentre from the northeastern and south/southeastern corners of the Central Bredasdorp Basin. The steep gradient of the northern and southern basin margins caused sediments to enter the submarine environment through a combination of mass wasting (e.g. slumps) and channels that flowed downslope onto the basin floor with little fault influence on the sand distribution. Simultaneously, sediment was being fed from the more dominant paleo shelf source in the northwestern corner of the basin as well as from the closer fluvial-deltaic onshore source on the paleo shelf in the western margin of the basin. The more gradual gradient of the continental slopes in the northwestern margin of the basin allowed for sediments to flow from the paleo shelf and over the shelf edge via incised channels but, depending on the volume of sediment and therefore the energy of the flow, the sands were either deposited on the lower slope to base of slope setting as fans or they flowed deeper via fault-controlled meandering channels to the main depocentre in the eastern part of the central basin where the flows terminated beyond the fault control and due to a loss of energy and left the sands to settle in depressions as fans and lobes. The gradient of the western margin of the basin was even more gradual and resulted in stepwise channel and fan-lobe pulses of deposition, perhaps influenced more by flooding and other triggers of fluctuating fluvial-deltaic input. The depositional trend of the western sourced sands headed in a southeast direction with the orientation and influence of the faults. The flow then diverted around the small central basin structural high to then follow a trend approximately parallel to the southern basin

margin. However, the flow ultimately terminated on the western side of the main basin depocentre due to a loss of energy and a lack of fault controlled flow guidance.

9.7.2 14A Sequence Proposed Depositional Models

The Albian aged 14A sequence was deposited as a progradational package of continental-derived sediments during a time of a local sea level fall. The 14A sequence sands, specifically, are strongly associated with a lowstand systems tract and overall the sand distribution appears to have been guided by the paleo seabed topography (i.e. especially the previous 13A deposits) within confined channels in the northern part of the basin and as mass wasting combined with shorter channels in the southern part of the basin. The alternate models of the deposition of the 14A sequence sands into the Central Bredasdorp Basin are described below. See **Figure 65**.

9.7.2.1 14A Model 1: Simultaneous northern and southern fairway development

A falling local sea level prompted erosion of the subaerially exposed southern basin margin (i.e. Agulhas Arch) and the transport of the erosive sediments in the form of turbidity flows deeper into the basin in a northeast direction where the sediments started to settle out of suspension and form small fan-like splays of fining upward sequences. Furthermore, the regression (sea level fall) had caused a basinward shift of the shoreline and an associated influx of onshore-sourced sediment from the west/northwest direction. The weight of this additional sediment coupled with a lack of accommodation space on the shelf caused the shelf edge to become unstable and led to slope failure, mass wasting debris flows and slumps. The energy of this mass in combination with the angle of the slope promoted the downward, gravity-driven movement of the sediments onto the basin floor. Deep seated faults that were active prior to the formation of the 14At1 unconformity significantly influenced the depositional trends of the sequences older than 14A, such as those during the Aptian deposition of the 13A sequence. This left behind a basin floor topography of depressions and structural highs which ultimately influenced the depositional trend of the 14A sequence. The sediments sourced from the west/northwest margin of the basin were guided by the seabed topography into a west-east trending channel extending across the Central Bredasdorp Basin. Weak points along the banks of this confined channel were overcome by the fast flowing mass and gave rise to levees and overbank splays. As the sedimentary input continued to enter from the west/northwest, the northern fairway accumulated sands and its meander pattern led it to migrate slightly towards the south. It did not, however, flow south of the structural high observed on the gross isochron maps in the central part of the basin between the northern and southern fairways. Whilst the northern fairway was forming, the less confined southern fairway had also developed into more than just a few turbidite fans. The steady input of sediment from the basin margin basement high in the southwest/south continually formed fans on the mid slope to base of slope. Amongst these fans there was also the development of some slope channels that carried the sands deeper into the basin depocentre and some even developed levees. The southern fairway appears to have a trend of sand-rich channels in the southeastern part of the basin and more mud-rich fans in the southwestern part, which is a direct reflection of the composition and sand capacity of the Agulhas Arch source.

9.7.2.2 *14A Model 2: Migrating source input*

The falling local sea level encouraged sediments to erode off the subaerially exposed southern basin margin (i.e. Agulhas Arch) to flow into the submarine Central Bredasdorp Basin. The steep gradient of the southern basement high caused sediments to enter the submarine environment via channels flowing down the slope and onto the basin floor, towards the depocentre in the east. Weak points along the banks of these channels were overcome by the fast flowing input and formed levees and overbank splays. The fourth order (local) fall in the sea level during this time, coupled with a lack of accommodation space on the shelf, caused some instability on the top of the slope/at the shelf edge and led to mass wasting. Sedimentary flows moved quickly down the slope and splayed as lower slope to base of slope fans, particularly on the southwestern part of the southern fairway of sand deposits. At the same time the channelised deposition of the sands into the main depocentre started to dwindle as the sediment source input started shifting westward and the sand concentration from the source started to decrease. Since the second order (global) sea level was on a rise, more of the southern margin basement high was flooded than it was during the Aptian deposition of the 13A sequence and this had caused onshore rivers to connect with the shoreline, which ultimately led to a later switch in the source location to the west/northwest. The energy of the onshore-derived sediment flows caused a new influx of sands to accumulate as added weight on the shelf edge and to then flow down the slope as mass transport deposits from the shelf edge. The mass transport deposit slumps and debris flows moving down the slope fed a broad channel that had formed as a west-east trending, meandering conduit which most likely originates from the inherited sea floor topography. Weak points along the banks of this confined channel were overcome by the fast flowing mass and gave rise to levees and/or overbank splays. As the source of sediment started to diminish and the northern fairway experienced a decrease in energy and sand input, the channels became narrower and shorter and meandered slightly more towards the northern margin until a change in the sea level led to the start of the transgressive systems tract deposition.

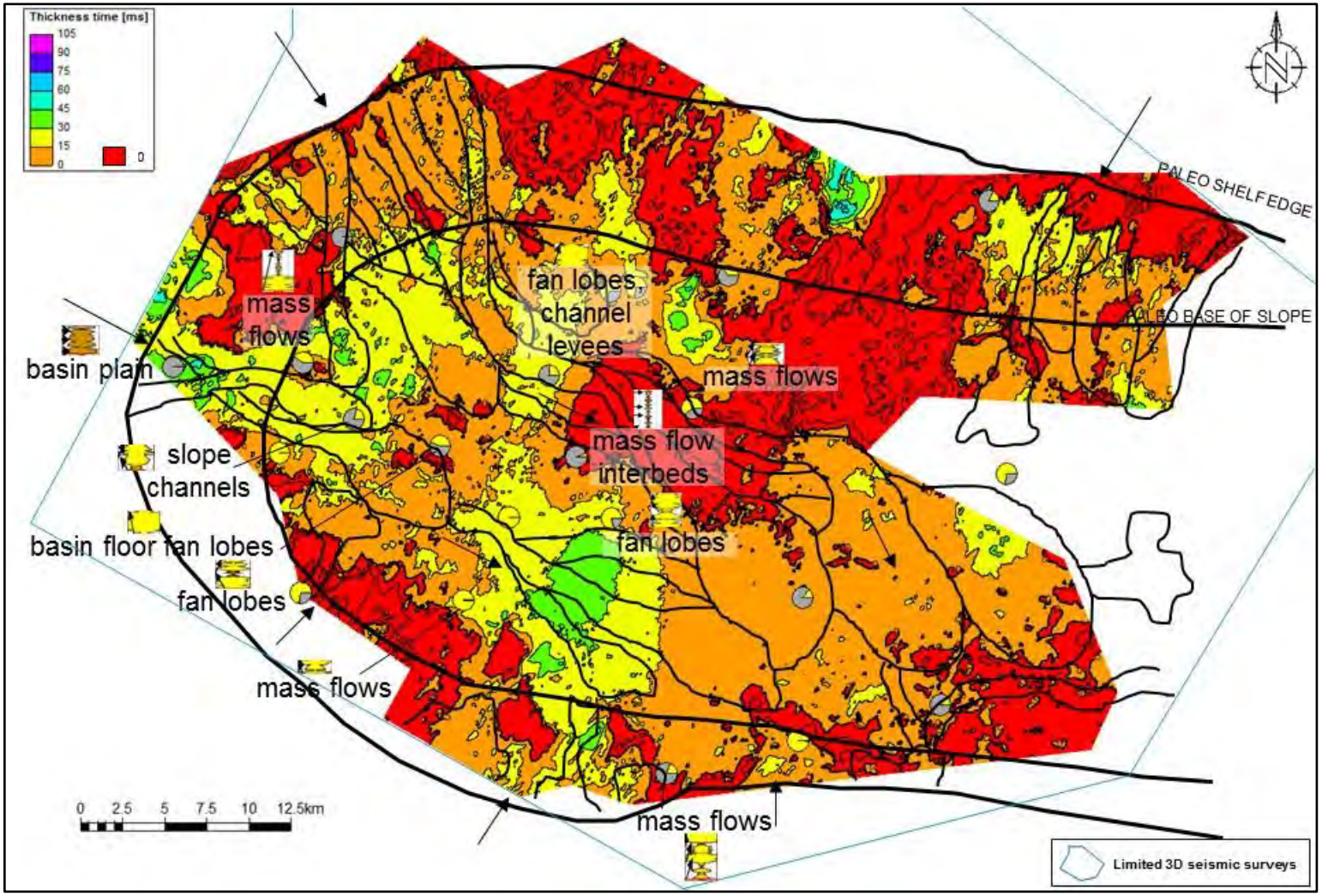

Figure 64 A summative description of the 13A depositional model. Gross isochron map of the 13A sequence (13A sand top-13At1) overlain with sand fraction pie charts at the key wells and the accompanying 13A sand segments of gamma ray log to illustrate the inferred depositional settings as supported by the overlying line drawing of the sand distribution across the basin, based on the 13A sand base amplitude map.

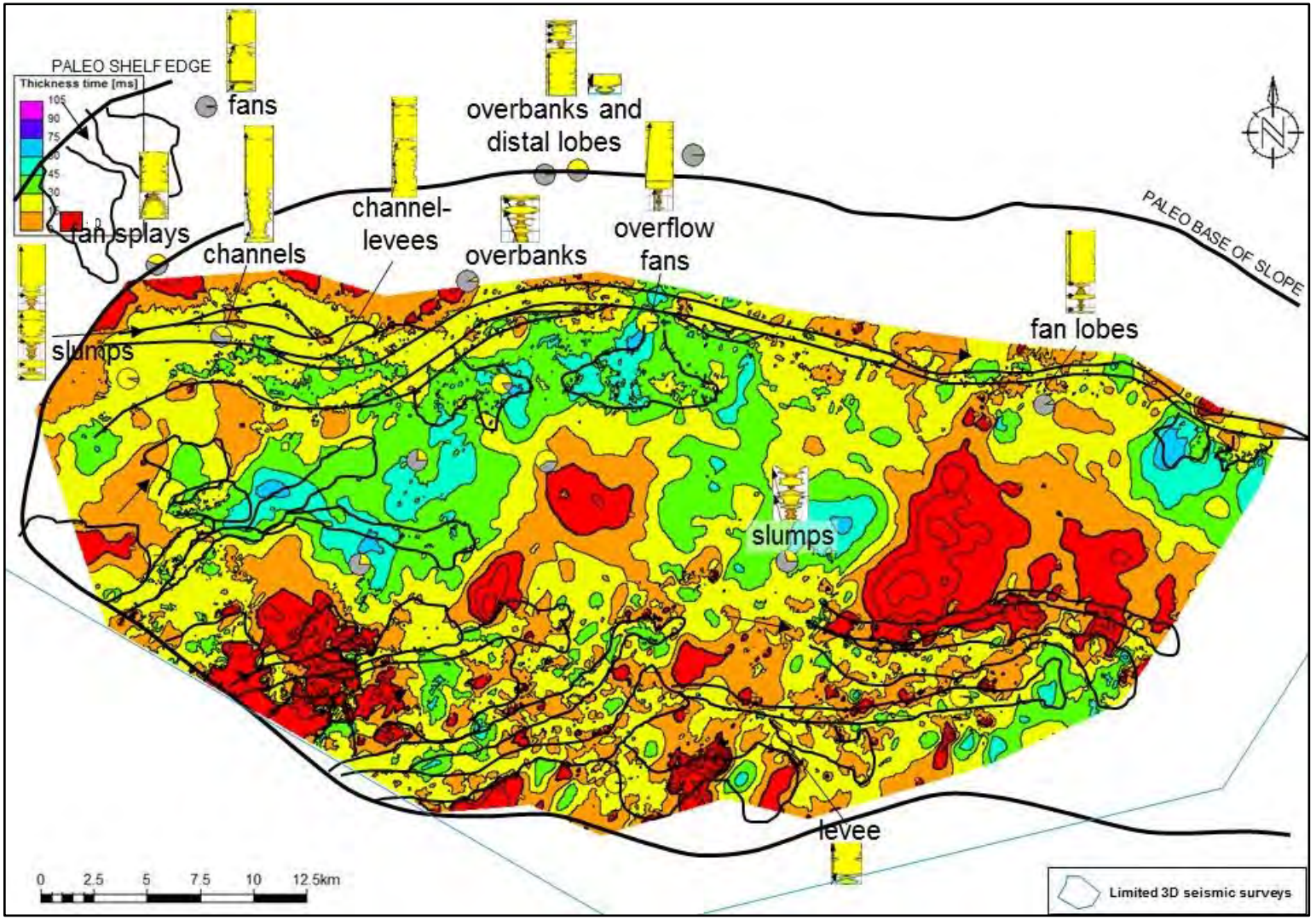

Figure 65 A summative description of the 14A depositional model. Gross isochron map of the 14A sequence (14A sand top-14At1) overlain with sand fraction pie charts at the key wells and the accompanying 14A sand segments of gamma ray log to illustrate the inferred depositional settings as supported by the overlying line drawing of the sand distribution across the basin, based on the 14A sand base amplitude map.

9.8 Discussion of the 13A and 14A Sands Distribution

9.8.1 13A Sand Distribution

The 13A sands were mainly sourced from the paleo shelf on the northwest margin of the basin, as demonstrated by the absence of shelf edge sands. However, there appears to be sediment input from a subordinate onshore fluvial source in the west too, as suggested by the thick succession of 13A deposits against the western margin of the basin.

The 13A sands were transported across the shelf and flowed down the slope primarily via channels. At some points, however, the sedimentary mass failed at the shelf edge, most likely as a result of tectonic readjustments or a local sea level fall, and gave rise to slumping and bypass with the sands ultimately being deposited on the base of slope as fans or they continued to flow deeper into the basin via channels that terminated in the form of splaying fans and lobes on the basin floor. Overall the 13A sands demonstrate a distributary type of depositional pattern across the basin.

The 13A sands trend in a northwest to southeast orientated transport regime across the Central Bredasdorp Basin with features that are indicative of a final swing in orientation towards the east. The deposition of the sands occurred in pulses coinciding with falls in the local sea level and an associated period of thermal sag, or subsidence, of the basin.

The main depocentre in the Aptian time was approximately ~130 km from the southeastern coastline area source and positioned in the eastern part of the of the Central Bredasdorp Basin as a circular depression. On its western edge was a subtle structural high situated below the stacked succession of channels, fans and lobes and onlapped by a thick succession of 13A deposits on its southwestern limb (**Figure 66**).

A more prominent physical influence on the 13A sand distribution was the fault set that intersected the Aptian-aged deposits in a primarily NW-SE orientation, thereby directing the 13A sands from the shelf to as far as the main basin depocentre in conduits aligned parallel to the faults. The subordinate, orthogonal faults on the other hand, coincide with some of the 13A sequence termination points, where the fan and lobe-like features on the amplitude map abruptly end as if acting like a barrier to the sand flow. The influence of all of the faults on the distribution of the 13A sands is illustrated on the gross isochron map as patterns of sand thickness variations within what has been identified as structural-bound transfer zones (delineated by blue polygons in **Figure 66**). **Figure 66** is a sketched map view of the areal distribution of the 13A sands, which captures the interpretations of seismic and well data performed in this study and clearly illustrates the presence of fault control and the associated transfer zones. The sketch also shows that the orientation and length of the faults intersecting the 13At1 surface compares very well to the dimensions of the sands distributed across the basin floor (as seen in the gross isochron map **Figure 64**).

The overall driver of the ~2.5 million year-long sequence of 13A sands distribution was primarily the faults that were active before and during the Aptian time in the Central Bredasdorp Basin. Naturally, the inherited topography of the seabed will play a role in influencing distributional trend patterns too even though there were no prominent obstructions on the seabed of the Central Bredasdorp Basin at the Aptian time.

This overall interpretation of the 13A sand distribution in the study area is summarised in the 3D schematic in **Figure 67**, which illustrates the role of faulting in guiding the sands in a NW to SE to east

trend from the primary continental source in the NW corner of the basin, collapsing off the unstable shelf edge as channelised mass flow sands down the slope and ultimately onto the basin floor where they splayed as submarine fans and lobes.

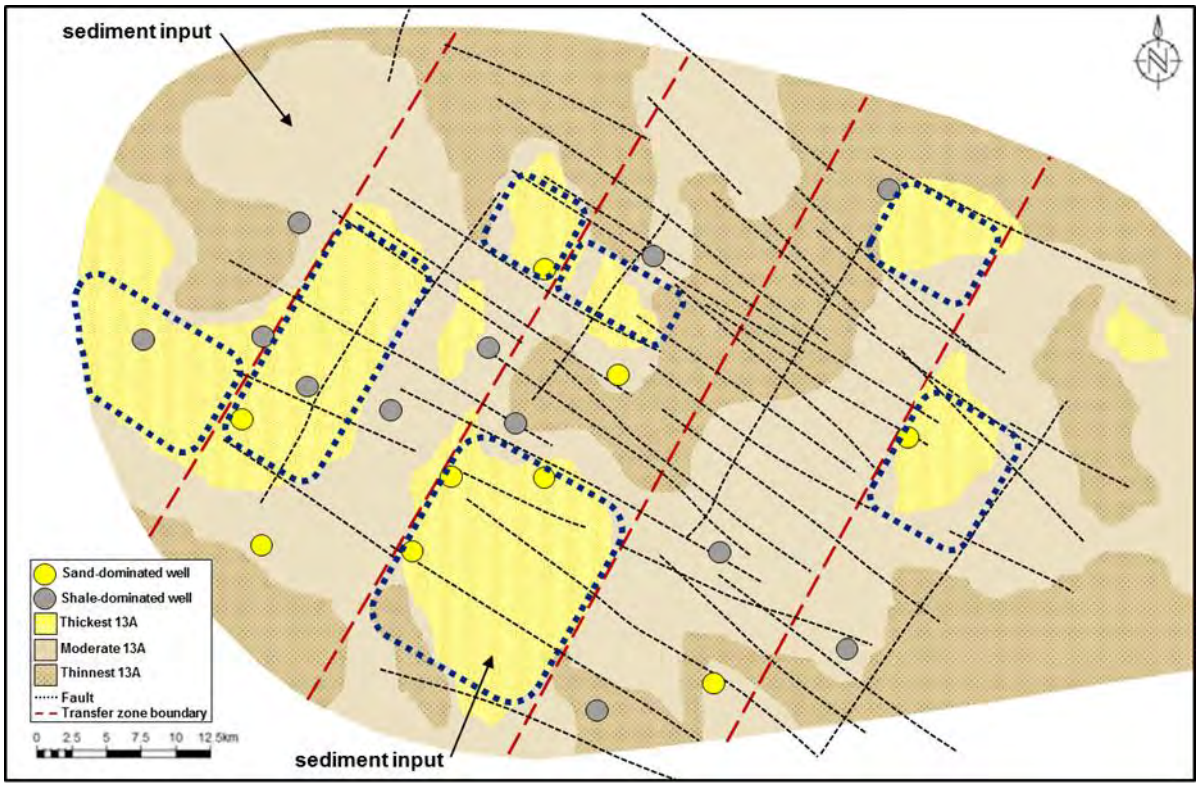

Figure 66 Summary sketch of the 13A sand distribution across the Central Bredasdorp Basin, generated using the isochron maps, with the interpreted faults and generalised sand/shale dominance represented at the key well locations, based on the sand fraction pie charts. Blue dashed outline polygons highlight the clusters of thickest 13A sand accumulations in the transfer zones.

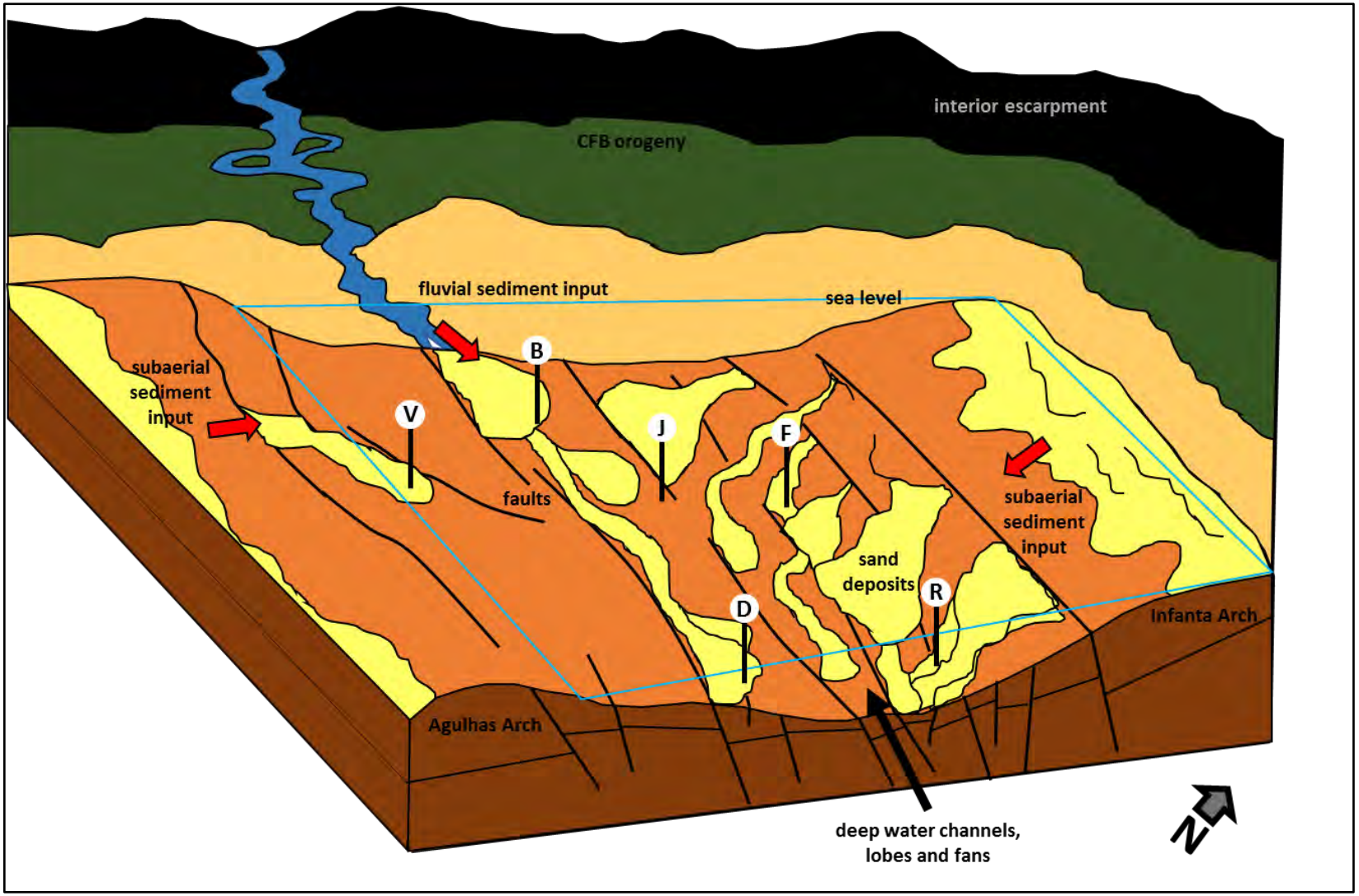

Figure 67 Summary 3D schematic of the 13A sand distribution across the Central Bredasdorp Basin, sketched based on the isochron maps, interpreted faults and generalised sand/shale dominance represented at the key well locations (based on the sand fraction pie charts).

9.8.2 14A Sand Distribution

The main source of the 14A sands was located on the western margin of the Bredasdorp Basin and represented the onshore fluvial environment. A subordinate source in the southwest provided continental sediments from the Agulhas Arch basement high.

Sediments were transported across the shelf in the west and eroded from the structural high in the southwest. The combination of a local sea level fall with basin margin uplift and gradual thermal sag, or subsidence, of the basin prompted the sediments to be transported downslope under the influence of gravity via channels or as a mass flow in the form of slumps up to the base of slope environment where they continued to flow deeper in levee-bound channels, alternatively high energy caused the sediments to breach and spill over the channel levees to form splays.

The 14A sands are generally distributed west to east across the Central Bredasdorp Basin as two channelised sand fairways with features that are indicative of an easterly directed transport regime. The northern fairway comprises of strongly confined and narrowly channelised sands with a distinct meandering trend whilst the southern fairway is comprised of more weakly confined channels intermingled with mass wasting features, particularly slumping, from the southern basin margin. The deposition of the sands occurred in pulses coinciding with falls in the local sea level and an associated period of thermal subsidence of the basin.

The main depocentre was positioned in the eastern part of the Central Bredasdorp Basin and approximately ~160 km from the Albian coastline source area in the west. On its western edge a structural high consisting of two adjacent mini horsts was present between the northern and southern fairways, bearing limited to no sand. This feature is seen more subtly on the 13At1 maps but very clearly on the 1At1 and Basement time structure surfaces, which serve as ancient topographical influences of the 14A sands distribution.

An additional physical influence on the 14A sand distribution was the fault set of the basin that intersected the Albian-aged deposits in a primarily NW-SE orientation and caused the 14A sands to diverge slightly from their west-east trend as they “jumped” across the faults. It was, however, the subordinate, orthogonal faults and their associated transfer zones that seemed to have had the most influence on the 14A sand distribution in this regard, as recognised by the patterns of structurally-induced sand distribution patterns across the basin floor (seen on the gross isochron map in **Figure 65** and delineated by blue polygons in **Figure 68**). **Figure 68** is a sketched map view of the areal distribution of the 14A sands, which captures the interpretations of seismic and well data performed in this study and clearly illustrates the presence of fault control and the associated transfer zones.

The overall driver of the ~2.5 million year-long sequence of 14A sands distribution was primarily the inherited topography of the seabed of the Central Bredasdorp Basin at the Albian time, which is owed to structural and stratigraphic factors. The role of the faults that were active at the Albian time was minimal in redirecting some of the 14A sands from their initial flow trend but this suggests that they had more influence on the broader sand distribution pattern instead.

The overall interpretation of the 14A sand distribution across the study area is summarised in the 3D schematic in **Figure 69**, which illustrates the transport of the sands in two fairways as a northern

channel complex and a southern channel complex, extending from the primary continental source in the west across the basin towards the depocentre in the east in a pattern demonstrating divergent "jumping" of the sands between adjacent, subtle fault compartments perpendicular to the main NW-SE fault trend (as illustrated in **Figure 46**).

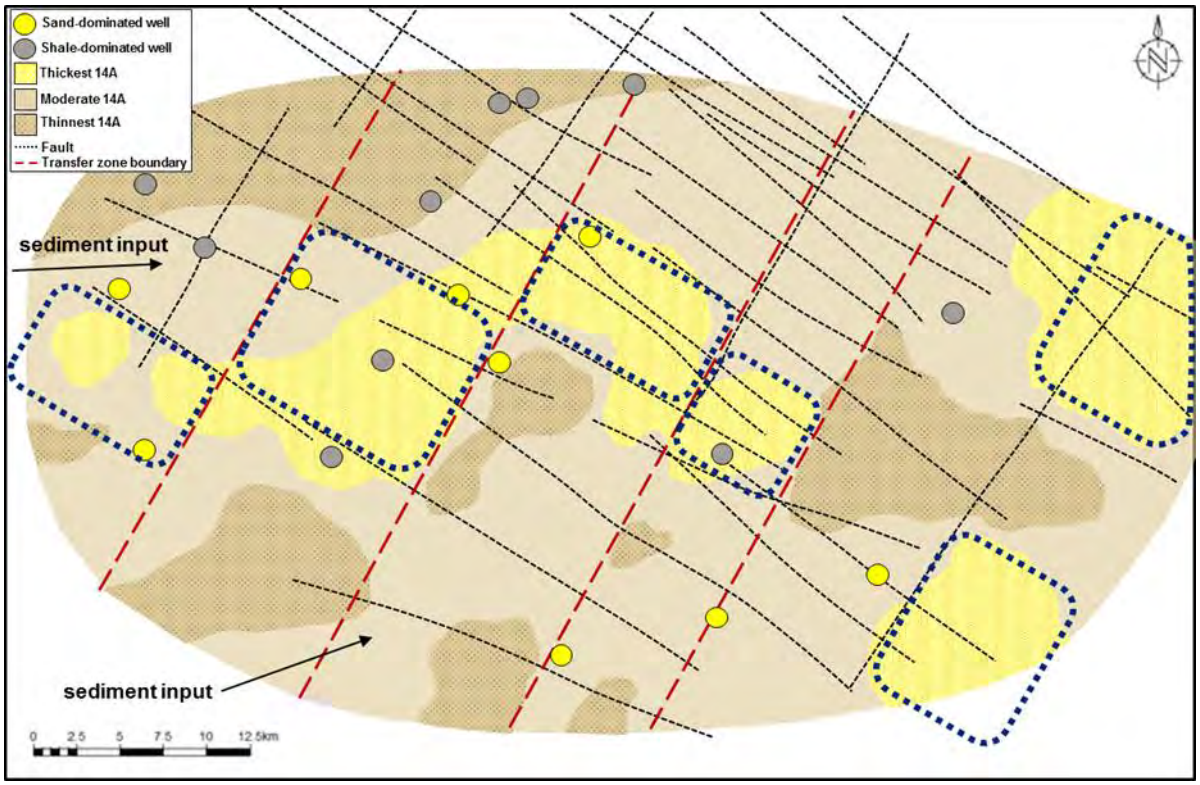

Figure 68 Summary sketch of the 14A sand distribution across the Central Bredasdorp Basin, generated using the isochron maps, with the interpreted faults and generalised sand/shale dominance represented at the key well locations, based on the sand fraction pie charts. Blue dashed outline polygons highlight the clusters of thickest 14A sand accumulations in the transfer zones.

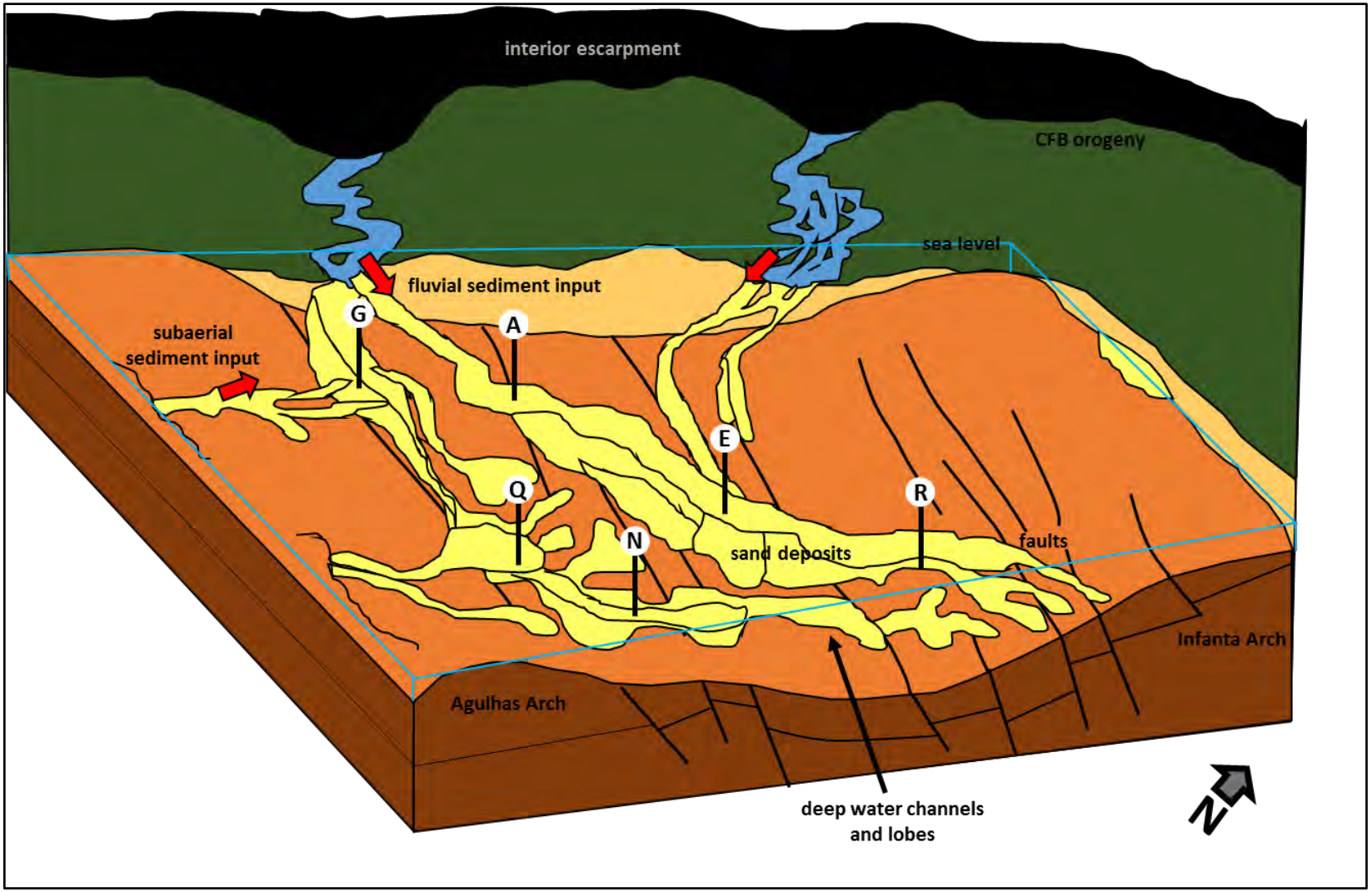

Figure 69 Summary 3D schematic of the 14A sand distribution across the Central Bredasdorp Basin, sketched based on the isochron maps, interpreted faults and generalised sand/shale dominance represented at the key well locations (based on the sand fraction pie charts).

CHAPTER 10

CONCLUSION

10.Conclusion

The primary objective of this study was to determine the physical regional controls and to perform a local assessment of the distribution of the Aptian (13A) and Albian (14A) deep water, gravity mass flow sands deposited in the Central Bredasdorp Basin of South Africa.

To begin making this assessment, seismic and well data in the defined study area were gathered, checked and analysed. The first key deliverable of the project was the mapped surfaces of the top and base of the 13A and 14A sequences in the time domain using the "3D only" set of seismic surveys. Amplitude values were extracted from these surfaces to generate maps that reflected the expected distributions of the 13A and 14A sequence sands across the study area. The best results for indicating this was the amplitude extraction map and the RMS attribute with the Variance or Standard Deviation volume attributes providing support in indicating the general depositional trend.

The seismic based identification of the Aptian-Albian sand distribution and insight into the possible environmental factors present in the Bredasdorp Basin at that time required support from the well data. The gamma ray wireline logs of the key wells located within and adjacent to the mapped amplitudes representing the 13A and 14A sands were reviewed over the unconformity-bound intervals of interest: 13At1 to 14At1 and 14At1 to 15At1, respectively. There was generally a good correlation between these datasets but for a more precise investigation the well markers for the tops of the 13A and 14A sand sequences were created. Sand fraction pie charts were calculated between the well markers of the sand top (i.e. 13AST for 13A and 14AST for 14A) and the sand base (i.e. 13At1 for 13A and 14At1 for 14A). Using the time structure surfaces, gross isochron (time thickness) maps were generated to give a basinwide representation of the volumetric distribution of the 13A and 14A sequences and to also visualise the possible structural features present in the basin at the Aptian-Albian times.

With an idea of the areal and thickness distribution of the 13A and 14A sands, faults intersecting the basement rocks and the 13At1 and 14At1 horizons were interpreted in the study area to gain an understanding of whether there was a strong element of tectonic control of the pattern of sand transport and the location of deposition. The character of the interpreted faults was verified using the dip azimuth attribute maps as a comparison, whilst the dip angle attribute map gave a clear indication of the position of the paleo shelf edge during the Aptian and Albian times. Generally, the main faults trend NW to SE but that there is a subordinate set of orthogonal faults that bound the NE-SW transfer zones. The distribution of the 13A and 14A sequences on the respective isochron maps recognise the transfer zone trend and initiated the concept of sands "jumping" across fault compartments, particularly in the 14A sequence.

The 13A sands appear to have been guided quite significantly by fault-bound channels and in some places they cross-cut the splays of the broadly deposited, progradational packages. The sand typically

splayed out of the channels as fans and lobes where fault control terminated within the main depocentre in the eastern part of the basin.
The distribution of the 14A sequence sands, on the other hand, does not appear to be directly influenced by the faults since many of them do not appear to have been active during the Albian, despite the apparently stronger confinement of the sands. Alternatively, there is the probability that the sands flowed within structural lows that were elongated west-east alongside the northern and southern basin margin. This inherited topography was created by the influence of faulting on the older sequences which also caused the formation of a mid-basin structural high which redirected the flow of the 14A sands from the onshore source accordingly. The 13At1 unconformity was formed in response to extensive tectonic uplift and intense subaerial erosion at the time that the Falkland plateau passed the Agulhas platform and it was followed by the initiation of four major subsidence episodes in the Bredasdorp Basin until around the Maastrichtian. The deposition of the 13A sequence occurred soon after the formation of the 13At1 unconformity and the associated major tectonic activity so this may be the reason why the distribution of the 13A sands is more prominently controlled by faults and the 14A sequence sands distribution is less guided by fault presence.

Overall the trend displayed through the Aptian and Albian depositional sequences is one which demonstrates a primary onshore sedimentary source in the west/northwest corner of the basin. The rising global (second order) sea level from the Aptian into the Albian shows little effect on the 13A and 14A sequences but the episodes of falling local (fourth order) sea level and the associated shelf and slope incision were captured. Bound by a basal regional unconformity and an upper maximum flooding surface and separated by a more mud-rich highstand systems tract, the progradational lowstand packages represent the sand-rich intervals of the 13A and 14A sequences. Within the Central Bredasdorp Basin, the 13A sequence displays mass wasting, primarily as slumps on the slopes, which develops into meandering distributary channels across the basin floor and ultimately splaying the sands into fans and lobes in the main depocentre in the east. The 14A sequence displays mostly channelised sands that are confined into west-east trending northern and southern fairways that are typically confined by levees and the occasional associated overbank splays, at an angle offset from the main fault trend.

The successions of sand that have been specifically identified as “turbidites” in the Tankwa Basin are referred to as mass flow or mass transport deposits in the Central Bredasdorp Basin. They represent fining upwards successions of massive sands to muds but are present as an “incomplete” Bouma sequence, having formed due to a gravity-driven mechanism of sediment transport in a depositional setting ranging from the shelf edge to basin floor in the Tankwa and in the Central Bredasdorp basins. The scale of the case study and the primary (project) study makes it difficult to compare individual fans between the Tankwa and Bredasdorp basins, so a regional comparison of the fan complex had to suffice with a particular focus on fan sand geometry across the basin and hence sand distribution patterns in a confined setting. It was increased sediment transport through stronger confinement, in the form of erosion and levee development that enhanced the action of sediment bypass and

resulted in incisions of the submarine basin slope and the ultimate deposition of fans and lobes further downdip in the base of slope to basin floor region of the Bredasdorp Basin (Hodgson, 2009). The highly faulted nature of the Bredasdorp Basin would have played a significant role in generating the conduits and creating confinement as a series of parallel and adjacent horsts and grabens, which appear to have boldly influenced the channel patterns and sand distribution trends. The Tankwa Basin does not show evidence of fault control on the channel and fan lobe patterns nor on the general sand distribution and in the outcrops there is no indication of syn-kinematic fill during deposition of the fan complex. Performing field studies in the Tankwa Basin of the Karoo gave a lot of practical insight into understanding the variation in resolution and the applicability of different types of data in a study of features on a basinwide scale. Although there are notable differences between the history of deposition in the Tankwa Basin and the Bredasdorp Basin, the field and literature based study of the submarine turbidite fans in the Tanwka Basin demonstrated the same principle as that identified in the Bredasdorp Basin of an increased volume of sediment transported through increased confinement in the form of erosional incisions and levees. The confinement of the mass sedimentary flows typically enhances bypass zones and results in incisions of the slope and fan lobes, which are ultimately deposited further downdip in the base of slope to basin floor setting.

The range in physical controls and the variety of mass flow deposits in the 13A and 14A sequences described in this thesis demonstrates the dynamic nature of the depositional environment of the central part of the Bredasdorp Basin over a span of a merely a few million years. The depositional models for the Aptian (13A) and Albian (14A) sequence sands reflect a fairly clear tectono-stratigraphic history and provide supporting evidence of the physical controls on the deposition of these deep water, gravity mass flow sands across the Central Bredasdorp Basin.

CHAPTER 11

RECOMMENDATIONS

11.Recommendations

It is recommended that further work be performed to refine the sand distribution of the 13A and 14A sequences through using additional seismic-based techniques. Neural Network and Spectral Decomposition tools in Petrel can be applied to try delineate the geometry of the sand bodies across the Central Bredasdorp Basin above the 13At1 and 14At1 levels.

Furthermore, using the pre-stack 3D seismic data in combination with the suggested seismic attribute extractions will perhaps contribute to finer scale interpretation of the sand tops and bases, ultimately enabling a more defined delineation of the basinwide 13A and 14A sequence deposits.

The study can be expanded in the geological perspective too through making more detailed studies of the wireline well logs and analysing available core samples and reports. This may generate results that define the interpreted depositional environments on a finer scale and will subsequently enable the identification of individual sand facies types.

A combination of decompaction analysis to reconstruct sea floor sand body geometry at the time of deposition and lithofacies analysis from core data and samples may then be used to represent the sand body morphology quantitatively and therefore qualitatively determine the specific sediment flow process (as suggested by Jeanette *et. al.*, 2000).

CHAPTER 12

REFERENCES

12.References

Allen, P.A. and Allen, J.R. (2013). Basin Analysis: Principles and Application to Petroleum Play Assessment. Third Edition. Fig. 8.9.

Beaubouef, R.T. (2004). Deep-water leveed-channel complexes of the Cerro Toro Formation, Upper Cretaceous, southern Chile. AAPG Bulletin, v. 88, pp. 1417 – 1500.

Bouma, A.H. (1999). Coarse-grained and fine-grained turbidite systems as end member models: applicability and dangers. Marine and Petroleum Geology, v. 17, pp. 137 – 143.

Bouma, A.H. (2000). Coarse-grained and fine-grained turbidite systems as end member models: applicability and dangers. Marine and Petroleum Geology, v. 17, pp. 137 – 143.

Bouma, A.H. (2004). Key controls on the characteristics of turbidite systems. *From* Lomas, S.A. & Joseph, P. (eds) (2004). Confined Turbidite Systems. Geological Society, London, Special Publications, v. 222, pp. 9 – 22.

Broad, D.S.,Jungslager, E.H.A., McLachlan, I. R. and Roux, J. (2006). Geology of the offshore Mesozoic basins. *In* The Geology of South Africa, M. R. Johnson et al. (eds), pp. 553 – 571, Geological Society of South Africa, Pretoria.

Brown, L.F. Jr., Benson, J.M., Brink, G.J., Doherty, S., Jollands, A., Jungslager, E.H.A., Keenan, J.H.G., Muntingh, A. and Van Wyk, N.J.S. (1995). Sequence stratigraphy in offshore South African divergent basins. An atlas on exploration for Cretaceous lowstand traps by Soekor (Pty) Ltd., American Association of Petroleum Geologists, Studies in Geology, v. 41, pp. 184.

Burbank, D.W. and Anderson, R.S. (2012). Tectonic Geomorphology. Second Edition. p. 99.

Burden, P.L.A. (1992). Soekor, Partners explore possibilities in Bredasdorp Basin off South Africa. Oil & Gas Journal website (December 21, 1992).

Burden, P.L.A. and Davies, C.P.N. (1997). Exploration to first production on Block 9 off South Africa. Oil & Gas Journal website (September 08, 1997).

Catuneanu, O., Hancox, P.J., Cairncross, B. and Rubidge, B.S. (2002). Foredeep submarine fans and forebulge deltas: orogenic off-loading in the underfilled Karoo Basin. Journal of African Earth Sciences, v. 35, pp. 489 – 502.

Catuneanu, O., Wopfner, H., Eriksson, P.G., Cairncross, B., Rubidge, B.S., Smith, R.M.H., Hancox, P.J. (2005). The Karoo basins of south-central Africa. Journal of African Earth Sciences, v. 43, pp. 211 – 253.

Clarke, L.J. and Jenkyns, H.C. (1999). New oxygen isotope evidence for long-term Cretaceous climatic change in the Southern Hemisphere. Geology, v. 27, no. 8, pp. 699 – 702.

Davies, C.P.N. (1997). Hydrocarbon evolution of the Bredasdorp Basin, offshore South Africa: From source to reservoir. Thesis for Degree of Doctor of Philosophy, University of Stellenbosch, South Africa.

De Wit, M.J. and Ransome, I.G.D. (1992). Regional inversion tectonics along the southern margin of Gondwana. *In* De Wit and Ransome (eds) (1992). Inversion Tectonics of the Cape Fold Belt, Karoo and Cretaceous Basins of Southern Africa. A.A. Balkema, Rotterdam, pp. 15 – 21.

Dudley, P.R.C., Rehmer, D.E. and Bouma, A.H. et al. (2000). Reservoir-Scale Characteristics of Fine-Grained Sheet Sandstones, Tanqua Karoo Subbasin, South Africa. GCSSEPM Foundation 20th Annual Research Conference: Deep-Water Reservoirs of the World (December 3 – 6, 2000), pp. 318 – 341.

Fildani, A., Drinkwater, N.J., Weislogel, A., McHargue, T., Hodgson, D.M. and Flint, S.S. (2007). Age Controls on the Tanqua and Laingsburg Deep-Water Systems: New Insights on the Evolution and Sedimentary Fill of the Karoo Basin, South Africa. Journal of Sedimentary Research, v. 77, pp. 901 – 908.

Flint, S.S., Hodgson, D.M., Sprague, A.R., Brunt, R.L., Van der Merwe, W.C., Figueiredo, J., Prelat, A., Box, D., Di Celma, C. and Kavanagh, J.P. (2011). Depositional architecture and sequence stratigraphy of the Karoo basin floor to shelf edge succession, Laingsburg depocentre, South Africa. Marine and Petroleum Geology, v. 28, pp. 658 – 674.

Goldhammer, R.K., Wickens, H.D., Bouma, A.H. and Wach, G. (2000). Sequence Stratigraphic Architecture of the Late Permian Tanqua Submarine Fan Complex, Karoo Basin, South Africa. *In* A.H. Bouma and C.G. Stone (eds) (2000). Fine-grained turbidite systems. AAPG Memoir 72/SEPM Special Publication, v. 68, pp. 165 –172.

Haq, B.U., Hardenbol, J. and Vail, P.R. (1987). Chronology of Fluctuating Sea Levels Since the Triassic. Science, v. 235, pp. 1156 – 1166. *Downloaded from* www.researchgate.net/publication/245660687.

Heezen, B.C. and Ewing, M. (1952). Turbidity currents and submarine slumps, and the 1929 Grand Banks earthquake. American Journal of Science, v. 250, pp. 849 – 878.

Hus, R., Acocella, V., Funiciello, R. and De Batist, M. (2005). Sandbox models of relay ramp structure and evolution. Journal of Structural Geology, v. 27, pp. 459 – 473.

Janocko, M., Nemec, W., Henriksen, S. and Warchol, M. (2013). The diversity of deep-water sinuous channel belts and slope valley-fill complexes. Marine and Petroleum Geology, v. 41, pp. 7 – 34.

Jeanette, D.C., Garfield, T.R., Mohrig, D.C. and Cayley, G.T. (2000). The Interaction of Shelf Accommodation, Sediment Supply and Sea Level in Controlling the Facies, Architecture and Sequence Stacking Patterns of the Tay and Forties/Sele Basin-Floor Fans, Central North Sea. GCSSEPM Foundation 20th Annual Research Conference: Deep-Water Reservoirs of the World (December 3 – 6, 2000), pp. 402 – 421.

Johnston, S.T. (2000). The Cape Fold Belt and Syntaxis and the rotated Falkland Islands: dextral transpressional tectonics along the southwest margin of Gondwana. Journal of African Earth Sciences, v. 31(1), pp. 51 – 63.

Jungslager, E.H.A. (1996). Geological evaluation of the remaining prospectivity for oil and gas of the pre-1At1 “synrift” succession in Block 9, Republic of South Africa. Soekor (Pty.) Ltd. *internal publication.*

Martin-Algarra, A., Ruiz-Ortiz, P.A. and Vera, J.A. (1992). Factors controlling Cretaceous Turbidite deposition in the Betic Cordillera. Rev. Soc. Geol. Espana, v. 5, pp. 53 – 80.

Mcmillan, I.K., Brink, G.I., Broad, D.S. and Maier, J.J. (1997). Chapter 13: Late Mesozoic Sedimentary Basins Off the South Coast of South Africa. Sedimentary Basins of the World, v. 3, pp. 319 – 376.

Meckel, T. (2010). Classifying and Characterizing Sand-Prone Submarine Mass-Transport Deposits. *Adapted from the oral presentation at* AAPG Annual Convention and Exhibition, New Orleans, Louisiana (April 11 – 14, 2010). Search and Discovery, Article #50270.

Meiburg, E. and Kneller, B. (2010). Turbidity currents and their deposits. Annual Review of Fluid Mechanics, v. 42, pp. 135 – 156.

Miller, K.G., Mountain, G.S., Wright, J.D. and Browning, J.V. (2011). A 180-Million-Year Record of Sea Level and Ice Volume Variations from Continental Margin and Deep-Sea Isotopic Records. Oceanography, V. 24, no. 2, pp. 40 – 53.

Mitchum Jr., R.M. (1977). Seismic stratigraphy and global changes of sea level. Part 11: glossary of terms used in seismic stratigraphy. In Payton, C.E. (ed.), Seismic Stratigraphy— Applications to Hydrocarbon Exploration, v. 26. A.A.P.G. Memoir, pp. 205 – 212.

Mutti, E. (1985). Turbidite systems and their relations to depositional sequences. *In* Zuffa, G.G. (ed.), Provenance of Arenites, D. Reidel Publishing Company, Dordrecht, pp. 65 – 93.

Mutti, E. (2011). Turbidites. *Adapted from special lecture at* AAPG International Conference and Exhibition, Milan, Italy (October 23 – 26, 2011). Search and Discovery, Article #30214.

Mutti, E., Tinterri, R., Magalhaes, P.M. and Basta, G. (2007). Deep-Water Turbidites and Their Equally Important Shallower Water Cousins. *Adapted from Extended Abstract prepared for presentation at* AAPG Annual Convention, Long Beach, California (April 1 – 4, 2007). Search and Discovery, Article #50057.

Nfor, N.E. (2011). Sequence stratigraphic characterization of petroleum reservoirs in block 11b/12b of the Southern Outeniqua Basin. Thesis for Degree of Masters in Petroleum Geosciences, University of the Western Cape, South Africa.

Petroleum Agency South Africa (2012). Petroleum Exploration in South Africa: Information and Opportunities brochure. Downloaded off *www.petroleumagencysa.com*.

Posamentier, H.W., Jervey, M.T. and Vail, P.R. (1988). Eustatic controls on clastic deposition. I. Conceptual framework. *In* Wilgus, C.K., Hastings, B.S., Kendall, C.G.St.C., Posamentier, H.W., Ross, C.A. and Van Wagoner, J.C. (eds.), Sea Level Changes – An Integrated Approach, v. 42. SEPM Special Publication, pp. 110 – 124.

Posamentier, H.W. and Martinsen, O. (2006). The Character and Genesis of Mass Transport Complexes I: Geomorphology and Process Sedimentology from 3-D Seismic Data. SEPM Research Symposium: The Significance of Mass Transport Deposits in Deepwater Environments, AAPG Annual Convention (April 9 – 12, 2006), Technical Program.

Prelat, A., Covault, J.A., Hodgson, D.M., Fildani, A. and Flint, S.S. (2010). Intrinsic controls on the range of volumes, morphologies, and dimensions of submarine lobes. Sedimentary Geology, v. 232, pp. 66 – 76.

Richards, M. and Bowman, M. (1998). Submarine fans and related depositional systems II: variability in reservoir architecture and wireline log character. Marine and Petroleum Geology, v. 15, pp. 821 – 839.

Roux, J. (1997). Potential outlined in Southern Outeniqua off South Africa. Oil and Gas Journal, v.95 (25).

Salles, T., Lopez, S., Eschard, R., Lerat, O., Mulder, T. and Cacas, M.C. (2008). Turbidity current modelling on geological time scales. Marine Geology, v. 248, pp. 127 – 150.

Sawyer, D.E. (2006). Seismic Geomorphology, Lithology, and Evolution of the Late Pleistocene Mars-Ursa Turbidite Region, Mississippi Canyon Area, Northern Gulf of Mexico. *Partial* Master of Science Thesis, pp. 22 – 31. College of Earth and Mineral Sciences, The Graduate School, Pennsylvania State University.

Shanmugam, G. (1997). The Bouma Sequence and turbidite mind set. Earth-Science Reviews, v. 42, pp. 201 – 229.

Sloss, L.L., Krumbein, W.C. and Dapples, E.C. (1949). Integrated facies analysis. *In* Longwell, C.R. (ed.), Sedimentary Facies in Geologic History, v. 39. Geological Society of America Memoir, pp. 91–124.

Smith, R.M.H. (1990). A review of stratigraphy and sedimentary environments of the Karoo Basin of South Africa. Journal of African Earth Sciences, v. 10, pp. 117 – 137.

Soekor (Pty.) Ltd. *internal publication* (1993). The distribution of and controls on sandstone deposition in sequences 1A-to-14A, Bredasdorp Basin, South Africa.

Soekor (Pty.) Ltd. *internal publication written by* Hodges, K.J., Van Rooyen, W. and Van Wyk, N.S.J. (1991). Report on the geology of the 14A sequence in the Central Bredasdorp Basin, South Africa.

Sonibare, W.A., Mikes, D. and Cole, D.I. (2011). Facies architecture of Kookfontein shelf edge delta, Tanqua-Karoo Basin (South Africa): Implications for facies analysis and modelling. South African Journal of Geology, v. 114, pp. 299 – 324.

Sprague, A.R.G., Garfield, T.R., Goulding, F.J., Beaubouef, R.T., Sullivan, M.D., Rossen, C., Campion, K.M., Sickafoose, D.K., Abreu, V., Schellpeper, M.E., Jensen, G.N., Jennette, D.C., Pirmez, C., Dixon, B.T., Ying, D., Ardill, J., Mohrig, D.C., Porter, M.L., Farrell, M.E. and Mellere, D. (2005). Integrated slope channel depositional models: The key to successful prediction of reservoir presence and quality in offshore West Africa. *From the article prepared for presentation and poster at* E-Exitep, Veracruz, Ver., Mexico *and edited by* CIPM (February 20 – 23, 2005).

Tankard, A., Welsink, H., Aukes, P., Newton, R. and Stettler, E. (2009). Tectonic evolution of the Cape and Karoo basins of South Africa. Marine and Petroleum Geology, v. 26, pp. 1379 – 1412.

Tinker, J., de Wit, M. and Brown, R. (2008). Linking source and sink: Evaluating the balance between onshore erosion and offshore sediment accumulation since Gondwana break-up, South Africa. Tectonophysics, v. 455, pp. 94 – 103.

Vail, P.R. (1975). Eustatic cycles from seismic data for global stratigraphic analysis. American Association of Petroleum Geology Bulletin, v. 59, Abstract, pp. 2198 – 2199.

Vail, P.R., Mitchum Jr., R.M. and Thompson III, S. (1977). Seismic stratigraphy and global changes of sea level. Part 3: Relative changes of sea level from coastal onlap. *In* Payton, C.E. (ed.), Seismic Stratigraphy – Applications to Hydrocarbon Exploration, v. 26. American Association of Petroleum Geologists Memoir, pp. 63 – 81.

Van der Werff, W. and Johnson, S. (2003). High resolution stratigraphic analysis of a turbidite system, Tanqua Karoo Basin, South Africa. Marine and Petroleum Geology, v. 20, pp. 45 – 69.

Van Rensburg, T. (2012). Deepwater Fan Complexes of the SW Karoo Basin: Facies Architecture, Stratigraphy and Reservoir Potential of the Tanqua and Laingsburg Basin Sedimentary Deposits. PetroSA Pty. Ltd., unpublished paper.

Van Wagoner, J.C. (1995). Overview of sequence stratigraphy of foreland basin deposits: Terminology, summary of papers, and glossary of sequence stratigraphy. *In* Van Wagoner, J.C. and Bertram, G.T. (eds.), Sequence Stratigraphy of Foreland Basin Deposits, v. 64. American Association of Petroleum Geologists Memoir, pp. ix – xxi.

Van Wagoner, J.C., Mitchum Jr., R.M., Campion, K.M. and Rahmanian, V.D. (1990). Siliciclastic sequence stratigraphy in well logs, core, and outcrops: Concepts for high resolution correlation of time and facies. American Association of Petroleum Geologists, Methods in Exploration, Series 7, pp. 55.

Visser, J.N.J. and Loock, J.C. (1978). Water depth in the main Karoo Basin, South Africa, during Ecca (Permian) sedimentation. Trans. Geological Society of South Africa, v. 81, pp. 185 – 191.

Wach, G.D., Lukas, T.C., Goldhammer, R.K., Wickens, H.D. and Bouma, A.H. (2000). Submarine Fan Through Slope to Deltaic Transition Basin-Fill Succession, Tanqua Karoo, South Africa. *In* A.H. Bouma and C.G. Stone (eds) (2000). Fine-grained turbidite systems. AAPG Memoir 72/SEPM Special Publication, v. 68, pp. 173 – 180.

Watkeys, M.K. (2006). The break-up of Gondwana: a South African perspective. *In* Johnson, M.R, Anhaeusser, C.R. and Thomas, R. (eds.), The Geology of South Africa. Geological Society of South Africa and Council for Geoscience, pp. 531 – 539.

Weimer, P. and Slatt, R.M. (2007). Introduction to the Petroluem Geology of Deepwater Settings. American Association of Petroleum Geologists, AAPG Studies in Geology, v. 57. *Also in* AAPG/Datapages Discovery Series 8.

Wickens, H.D. and Bouma, A.H. (2000). The Tanqua Fan Complex, Karoo Basin, South Africa – Outcrop Analog for Fine-Grained, Deepwater Deposits. *In* A.H. Bouma and C.G. Stone (eds) (2000). Fine-grained turbidite systems. AAPG Memoir 72/SEPM Special Publication, v. 68: 153 – 164.

Wickens, D. (2015 and 2011). Turbidites of the Southwestern Karoo Basin: Facies Architecture, Reservoir Applications and Predictive Stratigraphy. Field Excursion Guidebook.

Wood, M. (1995) Development potential seen in Bredasdorp Basin off South Africa. Oil and Gas Journal, v. 93, i. 22.

Zhao, N., Wuan, L., Mao, F., Huang, J. and Li, Z. (2015). High Resolution Sequence Stratigraphy Correlation and Sedimentary Model of Turbidites: A Case on the 1st Member of the Kqn Formation in the Dabusu Area, South Songliao Basin. *Adapted from extended abstract prepared for poster presentation at* AAPG 42nd Eastern Section Meeting, London, Ontario, Canada (September 27 – 30, 2014). Search and Discovery, Article #10698.

Website references:

www.geologycafe.com

www.sepmstrata.org

www.seddepseq.co.uk

www.slb.com

www.earthjay.com

CHAPTER 13

APPENDICES

13.Appendices

Appendix I

3D Q-Marine Over/Under (DISCover) seismic survey over Block 9, Bredasdorp Basin, South Africa

Tamsyn van Rensburg (Geoscientist, PetroSA)

September 2012

Abstract

A 3D Q-Marine Over/Under (DISCover) seismic survey was performed by PetroSA for the first time in South Africa over Block 9 in the Bredasdorp Basin during 2011/12. The aim of the survey was to assess the hydrocarbon potential and confirm the hydrocarbon reserves of this currently-producing offshore basin. Although the latest 2D seismic data was acquired in 2011, a more recent and technologically-advanced 3D seismic survey was the ultimate solution in producing a more detailed image of the subsurface. The Q-Marine Over/Under (DISCover) 3D method of shallow and deep cable pairs has yielded better seismic results and provided a processed dataset with far less noise – even in rough weather and strong currents, which was PetroSA's biggest concern during acquisition of seismic data off the south coast of South Africa.

Introduction

The 3D Q-Marine Over/Under (DISCover) survey layout plan consisted of roughly east-west trending sail lines orientated in a strike-direction to the basin geology and although the survey area included the Orca platform and the EM Buoy, amongst a few other permanent structures, the sail lines were dead-ended just short of these obstructions so that they did not interfere with the survey. The direction in which the survey sail lines were planned and acquired was predetermined based on a number of factors: 1) the sites of previous surveys, 2) the location of the wells drilled in and around this basin, 3) turning points between sail lines, 4) the weather and 5) the ocean currents, such as the Agulhas current along the south coast of South Africa which reached a strength of 2.6 knots during this survey.

This marine seismic survey followed the method of Over/Under towed-streamer acquisition. The survey spread consisted of seven over (shallow) cables separated at 100 m and three under (deep) cables with an ideal separation of 233 m (Fig. 1). The separation was critical because the efficiency of this method of acquisition and processing depends on the width of the over/under cable spread. The over cables were 6000 m long at a depth of 9 m below the sea surface whilst the under cables were at a depth of 20 m with a length of 6800 m.

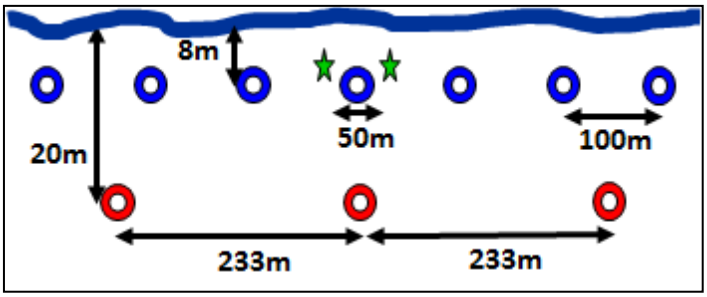

Figure 1: Q-Marine Over/Under streamer (DISCover) configuration of the CB3D survey. View from the vessel stern, below the surface of the water. Shallow cables = blue rings; Deep cables = red rings (Western Geco).

The two source arrays were 15 m-long at a depth of 7 m below the sea surface. Each of the source arrays consisted of three sub-arrays, hosting two cluster guns and four single guns (Fig. 2). The sub-arrays were spaced approximately 8 m apart and connected to one another by

ropes but the source arrays, however, were not connected to one another because of the Lead-Ins in the 50 m wide stretch of water between them.

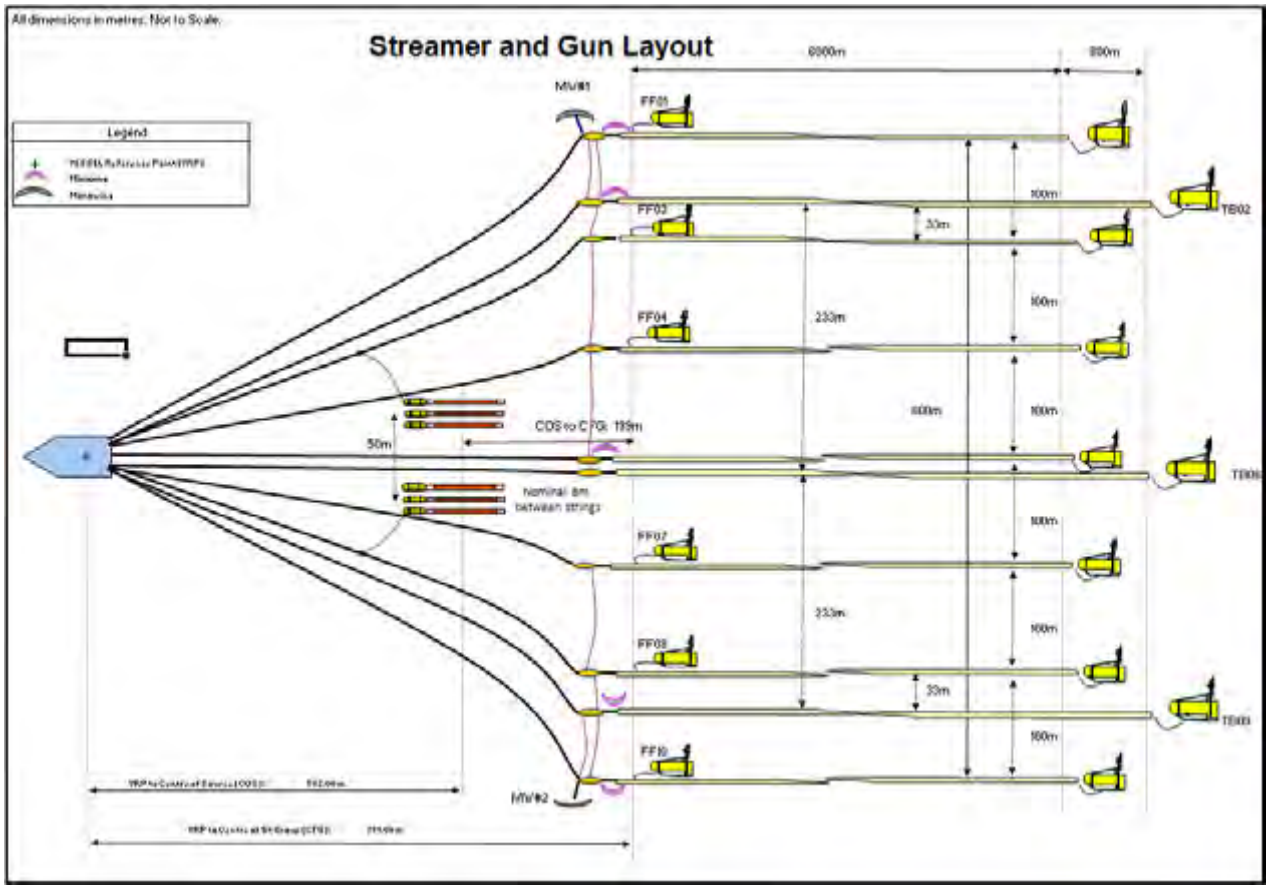

Figure 2: Seismic survey configuration. **COS = Centre Of Source; FF = Front Float; MW = Monowing; Paravane (orange); Miniwing (pink); TB = Tail Buoy (Western Geco).**

DISCover Technique

The key function of DISCover is the combination of the over (shallow) cable data with the under (deep) cable data to produce an image with well-defined geological structures and layers from the surface down to the basement. The quality of the deeper image is improved by increasing the low frequency signals by laying a set of under cables. These deeper cables allow a cleaner set of data because they are clear of the swell at the water surface which generates noise, particularly during the numerous episodes of rough weather that are encountered along the south coast of South Africa. In this regard, the Q-Marine Over/Under method of acquisition also improves the overall signal to noise ratio.

The Temperature/Salinity (T/S) dip is a subsurface factor to consider too because it represents the temperature and salinity values of the survey area. These variables influence the speed

of acoustic sound through the water therefore directly affecting the quality of the seismic data. The T/S dip was thus recorded on a weekly basis since it changes with the currents and temperature-depth profiles in the ocean as a result of seasonal fluxes.

The under cables were sparsely-sampled because their sole purpose was to capture the low frequency data to enhance the 3D data, whilst the data received from the over cables was calibrated from single sensors at a regular spacing of 3.125 m. This created seismic data with a higher resolution and data that is flexible in terms of filtering and processing. The data received by every set of three hydrophones was firstly sent to a Digital Sensor Unit (DSU) digitizing device within the cable, then forwarded to the In-sea Concentrator Unit (ICU) device located every 200 m along the cable and finally transferred via fibre optic cables to the data system on the vessel.

Onboard Processing

Once the 1.761×10^{13} samples of raw data reached the Acquisition department onboard, low and high cut filters were applied to the data to eliminate the primary noise by removing traces with frequencies greater than 200 Hz and less than 2 Hz. Interpolation was then performed to eliminate the "bad" traces by selecting 11 traces either side of each dead/missing/poor trace and, from this set, selecting the seven "best" traces to create a "good" trace to replace them. Extrapolation is a similar method that was used to improve that seismic data set by using selected inner traces to predict five outer traces on the ends of the seismic line. The Quadrant Mirror Filter (QMF) was applied after that to separate the filtered data set into high and low frequencies so that Lacona could be applied only to the lower frequencies (less than 32 Hz) to attenuate them to eliminate more swell noise. The enhanced low frequency data was then re-interpolated and regularised to the positions defined by the shallower, over cable spread. Interpolation of the under cables was performed to create additional (theoretical) under cables to ensure that there were seven over/under cable pairs in total and, once complete, the data was anti-QMF'd and anti-aliased using the T-X filter. The high frequency data from the over cable spread was then merged with the low frequency data as over/under cable pairs at 20 Hz, which was the dominant frequency of the under cable data (Fig. 3). The

final step in Acquisition was applying the K-filter tool during a process referred to as Decimation.

Decimation is performed using the concept of a Calibrated Marine Source (CMS) which is simply described as shot-by-shot evaluations of the data, as opposed to the conventional process of assuming that all of the shots produce a uniform signature. CMS removed the water bottom multiples and artefacts in the seismic data, like reflections off the vessel hull, but it was also used for interpolating dead and/or missing traces, generating the Far Field signature and performing the Near Field Hydrophone Trace Quality Evaluation.

Data Quality Control (QC) then came into action by performing Brute stacks. This process is applied to stack all of the shot points and their traces for each of the over and under cables, individually. In this survey, 7 billion seismic traces were recorded from 695 316 shot points so Brute stacking was followed by Anomalous Amplitude Attenuation to enhance the signal to noise ratio by removing all types of noise. Once a fair amount of QC had been applied, Cable Rotation was performed to gather the shots by rotating through each cable for each shot of each sequence. This process enabled the QC scientist to quickly identify the low frequency swell noise, the high frequency ship noise, turn noise, as well as the direct and first arrivals in the traces for the whole seismic data set (Fig. 4). This was based on the understanding that if cable 1 contains noise associated with shot 1 then it is very likely that the other nine cables of this survey will also contain some noise associated with shot 1.

After the seismic data had been QC'd, a selected sub-set of the data was briefly edited (for approximately 6 hours) by a Geophysicist to produce an unrefined, stacked 2D seismic image, unaffiliated with any of the Navigation data that had been recorded. This image was assessed by the Client onboard to determine whether the specifications set by PetroSA were being met and if the data would be acceptable after the major processing has been completed onshore. The selected set of seismic data used in onboard processing in this survey was sourced from a combination of the middle over cable (shallow streamer #5) and the middle under cable (deep streamer #6) from the 10-cable spread. These two cables made a good pair because they were positioned and maintained vertically in line with one another so their data could be merged easier than the data of the other over and under cables, which were offset.

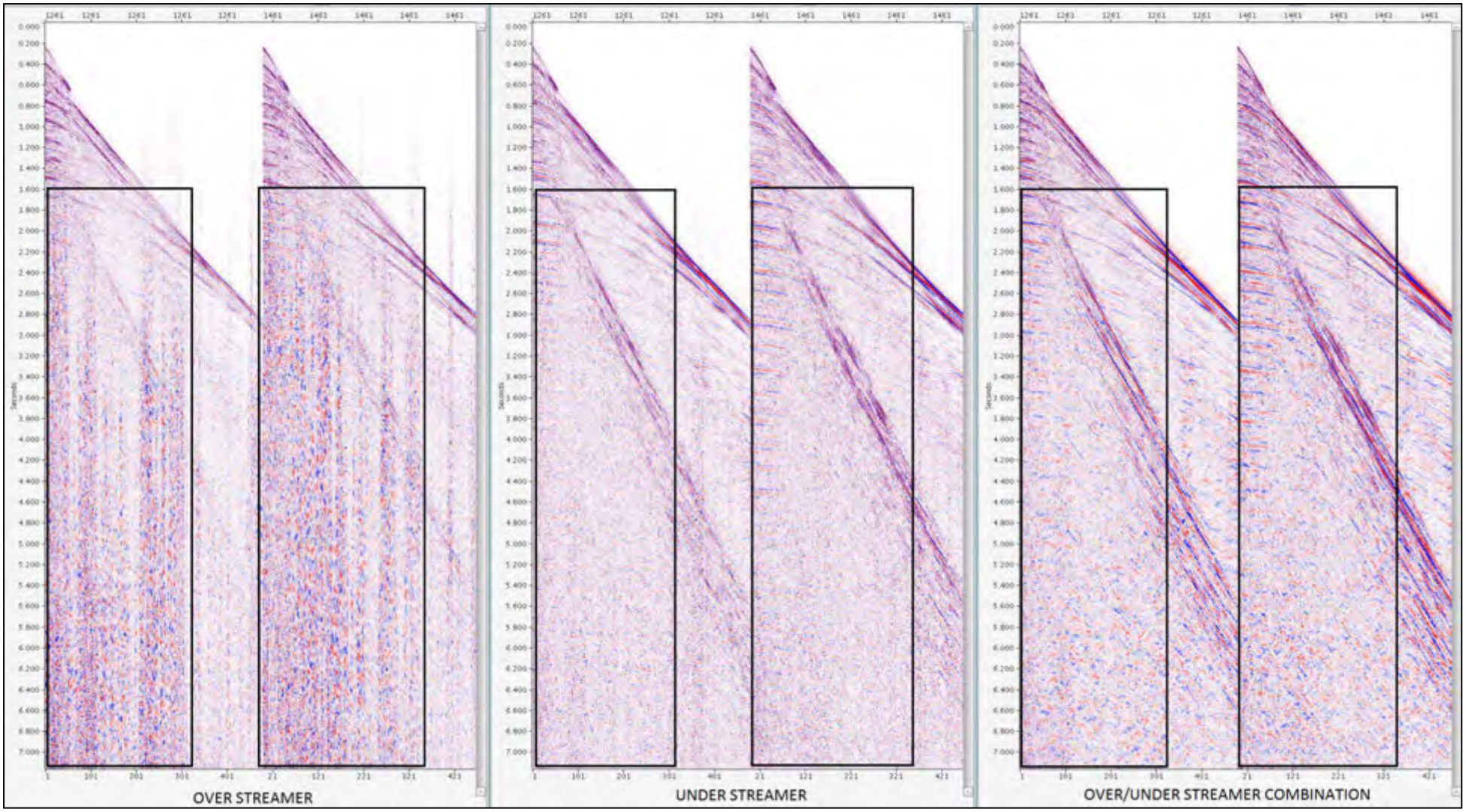

Figure 3: Comparison of Over streamer; Under streamer; Over/Under streamer raw seismic data (Western Geco).

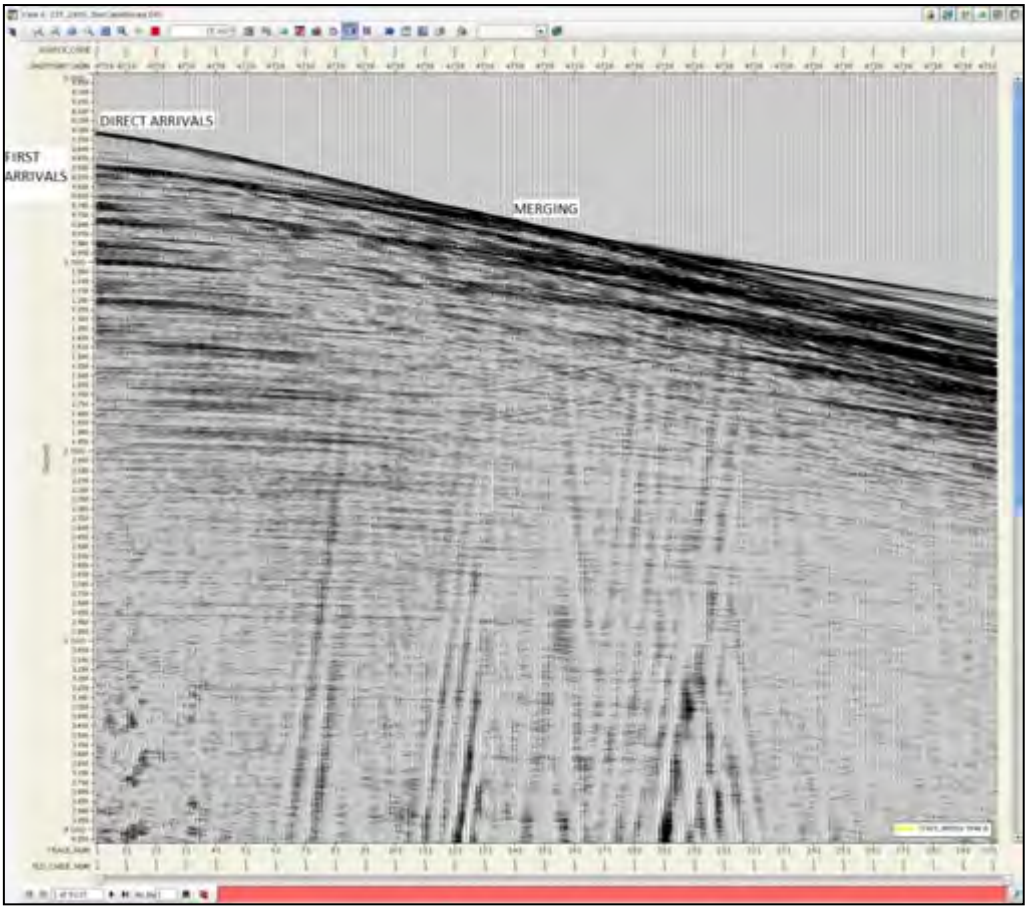

Figure 4: Cable Rotation. The Direct arrivals and First arrivals can be clearly identified at the first shot points but at some point the Direct arrivals merge into the First arrivals. The Direct arrivals need to be removed by frequency filtering the data (Western Geco).

Discussion

The 3D Q-Marine Over/Under (DISCover) seismic survey acquisition and data processing method was chosen instead of a conventional technique because it offers a major advancement by providing a broader signal bandwidth, enhanced resolution and a higher signal to noise ratio. Although the noise levels in this survey were higher than normal (well over 30 microbars) due to the strong ocean currents and 466.75 hours of weather downtime, the effect was minimised by the DISCover method which offered an extended weather window. The DISCover method is also favourable because it is not dependent on optimising data over a specific target depth or time, like the conventional methods. *Figure 6* clearly illustrates the difference in the quality of the seismic data acquired in a conventional 2D marine survey and a Q-Marine Over/Under (DISCover) 3D survey over the same area in the Bredasdorp Basin.

The only downfall encountered with the Q-Marine Over/Under (DISCover) method was that the cables were affected by the changing current profile and the varying speed of sound with depth

below the surface, hence the importance of recording the T/S dip daily. Additionally, the position of the seismic cables relative to the vessel and, more importantly, relative to one another was continuously monitored to determine the presence and influence of the current profile and surface swell. This screening ensured that the data recorded by the over and under cables yielded the maximum coverage of the survey area and that the data could be interpolated and merged as over/under cable pairs in the processing phase of the survey. In the cases where the coverage was poor and/or there was feathering, infill lines were acquired to improve the dataset. Infill lines accounted for 26.9% of this survey, as illustrated in the Daily Production Graph (Fig. 5) where the number of infill lines increased significantly over December 2011 during a break in the bad weather, which gave the opportunity for additional passes, and during the tail end of the survey in April as the last chance to better the survey coverage. Upon completion of this seismic survey, a total of 340 TB (terra bytes) of data had been recorded during navigation, seismic acquisition and onboard processing. The more intense onshore processing of all of this seismic data is expected to yield results that will enable the most advanced assessment of the hydrocarbon potential as well as the confirmation of the hydrocarbon reserves in the actively-producing Bredasdorp Basin in PetroSA's Block 9.

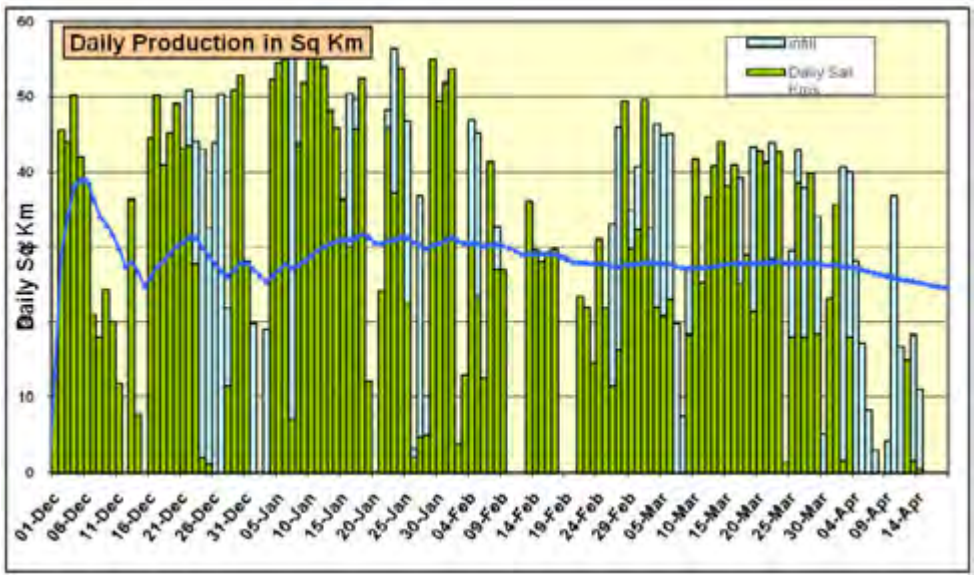

Figure 5: Daily Production Graph illustrating the scope of infill lines out of the total daily sail lines in squared kilometres (sq km) from 01 December 2011 to 14 April 2012 (Brown and Hopgood, 2012).

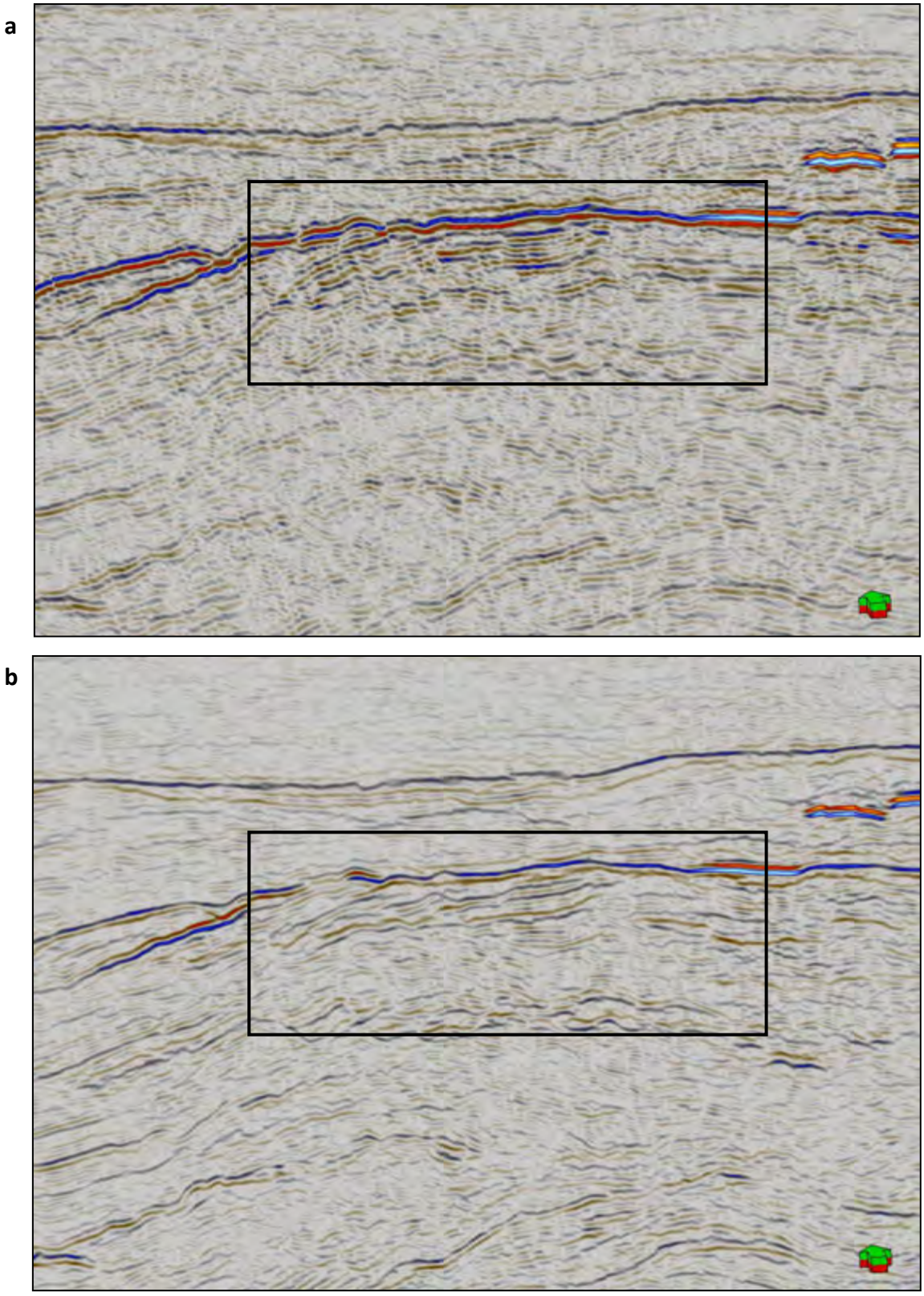

Figure 6: A comparison in the quality of (a) reprocessed vintage data acquired in a conventional 2D marine survey and (b) data acquired in the Q-Marine Over/Under (DISCover) 3D survey by Western Geco. Both surveys were managed by PetroSA over the F-O field in Block 9 in the Bredasdorp Basin of South Africa. The 2D survey data was reprocessed in 2011 at the same time that the 3D survey was acquired and processed.

References

Brown, Robert. Consultant Geophysicist for Verif-I onboard the Western Regent during the second half of the Central Bredasdorp Basin 3D seismic survey acquisition.

Brown, R. and Hopgood, P. (2012) Weekly QA Summary Report. 3D Seismic Survey – Central Basin Block 9: Week 21 (9th – 15th April).

Hill, D.I., Combee, L., Bacon, J. (2006) Over/under acquisition and data processing: the next quantum leap in seismic technology. Special Topic: Multi-disciplinary issue in *First Break*; 24:81-95.

Hill, D.I., Bacon, J., Brice, T., Combee, L., Koeninger, C., Leathard, M. and McHugo, S. (2007) Over/Under a Technology for Illuminating Deep Objectives. *Presented in* EAGE 69th Conference & Exhibition, London, UK.

Kragh, E., Muyzert, E., Curtis, T., Svendson, M. and Kapadia, D. (2010) Efficient broadband and marine acquisition and processing for improved resolution and deep imaging. Special Section: Offshore Technology in *The Leading Edge:*464-469.

Moldoveanu, N., Combee, L., Egan, M., Hampson, G., Sydora, L. and Abriel, W. (2007) Over/under towed-streamer acquisition: A method to extend seismic bandwidth to both higher and lower frequencies. *The Leading Edge*:41-58.

Monik, D.J. (2009) Fresnel zone binning: Application to 3D seismic fold and coverage assessments. *The Leading Edge*:288-295.

Young, P. and Monk, D. (2009) Reducing Infill Requirements Using Fresnel Zone Binning And Steerable Streamers. Focus: Streamer Technology in *PESA News*:49-51.

Appendix II

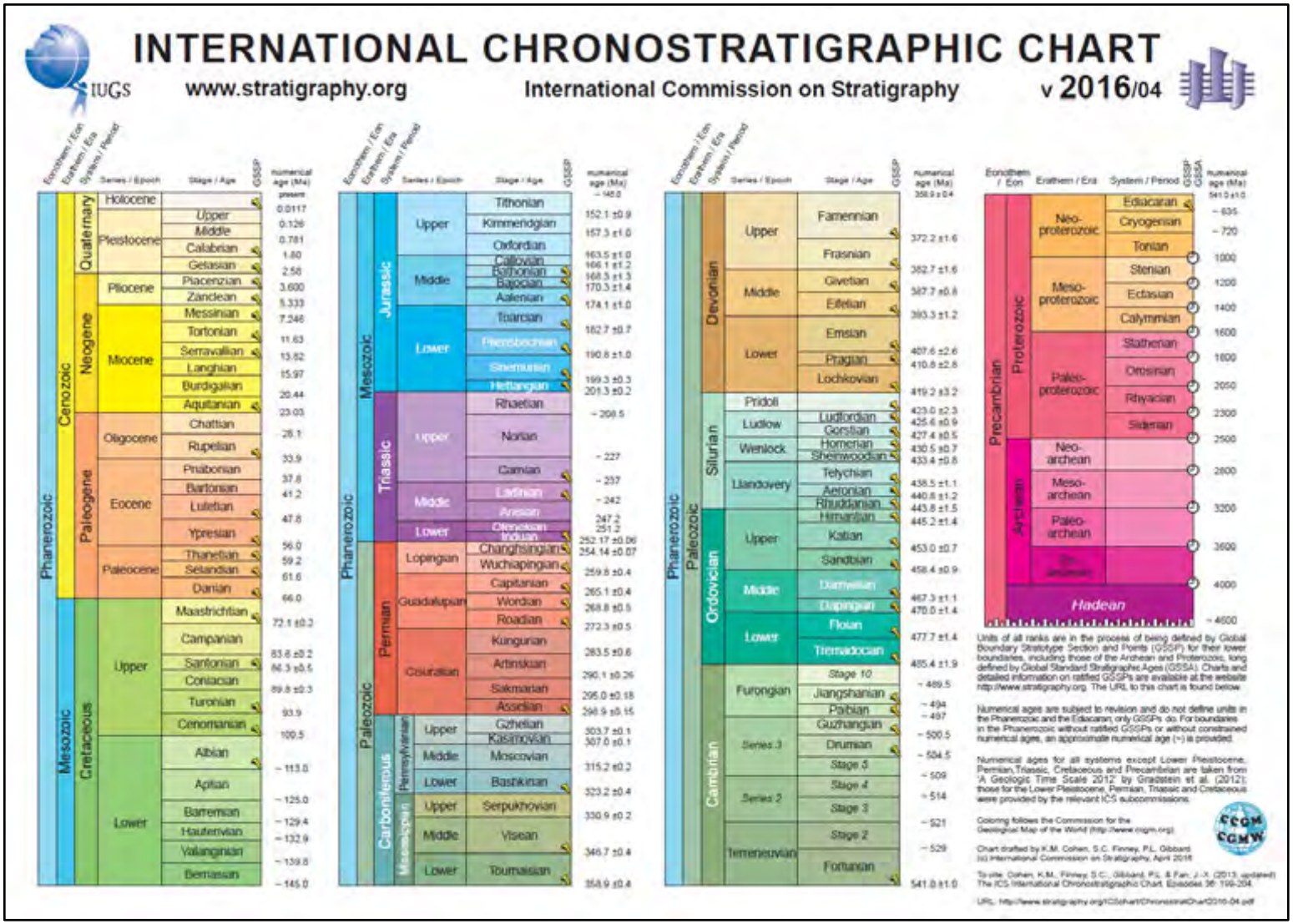

International chronostratigraphic chart – v.2016/04 (www.stratigraphy.org)

Appendix III

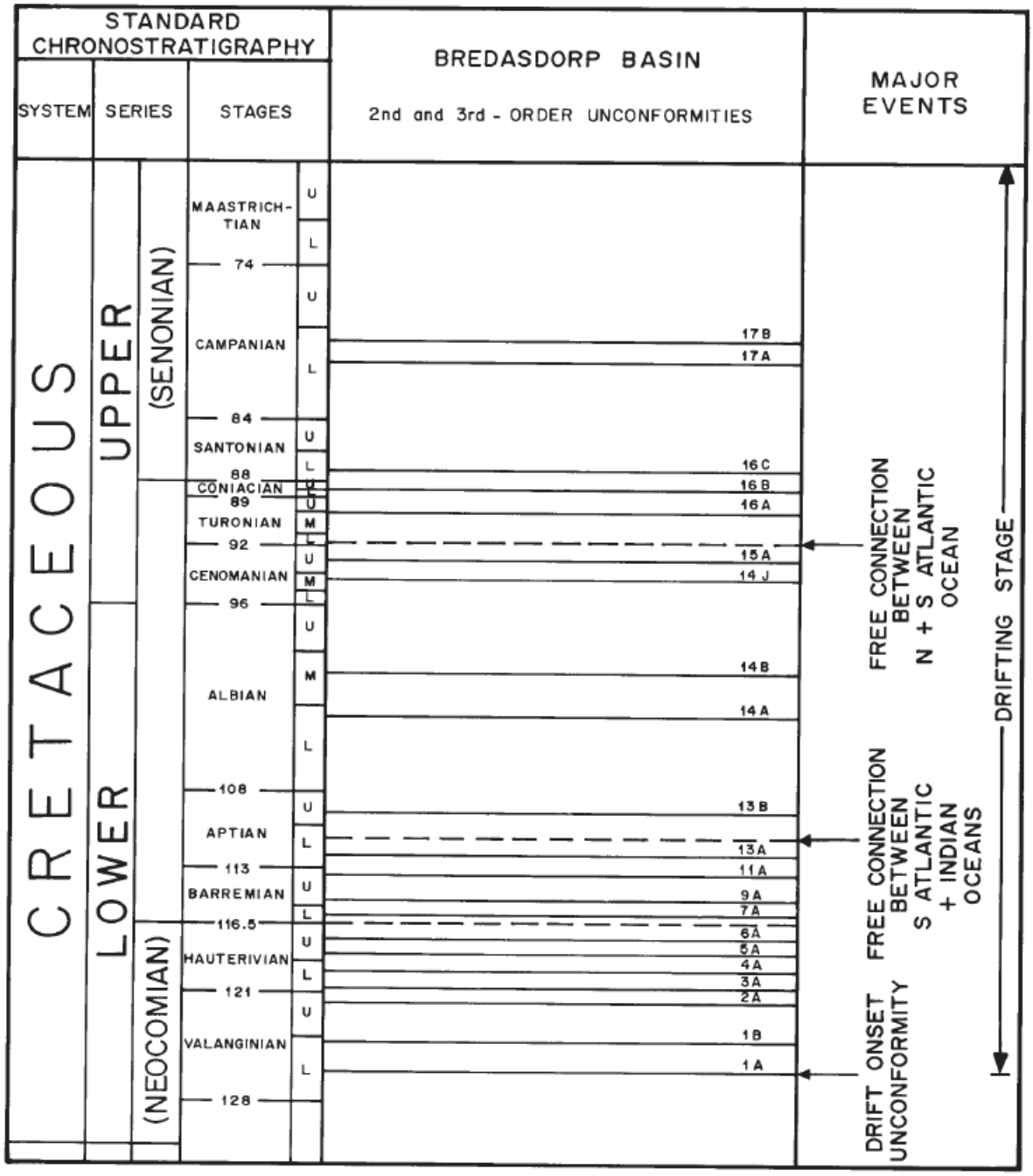

Linear time chart of the international standard Cretaceous chronostratigrpahy showing absolute dates of stage boundaries (Haq *et. al.*, 1987, 1988) and provisionally correlated second and third order unconformities in the Bredasdorp Basin. Solid lines are t1 unconformities and dashed lines are well-developed marine condensed sections (Brown *et. al.*, 1995).

Appendix IV

Turbidites

Earthquakes, compaction/subsidence, an uplift of sedimentary source areas, a lowering of the base level and a narrowing of the shelves that bound deep water basins are activities that may affect accommodation space and result in the spilling of shelfal sands from the shelf edge and down the slope, flowing onto the basin floor as turbidity currents (Zhao *et. al*., 2015) within tectonically-active basins.

As a turbidity current covers an increasing distance along the seabed from its shelfal source, it starts to deposit the coarsest sand grains as submarine fans from the head of the suspended, flowing mass. The lighter, fine grains of sand and silt continue flowing with the current as a fast mass and may scour channels into the previously-deposited coarse-grained fans on the seabed as they continue to be transported down slope towards the deeper basin. Flows are guided directionally by the basin configuration, such as pre-existing basement highs, topographic incisions (e.g. canyons, valleys, channels), tectonic features and pre-existing deposits, but the flow typically terminates once it has lost its energy due to friction with the seafloor. This results in a final sediment load being deposited in the form of channel lobes and splays on the basin floor.

Turbidites are generally deposited into a terrigenous or submarine trough on the base of slope to basin floor region on a passive continental margin during a sea level fall as the shelf is drastically eroded by a Type 1 unconformity (Martin-Algarra *et. al*., 1992). The coincidental occurrence of a major sea level fall with the formation of Type 1/2 unconformities has been identified by Haq *et. al*. (1987) and found to coincide with the mid-Hauterivian, Aptian and Albian geological ages. This covers the 13A and 14A sequences which are the focus of this study. Eustatic factors typically influence the form of the basin, like the position of the coastline and erosion base level, and ultimately affect the possibility of large volumes of sediment reaching the distal areas of the basin and continental margins (Martin-Algarra *et. al*., 1992). Analysis of the spatio-temporal distribution of these facies helps in understanding the basin morphology, the nature of the sedimentary contributions and their source, prevailing sedimentary conditions and their changes throughout time (Martin-Algarra *et. al*., 1992).

The depositional characteristics of turbidites vary greatly between basins and even within a single basin so Bouma (2004) classified two end members of turbidite systems: coarse-grained/sand-rich and fine-grained/mud-rich. The coarse-grained/sand-rich turbidite system is typically present in a proximal location within a tectonically confined basin on an active margin, whilst the fine-grained/mud-rich turbidite deposits are found in the complete opposite setting. Since the Bredasdorp Basin is a divergent margin, channelised and/or patchy, thick bedded sandstone deposited via poorly efficient turbidity currents is expected in the deep water region. Collisional margin type foredeep turbidites, on the other hand, are characterisitically deposited as sheet-like outer fan sandstone lobes transitioning distally into basin plain deposits via highly efficient, large volume and sustained turbidity currents (Mutti, 2011) (See the figure below).

Sheet-flow turbidite facies association		Channel-levee facies association	
Typical sedimentary column	*Description* Thick accumulation of rhythmic alternating beds of turbidite sandstone and mudstone with some thicker sandstone layers; minor occurrences of upward thickening and thinning trends	Typical sedimentary column	*Description* Combination of thick amalgamated sandstone facies and thinly bedded alternating beds of Bouma Tc sandstone and mudstone (several cm order); Thick amalgamated sandstone facies frequently contains slump blocks and rip-up clasts.
	*Interpretation* Sheet flow turbidites as trough-like foreland basin fill as described in Takano et al. (2005) with minor occurrences of depositional lobes.		*Interpretation* Channel-levee system Thick amalgamated sandstone: channel-fill deposits; thinly bedded alternating beds: overbank deposits in a levee beside the channel.

Table with illustrations and text describing the characteristic traits of a sheet-flow turbidite facies association in comparison to a channel-levee facies association (Mutti, 2011).

The deep sea fan model is based on outcrop studies of ancient turbidite basin fill and it identifies a canyon, inner fan, middle fan, outer fan and finally a basin plain as the segments of the fan system. The deep sea model is similar to that of a delta system in that it has distributary channels within the inner fan and prograding lobes in the outer fan. These channels and lobes form complexes over time, acting as conduits for turbidity currents, which carry shallow marine sediments into the deeper basinal environment (Reading and Richards, 1994) (See the figure below).

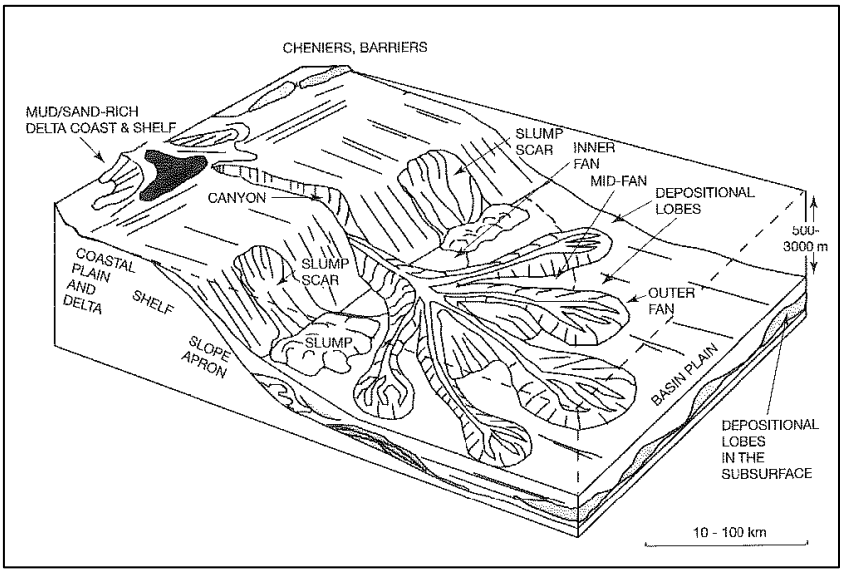

Depositional model for point-source mud/sand-rich submarine fan (Reading and Richards, 1994).

Often there is difficulty in distinguishing deep water turbidite deposits from detached delta-front sandstone bodies where they have been deposited into a fault-bound depression. This is due to the fact that fluvial floods tend to create hyperpycnal flows at river mouths which flow to the shoreline and onto the shelf like a shallow water turbidity current, creating a depositional sequence and a gamma ray log profile which looks like a regular deep water turbidity flow sequence of deposits (See the figure below).

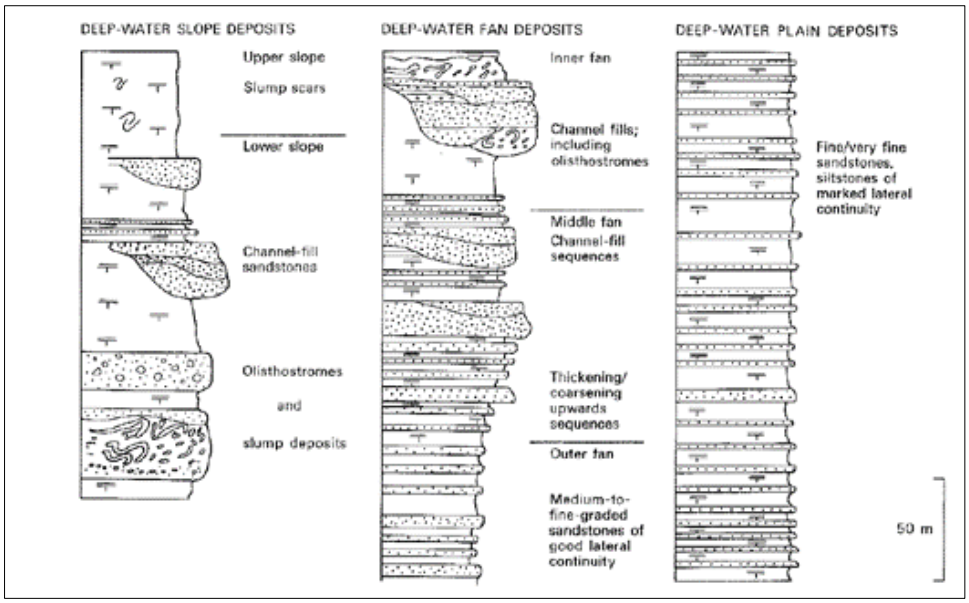

Sequence characteristics of deep water slope, fans and basin plain facies (Mutti and Ricci-Lucchi, 1972).

It has been long-assumed that the presence of a partial or complete Bouma sequence of strata is indicative of a turbidite deposit (Shanmugam, 1997) but studies have since shown that Bouma sequences may be formed by processes other than turbidity currents, such as debris flows, slumps and sea bottom reworking currents (Shanmugam, 1997). The clear and crucial differences between a deposit from a turbidity current versus from a debris flow are summarised in the table below and illustrated in the accompanying figure. Key differences are the turbulent flow versus a laminar flow, fine-grained sediment versus mixed grain sizes and low versus high sediment concentration for the turbidity current and debris flow, respectively.

TURBIDITY CURRENT	**DEBRIS FLOW**
Turbulent flow	Laminar flow
Two phase flow: water / solid	One phase flow: mass deformation
Fluidal rheology (Newtonian)	Plastic rheology (non-Newtonian)
Sediment held in suspension by turbulence	Sediment supported by matrix strength
Mainly fine-grained sediment	All grain sizes of sediment
Rare grain-to-grain contact	Frequent grain-to-grain contact
Low sediment concentration (1 – 23% by volume)	High sediment concentration (50 – 90% by volume)
Sediment settles from suspension	Sediment deposited by freezing en masse

A comparison between a turbidity current and a debris flow (Modified from Shanmugam, 1997).

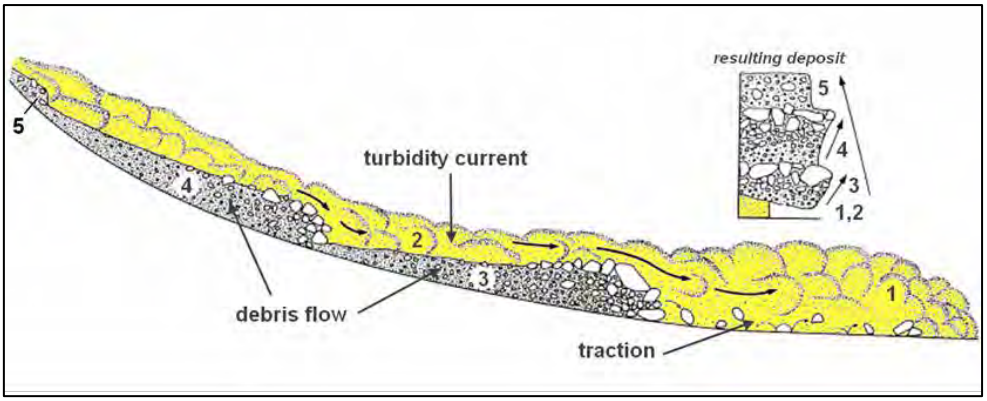

Diagram showing debris flow, turbidity current and traction processes operating in a sediment gravity flow (Modified from Young, K.S. (2000) Depositional Processes of Submarine Debris Flows in the Miocene Fan Deltas, Pohang Basin, SE Korea with Special Reference to Flow Transformation, Journal of Sedimentary Research, v. 70, pp. 491-503.).

Appendix V

Channel-fill Development

As a submarine current flows over the shallow subsurface and the sea floor, its turbulent energy erodes the substrate and starts to form an incision which may quickly develop into a channel. Finer material in the upper layer of the current spills over the edges of the channel and forms positive relief deposits referred to as channel levees. Levees occur on either side of the submarine basin floor channels (Janocko *et. al*., 2013) where (1) the channel is volumetrically too large for its capacity, (2) where there is hydraulic disequilibrium with the channel geometry, or (3) where there is a local plugging of the channel by mass transport deposits (Janocko *et. al*., 2013). Internal levees are constructional features fed by flows that have partially spilled out of the channel confinement but are unable to fully escape the confinement and hence ultimately exposed to erosion by channel avulsion/migration. External levees develop when a depositional body forms a constructional wedge of sediment pinching away from the channel, during the evolution of a genetically-related channel belt through flows that spill partially out of the confinement.

The weight of the levees combined with the lack of lateral support initiates faults on the edges of the channel, typically on the levee crest, with a failure plain that soles out close to the floor of the submarine channel. In some instances, fault blocks may rotate causing the channel margins to momentarily slide, as they simultaneously deposit a toe thrust into the adjacent channel axis. This motion suspends unconsolidated sediment in the body of water immediately above the seabed and passing turbidity currents entrain it whilst the levees continue to grow, thereby creating a “flushing” of the channel axis. Channel back-filling may occur in response to changes in the base level, thereby forcing subsequent turbidity currents to spill over the confinement of the channel (as illustrated in the figure below). This creates new pathways and ultimately initiates a new channel-levee system (Sawyer, 2006).

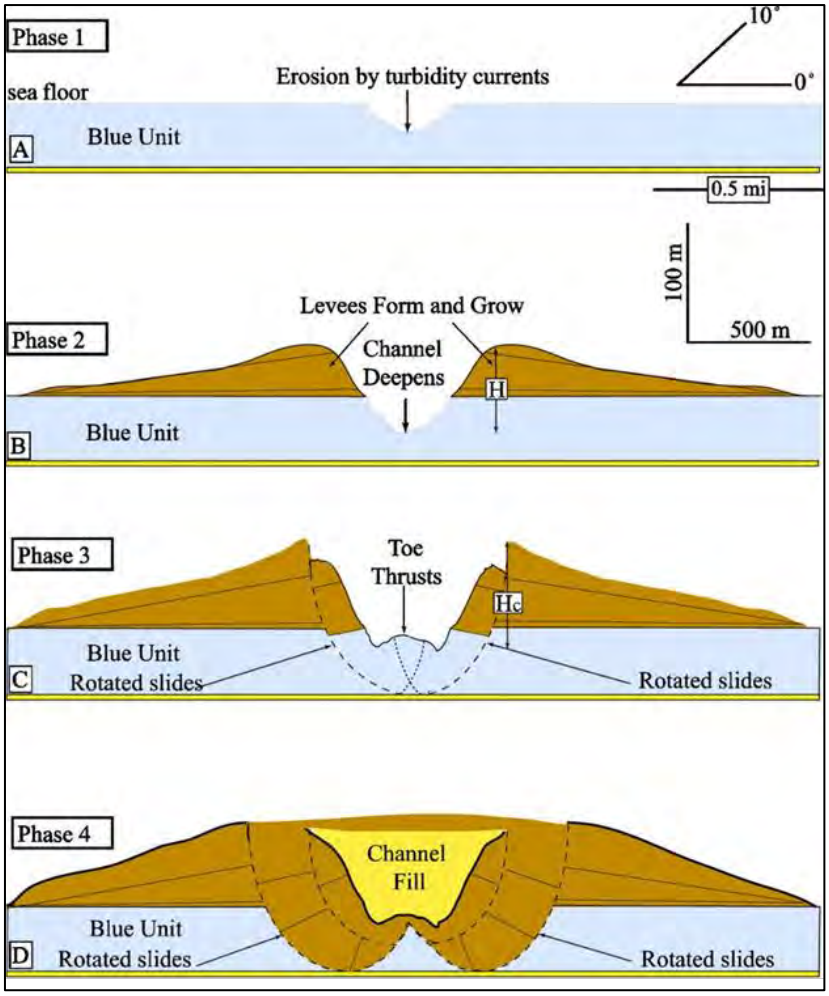

Schematic illustrating the stepwise development of channel-fill in an extensional tectonic setting (www.aapgbull.geoscienceworkd.org).

Appendix VI

Sequence Stratigraphy

A sequence is a relatively conformable succession of genetically related strata bound by unconformities or their correlative conformities (Mitchum, 1977). Sequences tend to show cyclicity of changes in the relative sea level and widespread unconformities, the sources and processes of sedimentation, and also climate and tectonic activity over time. The term "sequence'' was first introduced by Sloss *et. al.* in 1949 (Nfor, 2011) and developed into the principle of sequence stratigraphy in the 1960s as the study of several sequences of rock within a time-stratigraphic framework, which are grouped into genetically-related strata and separated by major surfaces of erosion or non-deposition or the correlative unconformities (Posamentier *et. al*., 1988; Van Wagoner, 1995). Unconformities are erosional surfaces that form as a result of major changes in the position of the shoreline as caused by relative sea level changes or global-scale tectonic events (Nfor, 2011). It is this knowledge which helps us to associate particular sequences of rock that are bound by unconformities and linked to specific events in the history of the Earth on a regional or global scale based on their unique age and lithologies, fossil content or other unique traits. As the concept of sequence stratigraphy grew and principles like turbidity flows and plate tectonics emerged, sequence stratigraphy became recognised in seismic studies through the inclusion of outcrop and well data (Posamentier *et. al*., 1988; Van Wagoner *et. al*., 1990; Nfor, 2011). Today, the concept of seismic sequence stratigraphy is widely used in seismic data interpretation due to the scale and resolution of the data, which allows geoscientists to identify the upper and lower boundaries of sequences of rock in the subsurface. Relating the sea level curve to these erosional surfaces enables the identification of transgressions and regressions by placing an associated age with a particular sequence of sediments, as first done by Vail in the 1970's (Vail, 1975; Vail *et. al*., 1977). This is particularly useful in the petroleum industry for the identification of source and reservoir rocks and to understand the evolution of basins.

Systems Tracts

The bounding surface types, stratal stacking patterns and position within the sequence define "systems tracts" which may be tied to particular positions on the global sea level curve since the bounding surfaces are typically global-scale unconformities. It is typically the depositional profile, rate of sediment supply and rate of relative sea level fall that control the stratal stacking patterns as illustrated below.

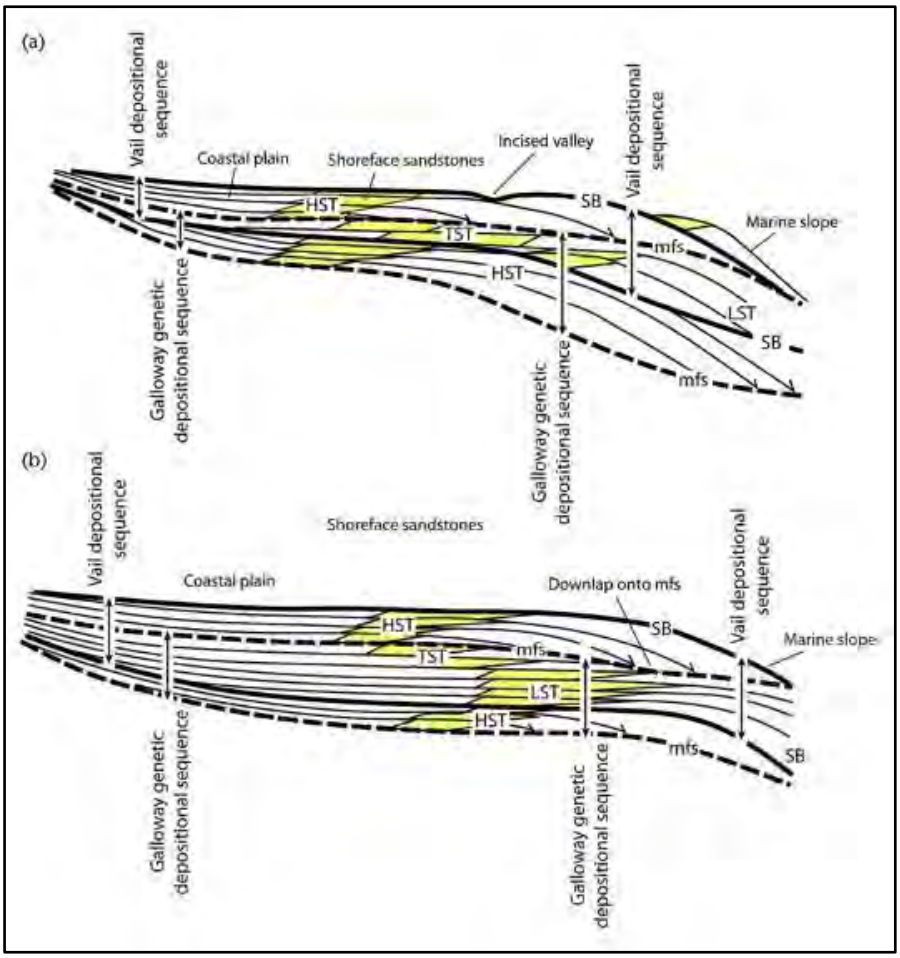

Schematic of depositional sequences and genetic stratigraphic units using their bounding unconformities and maximum flooding surfaces for a (a) shelf slope system and a (b) ramp system. The Vail type of depositional sequence is bound by erosional surfaces whereas the Galloway type is bound by maximum flooding surfaces (Allen and Allen, 2013).

The concept of a systems tract was introduced in the 1970's to describe the relationship between several depositional systems with one sequence. A depositional system is the fundamental mapping unit for sequence stratigraphy, defined in Van Wagoner (1995) as "…three-dimensional assemblages of lithofacies that are genetically linked by active or inferred ancient processes and environments seen as the laterally-grading sedimentary product of associated, coeval depositional environments." (Nfor, 2011). In essence, a depositional system consists of several lithofacies that may be vertically stacked and may grade laterally into simultaneously-deposited, adjacent environment lithofacies.

Depositional sequences can be mapped using seismic surveys, wireline well logs and outcrop data. The identification and interpretative tracking of bold seismic reflectors and the correlation of prominent surfaces across wireline well logs in this manner defines time lines in the physical stratigraphy and places boundaries between the systems tracts within one or several depositional sequences (Weimer and Slatt, 2007). Ideally, a single depositional sequence will consist of a set of three systems tracts that formed in response to sea level changes (Weimer and Slatt, 2007) and these systems tracts have been identified in the Exxon sequence model (Catuneanu *et. al*., 2002; www.sepmstrata.org), as illustrated in the figure below.

- *Lowstand Systems Tract:* Bound by a subaerial unconformity and its marine correlative conformity at the base and by a maximum regressive surface at the top, it forms during the early stage of base level rise when the rate of rise is outpaced by the sedimentation rate (i.e. normal regression). The lowstand systems tract (LST) includes the coarsest sediment fraction of marine and non-marine sections identified as the upper part of an upward-coarsening unit in a marine succession and the base of a fining-upward profile in non-marine strata. This systems tract has stacking patterns that may include backstepping, onlapping or retrogradational aggrading clinoforms that thicken updip to fill or partially fill incised valleys cut into older sequence deposits during the HST and overlying the associated erosional Type 2 sequence boundary.
- *Transgressive Systems Tract:* Bound by a maximum regressive surface at the base and a maximum flooding surface (MFS) at its top, it can be recognised from the diagnostic retrogradational stacking patterns in the form of an overall fining-upward profile in marine and non-marine successions.
  The transgressive systems tract (TST) comprises of deposits that accumulated from the onset of shoreline transgression until its peak but ended just before the renewed regression of the highstand systems tract (HST). Stacking patterns show evidence of backstepping as well as onlapping, generally in the form of retrogradational clinoforms that thicken landward.
- *Highstand Systems Tract:* Bound by a maximum flooding surface at the base and overlain with a composite surface consisting of a subaerial unconformity and a regressive surface of marine erosion as well as a basal surface of forced regression, the highstand systems tract (HST) is a package of progradational deposits that form when sediment accumulation rates exceed the rate of accommodation space growth. Stacking patterns typically yield prograding to aggrading clinoforms that thin upwards in the HST succession.

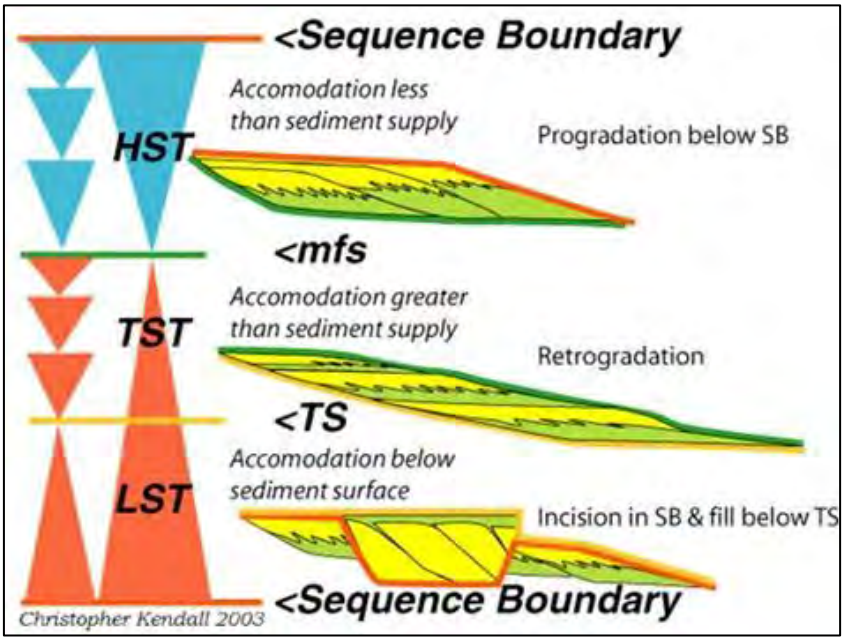

Schematic illustrating the relationship of the systems tracts within a single sequence (Kendall, 2003).

The maximum flooding surface (MFS) mentioned above is described as a widespread marine flooding surface that separates the underlying TST from the overlying HST. The MFS marks the deepest water facies within a sequence and represents a change from retrogradational to progradational stacking patterns. It is easily identified in seismic sections, like the one below, as a dominant trough since it is marked by the shales that immediately overlie it and it can often be well-recognised on the resistivity, gamma ray, neutron and density wireline well logs too.

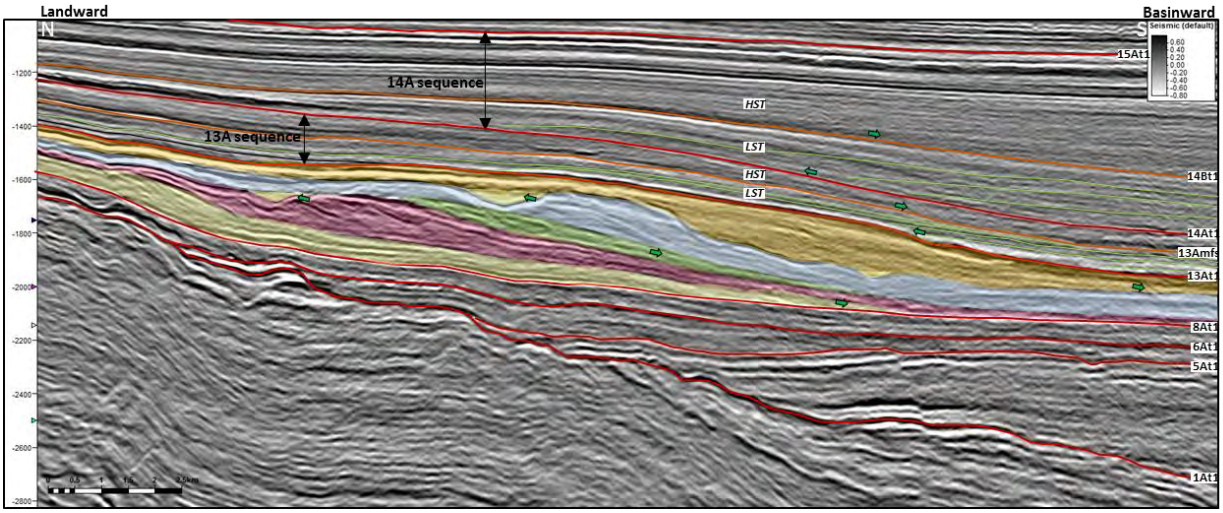

A seismic cross-section through the 14A and 13A sequences in the Central Bredasdorp Basin with HST and LST packages highlighted.

Depositional Cycles

It is believed that the deposition of sequences, such as those described above, occurs cyclically, albeit on different frequencies (see the figure below). First order cycles reflect sea level changes related to the movement of the global plates, occurring at a frequency of 250-300 myrs. Second order cycles reflect sea level changes related to tectonic processes at a frequency of 9-10 myrs. Third order cycles are 1-2 myrs in duration and represent the fundamental cycle on the proposed global eustatic cycle charts, typically consisting of the lowstand, transgressive and highstand systems tracts described above. Fourth order cycles have a ~0.1 myrs frequency; whilst fifth order cycles range from a 0.02 to 0.04 myrs frequency and have been interpreted as Milankovitch cycles (Mitchum *et. al*., 2002) since they appear to control high frequency variations in the global climate (Weimer and Slatt, 2007). Regional scale geological studies tend to focus on sequences deposited at the second and third order cycles scale. This principle that was applied in this study.

Tectono-Eustatic/ Eustatic Cycle Order	*Sequence Straigraphic Unit*	Duraction (my)	*Relative Sea Level Amplitude (m)*	*Relative Sea Level Rise/Fall Rate (cm/1,000 yr)*
First		>100		<1
Second	Supersequence	10-100	50-100	1-3
Third	Depositional Sequence Composite Sequence	1-10	50-100	1-10
Fourth	High Energy Sequence, Parasequence and Cycle Set	0.1-1	1-150	40-500
Fifth	Parasequence, High-Frequency Cycle	0.01-0.1	1-150	60-700

Hierarchy of the first to sixth order sea level cycles with the relative duration in millions of years (my) (www.sepmstrata.org).

Appendix VII

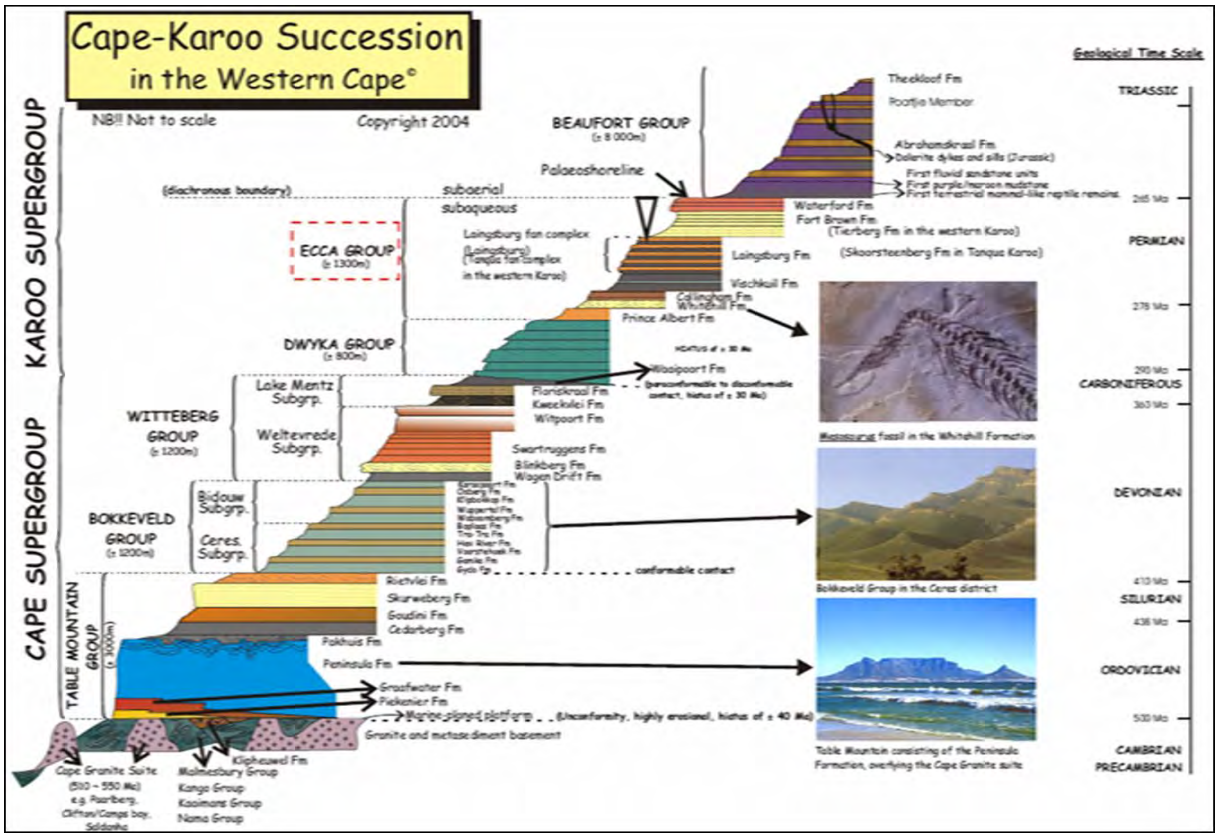

Stratigraphy of the Cape-Karoo succession. NB: NTS. (Modified after Wickens, 1994).

Appendix VIII

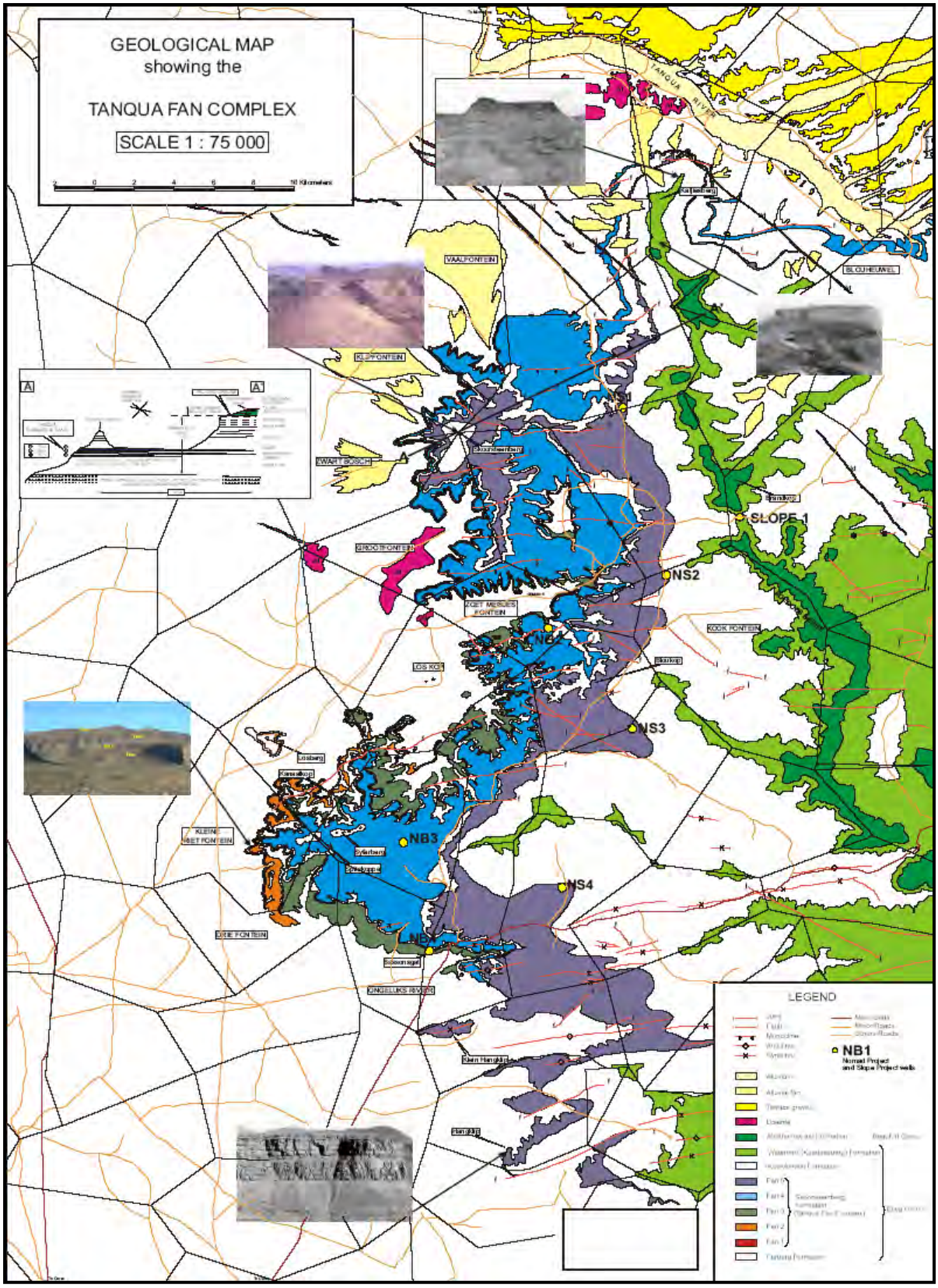

Geological map of the Tankwa fan complex (Wickens, 2015, 2011).

Appendix IX

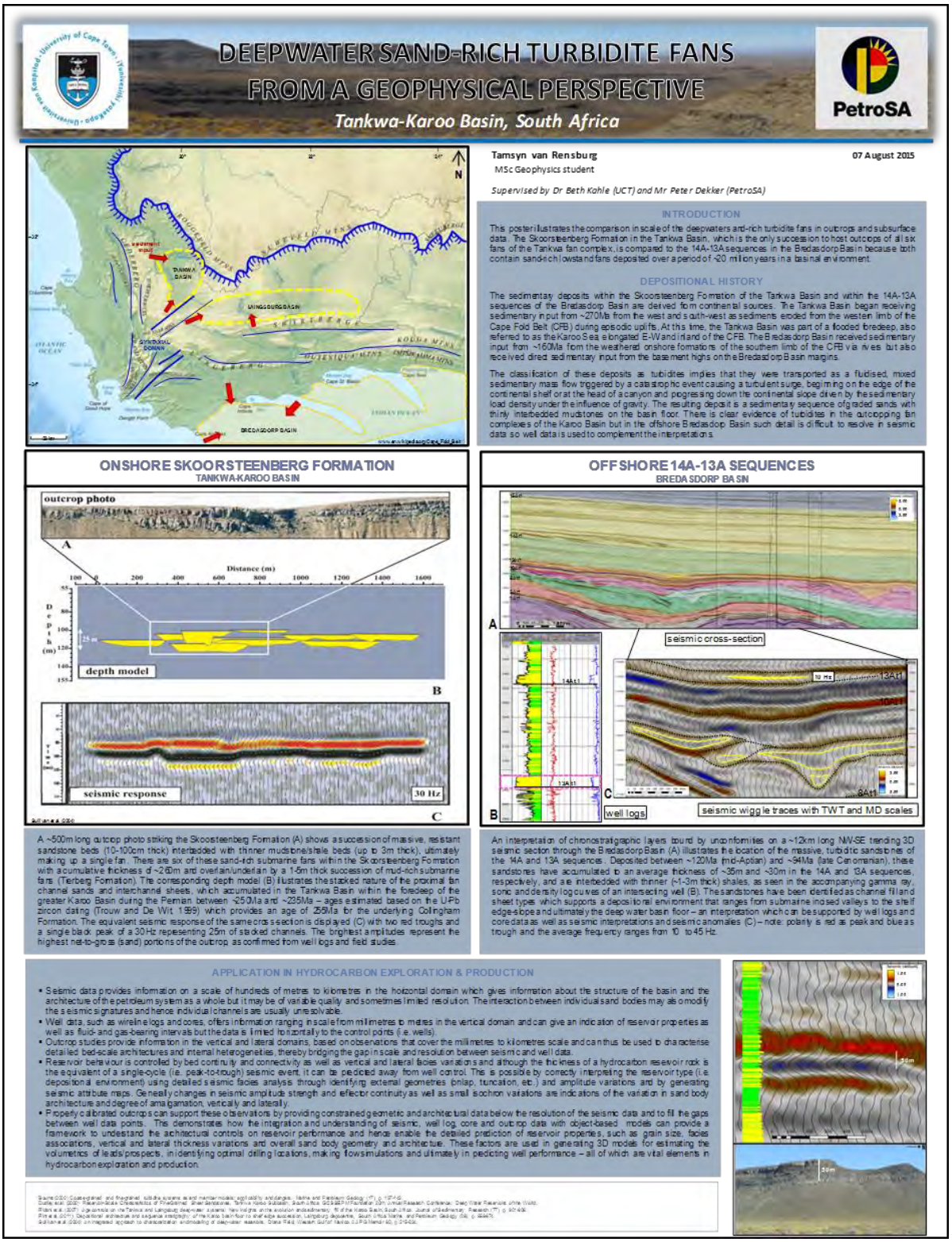

A poster demonstrating the role that scale plays in studying and modeling an ancient depositional environment of a turbidite complex by comparing data acquired in the Skoorsteenberg Formation of the onshore Tankwa-Karoo Basin versus the 13A-14A sequences in the offshore Bredasdorp Basin, South Africa (van Rensburg, 2012).